THE PRESENT DAY STRESS STATES IN THE MARMARA REGION

by

Yasemin Korkusuz

B.S., Physics, Marmara University, 2008

Submitted to the

Kandilli Observatory and Earthquake Research Institute

in partial fulfillment of the requirements

for the degree of Master of Science

Graduate Program in Geophysics

Boğaziçi University

2012

ACKNOWLEDGEMENTS

First, I want to place on record, my sincere gratitude to Assoc. Prof. Nurcan Meral Özel. As my thesis supervisor, she has shed light on my thesis research study and encouraged me at every point along the way. I am very fortunate to have benefited from her perspectives and extensive experience.

I am also grateful to Prof. Ali Pınar for his work cross-checking my results and his helpful advice, and Dr. Onur Tan for aiding my study through his programming and direction. In addition, I deeply appreciate Prof. Mustafa Erdik for his support.

With pleasure, I thank Prof. Balamir Üçer and Assist. Prof. Ethem Görgün for their efforts helping me to understand and evaluate fault mechanisms and seismotectonic features in a region. In addition, I would like to thank Dr. Mehmet Yılmazer, Dr. Ahu Kömeç Mutlu, Dr. Ayşegül Köseoğlu, Korhan Umut Şemin, Metin Kahraman, Ersin Çakır, Doğan Aksarı, and Mehmet Özer for their computer programming-related contributions. Also, I owe gratitude to Mustafa Çomoğlu, Gülten Polat, Ümit Çolpan and Zümer Pabuçcu for their help obtaining my very involved data set. In addition, I would like to acknowledge Öcal Necmioğlu for his broad perspective. I am grateful to Assist. Prof. Ali Özgün Konca and Nick Libassi for their precious helping, and my friend Mustafa Öztürk for his faithful encouragement.

Moreover, I wish to express my sincere thanks to Zafer Öğütçü, Nilay Başarır, and my brother Burak Korkusuz for their invaluable help and support.

I also would like to thank the Department of Geophysics, the National Earthquake Monitoring Center and the administration at KOERI-BU, as well as the Department of Earth and Marine Sciences at TUBITAK-MRC and the TURDEP Project.

Personally, I would like to thank to my dear friends Zeynep Yılmaz, Pelin Pündük, and my family, in particular, my mother Songül Korkusuz, as she has supported me every day of my life, as well as my father Orhan Korkusuz, and sister Neslihan Korkusuz.

ABSTRACT

THE PRESENT DAY STRESS STATES IN THE MARMARA REGION

Stress tensors with the aid of a large number of fault plane solutions provide important contributions for the evaluation of the seismotectonic setting of a region. In this study, recent earthquake activity at Ganos offshore, Tekirdağ Basin, Çınarcık Basin, Yalova Region and Gemlik Region, which are all located on the western branches of the North Anatolian Fault Zone, were analyzed using a current data set of fault plane solutions derived from a very dense seismic network.

For the analysis of high quality fault plane solutions, data from KOERI and the TURDEP project was merged. Data from a total of 105 stations, including 5 continuous SBO stations of KOERI was used. The earthquakes were selected with the following criteria; minimum local magnitude of 2.0, number of minimum P-wave first motion polarity of 10 and toleration of maximum misfit of 1. During the study 85, 75, 73, 102, and 63 source mechanisms were determined in Ganos Offshore, Tekirdağ Basin, Çınarcık Basin, Yalova Region and Gemlik Region, respectively. Through the determination of 9226 high quality P-wave first motion polarities for the selected 398 earthquakes, the number of average polarity per earthquake was 23. Average error depth, latitude, longitude, and GAP values were also obtained as 2.75 km, 0.98 km, 1.25 km and 63˚, respectively. Furthermore, using the algorithm of Horiuchi *et al.,* (1995), simultaneous focal mechanism solutions of individual earthquakes and recent stress regimes along with R-values have been determined for the five clusters. As a result, it was found out that NW-SE trending trans-tensional stress structures leading mostly normal and oblique faulting systems are predominant in Tekirdağ Basin, Çınarcık Basin, Yalova and Gemlik clusters. Nevertheless, Ganos Cluster was presented as a dextral strike-slip deformation system through the transition from normal to reverse faulting system. Vertically oriented Sigma-2 axis was obtained for the Ganos Offshore cluster, whereas in all other regions Sigma-1 axis was vertical.

Furthermore, data from KOERI and the TURDEP project was also merged in order to analyze 25.07.2011 Marmara Sea and 16.08.2011 Gemlik Gulf Earthquakes with local magnitudes of 5.2 and 4.0, respectively. It was stated that the stress tensor solutions obtained using mostly small size earthquakes fit the source mechanisms of these two moderate size earthquakes. Consequently, in this research, I have proposed a new and comprehensive approach to the fault geometries, present stress state, and seismotectonic structures of the Marmara Region by a detailed analysis of the results of the large number of fault plane solutions of earthquakes in the Marmara Region using the most dense seismic network of Turkey.

ÖZET

MARMARA BÖLGESİ'NDEKİ GÜNCEL STRES DURUMLARI

Çok sayıda fay düzlemi çözümünün kullanılması ile elde edilen stres tensörleri bir bölgenin sismotektoniğine önemli ölçüde katkı sağlar. Bu çalışmada, Kuzey Anadolu Fay Zonu'nun batı kollarında yer alan Ganos Kıyısı, Tekirdağ Havzası, Çınarcık Havzası, Yalova Bölgesi ve Gemlik Bölgesi'ndeki güncel deprem aktiviteleri, çok yoğun bir sismik ağdan elde edilen fay düzlemi çözümlerinin oluşturduğu yeni bir veri seti ile analiz edildi.

Yüksek kaliteli fay düzlemi çözümlerine ulaşmak için, KRDE ve TURDEP projesinin verileri birleştirildi. KRDE'nin 5 sürekli deniz dibi sismometresini de içermek üzere, toplamda 105 istasyon verisi kullanıldı. Depremler her bir depremin minimum 2.0 lokal magnitüde, minimum 10 P-dalgası ilk varış polaritesine ve maksimum 1 uyumsuz istasyona sahip olması kriterlerine göre elendi. Bu çalışma süresince, Ganos Kıyısı, Tekirdağ Havzası, Çınarcık Havzası, Yalova Bölgesi ve Gemlik Bölgesi'nde sırasıyla 85, 75, 73, 102 ve 63 kaynak mekanizması çözümü yapıldı. Seçilen 398 deprem için, 9226 adet yüksek kaliteli P-dalgası ilk varış polaritesinin kullanılmasıyla ortalama polarite sayısı 23 olarak belirlendi. Ortalama derinlik, enlem, boylam ve GAP hata değerleri de sırasıyla 2.75 km, 0.98 km, 1.25 km ve 63˚ olarak elde edildi. Dolayısıyla, bu çalışmadaki çoğu fay düzlemi çözümü çok yüksek kaliteye sahiptir. Ayrıca, Horiuchi *ve diğ.* (1995)'nin algoritmasını kullanılarak her bir depremin eşzamanlı fay düzlemi çözümü ve bu beş deprem kümesinin güncel stres rejimleri ile R-değerleri belirlendi. Sonuç olarak, Tekirdağ Havzası, Çınarcık Havzası, Yalova ve Gemlik kümelerinde, normal ve oblik fay sistemlerine neden olan, çoğunlukla KB-GD yönelimli açılma şeklinde stres yapılarının baskın olduğu görüldü. Bununla birlikte, normal fay sisteminden ters fay sistemine geçiş bölgesinde bulunmasından ötürü, Ganos Kümesi sağ yanal atımlı bir deformasyon sistemi olarak ortaya koyuldu. Ganos kıyısında Sigma-2 ekseni fay düzlemine düşey olarak yönelmiş iken, diğer tüm bölgelerde Sigma-1 ekseninin düşey doğrultuda olduğu elde edildi.

Ayrıca, KRDE ve TURDEP projesinin verileri, lokal magnitüdleri sırasıyla 5.2 ve 4.0 olan 25.07.2011 Marmara Denizi ve 16.08.2011 Gemlik Körfezi depremlerini incelemek için de birleştirildi. Çoğunluğu küçük magnitüdlü olan depremlerden elde edilen stres tensör çözümleri ile, bu iki orta büyüklüklü depremin kaynak mekanizmalarının birbirleriyle son derece uyumlu olduğu görüldü. Sonuç olarak, bu araştırmada, Türkiye'nin en yoğun sismik ağının yardımı ile Marmara Bölgesi'ndeki çok sayıda depremin fay düzlemi çözümlerinin ayrıntılı analiz sonuçları elde edilerek, Marmara Bölgesi'nin fay geometrileri, güncel stres durumu ve aynı zamanda sismotektonik yapıları için yeni ve kapsamlı bir yaklaşım ortaya koyulmaktadır.

TABLE OF CONTENTS

LIST OF FIGURES

LIST OF TABLES

LIST OF SYMBOLS / ABBREVIATIONS

σ	Sigma, principal stress axis
M	Magnitude
Md	Duration magnitude
ML	Local magnitude
Ms	Surface wave magnitude
Mw	Moment magnitude
P	Primary
R	Ratio of principal stress axes
S	Secondary
P (Az)	Azimuth of pressure axis
P (Pl)	Plunge of pressure axis
T (Az)	Azimuth of tension axis
T (Pl)	Plunge of tension axis
Vp	Velocity of primary wave
Vs	Velocity of secondary wave
AFAD	Presidency of disaster and emergency management
BB	Broad band
BU	Boğaziçi University
CMT	Centroid moment tensor
Dep	Depth
Erlt	Error of latitude
Erln	Error of longitude
Erdp	Error of depth
FOCMEC	Focal mechanism determinations
GCF	Guralp compressed format
CMG	Cansun Mehmet Guralp
GMT	Greenwich mean time
GMT	Generic mapping tools
H.In	Inconsistency of the method of Horiuchi *et al.* (1995)
In	Inconsistency

J	Geophone
KOERI	Kandilli Observatory & Earthquake Research Institute
KRDE	Kandilli Rasathanesi ve Deprem Araştırma Enstitüsü
Lat	Latitude
Lon	Longitude
MRC	Marmara Research Centre
NAF	North Anatolian Fault
NEMC	National Earthquake Monitoring Centre
SBO	Sea bottom observation system
Pl	Polarity
SAC	Seismic analysis code
Scream	Seismometer configuration, real-time acquisition and monitoring
SP	Short period
TUBITAK	Scientific & Technological Research Council of Turkey

1. INTRODUCTION

The Anatolian Block is located between the collision zone of the Arabian and Eurasian plates and moves to the west 2-2.5 cm per year along the North Anatolian Fault Zone. Holocene and GPS-derived slip rates imply an increase in this velocity from east to west (Dresen *et al.,* 2008). The Marmara Region accommodates the western branch of the 1500-km long North Anatolian Fault Zone. NAFZ is a dextral strike-slip faulting system starting from the Karlıova triple junction and vanishing in the Aegean Sea, having a 25.6±0.7 mm slip rate per year (McKenzie 1972, 1978; Dewey and Şengör 1979; McClusky 2003), and the slip rate for the Marmara Sea is 22±0.3 mm per year (Straub *et al.,* 1997; Kahle *et al.,* 2000). The M7.9 Erzincan Earthquake in 1939 initiated a new activity of seismic moment along the NAFZ (Parejas *et al.,* 1942). The seismotectonic features of the Marmara Region are complicated due to the transition from the right lateral strike-slip faulting regime of the NAFZ to the extensional regime of the Aegean Region. Moreover, the 1912 Ganos Earthquake in the Western Marmara Sea and 1999 İzmit Earthquake in the Eastern Marmara Sea were the last devastating earthquakes of the Marmara Region where occurrence periods of large earthquakes near İstanbul is about one century (Gürbüz *et al.,* 2000). Within that seismic gap a major Earthquake is expected (King *et al.,* 2001). Wright *et al.* (2001) asserted that the western end of the rupture of the 1999 İzmit event propagated below the Çınarcık Basin, while Bouchon *et al.* (2002) and Özalaybey *et al.* (2002) suggested that the rupture might be ended to the south of the Princes' Islands, and Pınar *et al.* (2001) claimed that it did not enter the Çınarcık Basin. As a result, gaining an understanding of the seismotectonic features of the Marmara would be a critical advance.

Crustal movement of Anatolia illustrated in Figure 1.1 (below) taken from Reilinger *et al.* (2010) better visualize the collision of the Anatolian Block between the Arabian and Eurasian plates. GPS-derived velocities with 95 per cent confidence ellipses of uncertainties also designate the movements with respect to Eurasia (Reilinger *et al.,* 2010). The Marmara Sea, shown in Figure 1.1 (top) has a GPS-derived slip rate of 25±2 mm/yr (Reilinger *et al.,* 2006; Reilinger *et al.,* 2010).

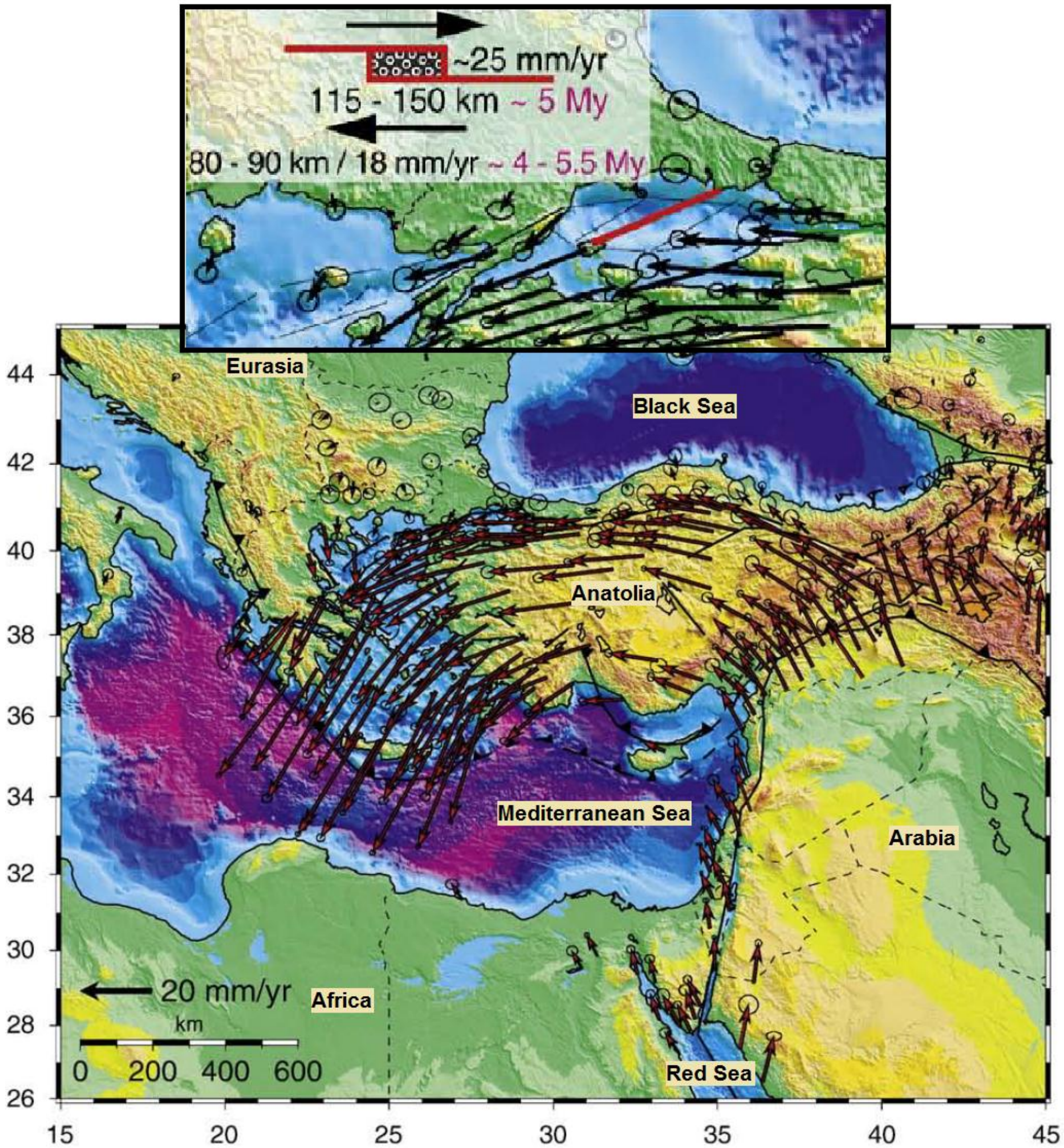

Figure 1.1. GPS velocity maps of the Marmara Region and the Anatolian Block (Reilinger *et al.,* 2010)

Deficiency in an understanding of transpression and especially transtension zones (Dewey, 2012) may be one of the most important problems for the Sea of Marmara. In order to reveal complex characteristic structures of the Marmara Region, numerous research studies have been done in recent years using P-wave first motion polarities or moment tensor inversion techniques to obtain fault plane solutions as well as principal stress axes (Gürbüz *et al.*, 2000; Kiratzi, 2002; Polat *et al.*, 2002; Pınar *et al.*, 2003;

Bohnhoff *et al.,* 2006; Pınar *et al.,* 2009; Görgün *et al.,* 2010; Örgülü, 2011). In addition, seismicities in some parts of the Marmara Region have been studied, and fault plane solutions without derivation of principal stress axes have been obtained (Karabulut *et al.,* 2002; Özalaybey *et al.,* 2002; Sato *et al.,* 2004; Bulut *et al.,* 2009; Karabulut *et al.,* 2011; Tunç *et al.,* 2011). A microearthquake seismicity study was also done by Barış *et al.* (2002). In addition, various explorations were also done to shed light on the Marmara Sea through sea bottom observations and geological investigations to define seismotectonic structures beneath the Sea of Marmara (Tüysüz *et al.,* 1998; Okay *et al.,* 2000; Le Pichon *et al.,* 2001; Yaltırak and Alpar, 2002; Elmas and Gürer, 2004; Robertson and Ustaömer, 2004; Seeber *et al.,* 2004; Armijo *et al.,* 2005; Oncel, 2006; Carton *et al.,* 2007; Laigle *et al.,* 2008; Avşar and İşseven, 2009; Janssen *et al.,* 2009; Becel, 2010; Yılmaz, 2010; Sorlien *et al.,* 2012). Moreover, Bohnhoff *et al.* (2007) investigated the seismotectonic setting of the NAFZ and Bekler *et al.* (unpublished) explored the rupture process of moderate events in the Southern Marmara Region which is important to evaluate the 24.10.2006 ML5.2 Gemlik Gulf event.

Gürbüz *et al.* (2000) obtained two regional stress regimes. One of them was achieved by compiling fault plane solutions of significant earthquakes from the global network (Eyidoğan, 1988) for the time period of 1943-1997, while the other one was achieved by using their own fault plane solutions of 23 microseismic events for the time interval of October-December 1995. The horizontal and vertical errors of relocations were better than 1.0 and 2.5 km, respectively. In order to get stress tensor alignments, they used the first motion polarities of P-waves through the method of Rivera and Cisternas (1990). The stress tensor inversion result of the global network yielded R=0.93 which is very close to an extensional stress regime, and the result of microseismic experiment indicated R=0.5 which is exactly between extension and compression. In addition, they found that the orientation of σ_1 is 145˚ from North implying a vertical σ_2 value. Furthermore, they achieved a new regional velocity model for the Marmara Region by the VELEST algorithm.

Kiratzi (2002) applied Gephart and Forsyth’s (1984) method to reinterpret regional stresses using a total of 163 fault plane solutions along the NAFZ, and its westward progression to the North Aegean Sea and Greece. The region was divided into 9 study areas, and the author used both previously obtained focal mechanism solutions through waveform modeling and focal mechanism solutions of microearthquakes through first motion polarities of P-waves. As selection of the correct fault plane is a significant problem, Kiratzi (2002) didn't make any choice and allowed the program of Gephart and Forsyth (1984) to determine correct fault planes although she revealed that the program doesn't give correct nodal planes every time. The author noted reactivation of the old NW-SE alignment features in Greece. Additionally, R-values vary between 0.2 and 0.7 with 90 per cent confidence limits of σ_1 and σ_3 for the 9 study regions. Furthermore, she discovered an inconsistent condition in the Marmara Region. Although the normalized average of the fault plane solutions implies strike-slip movements and resolved stress tensors indicate oblique strike-slip motions with strong normal components, the obtained R-value of the Marmara Region is 0.7 pointing to a transpressional stress regime. The author verified this result, signifying the region as an example of a shortening area which is indicated by source mechanisms.

Polat *et al.* (2002) performed a study in the Sea of Marmara for the time interval of 17 July-2 November 1999 that also includes the 17 August 1999 M7.4 İzmit Earthquake. They achieved 60 focal mechanism solutions for the purpose of obtaining the stress regime subsequent to the İzmit Earthquake with the analysis of the events recorded between 17 August and 24 September 1999. They were also able to forecast an alignment of approximation of N82˚ for the main shock and N78˚ for the precursor with the usage of P wave first motion arrivals. They pointed out that the recorded seismicity before the İzmit Earthquake, especially during the 1995 experiment, indicates a continuity of a seismic gap along the İzmit Bay soon before July and August 1999 when clustered earthquake activity was observed in the region. In addition, regarding previous different studies, they emphasized that before the 17 August main shock, σ_2 was vertical and σ_3 was N32˚ to N35˚ oriented, and after the İzmit main shock this condition was the same. On the other hand, σ_1 and σ_2 indicated an oblique faulting system instead of a strike-slip one.

Pınar *et al.* (2003) established the moment tensors of 64 small and moderate size earthquakes most of which were recorded beneath the Marmara Sea with the use of the method of Kuge. Separating the Eastern and Western Marmara regions, they reached principal stress axes through the method of Gephart & Forsyth (1984), Gephart (1985, 1990). As a result, they obtained the following azimuth and plunge values of σ_1, σ_2, and σ_3 for the Eastern and Western Marmara, respectively: 128˚-18˚; 19˚-69˚; 221˚-11˚, and 112˚-18˚; 9˚-36˚; 223˚-49˚. Azimuths of the Eastern and Western Marmara Sea were attributed to a counter-clockwise rotation from east to west. Plunge of σ_2 was vertical in the east, but closer to horizontal in the Western Marmara, indicating shear and transpressive tectonic regimes, respectively. They even found homogenous stress field in the Eastern Marmara and heterogeneous stress field in the Western Marmara on the alteration of strike of the NAFZ from E-W to WSW-ENE with the help of moment tensor solutions. Some secondary faults were also mentioned in the Sea of Eastern Marmara with the interpretation of nearly E-W trending NAFZ. Furthermore, they suggested a right step-over in the Eastern and left step-over in the Western Marmara Sea. Concerning the historical seismic activity of the Marmara Region, they proposed that the 1509 Marmara Sea Earthquake was the last major event between the Princes Islands and Ganos faults, and if the whole area were to rupture in a single earthquake, it may create an earthquake with Mw=7.9.

Bohnhoff *et al.* (2006) explored 446 focal mechanisms of aftershocks of the M7.4 1999 İzmit Earthquake for 4 earthquake clusters for the time span 17 August and 12 November. Focal mechanisms of 254 events were, determined from a 41-station network, obtained through a double-couple model (FPFIT program, Reasenberg and Oppenheimer, 1985), whereas focal mechanisms of 192 events originated from other published studies (Karabulut *et al.,* 2002; Özalaybey *et al.,* 2002; Polat *et al.,* 2002; Örgülü and Aktar, 2001). They also investigated stress regimes in order to obtain local stress areas using the method of Michael (1984, 1987). They pointed out that regions with small coseismic slip present mostly normal faulting features, whereas fields with large coseismic slip mainly exhibit strike-slip faulting features. A few thrust faults close to Yalova were also observed. They suggested that the NAFZ has three or more branches in the west. It was concluded that the regional stress field of the Marmara and local coseismic stress field of the İzmit Earthquake had nearly the same orientations, and stress partitioning and rotations were clearly seen in the local stress fields subsequent to the İzmit main shock.

Pınar *et al.* (2009) explored stress tensor orientations before and after the 1999 İzmit earthquake. They first used the Harvard CMT catalogue and the source mechanisms from

Eyidoğan *et al.* (1991) in order to determine a regional stress regime with the use of fault plane solutions of large events since 1943 through the method of Gephart and Forsyth (1984). Then, comparing FPFIT routine with the program of Horiuchi *et al.* (1995), they examined that even fault plane solutions of P-wave first motion polarities were not well constrained, and the program of Horiuchi *et al.* (1995) generated better fault parameters for a cluster of events and a uniform stress field. Therefore, after the analysis of 545 aftershocks with the criteria of a minimum of 10 P-wave first motion polarities and maximum 1 misfit, they obtained stress orientations of the seven aftershock clusters of the 1999 İzmit Earthquake using the program of Horiuchi *et al.* (1995) for the purpose of determination of postseismic stress field. Consequently, they asserted an extensional stress regime for the Çınarcık cluster and a vertical σ_3 around the area, and a compressive stress axis for the Yalova cluster which was attributed to negligible coseismic slip.

Görgün *et al.* (2010) determined 221 fault plane solutions of the 1999 İzmit Earthquake aftershocks recorded in Düzce and Karadere segments between 22 August and 17 October using FOCMEC (Snoke, 2003) program. Maximum azimuthal gap value is 110° and the minimum number of P-wave first motion polarities is 10 for every earthquake with an average of 15 first motion polarities and 92° azimuthal GAP. To obtain three principle stress orientations, they used the method of Michael (1984, 1987). The result is that the Düzce area has a vertical σ_1 orientation with a plunge of 84.

Örgülü (2011) investigated seismicity and principal stress axes of the Marmara Region, and most of the events in the Eastern Marmara were claimed as earthquake swarms triggered by the 1999 İzmit mainshock. She obtained fault plane solutions of 35 earthquakes ($3.3 \leq Mw \leq 4.9$) in the Eastern Marmara Region by the regional moment tensor inversion algorithm of Dreger and Helmberger (1991, 1993) and Dreger & Lanston (1995) for the time span 1999-2006. Source mechanisms of 54 earthquakes ($2.5 \leq Md \leq 5.0$) in the Marmara Sea were also achieved by the use of first motion polarities through FPFIT algorithm (Reasenberg & Oppenheimer 1985). The method of Michael (1984, 1987) was used to reach principal stress axes of the Marmara Sea. As a result, Örgülü (2011) asserted that Marmara Sea was predominantly under the right lateral strike-slip deformation with integration of normal and thrust faults in some local areas, and the Eastern Marmara has roughly two alignments after the İzmit Gulf; one is the fault of the

Çınarcık Basin and the other is the one or may be more branches on the Southern Çınarcık Basin. A limited number of normal faulting mechanisms were found in the town of Çınarcık. The author also suggested an unclear alternative between the negative flower and pull-apart structures for the Central Marmara Basin, but she drew attention to the extensional features. Furthermore, she pointed out a transpressive stress regime for the Western Marmara Sea.

It should also be noted that almost all of these scientific studies used the aftershock activity of the 17 August 1999 İzmit Earthquake for the analysis of the Eastern Marmara. Fortunately, 5673 earthquakes were recorded in the whole Marmara Region with ML≥1.0 between the dates 02.09.2006 and 31.03.2011, but due to the deficiency of a very dense network, very few earthquakes could be analyzed with ML≤3.0 up until now. Dresen *et al.* (2008) also remarked on the stress orientations of the NAFZ in the Marmara Region as these kinds of studies are mostly based on a small number of large earthquakes (Heidbach *et al.*, 2004) and aftershocks (Bohnhoff *et al.*, 2006). What is more, a magnitude ≥7.0 earthquake is expected in the Marmara Sea and would severely affect the İstanbul metropolitan area with its 13 million inhabitants. Therefore, this current thesis study was conducted with the purpose of exploring small earthquakes using a high quality data set in order to make substantial contributions regarding the seismotectonic features of the Marmara Region.

In this study, orientations of the principle stress axes for the five most obvious earthquake clusters in the Marmara Region were investigated with the use of a large number of simultaneously determined fault plane solutions for the time span 02.09.2006 and 31.03.2011. In order to achieve this purpose, data from the National Earthquake Monitoring Centre (NEMC) unit at the Kandilli Observatory & Earthquake Research Institute (KOERI) and the Scientific & Technological Research Council of Turkey (TUBITAK) were merged using the earthquake catalogue of TUBITAK. P and S phases and P-wave first motion polarities were defined with the visualization of waveforms on PQL-II screen. After the elimination of events in the Ganos Offshore, Tekirdağ Basin, Çınarcık Basin, Yalova and Gemlik clusters, the number of earthquakes decreased from 600 to 398. The criteria for the earthquake selections were that each event had to have at least 10 P-wave first motion polarities and no more than one inconsistent station. Then, 398 earthquakes were relocated through the method of HYPOCENTER 3.2 and source mechanisms were determined by the use of the FOCMEC algorithm (Snoke, 2003). Using the FOCMEC program was not actually an obligation to get individual fault plane solutions because the program of Horiuchi *et al.* (1995), which was used to reach stress tensors, can make simultaneous determinations of fault plane solutions for a single earthquake cluster. Minimum possible grid search interval on a focal sphere is five degrees for the program of Horiuchi *et al.* (1995). For this reason, the FOCMEC program was also used to obtain source mechanisms with the sensitivity of one degree of grid search interval. The average polarity per earthquake is 23 and depth error value is 2.75 km. Then, using the outputs of the relocations, simultaneous fault plane solutions and orientations of principle stress axes were determined by the program of Horiuchi *et al.* (1995).

As a result, some reverse fault mechanisms were obtained in the Ganos cluster and this corresponds to the Ganos uplift. Furthermore, stress tensor results of the Ganos cluster characterize a strike-slip regime, whereas the other four clusters are extensional stress regimes which are also compatible with the tectonic structure of the Sea of Marmara as pull-apart basins are involved. In addition, land earthquakes of the Gemlik cluster have right lateral strike-slip faulting mechanisms. Maximum principle stress axes in Ganos Offshore, Tekirdağ Basin, Çınarcık Basin and Yalova regions are NW-SE trending, while in the Gemlik region Sigma-1 is close to W-E orientation. Our results show that considering recent seismic activity in the region, all three branches of the NAFZ in the Çınarcık Basin are active faults.

2. TECTONIC SETTING AND SEISMIC ACTIVITY OF THE MARMARA REGION

Tectonic structure of the Marmara Region is run by the dextral strike-slip motion of the 1500-km long North Anatolian Fault Zone that starts from the Karlıova triple junction in the east and joins to the Aegean Sea in the west during the late Miocene Period. The NAFZ accommodates westward motion of the Anatolian block relative to Eurasia due to the collision between Arabian and Eurasian Plates. The length and width of the Marmara Sea Basin is about 230 km and 70 km, respectively, with a shallow shelf to the south and a series of sub-basins to the north--the Tekirdağ, Central, Çınarcık, Karamürsel, and İzmit Basins (Ambraseys, 2002). In general, transtensional and transpressional zones attribute to the unclear features (Dewey *et al.*, 2012) in particular regions. Since it involves many extension and strike-slip zones, the Marmara Region may be considered a very complex structure.

The western part of the NAFZ has especially complex features, splitting into three main strands in the Eastern Marmara Region. One of these branches passes by through Sapanca Lake and enters the Gulf of İzmit, while the central branch extends to the Gemlik Gulf via Pamukova and İznik Lake, forming the Gemlik pull-apart basin. The southern branch runs into the İznik Lake and Bursa. The southern strand splits again into central and southern strands, the former passing south of İznik and the latter south of Bursa, by the existence of the lakes of Apolyont and Manyas into the North Aegean extensional feature (Ambraseys, 2002; Yaltırak, 2002). Moreover, Bulut *et al.* (2012) found greater average velocity contrasts of Vp and Vs velocities in the Southern Mudurnu segment compared with the Northern one, using early P waveforms. The Adalar-Thrace Fault extends from Tuzla to Thrace and it loses its extensional character from east to west, since its fault character turns into strike-slip in the Central Marmara. The Ganos Fault inclines normal faults on the western, southern and northern boundaries, while compression characters such as Gelibolu Peninsula exist through the south (Yaltırak, 2002).

Throughout history, various views have been stated related to the active fault structure of the Marmara Region (Yaltırak, 2002), and some important tectonic models have been foreseen (Figure 2.1). The first column (Barka and Kadinsky-Cade, 1988; Wong *et al.,* 1995; Ergün and Özel, 1995; Barka, 1992), the second column (Parke *et al.,* 1999; Siyako *et al.,* 2000; Okay *et al.,* 2000) and the third column of Figure 2.1 (Le Pichon *et al.,* 1999; Aksu *et al.,* 2000; Imren *et al.,* 2001) characterize the investigated Pull-apart, En-echelon and Master Fault models for the Marmara Sea, respectively. Bold lines indicate the main faults and thin lines signify secondary faults. Yaltırak (2002) also stated that the Sea of Marmara is formed by the Tekirdağ Basin in the west, the Central Basin in the middle and the Çınarcık Basin in the east which split each other by NNE-SSW oriented ridges. The Sea of Marmara was found to be a graben or a structure of right-lateral faults exhibiting an overall normal motion (Barka and Kadinsky-Cade, 1988).

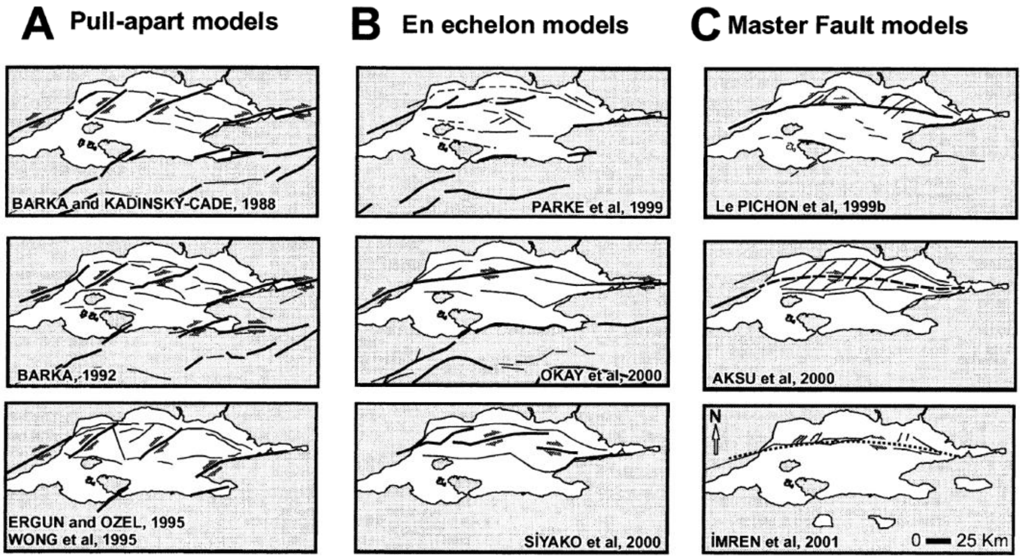

Figure 2.1. Tectonic models for the Sea of Marmara (Yaltırak, 2002)

The more recent study of Le Pichon *et al*. (2001) stated the basin of the Sea of Marmara as it was under the control of a strike-slip fault that extended between the Gulf of İzmit and the Gelibolu Peninsula. Nevertheless, a proposed bathymetry and fault model of Ambraseys and Jackson (2000) by the use of seismic reflection surveys and focal mechanisms of a few earthquakes indicate a series of pull-apart basins which are bounded by mostly short strike-slip and normal faults that implies a significant regional extension that is responsible for the formation of the Marmara Sea Basin. In addition, Ambraseys (2002) investigated the depths and steep bathymetric gradients for the demonstration of high seismicity in the Tekirdağ and Çınarcık sub-basins, the western and eastern portions of the Marmara Sea, respectively.

Using multi-beam bathymetry and high resolution multichannel seismic reflection data, Armijo *et al*. (2005) proposed that the geometry of submarine scraps in the Marmara Region is under the control of a segmentation of the pull-apart fault system. Additionally, they characterized a large component of normal slip along the southern margin of the Tekirdağ Basin. The pull-apart model of Armijo *et al*. (2005) is stated in Figure 2.2. This model proves to be very important for the tectonic and morphological structure of the Marmara Region. The figure also shows the inner pull-apart of Central Basin clearly. The trace of colour outlines and dates indicate the earthquake breaks with the pull-apart of the Marmara Sea.

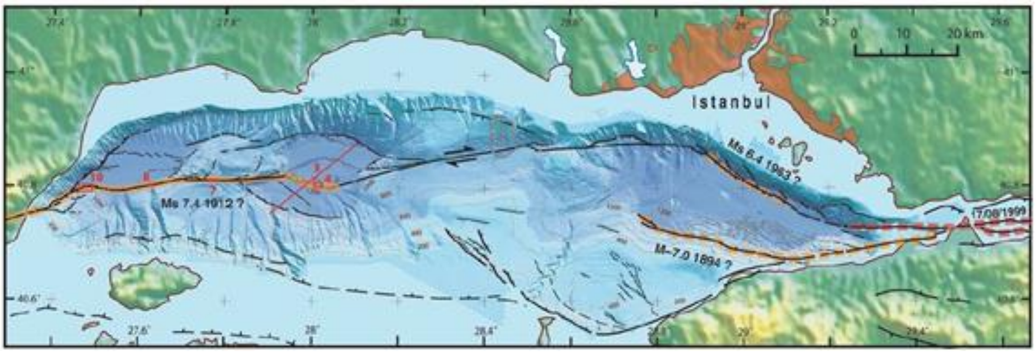

Figure 2.2. Active fault and bathymetry map of the Marmara Sea (Armijo *et al.*, 2005)

Long term seismicity analyses of the Marmara Region over the last 500 and 200 years are investigated by Ambraseys and Jackson (2000), and Ambraseys (2002). Ambraseys (2002) identified 581 earthquakes during the last 20 centuries in the Marmara Sea, and investigated the seismicity of the last 2000 years which might account for the 2.2±0.3 cm/yr dextral strike-slip. Earthquakes recorded on the northern strand of the NAFZ in the Marmara Region have dominantly right lateral strike-slip mechanisms with E-W orientation and their magnitudes alternate between 6.6 and 7.4 with ~10 km focus depth (Yaltırak, 2002). Yaltırak (2002) also stated that earthquakes smaller than M6.4 have different fault mechanisms such as the NW-SE trending extensional mechanism of the 1963 event on the Princes’ Islands Fault. Furthermore, right lateral strike-slip offsets of the

9 August 1912 Earthquake between Gaziköy and Saros Gulf were smaller than 5.5 m (Altunel *et al.,* 2000; Altınok *et al.,* 2001). Yaltırak (1996) also identified NE-SW trended reverse faults oblique to the main Ganos Fault. In addition, an earthquake that occurred in 1975 on the Northern branch of the NAFZ close to the Saros Gulf (Yaltırak and Alpar, 2002) identifies a dextral strike-slip offset with a normal component (Taymaz, 1990, 2000). Fault plane solutions in the Gemlik Gulf indicate oblique faults as a result of the investigation of Gürbüz *et al.* (2000), existing on the middle strand of the Western NAFZ. The largest earthquakes of the southern branch of the Western NAFZ are the 1964 Manyas (Ms6.8; Bekler *et al.,* unpublished) and the 1983 Yenişehir earthquakes (Ketin, 1966; Taymaz, 1990). Additionally, as historical seismicity is shown in Figure 2.3, the northern strand of the NAFZ in the Marmara Sea is seismically more active than the southern one (Gürbüz *et al.,* 2000). The latest destructive earthquakes of the northern strand of the NAFZ are the 1963 M6.3 Çınarcık, 17 August 1999 İzmit and 12 November 1999 earthquakes. Moreover, the 17 August İzmit Earthquake has a W-E aligned pure right lateral strike-slip mechanism, while the 12 November event has a W-E oriented right lateral strike-slip mechanism with a normal component (Bohnhoff *et al.,* 2007).

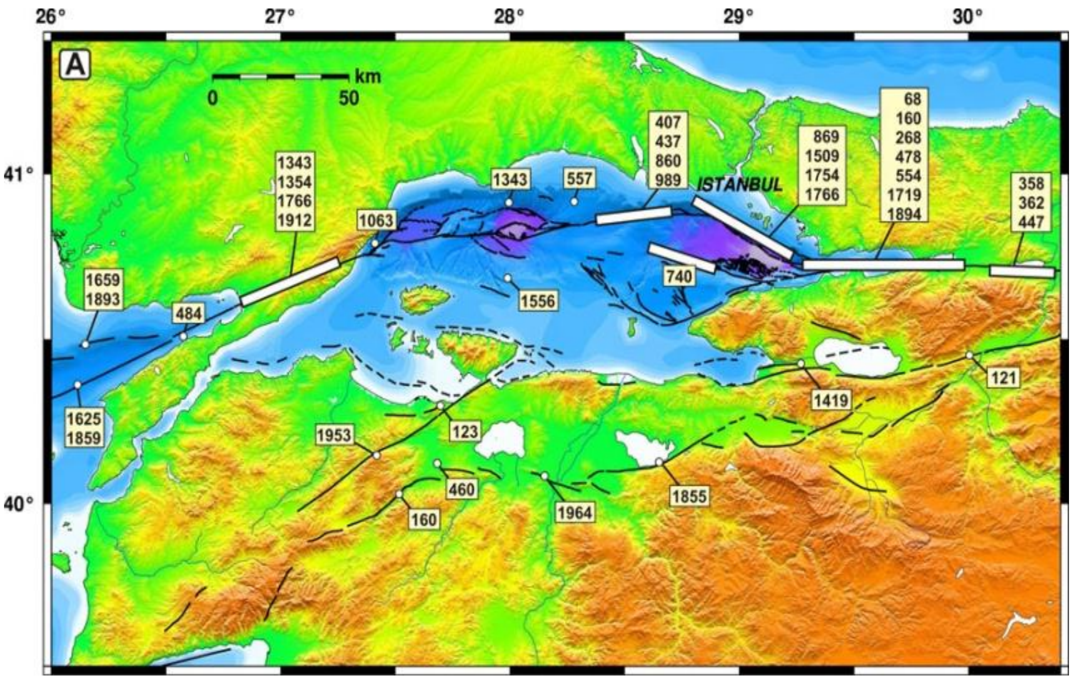

Figure 2.3. The occurrence years and possible locations of historical earthquakes (redrawn from Ambraseys, 2002)

3. DATA AND METHODS

3.1. General

Knowledge of the accurate state of stress in the Earth's crust is substantial to understand the mechanics of earthquakes and structural deformations (Görgün, 2008). Since obtaining direct stress measurements is impossible the radiation patterns of seismic waves must be used in order to achieve features of earthquakes and deformation of stress (Kostrov and Das, 2005). Therefore, observation of initial motion polarity and the amplitude of P waves provide the opportunity to obtain the direction of radiation of an earthquake.

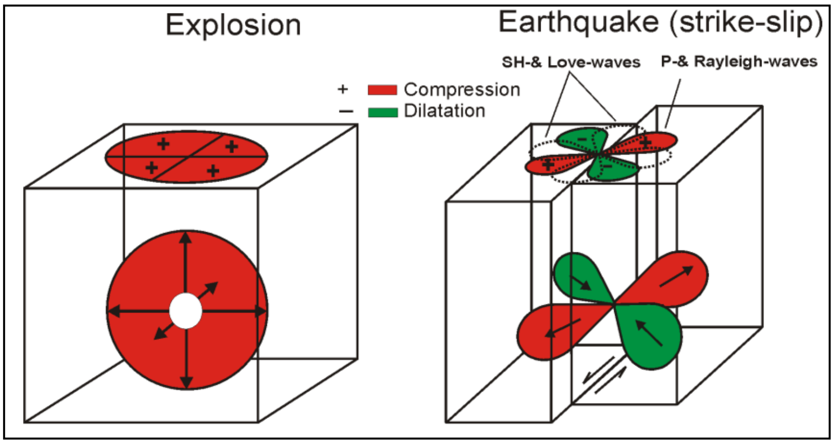

Figure 3.1.1. Schematic sketches of an idealised underground explosion and a pure left lateral strike-slip earthquake (Bormann, 2002)

An idealised underground explosion and a vertical pure left lateral strike-slip earthquake are depicted in Figure 3.1.1. As is clear, an ideal explosion produces outward oriented compressional initial motions in all radial directions (spherical symmetry), whereas an earthquake produces polarities in different directions and amplitudes, so earthquakes are examples of double couple forces (Bormann, 2002; Lay and Wallace, 1995). Considering an earthquake source and Doppler Effect, P wave first motion polarities and amplitudes change with the positions of seismic stations relative to the hypocenter of the event. The program of Focmec (Snoke, 2003), used in this study, provides the opportunity for different weight qualities for polarities which results in more accurate solutions.

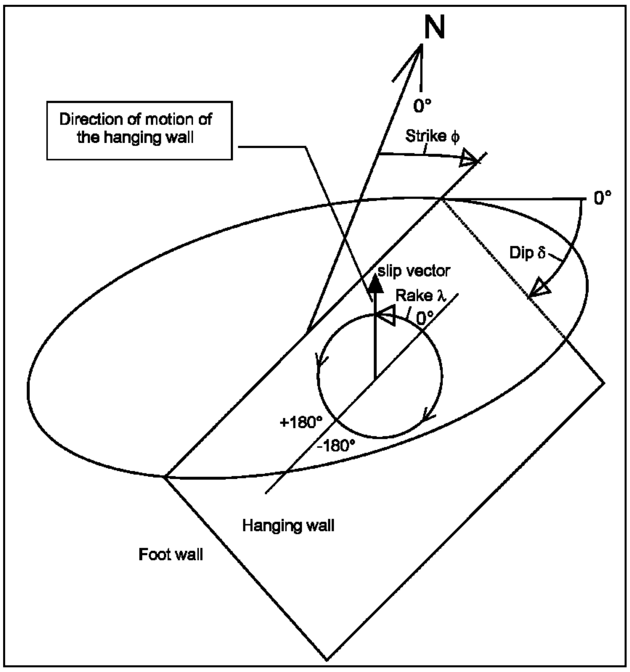

Figure 3.1.2. Angles describing a fault source (Bormann, 2002)

Fault geometry is defined by three angles which are called strike, dip, and rake, as can be seen in Figure 3.1.2. Fault strike is measured clockwise from north, depicting the orientation of the fault. Fault dip is measured from vertical to horizontal signifying the steepness of the fault. Fault rake/slip angle represents the direction of the slip vector of the hanging wall, the active fault plane of the fracture area relative to the foot wall.

The left part of Figure 3.1.3 represents pure normal, thrust, left lateral strike-slip, right lateral strike-slip and down-slip types of earthquake faulting mechanisms for some dip and rake angles (Bormann, 2002). In this figure, all the faults are NE-SW oriented, namely their strike angles are the same. Also, the right part of Figure 3.1.3 indicates lower hemisphere “Beach-ball” presentations of some basic earthquake faulting types (Bormann, 2002). White areas correspond to downside and black areas correspond to upside first motion polarities. “P” and “T” designate the dilatational (pressure) and compressional (tension) areas, respectively, and they are perpendicular to each other. Each event also has a “B” (Null) axis which is perpendicular to the others.

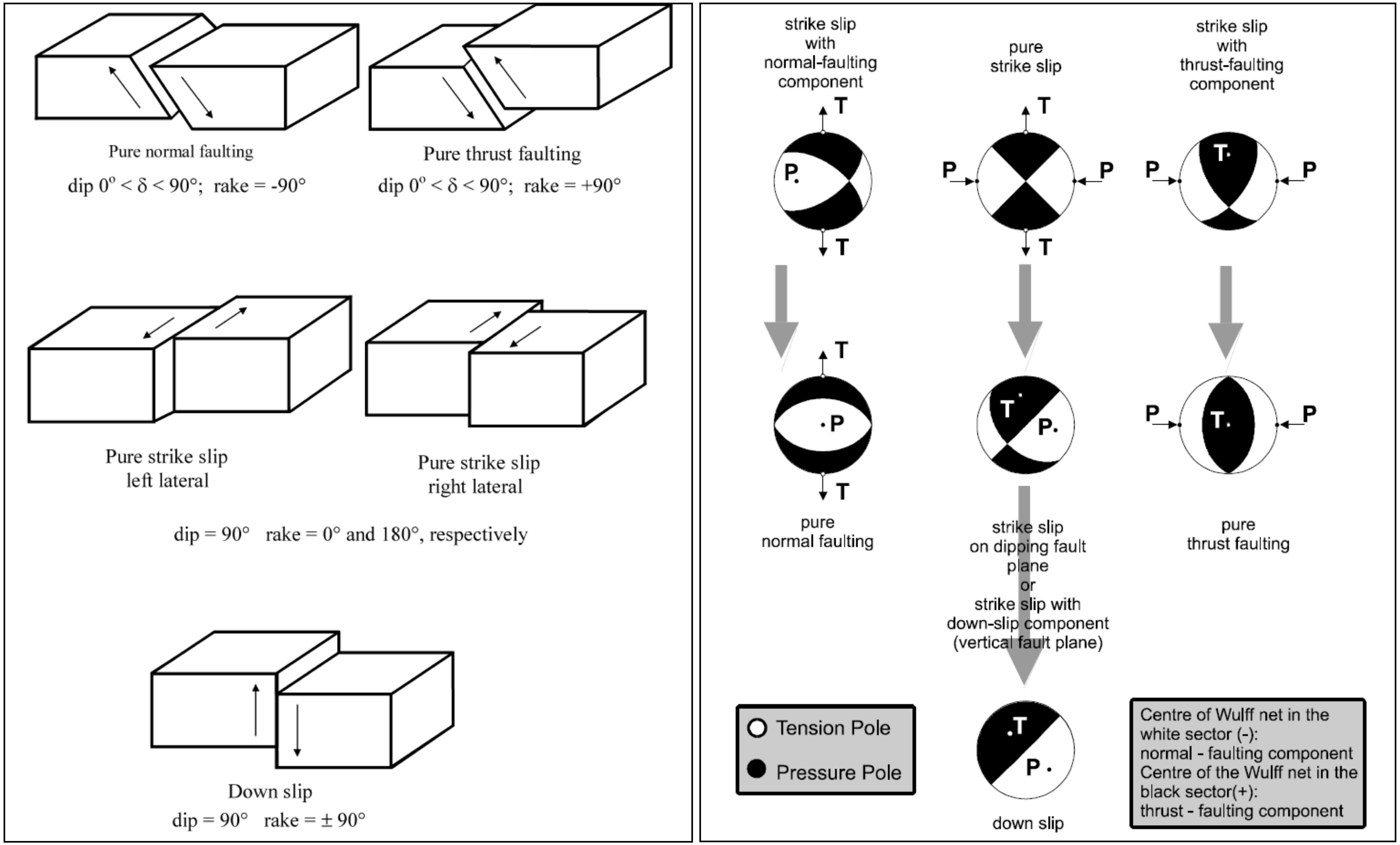

Figure 3.1.3. Basic types of earthquake faulting and some “Beach-ball” presentations (Bormann, 2002)

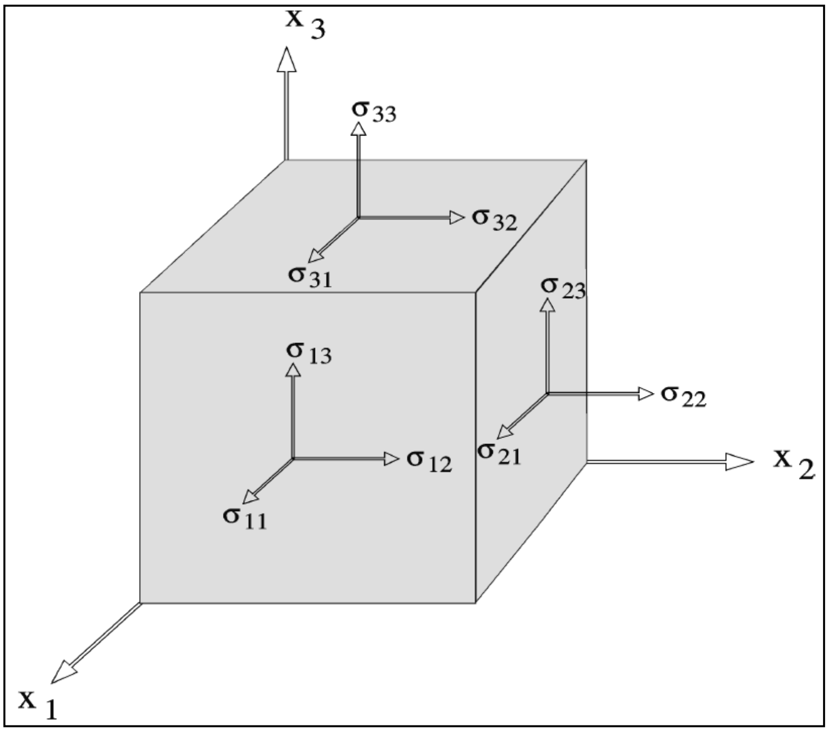

Figure 3.1.4. Nine components of a stress tensor (Bormann, 2002)

Obtaining many focal mechanism solutions for a specific area can allow a seismologist to state a regional stress regime by the use of source parameters such as P and T axes since they are vital for the stress analysis. As illustrated in Figure 3.1.4, an earthquake stress tensor consists of nine components. On the other hand, with the diagonalization of this stress tensor matrix, one can obtain three principal stress axes and rotation angles (Nowack). Governing a fault stress, the maximum compressive axis P, the intermediate axis B, and the minimum axis T, also called the greatest extensional axis, constitute the diagonal elements of this matrix.

3.2. The Data for Focal Mechanism Estimations

In order to reach the focal mechanisms with the best fit, I merged the data of 40-BB, 10-SP and 5-SBO stations of KOERI, and 50 BB and SP stations of the TURDEP Project consisting of 43 from TUBITAK, 5 stations from AFAD, and 2 stations from Sentez Company. The sampling interval of the KOERI stations is 50 sps (samples per second) and that of the AFAD stations was 50 sps historically but is now 100 sps. The sampling interval of all the TUBITAK stations is 100 sps.

Second, I selected clearly visible earthquake clusters which were located around the Ganos, Tekirdağ, Çınarcık, Yalova and Gemlik areas, using the current earthquake catalogue of TUBITAK-MRC. After the achievement of all the events in these clusters, I eliminated the earthquakes which have local magnitude values less than ML2.0 determined through the program of SEISAN. I used Tubitak local magnitude values following this selection, so some of the earthquakes in the catalogue were seen as smaller than ML2.0 in local magnitude value. I also checked the earthquakes around Gemlik and Yalova regions using the earthquake and explosion catalogues of M.S. Thesis of Deniz (2010) in order to confirm that the event catalogue of TUBITAK did not mistakenly include any explosions.

Figure 3.2.1 indicates the seismic station distribution of this current thesis study. Pink triangles in the figure represent BB stations of KOERI (40), and white triangles represent KOERI SP stations (10). Yellow triangles indicate BB and SP stations of TUBITAK (43), while green triangles stand for AFAD BB stations (5). Light green triangles signify BB stations deployed by other corporations (2). White and purple circles are SBO stations of KOERI (5).

Furthermore, I was able start to using data from the stations of the continuous Sea Bottom Observation (SBO) system of KOERI after 09.06.2010, as even at that date, only SBO5 station was ready for use. The others were deployed later. On the other hand, due to the fact that I have a very dense network, I was able to read a large number of P- and S-wave arrivals and polarities. Hence, I did not have to use any filter option when determining a types of first motions, as they can affect and even change the polarities of the P wave first motions, and reading the accurate P-wave first motion polarities is critical for this study. As an example, PQL II screen-shot from the SBO stations vertical component data of 29.02.2011 ML2.1 Yalova Earthquake can be seen from Figure 3.2.2. Being close to the Yalova Region, data of SBO1 and SBO5 stations are very clear.

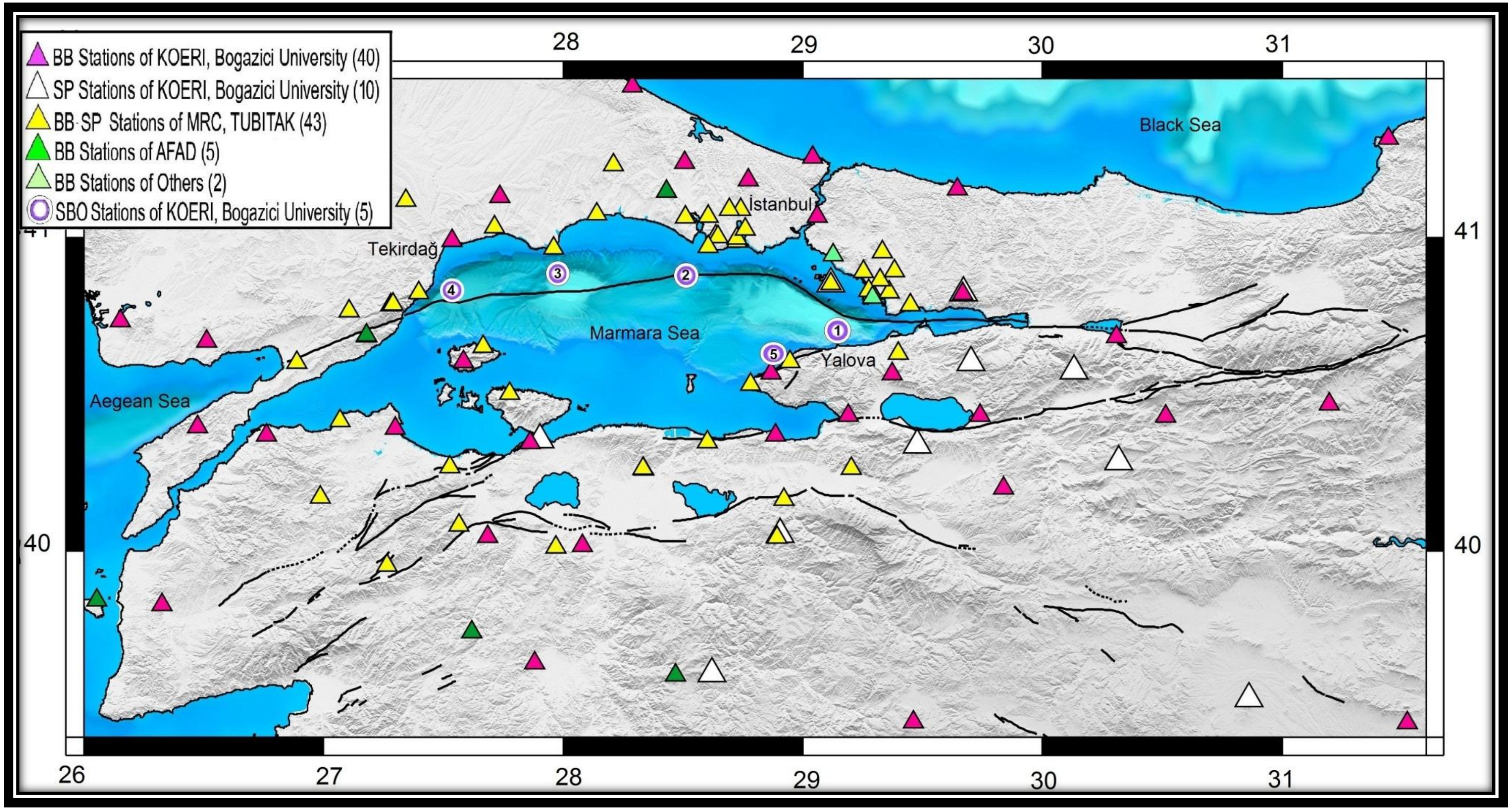

Figure 3.2.1. Seismic stations used in this the study

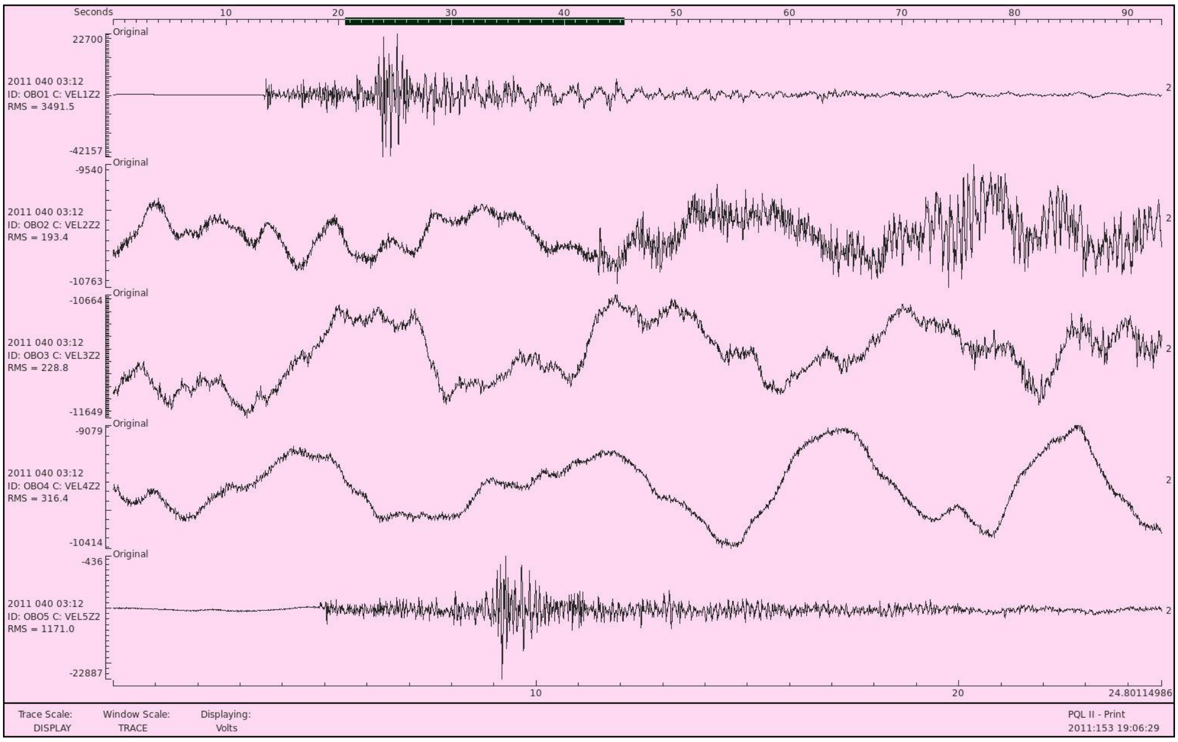

Figure 3.2.2. PQL II screen-shot from the SBO stations vertical component data of 29.02.2011 Yalova Earthquake with ML=2.1 and origin time 03:13 (GMT)

In the third stage, I chose arrival times of P and S phases and initial motion polarities of P waves. At first, I attempted to choose P and S phases and relocate earthquakes through zSacWin and SEISAN, but I encountered many problems in residuals and other error values. These problems most likely originated from having too many and so many different types of seismic stations, so the phase identification (P and S) was done by using PQL-II and HYPOCENTRE 3.2 to relocate earthquakes. However, in this case I had to convert the output files of PQL-II into Nordic format through a small program to be able to use observed phase times for relocations by the program of HYPOCENTRE 3.2. Stations further than 200 km were not involved in the relocations, but their polarities were used for only a few earthquakes which were greater in magnitude than others. In addition to this, I also had to write the types of the P wave first motions polarities manually, C for compression and D for dilatation, since PQL-II does not do that. Using data from 105 stations, I chose accurate P and S phases as well as P-wave first motion polarities of the 600 earthquakes cluster by cluster.

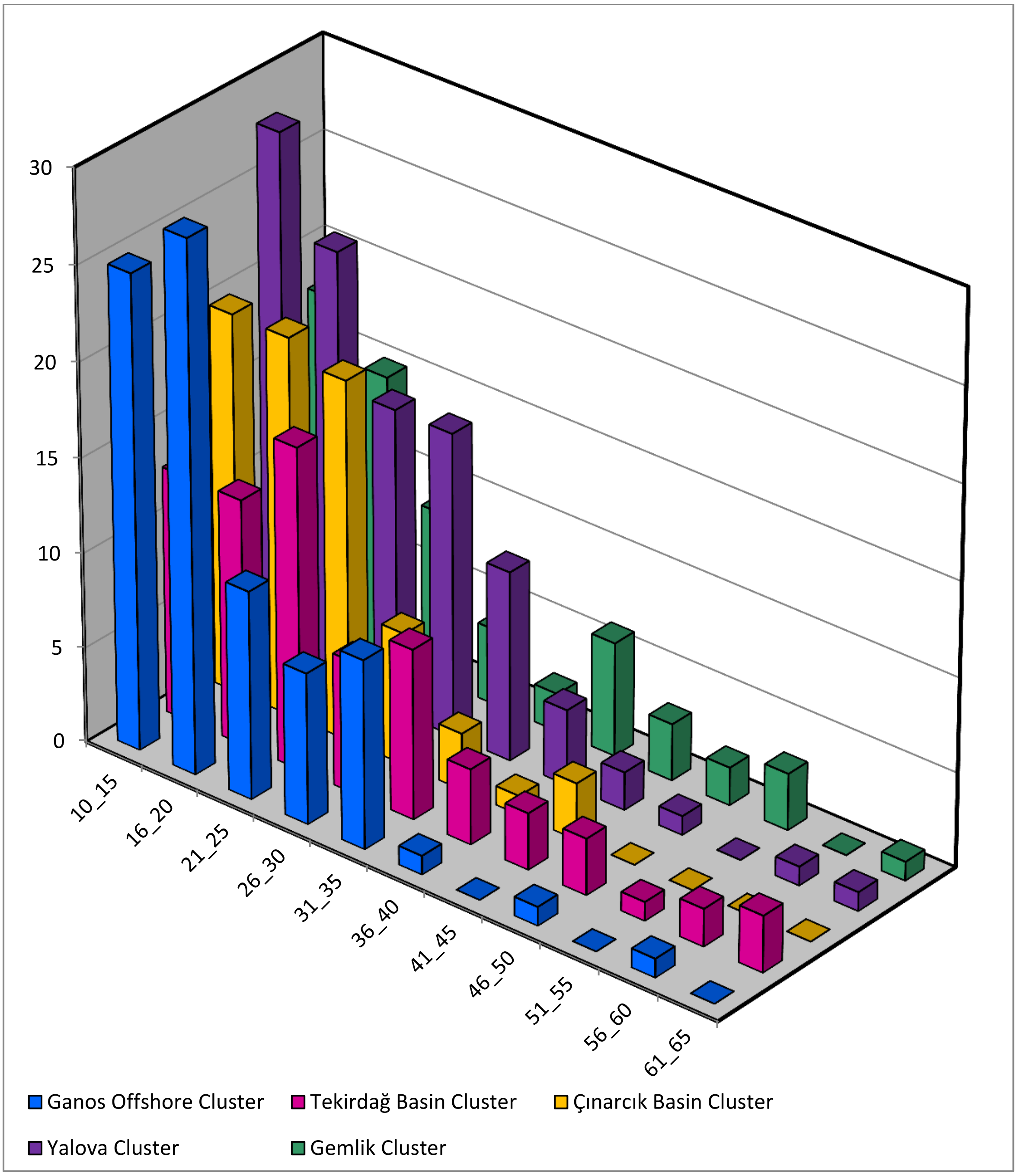

Figure 3.2.3. Cumulative frequency-polarity relationship of the five earthquake clusters

The cumulative number of earthquakes (vertical axis) versus the number of polarities (horizontal axis) can be seen in Figure 3.2.3 for 398 earthquakes selected from the total of 600 shown in five different clusters. As can be seen from the figure, the best quality data set belongs to the Tekirdağ Basin Cluster (pink) with an average of 28, whereas the worst data set belongs to the Çınarcık Cluster (orange) with an average of 20.

The number of polarities I read is 9226 for the 398 selected events as 195 earthquakes with less than 10 very accurate P-wave first motion polarities and 7 earthquakes with an inadequate number of polarities and very high error depth values were eliminated. In addition, to reach more accurate relocations, I used 5 different quality values from 0 to 4 for the determinations of P and S phases to be included in the relocations.

In the next stage, Vp/Vs ratio has been selected as 1.75 (Akyol *et al.,* 2006), and the velocity model of Karabulut *et al.,* (2003) was chosen after the comparison of the velocity models of Gürbüz *et al.,* (2000), Barış *et al.,* (2002), Karabulut *et al.,* (2002), Özalaybey *et al.,* (2002), and Bekler and Gürbüz (2008) concerning error values, residuals and take-off angles of these velocity models for 10 selected well-constrained earthquakes in the Gemlik and Yalova clusters. Fourth, using ready input files of the read phase records, I have relocated earthquakes one by one through HYPOCENTER 3.2 for each earthquake cluster. AZMTAK (Suetsugu, 1996) and FOCAL software were used to cross check the values of take-off angles and to see the differences in fault plane solutions to check the accuracy of the take-off angles and its effect to the fault plane solutions. Hence, fault plane solutions for a few well-constrained earthquakes were compared. As a result, the same fault plane solutions obtained with the similar take-off angles obtained by HYPOCENTRE 3.2, AZMTAK and FOCAL for the same earthquakes even though some small differences were seen in values of take-off angles. Therefore, the HYPOCENTER program was a suitable program to make relocations.

In the fifth stage, using the FOCMEC program as a package in the SEISAN software, I was able to obtain very high quality fault plane solutions with the help of accurate P wave first motion polarities. During this thesis study mostly “1 degree” and sometimes “2-5 degree” grid search intervals were used while performing the FOCMEC program to reach the best quality in fault plane solutions. When more than 1 degree of grid search interval was chosen, the program was sometimes unable to find any fault plane solutions without any inconsistent station which is crucial for the accuracy of the source mechanisms. Namely, one possible fault plane solution was obtained sometimes with the criteria of 1 degree of grid search without any misfit. Further, each earthquake being allowed no more than one inconsistent station was one of many strict criteria.

Finally, all the output documents of relocations were merged into one file for each cluster. After converting these overall output files into new input files, I subjected them to the program of Horiuchi *et al.* (1995) with the criteria of 5 degrees of grid search which is the possible minimum sensibility value. Again, no more than one inconsistent station was allowed for the fault plane solutions. Therefore, I was able to obtain two new focal mechanism solutions for each earthquake one before and one after obtaining the stress tensors and real fault planes. I eventually obtained the orientations of the principal stress axes with 5 degree grid intervals for each cluster by the program of Horiuchi *et al.* (1995). The last stage was the usage of the GMT 4.5.3 to obtain colorful contours in order to see orientations of stress tensors in detail and draw all the fault plane solutions on the topographic or bathymetric maps. All these programs were used on the Fedora 14 operating system, except for converting phase reading into the Nordic format as this required an operating system similar to that of Windows. Additionally, Figure 3.2.4 summarizes the general stages of data process in this current thesis study.

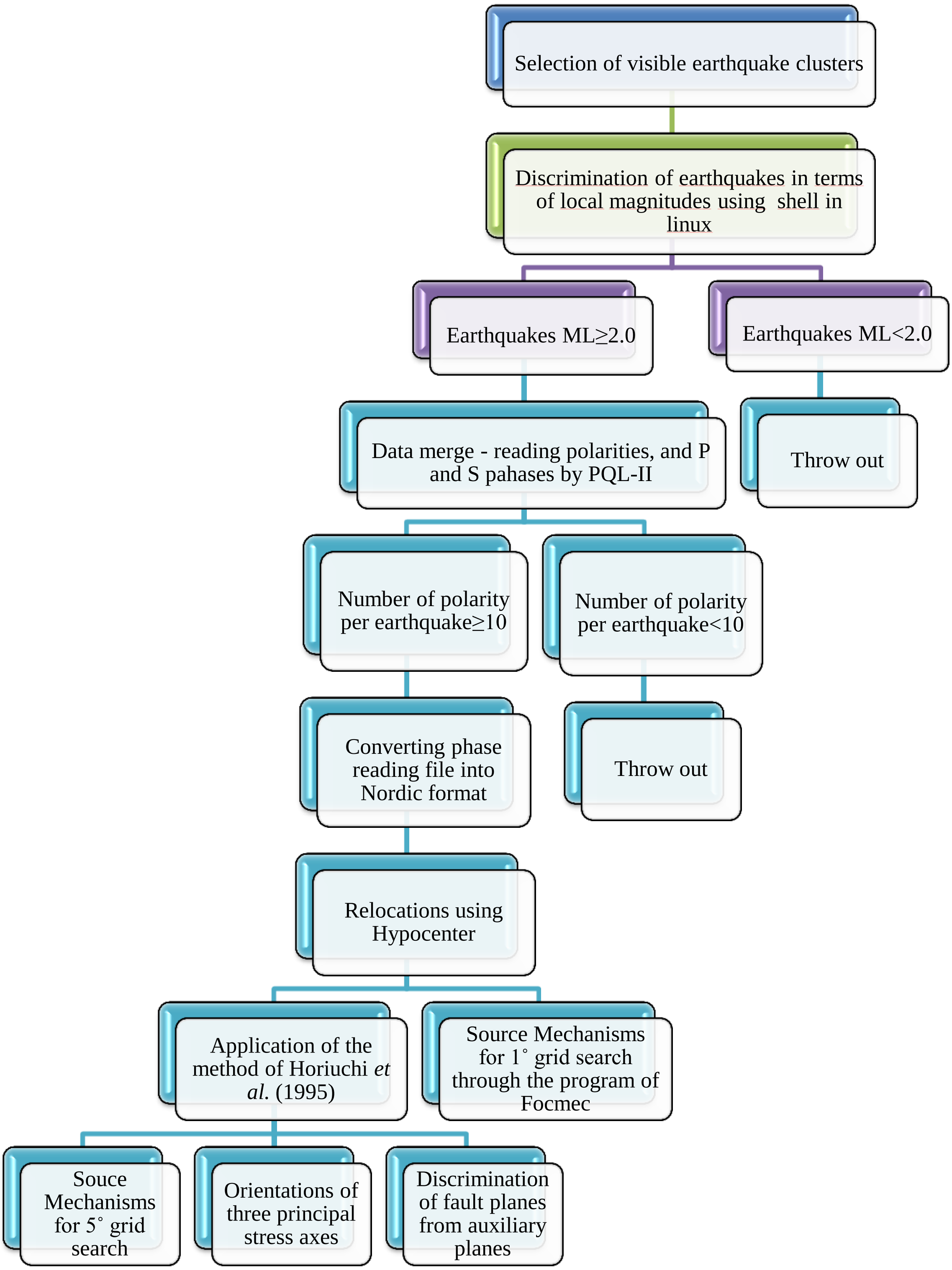

Figure 3.2.4. The methodology

3.2.1. Difficulties during Data Processing

One of the primary problems during data processing was that data of the most of the TURDEP Project stations does not include component information and station names in their headers for 2006 and the beginning of 2007 (Figure 3.2.1.1 and Figure 3.2.1.2). Because of this lack of information zSacWin 2010 yielded very high travel time residuals in the location process. These difficulties potentially could have been overcome by manually adding both component information and station names into the header files, but doing this for each earthquake and each station would have taken far too much time.

Moreover, when I attempted to use the SEISAN software, again because of the deficiency of header information and since there were so many waveforms, I was unable to convert all the waveforms into the SEISAN format. Even when I wrote station information into each header file for a selected earthquake, SEISAN could not open all the waveforms at the same time as it cannot convert SAC files to the SEISAN format when using more than 75-90 waveforms at once (Üçer, 2011) in most cases, I had over 100 components of data for every event.

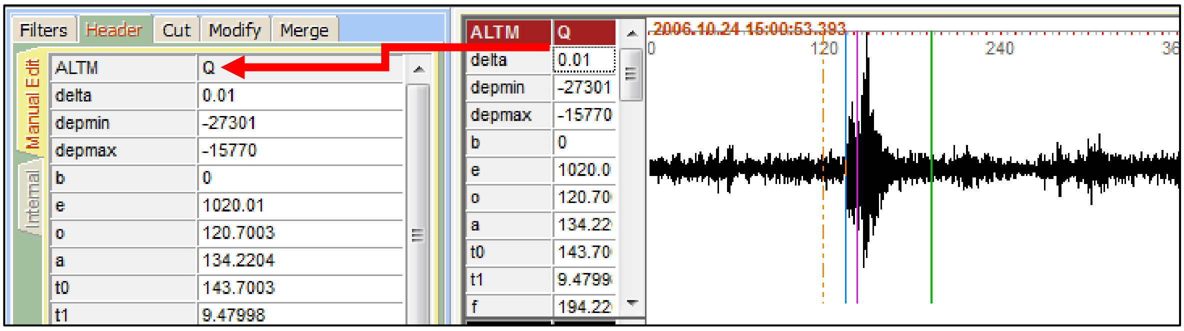

Figure 3.2.1.1. zSacWin screen-shot of one component data of ALTM station of TUBITAK from the 24.10.2006 ML3.3 Gemlik Earthquake showing the missing component information in the header of the station in 2006

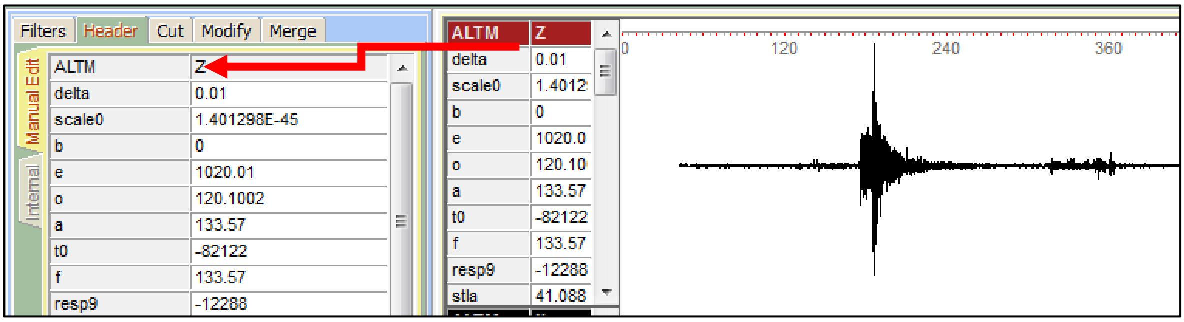

Figure 3.2.1.2. zSacWin screen-shot of one component data of ALTM station of TUBITAK from the 25.05.2009 ML2.9 Gemlik Earthquake showing that component information of the same station appears in the header file of the station in 2009

Furthermore, the KOERI and TURDEP datasets use are cut in different time intervals which may be another source of these issues (Figure 3.2.1.3). Consequently, I chose neither zSacWin nor SEISAN to select or relocate earthquakes directly. I decided to use PQL-II and HYPOCENTER for phase readings and relocations, respectively.

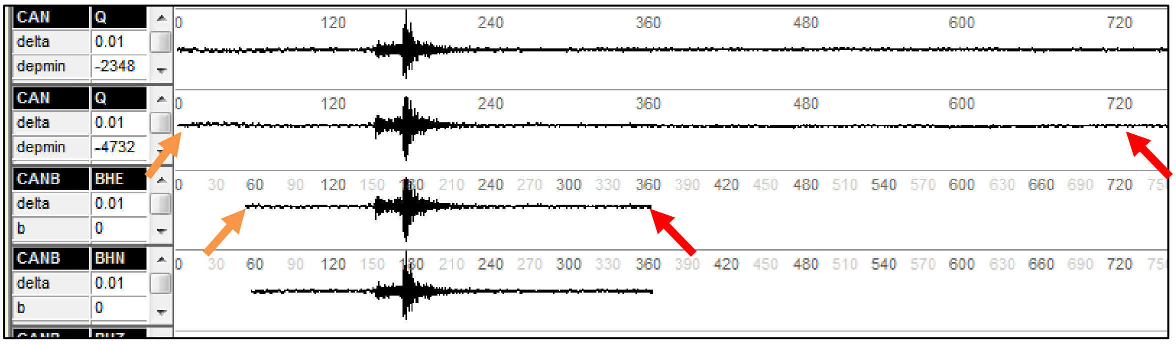

Figure 3.2.1.3. View of a waveform group indicating that the KOERI and TURDEP data are cut in different time intervals

Use of PQL-II also resulted in some visualization problems. PQL-II cannot be used on a laptop screen to select phases as the time bar cannot even be seen. This problem was solved using an external monitor. Obtaining KOERI's SBO data in a useful format was another difficulty as SBO data was saved in GCF format including one-hour data. Therefore, I obtained an earthquake list for each cluster and as well as SBO data for related times from NEMC using an external hard disk. Selecting velocity waveform files for the required hours for each earthquake, GCF data were converted into SAC data using Scream

4.5 on Windows 7. Furthermore, some small earthquakes were not included in the earthquake-based data storage of NEMC but were obtained from the earthquake catalogue of TUBITAK owing to their dense network in the Marmara Region. Downloading the required one-hour SAC data for each component of each station for all these absent earthquakes from the web page of NEMC, I obtained them with the help of zSacWin for Windows 7 and unified all the data together in order to be able to use all together.

In the meantime, using more than 10 arrival times of S phases for each earthquake resulted in increases in error depth values, but the use of many high quality S phases makes relocations much more accurate despite increasing hypocentral error values. Manually selecting each P and S phase, recording the type of each P-wave first motion polarity, and whether it is compressional or dilatational was quite time-intensive. In addition, each time I ran the program of Horiuchi *et al.,* (1995), I had to wait 3-4 hours to see the results and possible problems which required going back to the relocations to prepare a new suitable input file by finding and correcting the mistakes. All of these issues actually originated from writing polarities by hand, but each problem was carefully corrected. Hence, the program of Horiuchi *et al.,* (1995) allowed a cross-check for all the details of the fault plane solutions.

In addition, fault plane solution output files of the FOCMEC program were in PLT/HPGL format, so I was unable to convert them directly into JPEG format for use as figures in the lists of Appendix D as it was prepared using a Windows operating system. Therefore, I used the ‘Rename Man’ program to convert them into PS format. It was then possible to convert them into JPEG’s with the use of ‘Paint Shop Pro 9’ program.

3.3. The Methods for Stress Tensor Inversion Using Fault Plane Solutions

Numerous methods have been developed to obtain accurate values and orientations of stress tensors (Gephart and Forsyth, 1984; Michael, 1984; Rivera and Cisternas, 1990; Horiuchi *et al.*, 1995; Lisle *et al.*, 2001; Shan *et al.,* 2004; Sato, 2006; Otsubo *et al.,* 2008). The most common of these algorithms and the method of Horiuchi *et al.* (1995), which was used in this study, are explained in detail in the following sections.

3.3.1. The Algorithm of Horiuchi *et al.* (1995)

Shigeki Horiuchi, Guillermo Rocco, and Akira Hasegawa developed a method in 1995 for the purpose of determination of stress tensors and orientation of fault planes of a number of earthquakes. Here is a summary of the program and details can be found in Horiuchi *et al.* (1995). The method uses P wave first motion polarities and makes a simultaneous determination for stress tensors and fault plane solutions.

Approximation of fault planes is difficult when the number of P-wave first motion polarities is low with large estimation errors in individual source mechanisms. Scientists who use the program of Gephart and Forsyth (1984) don't determine orientations of fault planes, as is not easy every time with the use of theoretic data. Hence, it shouldn't be said that each fault plane can be distinguished from the auxiliary plane. On the other hand, Horiuchi *et al.* (1995) assert that it is possible to discriminate fault planes when original P-wave first motions are used even if some inconsistencies are smaller or greater than the observation errors.

In this method, it is assumed that earthquakes happen in randomly distributed weak planes for a uniform study region, and like Gephart and Forsyth, Horiuchi *et al.* (1995) also supposed that the slip direction of the faulting is parallel to the maximum shear stress direction. The aim of the method is to determine principle stress axes and orientation of fault planes simultaneously through P-wave polarities. Six independent components are present in a stress tensor, and they set σ_1(P), σ_2(B), and σ_3(T) as maximum, intermediate and minimum principle stress axes, respectively. With the negligence of hydrostatic term they obtained;

$$\sigma_1 + \sigma_2 + \sigma_3 = 0 \qquad (3.1)$$

Because of the usage of P wave polarities, absolute values of principal stress axes aren't obtained, and the ratio of stress tensors (R) is following;

$$\boxed{R = (\sigma_1 - \sigma_2)/(\sigma_1 - \sigma_3)} \qquad (3.2)$$

It is assumed that $\sigma_1 > \sigma_2 > \sigma_3$, so for the condition of nearly equivalent values of Sigma-2 and Sigma-3 the R-value approaches “1”, which indicate an axial compression, for the condition Sigma-1 and Sigma-2 are nearly equivalent the R-value approaches “0”, which characterizes also an axial extension, and for the condition of Sigma-2 is two times greater than Sigma-3 the R-value approaches “0.5” indicating a biaxial stress state (Kiratzi *et al.*, 2002).

Assuming X_g, Y_g and Z_g as unit vectors of geographical coordinates, θ_p and $\emptyset_p$ are inclination and azimuth of the P;

$$P = X_g cos\emptyset_p\ sin\theta_p + Y_g sin\emptyset_p\ sin\theta_p + Z_g cos\theta_p \tag{3.3}$$

With the use of ω_p as rotation angle about P, T and B are given as;

$$B = B_0 cos\omega_p + T_0 sin\omega_p \tag{3.4}$$

$$T = -B_0 sin\omega_p + T_0 cos\omega_p \tag{3.5}$$

Where B_0 and T_0 are;

$$B_0 = PZ_g/|PZ_g| \tag{3.6}$$

$$T_0 = PB_0 \tag{3.7}$$

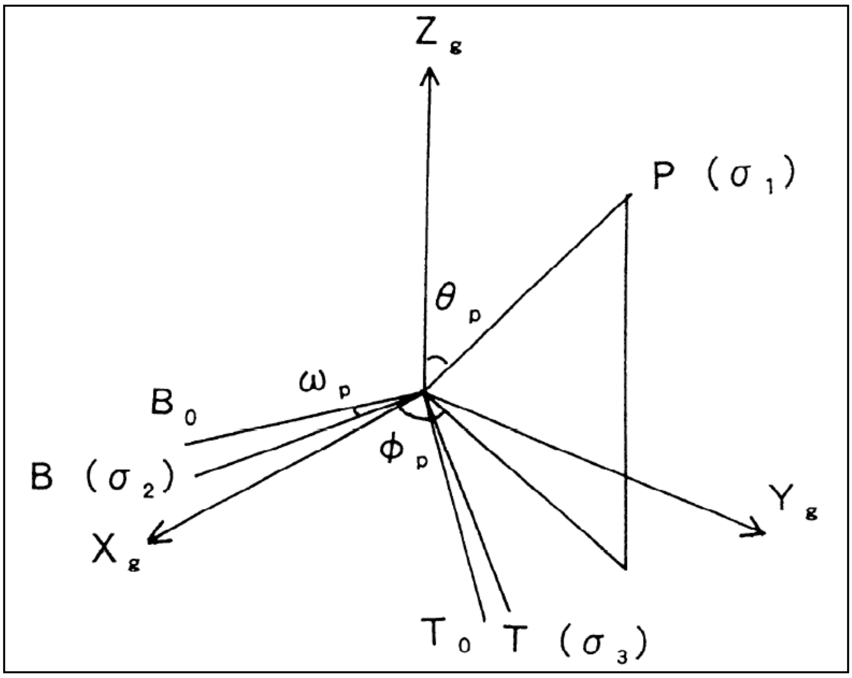

Figure 3.3.1.1 Cartesian coordinate system of the program of Horiuchi *et al.* (1995)

$X_g, Y_g, Z_g, P, B,$ and T are shown on the Cartesian coordinate system in Figure 4.1.1. The vector B_0 is perpendicular to P and Z_g. Rotations of B_0 and T_0 about P an amount of ω_p give the directions of *B* and *T* vectors (Horiuchi *et al.*, 1995).

With the assumption of C is a constant and A_{ij} is a unit vector indicating the direction of jth station of ith event, the theoretical amplitude of the P wave is defined as;

$$S_{ij} = C\left(A_{ij}X_i\right)\left(A_{ij}Y_i\right) \tag{3.8}$$

The number of inconsistent stations is calculated with the comparison of polarities of theoretical and observed amplitudes. Therefore, the function of the total number of inconsistent stations is given through inclination and azimuth of P and T axes $(\theta, \emptyset)$, rotation angle about P (ω_p), the ratio of stress tensors (R), unit vector (A_{ij}), reading of a P-wave polarity (P_{ij}), and a value of inconsistency (N_{ij}) that becomes zero when amplitudes of theoretical and observed polarities coincide each other and becomes 1 for vise verse.

$$N_{tot} = \sum_i \sum_j N_{ij}\left(\theta_p, \emptyset_p, \omega_p, R, \emptyset_t, \theta_t, A_{ij}, P_{ij}\right) \tag{3.9}$$

Nevertheless, calculation of derivatives of Equation (3.9) is difficult as they become infinite on the nodal planes, so the inversion is done numerically. Because making a grid search for all combinations of unknown parameters isn't necessary, the term of inconsistency could be omitted. Hence, the total number of inconsistency is given as;

$$N_{tot} = \sum_i M_i\,(\theta_p, \emptyset_p, \omega_p, R) \tag{3.10}$$

M_i is the minimum number of inconsistent stations of the ith earthquake. Number of inconsistent station is determined for all events and for all cases of the three variables of Equation (3.10), as they directly affect the orientations of the focal plane solutions.

Due to the discontinuities of the seismic velocity structure, the distribution range of take-off angles is very narrow. As a result, to have the most accurate grid searches is crucial. The computations of the amount of inconsistency are determined through the program of Horiuchi *et al.* (1972). The advantage of this process is that it is almost independent of ω_i which is the rotation angle around the vector perpendicular to the fault plane for the ith earthquake. The method computes a value of rotation angles around this vector that is perpendicular to the fault plane, from each station to the initially supposed positions of the nodal planes. Then, all the values of calculated inconsistencies are used for all the values of ω_i within a certain interval. The number of inconsistency is computed for 0.2° interval for ω_i. Besides, total number of inconsistency is $N_{eq} \times N_x \times N_w$, where N_x is the number of grid points of the fault plane and N_w is the number of grid points of the rotation angle around the pole.

3.3.2. The Algorithm of Rivera and Cisternas (1990)

Rivera and Cisternas (1990) developed an algorithm to achieve the orientations of principal stress axes and individual fault plane solutions with the use of parameters of real data, instead of predetermined fault plane solutions. Namely, their method uses the same input parameters (P wave initial polarities and take-off angles) with the program of Horiuchi *et al.* (1995). They asserted that their approach generally gives better results than the others which use individually determined focal mechanisms. Besides, this method also gives more accurate results than the methods composite fault plane solutions, as they give acceptable results in the case where some earthquakes have the same source mechanisms.

3.3.3. The Algorithm of Reasenberg and Oppenheimer (1985) / FPFIT

The method of Reasenberg and Oppenheimer (1985) also calculates stress regime of a region. The program FPFIT derives from only a double-couple source model and it uses a set of observed initial motion polarities. The program is based on observed and theoretical amplitudes of P wave first motions. It is executed by a two stage grid search process. Namely, two weighting factors are involved: one is presenting the estimated variance of the data set, based on the absolute value of the theoretical P wave amplitude (Aki and Richards, 1980), and the other indicates greater (lesser) weight to observations near radiation lobes (nodal planes). On the other hand, the program FPFIT requires well-fitted focal mechanism solutions to give a uniform stress regime comparing with the program of Horiuchi *et al.* (1995), since the latter can give a uniform stress regime even if the focal mechanisms are poorly constrained (Pınar *et al.,* 2009).

3.3.4. The Algorithm of Gephart and Forsyth (1984)

Gephart and Forsyth (1984) presented that it is necessary to select one of the nodal planes as a fault plane although this selection leads to differences between theoretical and observed slip directions. However, the method of Horiuchi *et al.* (1995) changes the pole of the fault plane to all directions, so it makes a grid search which doesn’t require a choice of a nodal plane (Horiuchi *et al.,* 1995).

Gephart and Forsyth (1984) developed a method to determine regional stress tensors and they claimed that with the help of the use of grid search models instead of linearization methods, they can carry out a realistic error analysis which constitutes the confidence limits for a selected regional stress. Besides, this approach allows objective choices of the selected nodal planes. Because the program of Gephart and Forsyth (1984) need to have chosen nodal planes in order to fit stress tensors, they select the smaller angles which indicate the misfits. As a result, they can select more consistent fault planes with the related stress tensors by the use of their method. On the other hand, when there is no sign to choose the correct nodal plane, the program uses just the misfit for that plane.

$$R = (\sigma_2 - \sigma_1)/(\sigma_3 - \sigma_1) \tag{3.11}$$

The Equation (3.11), showing the ratio of principal stress axes, is used by Gephart and Forsyth (1984). As a result, both the numerator and the denominator give negative results and the actual value of R is positive for the condition of $\sigma_1 \geq \sigma_2 \geq \sigma_3$. Namely, R-value formulas of the methods of Gephart and Forsyth (1984), and Horiuchi *et al.* (1995) give the same results for the same principal axes values.

3.3.5. The Algorithm of Michael (1984)

The relative relationship between the principal stress axes is given in the following equation;

$$R = (\sigma_2 - \sigma_3)/(\sigma_1 - \sigma_3) \tag{3.12}$$

Furthermore, Hardebeck and Hauksson (2001) compared the methods of Gephart and Forsyth (1984), and Gephart (1990a) with the method of Michael (1984, 1987b), as they are used by a majority. They asserted that both techniques obtain stress tensors correctly. On the other hand, the former one gives more accurate results when high quality data is used, while the latter one gives more accurate result when very noisy data is used.

4. RESULTS

In this study, I used 9226 high quality first motion polarity data of 398 earthquakes out of 600 with ML≥2.0 through 105-seismic-station data for the time span 02.09.2006 and 31.03.2011. Data of SBO stations is only used during the analysis of 50 earthquakes in total due to their late installations. Moreover, minimum 10 P wave first motion polarities, toleration of 1 inconsistent station, and maximum 5 km error depth value, in general 3 km, were the criteria for each event to be involved in the stress tensor inversion program.

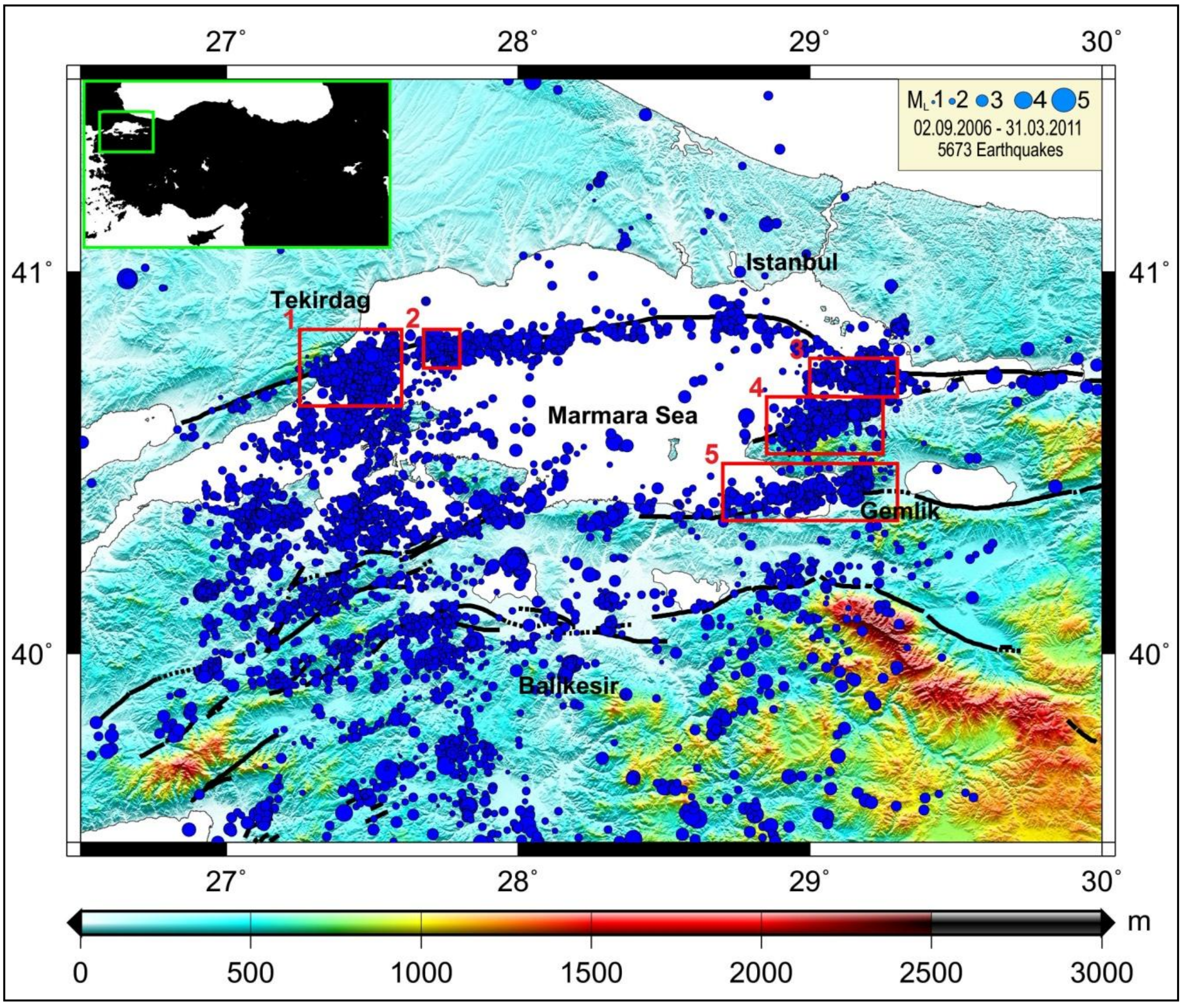

Figure 4.1. Recent earthquake activity of the Marmara Region

Blue dots indicate ML≥1.0 earthquakes during the time interval of 02.09.2006-31.03.2011 in Figure 4.1. Red rectangles show the most outstanding earthquake clusters which are selected to research in this study.

Furthermore, all the earthquakes are eliminated by TUBITAK-MRC and KOERI-NEMC if they are explosions or not. Since the most of the events have a small magnitude, these eliminations are crucial for this study. A cross check was made with the help of an earthquake and explosion catalogue for Yalova and Gemlik Regions between 2006 and 2009 (Deniz, 2010). No event was mistakenly identified as an earthquake. Besides, all the events have not only compressional but also dilatational polarities. Thus, differentiations of TUBITAK and KOERI for explosions and earthquakes confirmed for the Eastern Marmara Region.

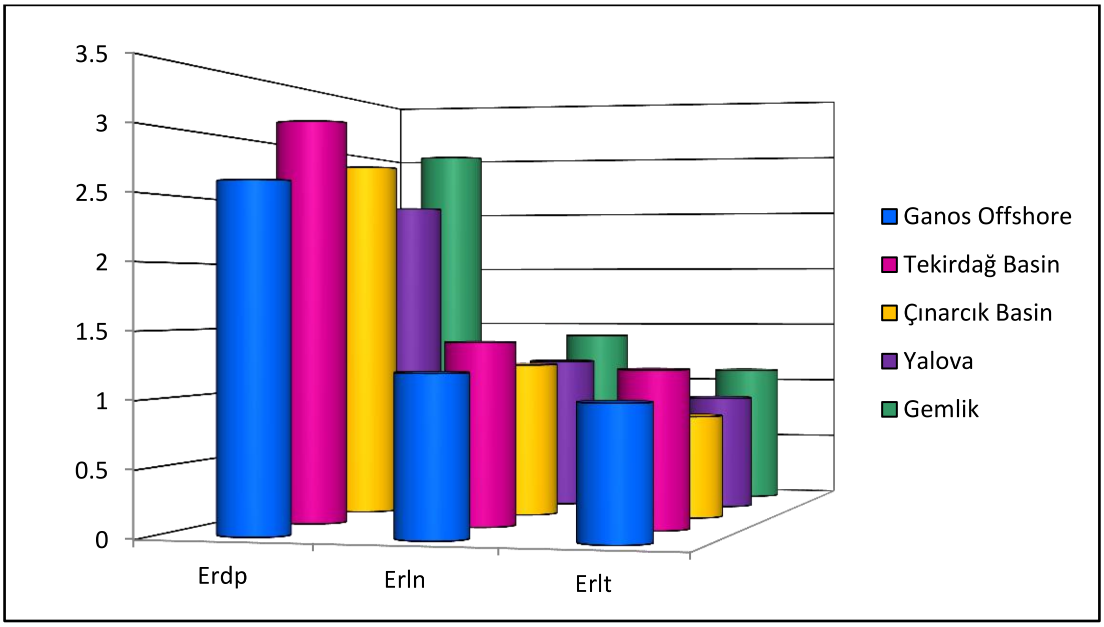

Figure 4.2. Average vertical and horizontal error values of five selected earthquake clusters

Furthermore, Figure 4.2 is the graphical representation of average vertical and horizontal error values for five selected earthquake clusters. The terms Erdp, Erlt, and Erln indicates average depth, latitude and longitude error values in km, respectively. Average Erdp-Erln-Erlt values are; 2.6-1.2-1.0, 3.1-1.4-1.2, 2.8-1.2-0.8, 2.5-1.2-0.9, and 3.0-1.4-1.1 for Ganos Offshore, Tekirdağ Basin, Çınarcık Basin, Yalova and Gemlik clusters, respectively. Even though average vertical error values aren't very small in amount, due to the usage of many arrival times of S phases for every event, it can be argued that these relocations are in very high quality.

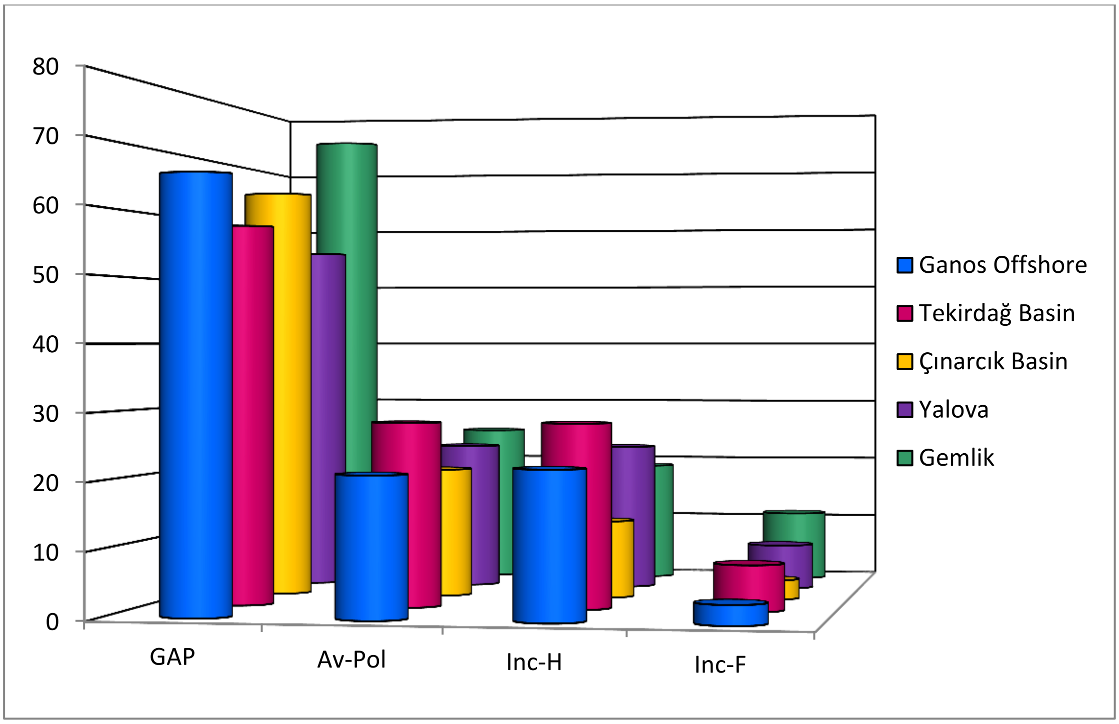

Figure 4.3. Average GAP, number of polarity and inconsistency values of five selected earthquake clusters

As it can be observed from Figure 4.3 average azimuthal GAP in station coverage of the Yalova Cluster is the smallest, while the number of average polarity of the Tekirdağ Basin Cluster is the highest. Inc-H and Inc-F characterize number of total inconsistency of the program of Horiuchi *et al.* (1995) and Focmec for each cluster, respectively. Because of the usage of 5 degree of grid search, the method of Horiuchi has higher misfit values, whereas the program of Focmec signatures much smaller values by using 1 degree of grid search interval on the projection of focal sphere. Moreover, most of the individual focal mechanism solutions obtained by the program of Focmec are more accurate than the ones obtained by the method of Horiuchi *et al.* (1995) concerning individual fault mechanisms. Namely, number of earthquakes with one inconsistent station is much less for the results of Focmec program than the simultaneous results of the program of Horiuchi *et al.* (1995). Average GAP, number of polarity, umber of inconsistency for the method of Horiuchi *et* *al.* (1995) and number of inconsistency for the program of Focmec are; 65, 21, 22, 3; 58, 28, 28, 7; 64, 20, 12, 3; 55, 23, 23, 7; 75, 25, 19, 11 for Ganos Offshore, Tekirdağ Basin, Çınarcık Basin, Yalova Region and Gemlik Region, respectively.

The number of average polarity per earthquake is 23 with average 2.75 km error depth, 0.98 km error latitude, 1.25 km error longitude, and 63° degree GAP values in terms of the analysis of selected five earthquake clusters during this current thesis study. Hence, most of the fault plane solutions have a very good quality. Figure 4.1 shows selected earthquake clusters extending from Ganos offshore to Gemlik as enumerated from 1 to 5. The stress tensor inversion results of these clusters determined by the program of Horiuchi are given in the Table 4.1, as well.

Table 4.1. Stress tensor inversion results of the program of Horiuchi *et al.* (1995)

Cluster Name	Used-All Events	Polarity Counts	$\emptyset - \delta$	$\emptyset - \delta$	$\emptyset - \delta$	R	Misfit Counts
1-Ganos O.	85-144	1768	315-35	141-50	221-7	0.66	22
2-Tekirdağ B.	75-105	2063	293-70	143-30	30-0	0.80	28
3-Çınarcık B.	73-116	1494	123-80	298-10	206-5	0.67	12
4-Yalova	102-125	2336	285-75	115-7	201-2	0.32	23
5-Gemlik	63-100	1565	90-65	285-30	209-12	0.54	19

The results are shown in the Table 4.1 indicate the stress tensor orientation results of the program of Horiuchi *et al.* (1995) which were obtained by the use of 9226 P-wave first motion polarities of 398 earthquakes with ML≥2.0 for selected five earthquake clusters in the Marmara Region. The time interval of the study is 02.09.2006-31.03.2011. Second column of the Table 5.1 denotes the number of used and all events recorded in the related cluster. $\emptyset$ and δ indicates azimuth and plunge of principal stress axes in degree, respectively, and plunge is measured from horizontal. σ_1, σ_2 and σ_3 are maximum, intermediate and minimum principal stress axes, respectively. The ratio among stress axes is R which is calculated using $R = (\sigma_1 - \sigma_2)/(\sigma_1 - \sigma_3)$ relationship and the last column in Table 4.1 indicates total number of misfits for each earthquake cluster.

4.1. The Ganos Offshore Cluster

Ganos Offshore Cluster is chosen at the eastern part of the location of the destructive 9 August 1912 M7.4 Ganos (Şarköy-Mürefte) Earthquake. In spite of the importance of the Ganos Fault, fault structure and seismicity of the Ganos Area still not well-defined (Tüysüz *et al.,* 1998; Okay *et al.,* 1999; Okay *et al.,* 2004; Seeber *et al.,* 2004; Altunel *et al.,* 2004; Armijo *et al.,* 2005; Motagh *et al.,* 2007). Motagh *et al.* (2007) obtained right lateral slip rate of 20-27 mm/yr on a vertical fault with the inversion of geodetic data, even though they thought a strike-slip rate as 18-24 mm/yr concerning viscoelastic rheology and seismic cycle effects of the region. Ganos Area is generally characterized by right lateral strike-slip movements (Başarır, 2011).

Earthquakes of this Ganos Offshore Cluster are close to the epicenter of the 1912 event, since most of the events of this study are stated in the Ganos Bend. During the process of the analysis of the Ganos Offshore Cluster, 85 out of 144 earthquakes were relocated and their fault plane solutions were obtained. The decrease in the number of selected earthquakes was originated from the low magnitude values and inadequate number of polarities. Data from SBO stations was used for the analysis of 4 earthquakes. 1768 P-wave first motion polarities were determined in order to obtain individually and simultaneously determined fault plane solutions, and also orientations of principal stress axes. Thus, the number of average polarity for every earthquake is 21. Also, fault plane solution results of 22 of 85 selected earthquakes depicted 1 inconsistent station for 5˚ grid search with the application of the method of Horiuchi *et al.* (1995), whereas just results of 3 of 85 events gave 1 misfit for 1˚ grid search through the use of the Focmec program. In addition to this, average error values of depth, latitude, longitude and azimuthal GAP in station coverage are; 2.6 km, 1.0 km, 1.2 km and 65˚, respectively. As a result of the application of the method of the Horiuchi *et al.* (1995) azimuth and plunge values of the orientations of maximum, intermediate and minimum axes are; 315˚-35˚, 141˚-50˚, and 221˚-7˚, respectively.

Fault plane solutions of 85 earthquakes, which were simultaneously determined by the program of Horiuchi *et al.* (1995) after the determination of orientations of principal stress axes, are presented in Figure 4.1.1. Blue dots with black circles represent the 59 eliminated earthquakes. Three black rectangles, designated as 1, 2 and 3, indicate focusing areas in order to see the fault plane solutions in detail (Figure 4.1.2, Figure 4.1.3, and Figure 4.1.4). Dark green line shows the profile of the AB cross section that indicates the depth distribution versus fault plane solutions (Figure 4.1.5).

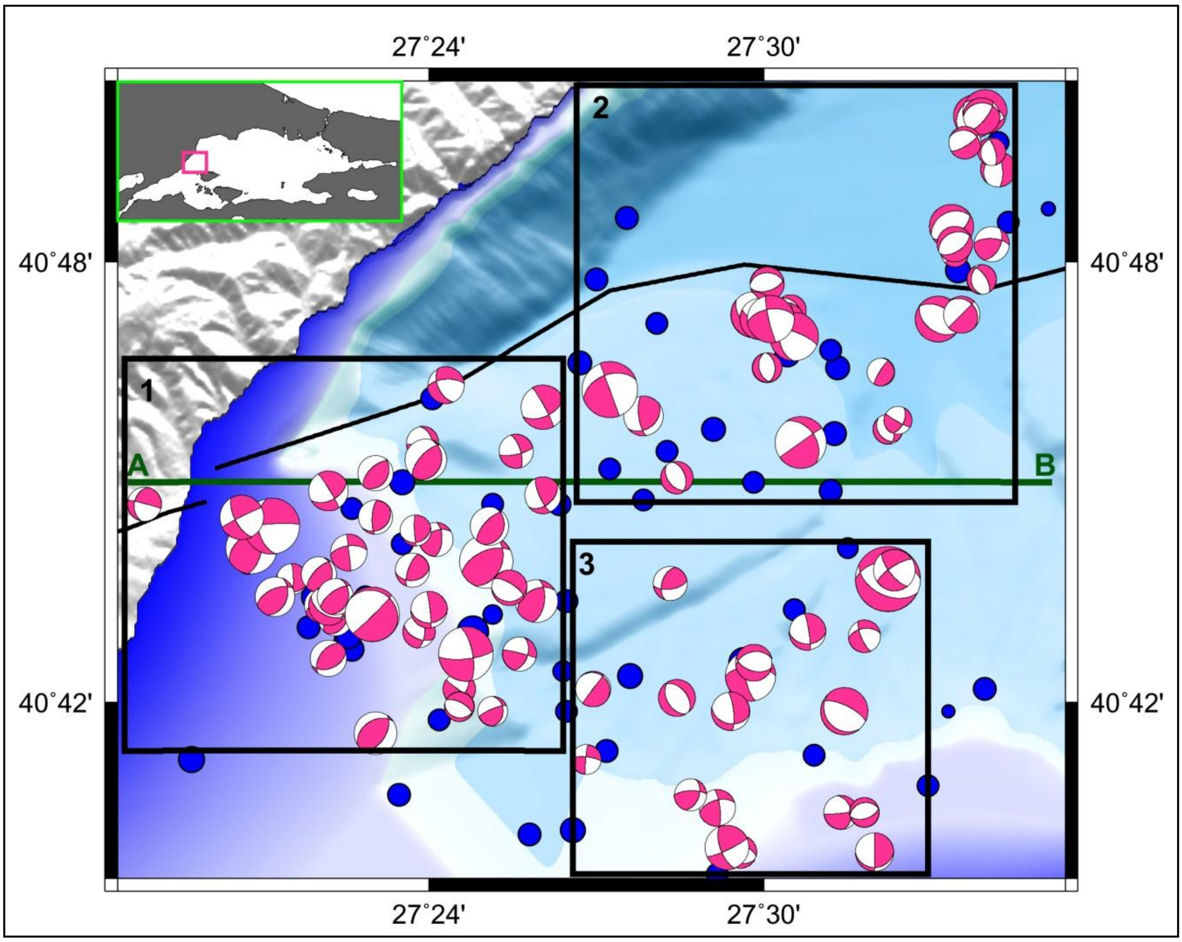

Figure 4.1.1. 85 fault plane solutions in Ganos Offshore Cluster

Figure 4.1.2, Figure 4.1.3, and Figure 4.1.4 are three focus maps of Figure 4.1.1 in order to see fault plane solutions more explicitly. Black dots are the epicenters of related earthquakes, as they are connected to each other by black lines. Each earthquake is enumerated time dependently. As it can be seen from these focus maps, nearly all thrust movements are located in the western part of the Ganos Cluster, and in this area the number of reverse and strike-slip mechanisms are nearly the same; additionally, 3 normal faulting mechanisms are also observed in this part of the cluster (Figure 4.1.2).

I have found that, every thrust fault mechanism in this cluster has NE-SW oriented T (tension) axis, being compatible with the dextral strike-slip regime. Besides, their relocations and fault plane solution parameters including the number of misfits and other error values can be seen from Table B1, in Appendix B. Detailed information of these simultaneous fault plane solutions, determined by the use of the program of Horiuchi *et al.* (1995), are also available under the Ganos Offshore Cluster title in Appendix C. Individual fault plane solutions obtained through FOCMEC software inside of SEISAN program are also taken part under the Ganos Offshore Cluster title in Appendix D. Designation of the earthquakes are the same for each earthquake cluster in maps, and Appendix B, C and D.

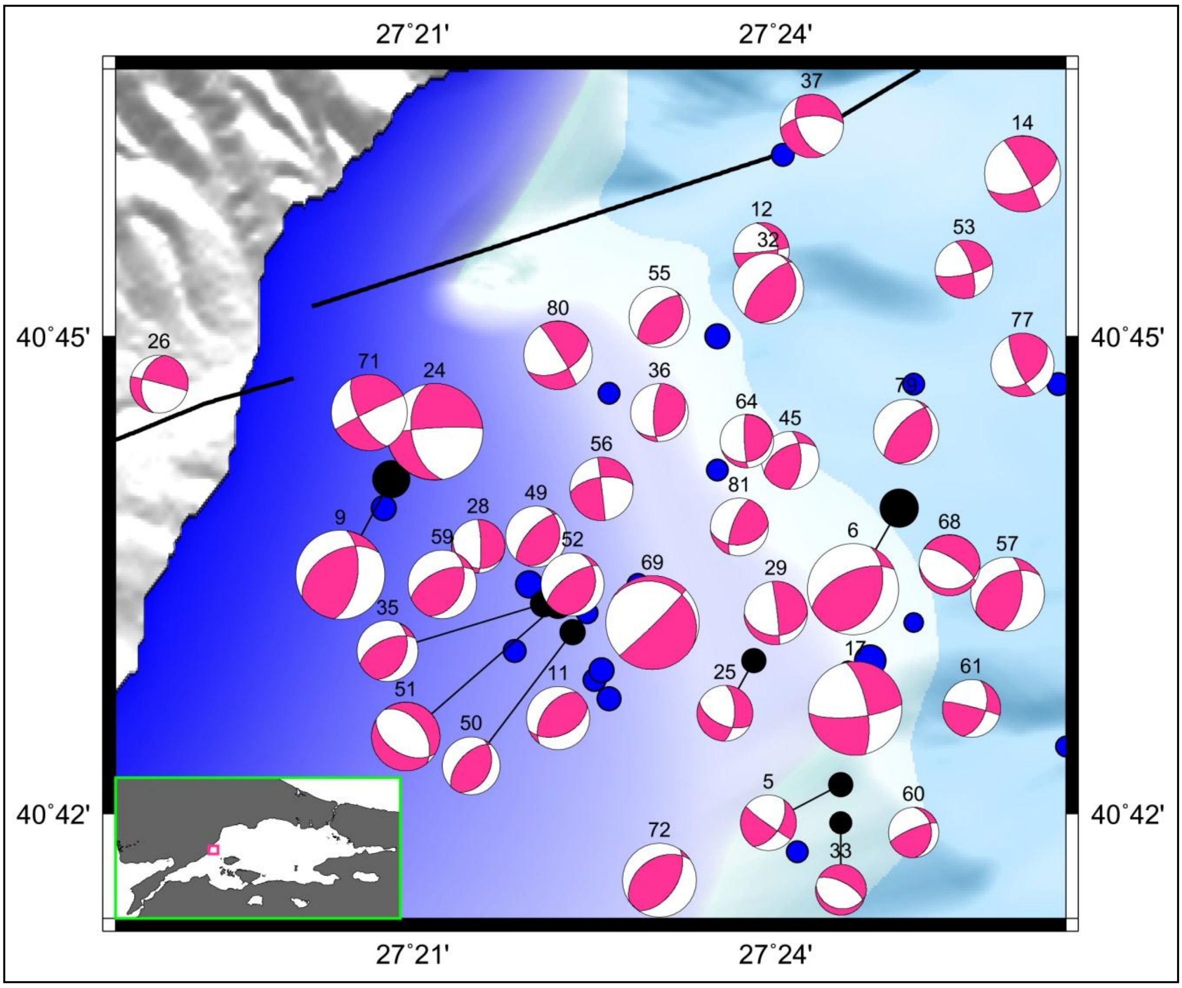

Figure 4.1.2. Focus of the 1st rectangle on the Ganos Offshore Cluster map

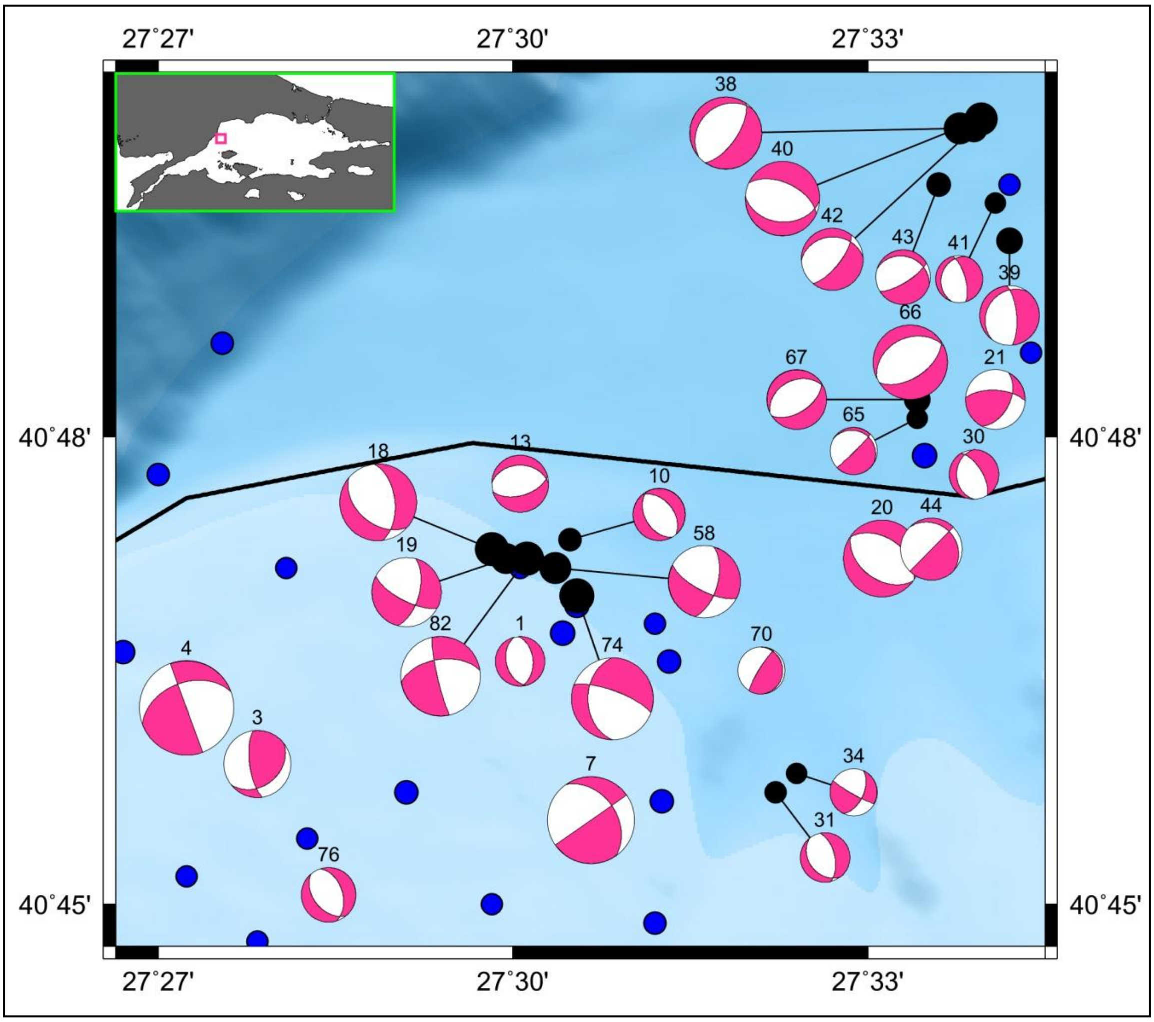

Figure 4.1.3. Focus of the 2nd rectangle on the Ganos Offshore Cluster map

Contrary to western part of the cluster, northeast part included mostly normal fault mechanisms. Some oblique fault systems are also present and very few of them have thrust fault mechanisms (Figure 4.1.3). Furthermore, in the southeast of the cluster right lateral strike-slip and normal fault mechanisms are predominantly obtained, but thrust components are also valid for very few of oblique mechanisms. Moreover, orientations of maximum, intermediate and minimum principal stress axes are shown in Figure 4.1.6 as (a), (b) and (c), respectively. Pink color indicates minimum number of the inconsistency. In Figure 4.1.6 (d) both Sigma-1 and Sigma-3 axes are indicated by pink circles and turquoise triangles, respectively. In graphic (e) number of misfits versus the R-value is shown. The colorful scale bar in the southeast of the Figure 5.1.6 shows the number of inconsistency from minimum to maximum, namely from pink to red color.

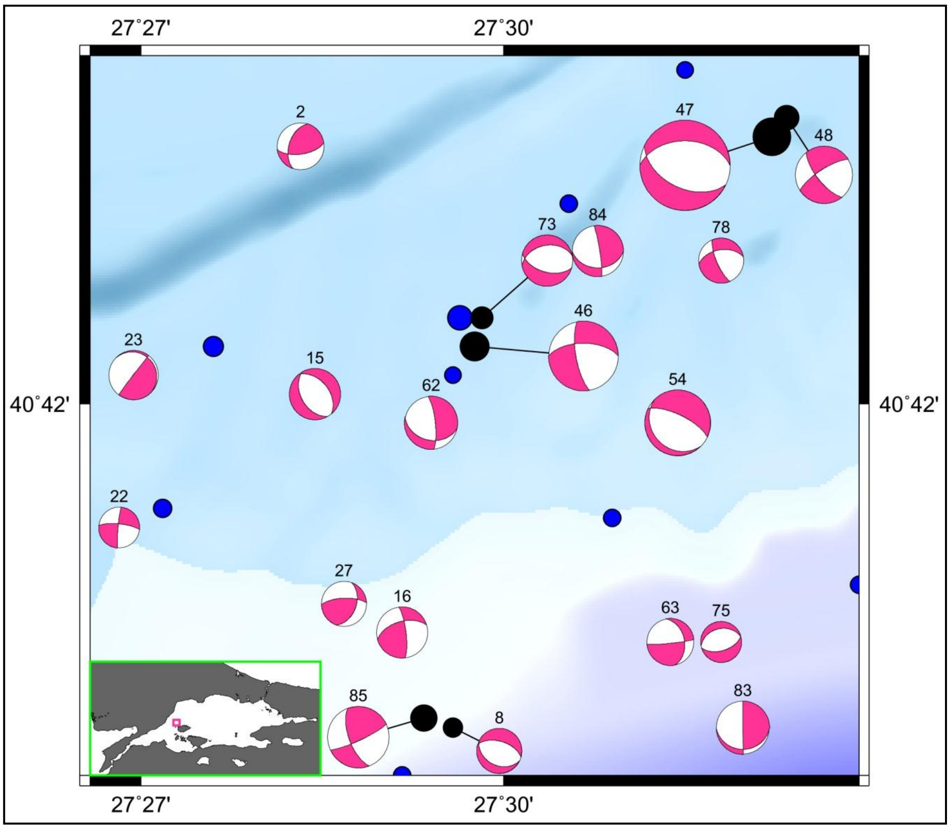

Figure 4.1.4. Focus of the 3rd rectangle on the Ganos Offshore Cluster map

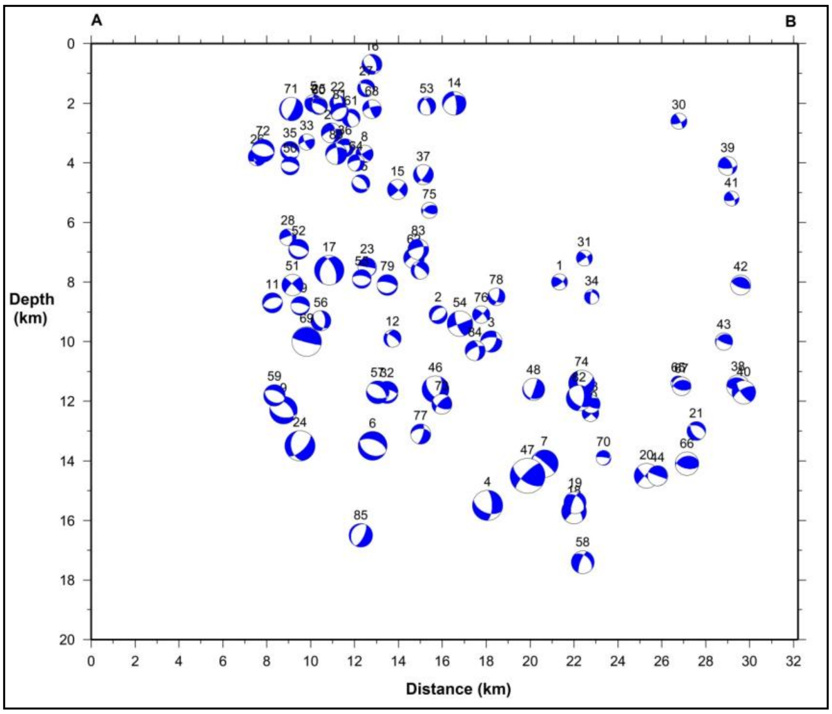

Figure 4.1.5. Depth distribution of fault plane solutions for Ganos Offshore Cluster

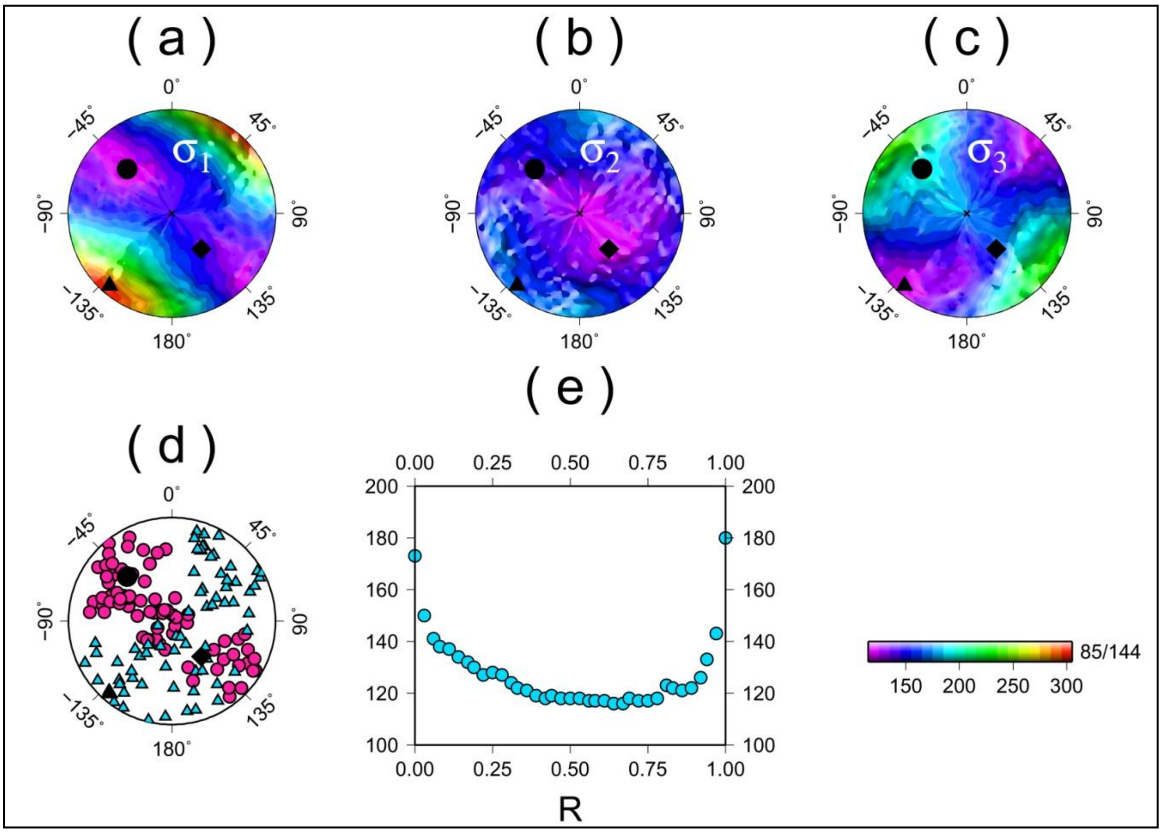

Figure 4.1.6. Stress orientations and Number of misfits versus R-value graphic of the Ganos Offshore Cluster

The cross section of the AB profile in Figure 4.1.5 characterizes a seismogenic zone between 2 km and 14.5 km depth. Fault plane solutions are randomly distributed concerning depth, but most of the events in the Western Ganos Offshore have thrust fault mechanisms, whereas events in the Eastern Ganos Offshore mostly have normal faulting mechanisms. Right lateral strike-slip fault mechanisms can be observed in every part of the cluster, as well. Maximum principal stress axis is N45˚W-S45˚E oriented with 35˚ dipping and minimum principal stress axis is S41˚W-N41˚E oriented with 7˚ dipping, so vertical motion is dominated by intermediate principle axes (Sigma-2) with 50˚ dipping in the Ganos Offshore. As it is also clearly seen from Figure 4.1.6(d), the region has a dextral strike-slip stress regime. The best-selected value of the R equals to 0.66, but the R-value of the Ganos Offshore Cluster has a wide range between 0.42 and 0.78.

4.2. The Tekirdağ Basin Cluster

Tekirdağ Basin is one of the three deepest structures below the Marmara Sea, settling the most western part of it with a large half-graben structure (Okay *et al.,* 2004). Concerning the right lateral slip rate, the Tekirdağ Basin might be younger than the NAFZ (Seeber *et al.,* 2004). Besides, it propagates towards the Ganos Mountain (Le Pichon, 2001). Actually, Tekirdağ Basin Cluster is located at an approximately 4-km-long area (Le Pichon, 2001) between the Tekirdağ and Central Basins. Namely, southern part of the Western High, which is much narrower than the Eastern High, occupies the study region (Le Pichon, 2001).

75 out of 105 earthquakes have been relocated during the analysis of the Tekirdağ Basin, and their individual and simultaneous fault plane solutions, and also stress tensor orientations of maximum, intermediate and minimum principal stress axes have been achieved with the use of 2063 high quality P wave initial motion polarities. The number of average polarity for the each event of the Tekirdağ Basin is 28, and achievement of this high quality, in particular in the sea, is very important to show the data quality of the stations used in this study. Actually, the reason of the obtaining higher quality in the fault plane solutions of the Tekirdağ Cluster is that just 2 of the 75 events occurred in 2006 and 2007, so 73 of them occurred after the beginning of 2008 and they could be analyzed with the help of a better data set. Also, 28 of 75 selected earthquakes give one inconsistent station for 5˚ grid search inside of the method of Horiuchi *et al.* (1995), whereas just 7 of 75 events depict one misfit for 1˚ grid search with the use of the Focmec program.

Average depth error value is 3.1 km with average latitude is 1.2 km, longitude is 1.4 km and azimuthal GAP in station coverage is 58˚. Using the stress tensor inversion method of Horiuchi *et al.* (1995), azimuth and plunge values of orientations of maximum, intermediate and minimum axes were obtained 293˚-70˚, 143˚-30˚, and 30˚-0˚, respectively.

In Figure 4.2.1 fault plane solutions of 75 earthquakes are seen. They were simultaneously determined by the program of Horiuchi *et al.* (1995) after the determination of orientations of principal stress axes. Three black rectangles indicate focusing areas to see the fault plane solutions in detail (Figure 4.2.2, Figure 4.2.3, and Figure 4.2.4). The dark green AB line symbolizes the profile of the cross section analyzed to present depth distribution versus fault plane solution (Figure 4.2.5).

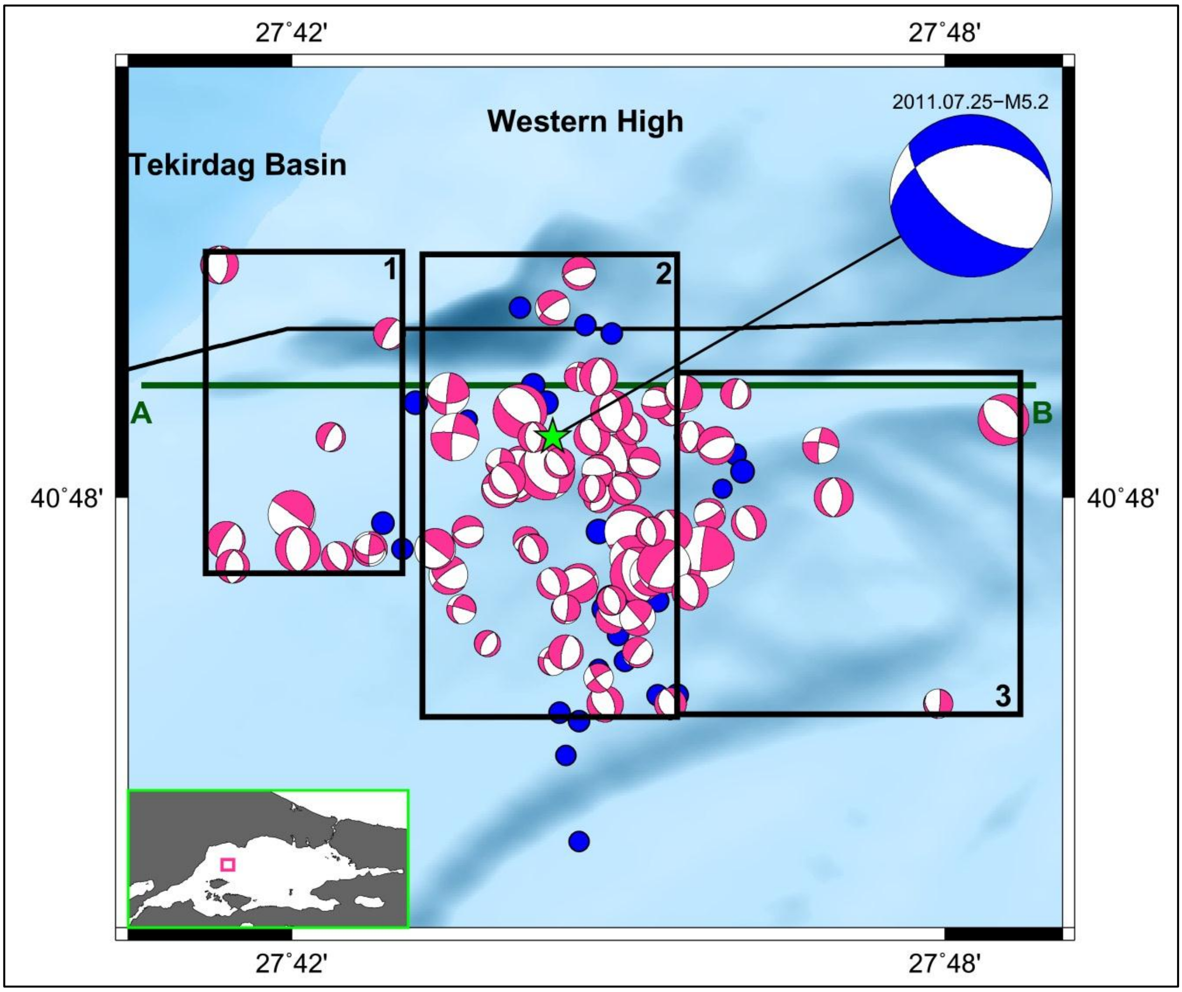

Figure 4.2.1. 75 fault plane solutions and source mechanism of the 25.07.2011 event in Tekirdağ Basin Cluster

Figure 4.2.2, Figure 5.2.3, and Figure 4.2.4 are the three focus maps of Figure 4.2.1, representing fault plane solutions in detail. Earthquakes are in these three maps also enumerated time dependently. Earthquakes of the Western Tekirdağ Basin mostly have normal fault mechanisms while 3 of them have oblique faults systems (Figure 4.2.2). Their location and fault plane solution parameters including number of misfits can be seen from Table B2, in Appendix B. Details of these simultaneous fault plane solutions, obtained by the use of the method of Horiuchi *et al.* (1995), can be seen under the Tekirdağ Basin

Cluster title in Appendix C, as well. Besides, individual fault plane solutions obtained by the use of FOCMEC software inside of SEISAN program are located under the Tekirdağ Basin Cluster title in Appendix D. Each earthquake has the same number in maps, and Appendix B, C and D.

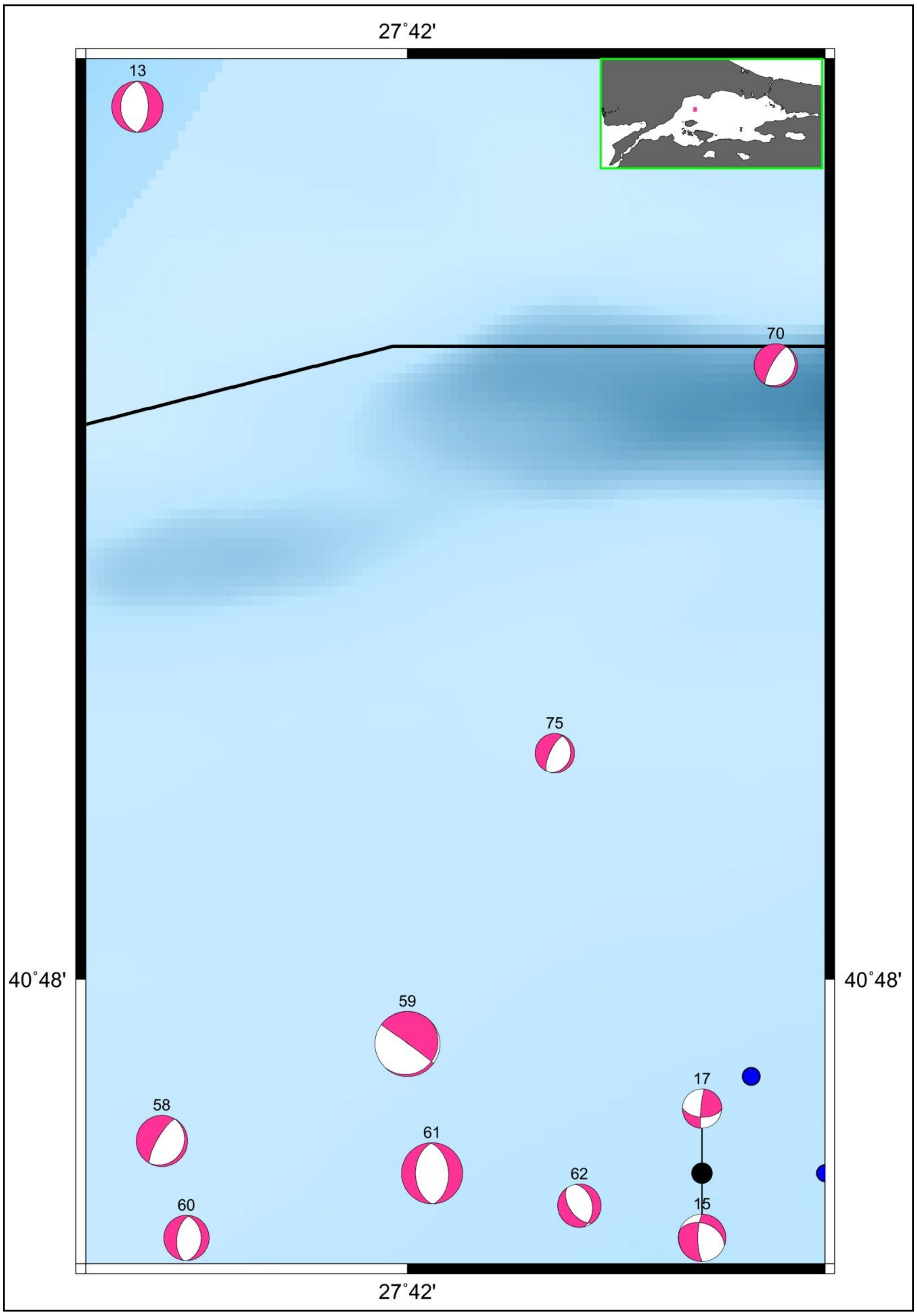

Figure 4.2.2. Focus of the 1st rectangle on the Tekirdağ Basin Cluster map

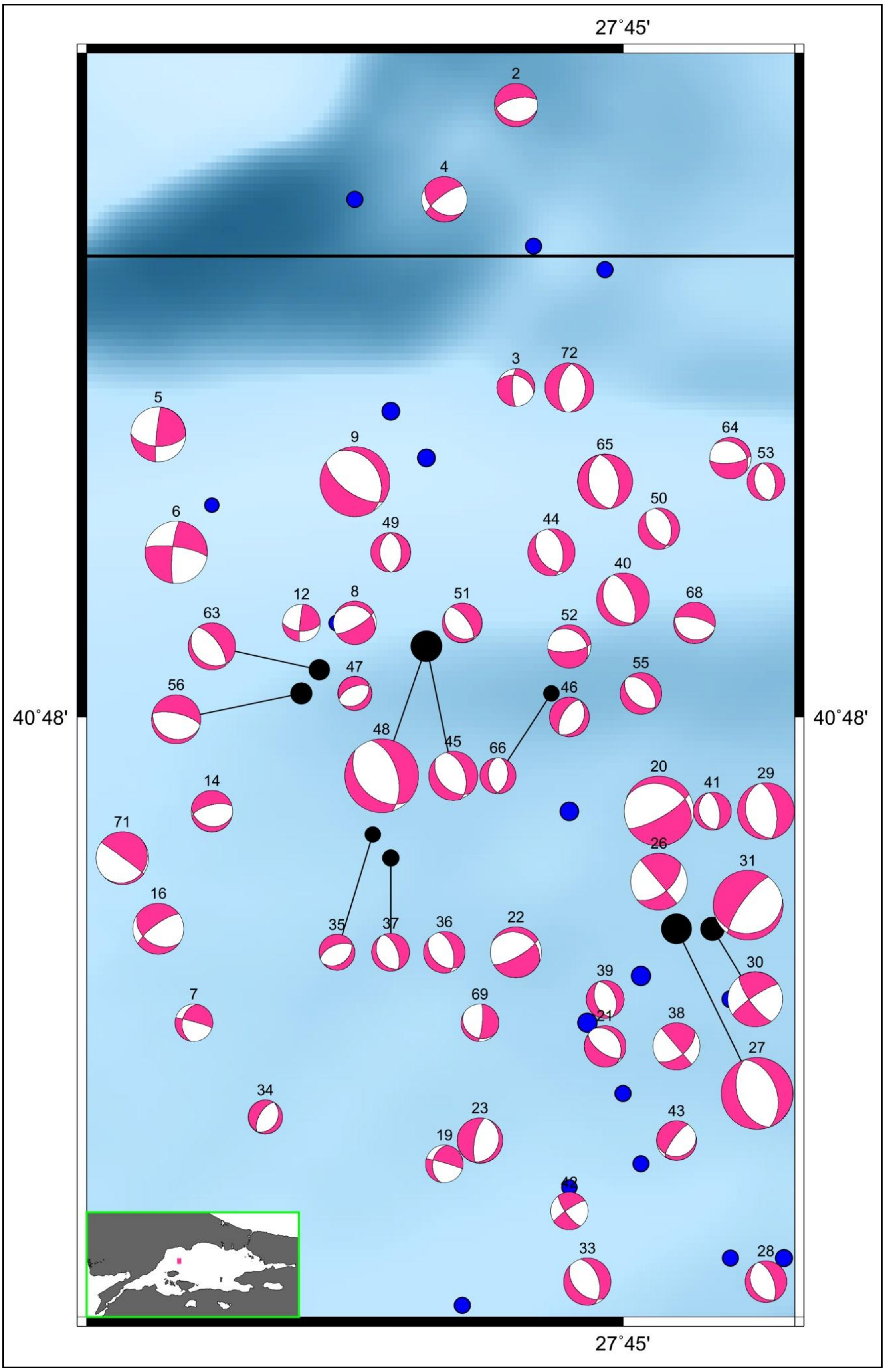

Figure 4.2.3. Focus of the 2nd rectangle on the Tekirdağ Basin Cluster map

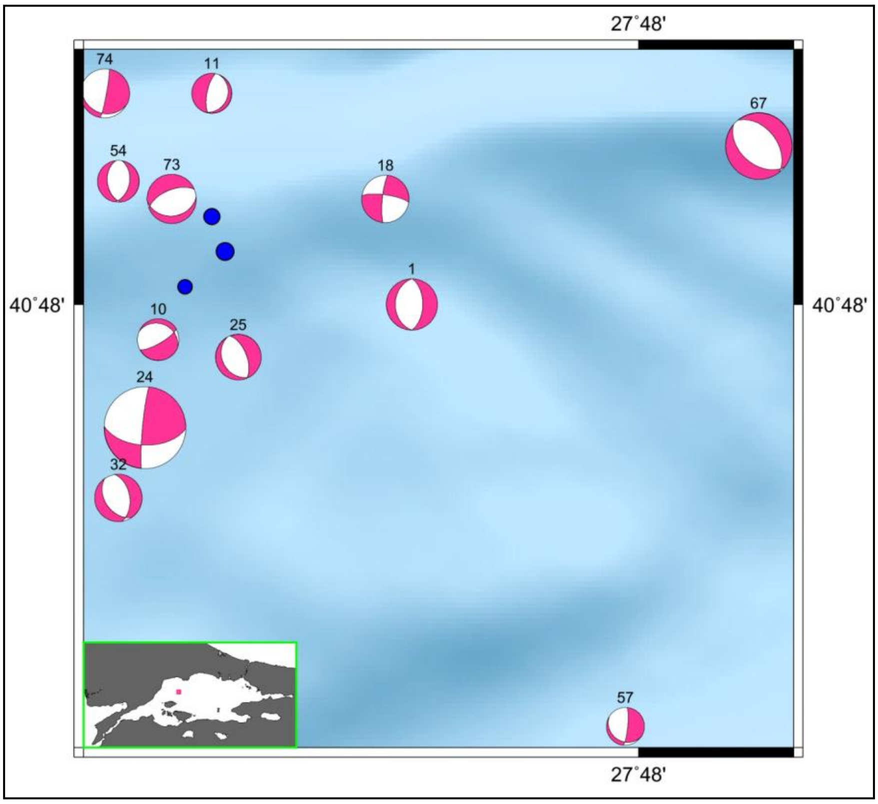

Figure 4.2.4. Focus of the 3rd rectangle on the Tekirdağ Basin Cluster map

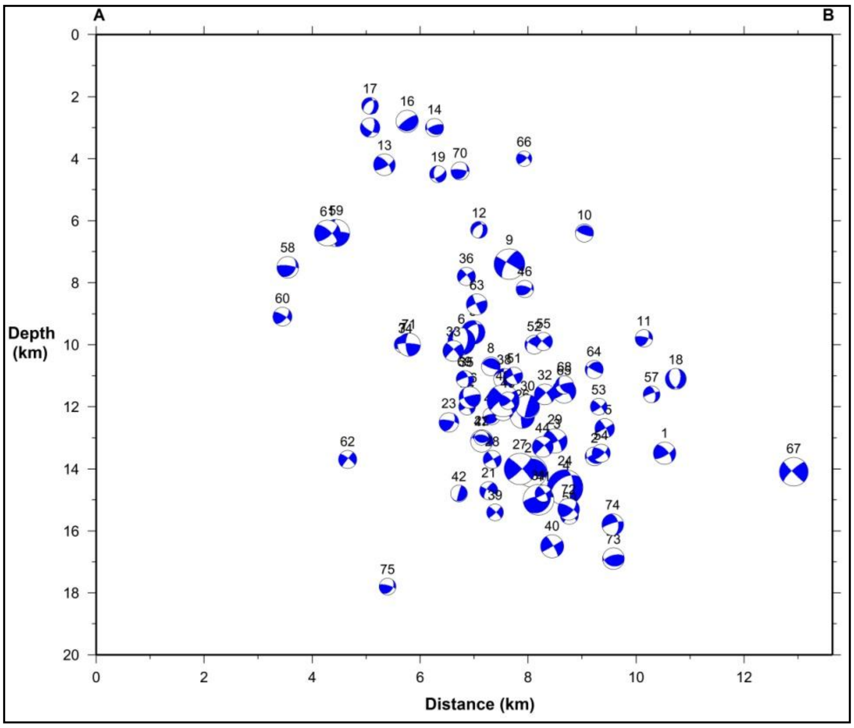

Figure 4.2.5. Depth distribution of fault plane solutions for Tekirdağ Basin Cluster

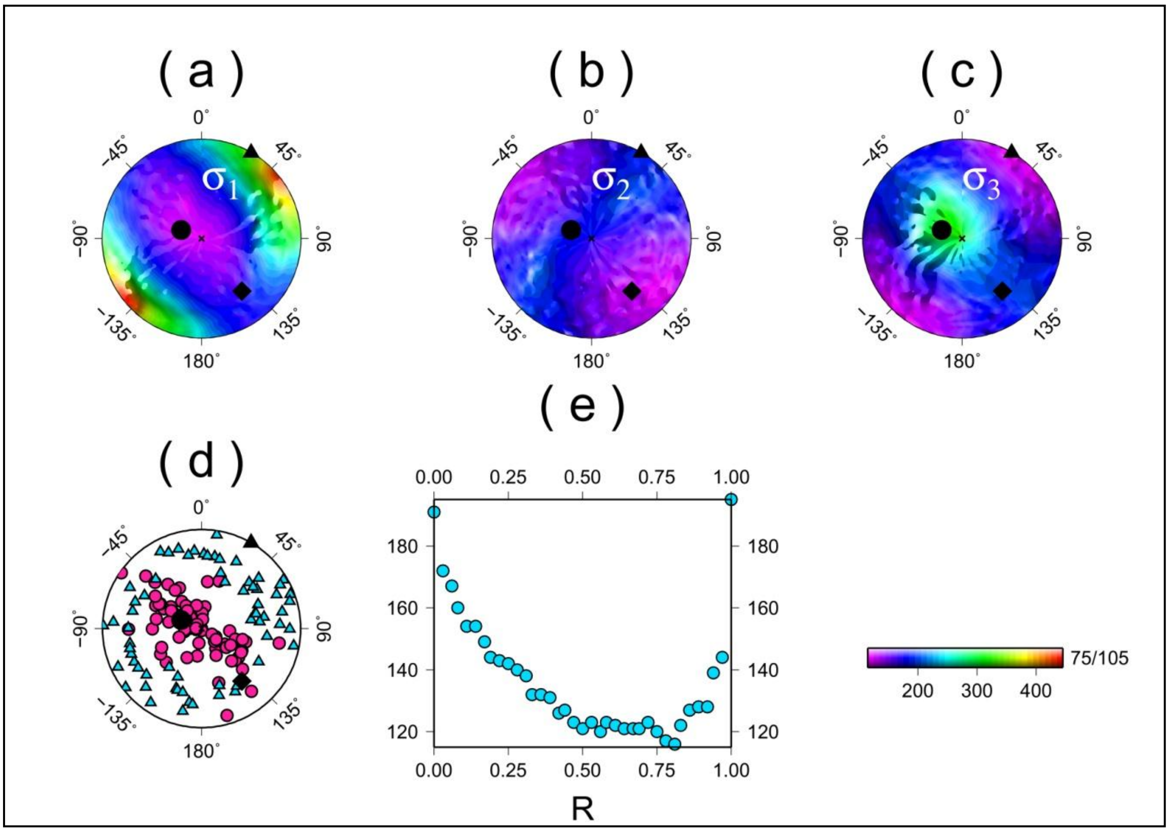

Figure 4.2.6. Stress orientations and graphic of R-value of the Tekirdağ Basin Cluster

Most of the earthquakes of the Tekirdağ Basin are located in the middle of the cluster (Figure 4.2.3), and they have nearly pure normal fault mechanisms. Besides, some strike-slip and oblique fault mechanisms also exist. In the eastern part of the Tekirdağ Basin Cluster, 9 normal, 2 strike-slip and one oblique fault mechanisms are obtained (Figure 4.2.4). Graphic of the depth distribution of the events, recorded in Tekirdağ Basin Cluster, versus the distance is shown in Figure 4.2.5, representing the cross section of the profile AB. This depth distribution points out a seismogenic zone between 3 km and 15.5 km depth even though most of the events are located between 10 km and 15.5 km depth interval. Actually, relatively bigger earthquakes are also located between 14 km and 15 km depth. Furthermore, as it can be seen from Figure 4.2.5, focal mechanisms of earthquakes are randomly distributed, so it is not easy to classify events in terms of depth.

Orientations of maximum, intermediate and minimum principal stress axes are shown in Figure 4.2.6 as (a), (b) and (c), respectively. Maximum principal stress axis (Sigma-1) is NW-SE oriented (Figure 4.2.6(d)) with 70˚ dipping. Minimum principal stress axis (Sigma-3) is exactly horizontal with 0˚ dipping. Stress tensor inversion results of the Tekirdağ Basin Cluster point out an R-value of 0.80. In the Tekirdağ Basin Cluster 3 of the 75 earthquakes have thrust faulting components, but one of them is the biggest earthquake of this cluster having a local magnitude value of 4.3 and it has as right lateral strike-slip faulting mechanism (Earthquake with the number of 24, Figure 4.2.4).

4.2.1. 25 July 2011, ML5.2 Marmara Sea Earthquake

The ML5.2 Marmara Sea Earthquake is located in the Tekirdağ Basin where an earthquake activity is present (Figure 4.2.1, Tekirdağ Basin Cluster). No event with M≥5.0 was recorded in the Marmara Region between 1989 and 1999 (Durand, 2010). Nevertheless, after the 17 August 1999 İzmit event 3 earthquakes occurred in one year in the different parts of the Marmara Region with M≥5.0 and one of these was located in Tekirdağ Basin, namely, very close to the epicenter of the 2011 event (Durand, 2010).

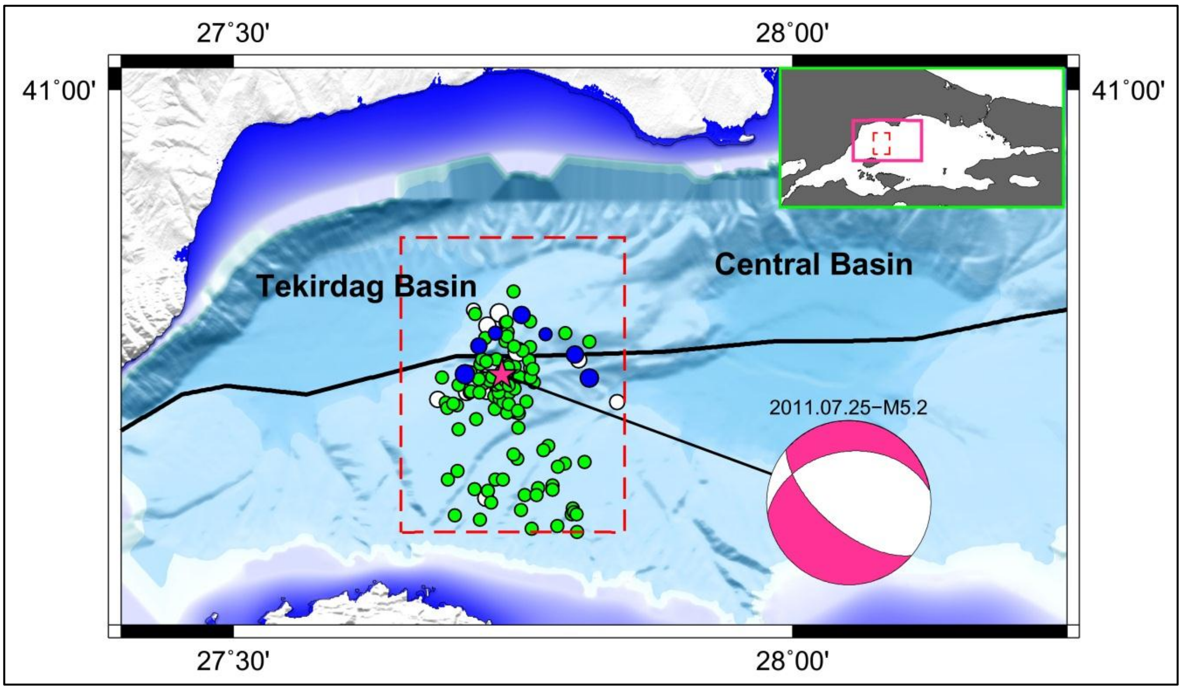

Figure 4.2.1.1. Aftershock distribution of 25.07.2011 ML5.2 Marmara Sea Earthquake

In Figure 4.2.1.1 blue dots indicate 7 small earthquakes occurred during the last 7 months before the 25.07.20011 main shock, and one of them with Md=2.2 was originated just 5 days before the 25 July 2011 earthquake. 104 green dots characterize aftershock activity of the event took place in 49 days after the main shock which is symbolized with a pink star. 12 white dots show the earthquakes recorded between September 2011 and December 2011.

Moreover, a quiescence process was observed before the 25.07.2011 M5.2 Marmara Sea earthquake. No earthquake has been relocated for the time span of 23.12.2010 and 31.03.2011 (Appendix B). During the analysis of this study, all the clusters except for the Tekirdağ Basin Cluster include visible earthquake activities in the first 3 months of 2011. Actually, even after earthquake catalogues of both TUBITAK-MRC and KOERI were checked, only one small event was found in the catalogue of TUBITAK, whereas 2 small events were observed in the catalogue of KOERI, being close to the epicenter of this event for the first three months of 2011. Besides, the whole 2011 earthquake catalogue of KOERI has also examined for the red rectangle area in Figure 4.2.1.1, and just 7 small earthquakes have been observed in the region during the first seven months of 2011. Furthermore, 104 earthquakes were recorded after the 25 July main shock until 11.09.2011. A very clear decrease in aftershock activity was observed after 11.09.2011, and it may be stated that the aftershock activity was ended in 49 days.

The occurrence date of this 2011 earthquake is out of the time interval of this study, but the analysis of this earthquake also gave the opportunity of comparison of this moderate size earthquake with the general stress tensor inversion results of the Tekirdağ Basin Cluster which included relatively smaller events. Moreover, relocations and possible fault plane solutions of the ML5.2 Marmara Sea Earthquake were done twice in order to evaluate the contribution of SBO data to the analysis of earthquakes in the Marmara Sea. First, only data of land stations were used to obtain hypocentral parameters and the best fitted focal mechanism solutions; then, data of SBO stations was added to land stations (two stations for the relocation and four stations for the focal mechanism estimation) in order to analyze the contribution of the data from SBO stations to location and quality of possible fault plane solutions.

In the case of land stations data only, horizontal error value (ERH) is a slightly better (1.0 km) rather than the case of all stations (0.9). However, this problem most probably originated from the fact that the sea bottom seismometers are located in mud at the bottom of the Marmara Sea, so all the P and S phases arrive the stations lately. So, the little increase in location error may come from late arrival of P and S phases. That is why most of the S phases weren’t included during the relocations of earthquake clusters. On the other hand, number of inconsistent polarities decreased from 6 to 5 when SBO data was used for this earthquake, and for the 1 degree of grid search interval through the FOCMEC software gave 46 possible fault plane solutions for the case of all stations, whereas the solutions were not stable for 1-2 degree of grid search when SBO data wasn’t used. Thus, for the case of land stations 3 degree of grid search interval is used (Table 4.2.1.1), as it gave 55 solutions. Azimuthal GAP in station coverage was also better when data of sea bottom observation system is used, since it decreased from 46˚ to 42˚.

In summary, adding SBO stations for the relocation process of this ML5.2 Earthquake did not lead to significant increase in horizontal and vertical error values. On the other hand, they caused increase in residuals and also horizontal and vertical errors during the analysis of small events. Furthermore, due to the fact that data from 4 SBO stations for this event were used, an increase in the quality of fault plane solutions observed although the general stress regime seems the same.

The ML5.2 Earthquake has an extensional stress feature which coincides with the stress tensor inversion results of the Tekirdağ Basin Cluster. Especially, orientations of minimum principle stress axes are very close to each other (Table 4.2.1.2 and Table 4.1).

Figure 4.2.1.2 represents possible focal mechanism solutions when only land stations are used, while Figure 4.2.1.3 denotes possible solutions when both sea and land stations are used. Besides, three component waveform data of four SBO stations are seen in Figure 4.2.1.4.

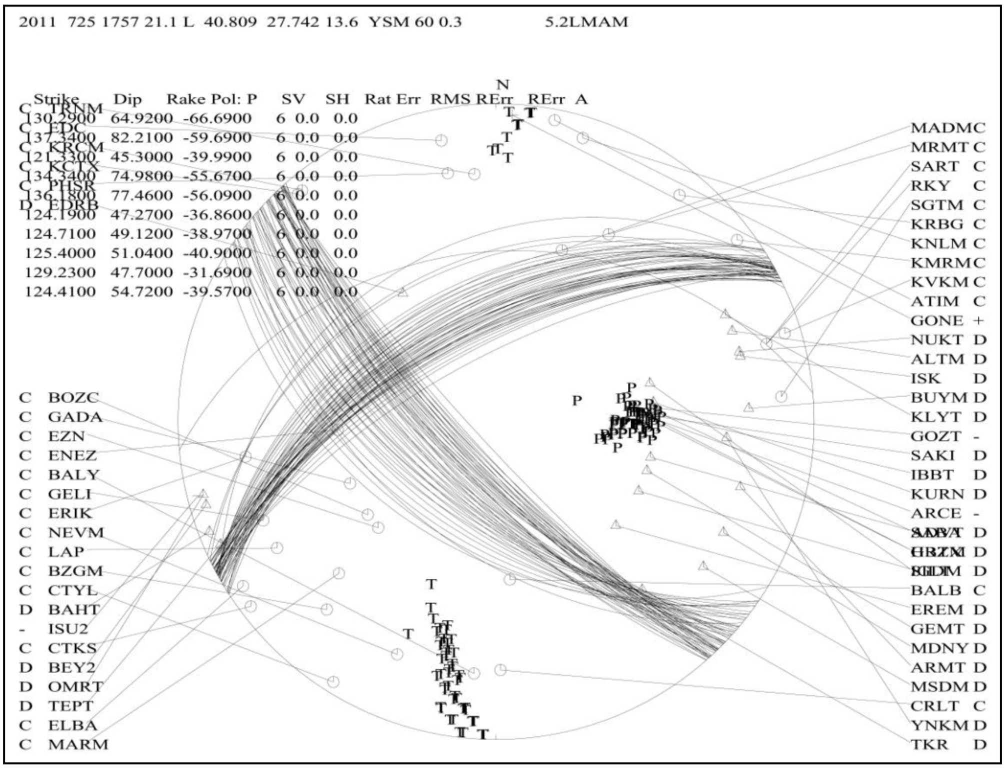

Figure 4.2.1.2. Output of the FOCMEC program with the use of only land stations

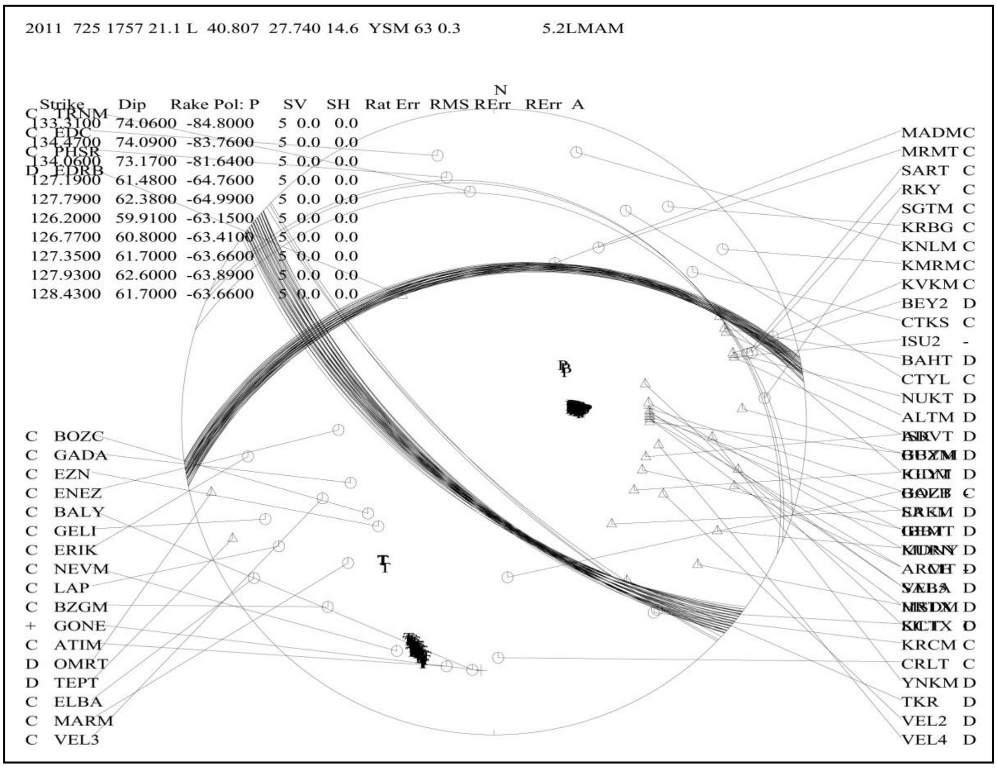

Figure 4.2.1.3. Output of the FOCMEC program with the use of SBO and land stations

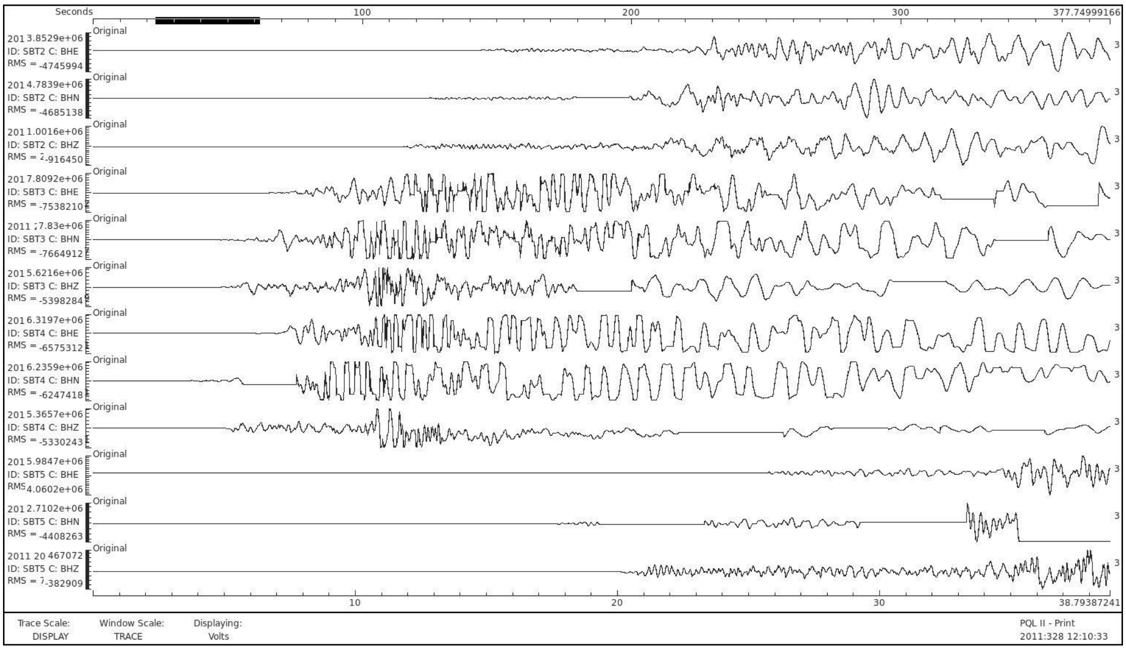

Figure 4.2.1.4. PQL-II screen-shot from the SBO stations three component data

Table 4.2.1.1. Detailed information of the relocation and fault plane solutions

Quality	4 SBO data used	SBO data not used
Number of Polarities	65	61
Number of Misfits	5	6
Degree of Grid Search Interval	1	3
Number of Acceptable Solutions	46	55
Azimuthal GAP	42	46
ERH	1.0	0.9
ERZ	1.6	1.6

Table 4.2.1.2. Fault plane solution information of ML5.2 Marmara Sea Earthquake

Focmec results of 25.07.2011 ML5.2 Marmara Sea Earthquake	
N1-Strike/Dip/Rake	130/63/-63
N2-Strike/Dip/Rake	262/37/-132
P (Trend, Plunge)	83, 62
T (Trend, Plunge)	201, 14

4.3. The Çınarcık Basin Cluster

Çınarcık Basin is bounded by two conjugate anomalous normal faults (Laigle *et al.*, 2008). The basin is of 50 km length, about 20 km width and 1250 m depth (Okay *et al.*, 2000). Eastern part of the Çınarcık Basin, the study area, is located at the northern offshore of the Armutlu Peninsula. Çınarcık Basin is the most complex area of the main branch of the NAFZ in the Marmara Sea (Le Pichon *et al.*, 2001). Northern margin of the Çınarcık Basin is more regular and steep comparing with the southern part (Le Pichon *et al.*, 2001). Thrust faults and folds exist in the Western Çınarcık Basin with notable highly complex structure, due to the formation of the boundary between the Çınarcık Basin and Central High (Le Pichon *et al.*, 2001).

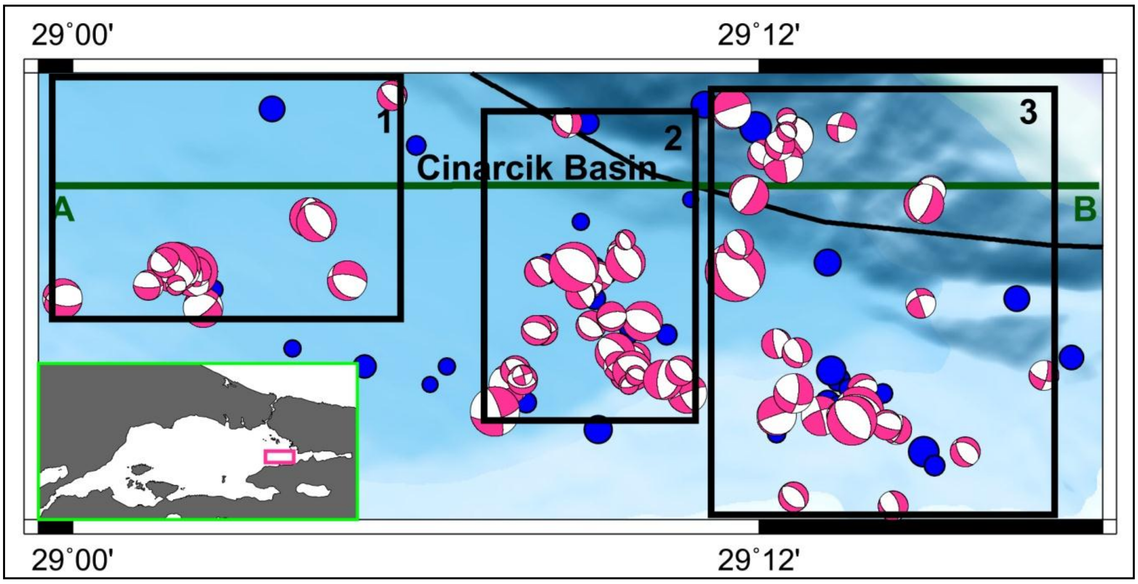

Figure 4.3.1. 73 fault plane solutions of the Çınarcık Basin Cluster

During the process of the analysis of the Çınarcık Basin Cluster, 73 out of 116 earthquakes have been relocated and data of SBO stations is used for the analysis of 22 events. Also, individual and simultaneous fault plane solutions and also stress tensor orientations of principal stress with the help of 1494 high quality P-wave first motion polarities have been obtained. Hence, number of average polarity for each earthquake in the Çınarcık Basin Cluster is 20. 12 out of 73 selected earthquakes depict one inconsistent station for 5˚ grid search using the method of Horiuchi *et al.* (1995), while just 3 of 73 events give one misfit for 1˚ grid search through the use of the Focmec program. Average depth error value is 2.8 km with average latitude is 0.8 km, longitude is 1.2 km and azimuthal GAP in station coverage is 64˚. Azimuth and plunge values of orientations of maximum, intermediate and minimum axes are; 123˚-80˚, 298˚-10˚, and 206˚-5˚, respectively.

In Figure 4.3.1 fault plane solutions of 73 earthquakes simultaneously determined by the program of Horiuchi *et al.* (1995) before and after the determination of orientations of the principal stress axes are provided. Three black rectangles indicate focusing areas in order to see the fault plane solutions in detail (Figure 4.3.2, Figure 4.3.3, and Figure 4.3.4). Dark green AB line shows the cross section profile of the depth distribution versus fault plane solution (Figure 4.3.5).

Figure 4.3.2, Figure 4.3.3, and Figure 4.3.4 are three focus maps of Figure 4.3.1 to present fault plane solutions accurately. Earthquakes are enumerated time dependently. Their location and fault plane solution parameters including number of misfits can be seen from Table B3, in Appendix B. Detailed information of these simultaneous fault plane solutions, determined by the use of the program of Horiuchi *et al.* (1995), are also available under the Yalova Cluster part in Appendix C. Additionally, individual fault plane solutions obtained through FOCMEC software inside of SEISAN program are located under the Yalova Cluster title in Appendix D. Numbering of the earthquakes are the same in the maps of this cluster, and Appendix B, C and D.

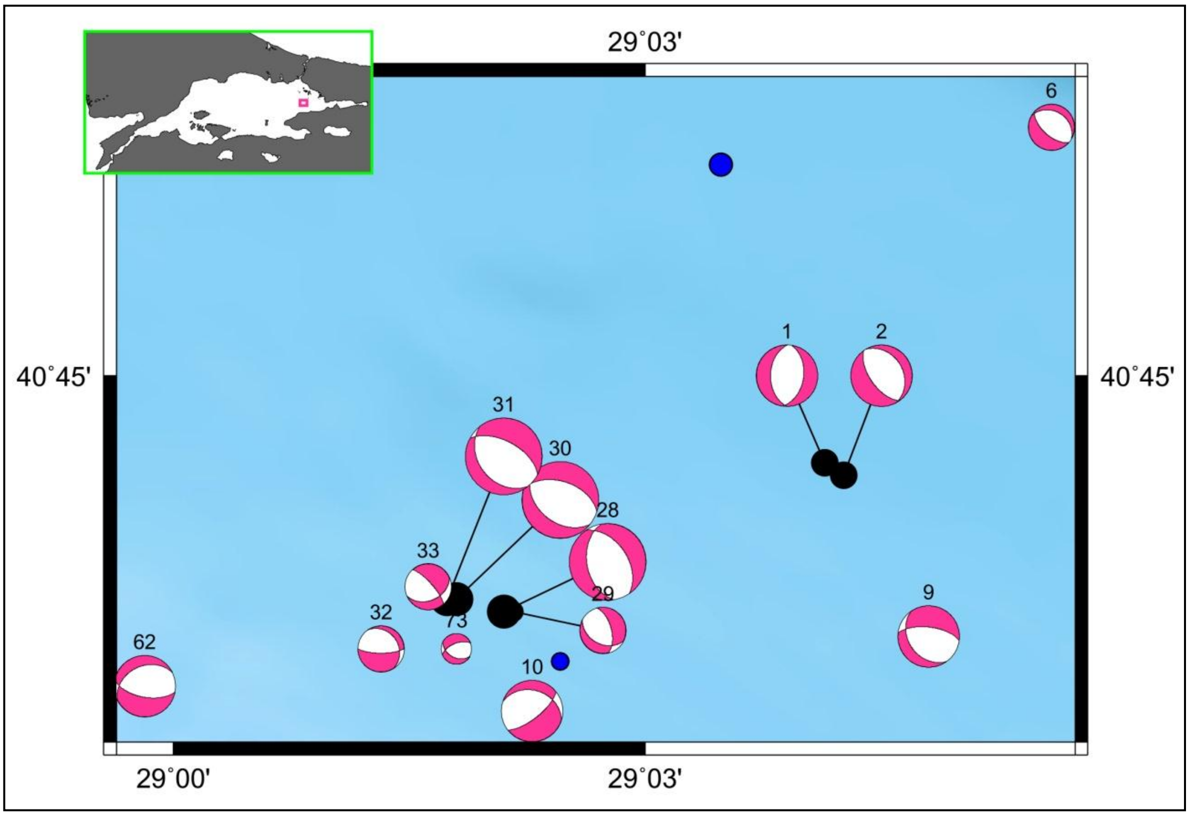

Figure 4.3.2. Focus of the 1st rectangle on the Çınarcık Basin Cluster map

As it can be seen from Figure 4.3.2 Western Çınarcık Basin Cluster has mostly NW-SE oriented normal faulting mechanisms. Besides, 7 of 13 fault plane solutions have small right lateral components. In the middle of the Çınarcık Basin Cluster again most of the events are NW-SE oriented having nearly pure right lateral components (Figure 4.3.3). On the other hand, 3 nearly pure right lateral strike-slip fault mechanisms and one oblique fault system with right lateral orientation are also clearly visible in the southern part of the cluster. Furthermore, in the eastern part of the cluster most of the events have normal fault mechanisms, as well. Nevertheless, dextral strike-slip motions can be seen in the north and east parts of the map seen in Figure 4.3.4. One is located at the eastern starting point of the Çınarcık Basin, and other 3 strike-slip motions are seen in the northern part of the basin. Additionally, other 2 strike-slip motions can be evaluated close to the south.

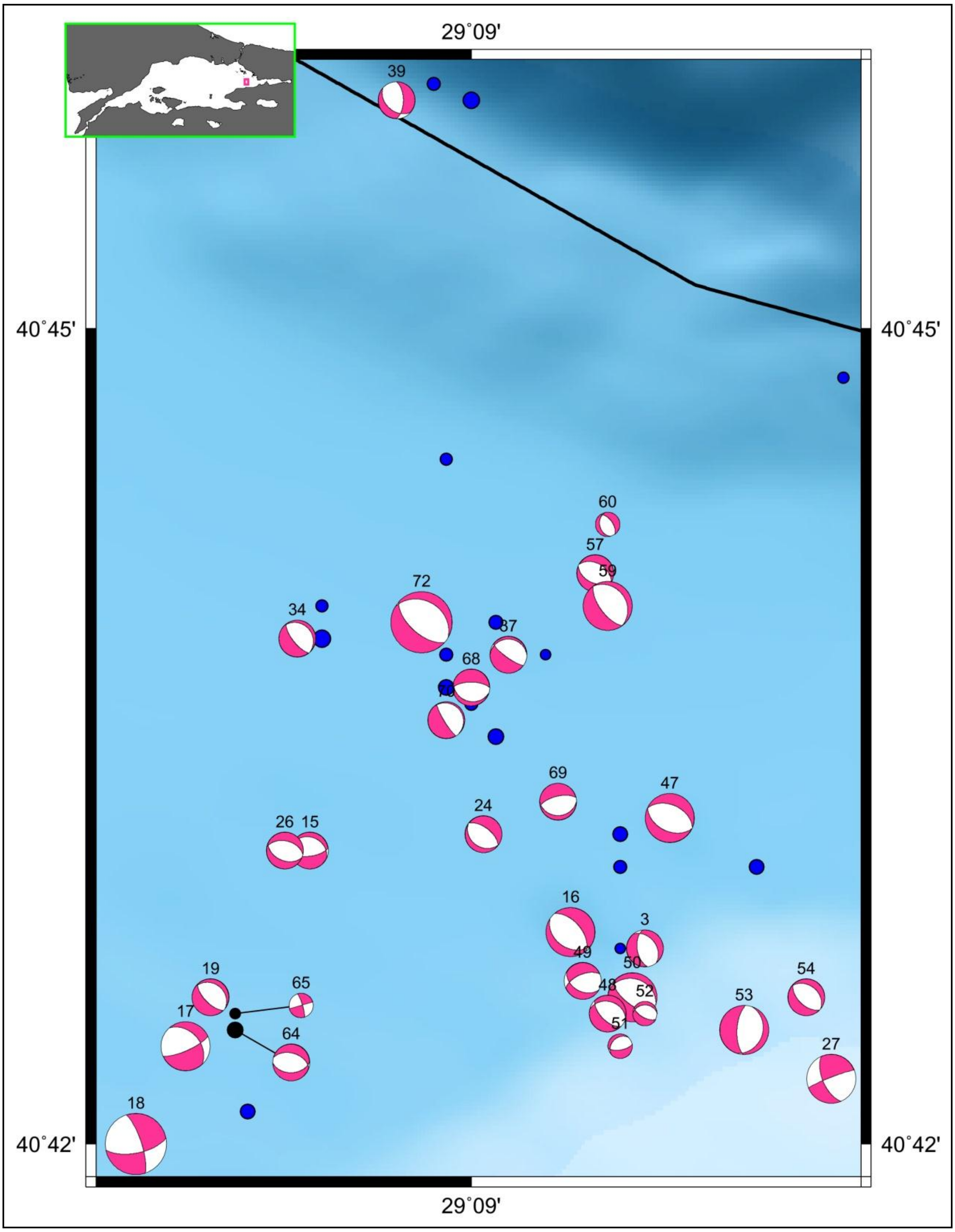

Figure 4.3.3. Focus of the 2nd rectangle on the Çınarcık Basin Cluster map

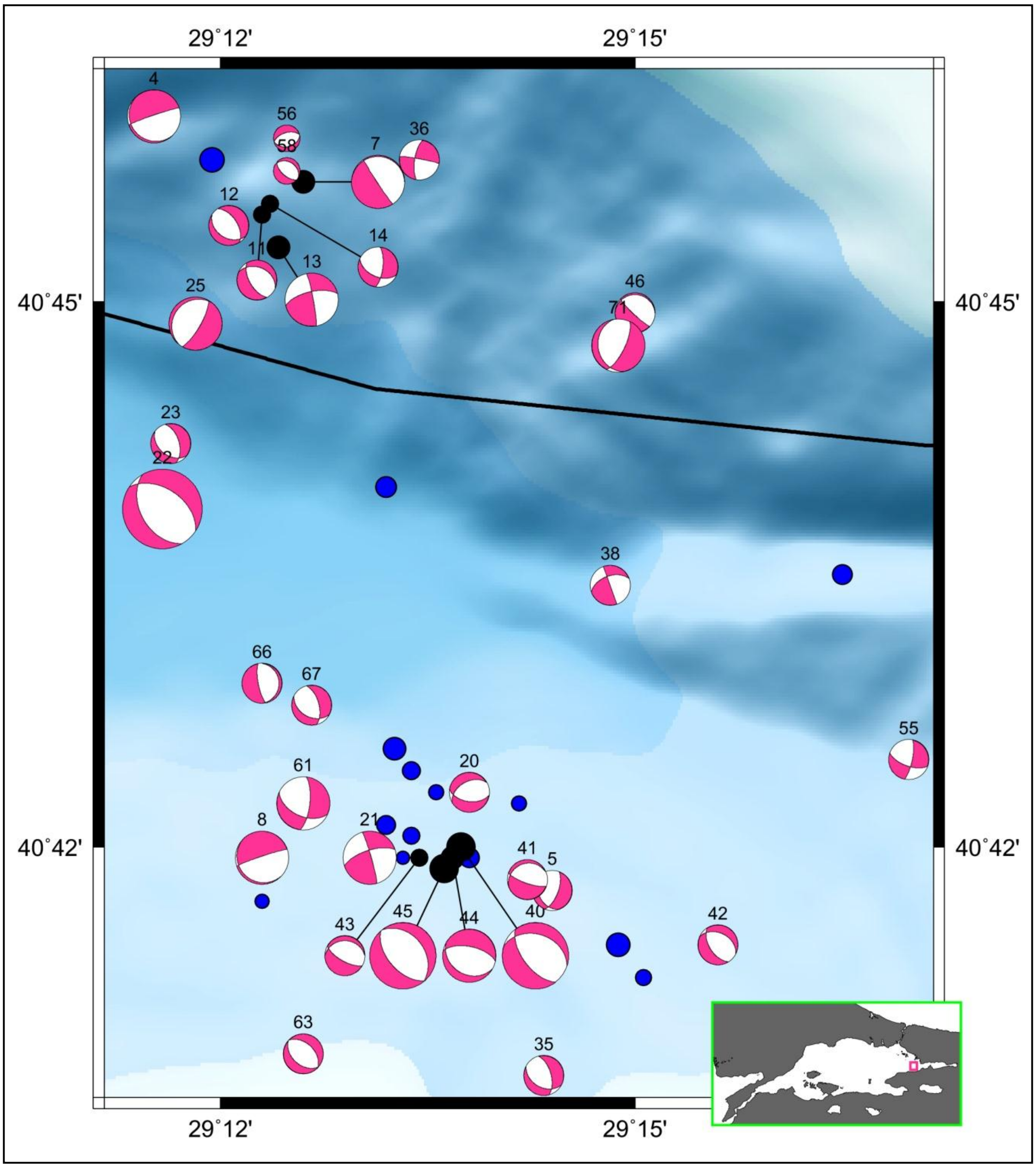

Figure 4.3.4. Focus of the 3rd rectangle on the Çınarcık Basin Cluster map

Orientations of maximum, intermediate and minimum principal stress axes are represented in Figure 4.3.6 as (a), (b) and (c), respectively. Pink color shows the number of minimum misfit. In Figure 4.3.6 (d) both Sigma-1 and Sigma-3 axes are indicated by pink circles and turquoise triangles, respectively. In graphic (e) number of inconsistency versus R-value is characterized and the best value of R equals to 0.67. The colorful scale bar in the southeast of the Figure 4.3.6 shows the number of inconsistency from minimum to maximum, namely from pink to red color.

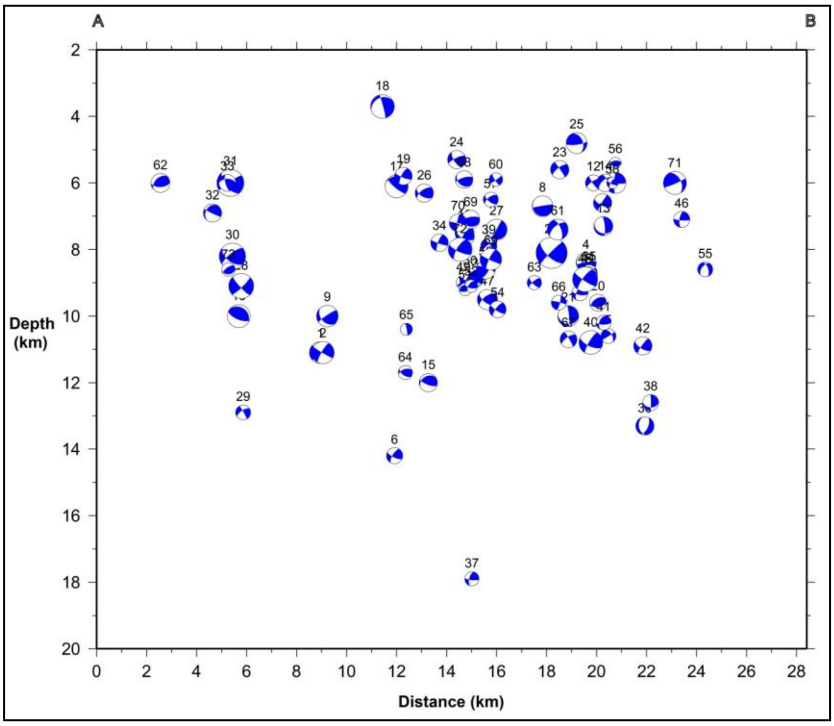

Figure 4.3.5. Depth distribution of fault plane solutions for Çınarcık Basin Cluster

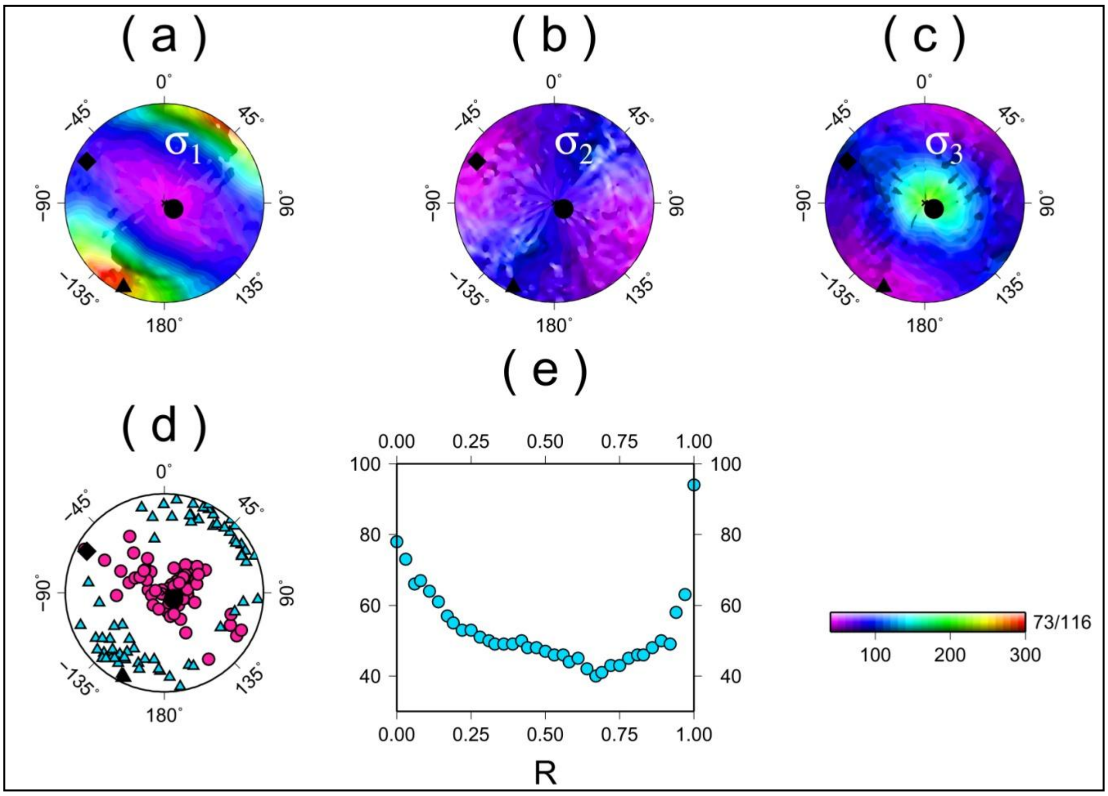

Figure 4.3.6. Stress orientations and R-value graphic of the Çınarcık Basin Cluster

Figure 4.3.5 is the cross section of the AB profile, indicating a seismogenic zone between 4.5 km and 11 km depth. Fault plane solutions are randomly distributed and most of the events are located in the middle and Eastern Çınarcık Basin. As it is clearly seen from Figure 4.3.6(d), the region has a transtensional stress regime, as a result of a NW-SE oriented maximum principal stress axis with 80˚ dipping. In other words, Sigma-1 has a strong vertical dipping, whereas Sigma-3 has a very weak vertical motion with 5˚ plunge, so it is horizontally oriented. Furthermore, the most appropriate value of R is 0.67, and just 2 of the 73 source mechanisms of the region have thrust faulting components.

4.4. The Yalova Cluster

Locating on the Armutlu Peninsula, Yalova and Çınarcık areas consist of metamorphic rocks (Eisonlohr, 1996). Namely, Armutlu Peninsula is a seismologically very active region. Earthquakes of the Yalova Cluster are mostly recorded on the 50 km Yalova-Hersek Fault (Pınar *et al.* 2003). During the study of Yalova Cluster, 102 out of 124 earthquakes were relocated, and data from SBO stations was used for the analysis of 14 earthquakes. Besides, individual and simultaneous fault plane solutions for these 102 earthquakes were obtained, and also stress tensor orientations of the principal stress axes using 2336 high quality P wave initial motion polarities. Hence, number of average polarity for each event in the Yalova Cluster is 23 and it is directly related to the quality of the source mechanisms. Also, 23 of 102 selected earthquakes depict one inconsistent station for 5˚ grid search through the method of Horiuchi *et al.* (1995), whereas just 7 of 102 events give one misfit for 1˚ grid search by the use of the Focmec program. Average depth error value is 2.5 km with average latitude is 0.9 km, longitude is 1.2 km and azimuthal GAP in station coverage is 55˚. As a result of stress tensor inversion, azimuth and plunge values of orientations of maximum, intermediate and minimum axes are; 285˚-75˚, 115˚-7˚, and 201˚-2˚, respectively.

In Figure 4.4.1 fault plane solutions of 102 earthquakes are seen, and these solutions have been simultaneously determined by the program of Horiuchi *et al.* (1995) after the determination of orientations of the principal stress axes. Three black rectangles indicate just focusing areas to see the fault plane solutions in detail (Figure 4.4.2, Figure 4.4.3, and

Figure 4.4.4). Dark green AB profile shows the cross section which was analyzed to present depth distribution versus fault plane solutions (Figure 4.4.5).

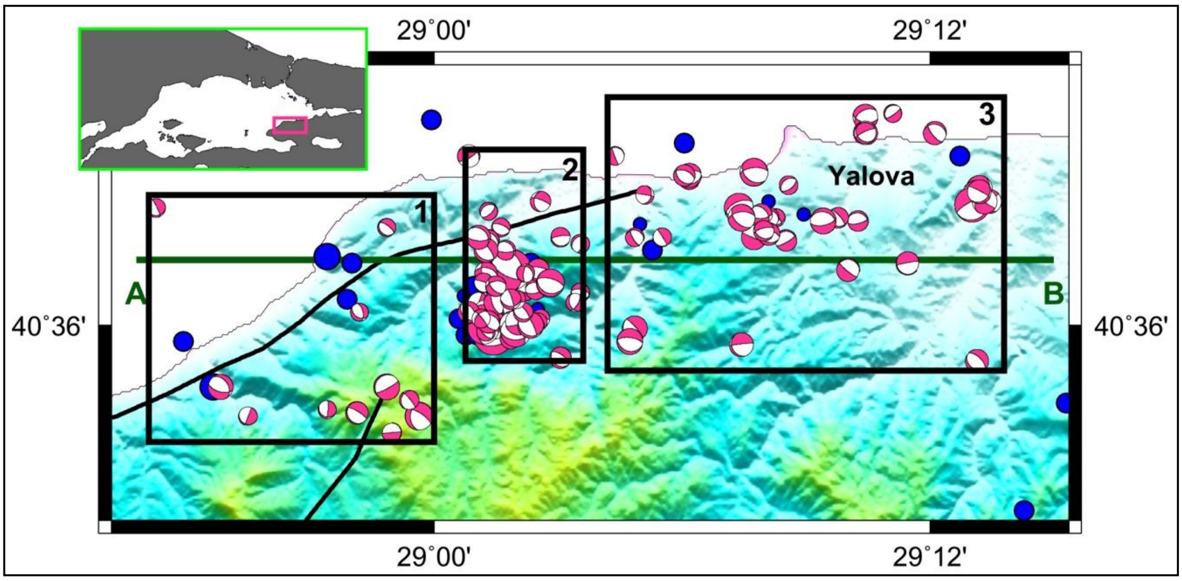

Figure 4.4.1. 102 fault plane solutions in Yalova Cluster

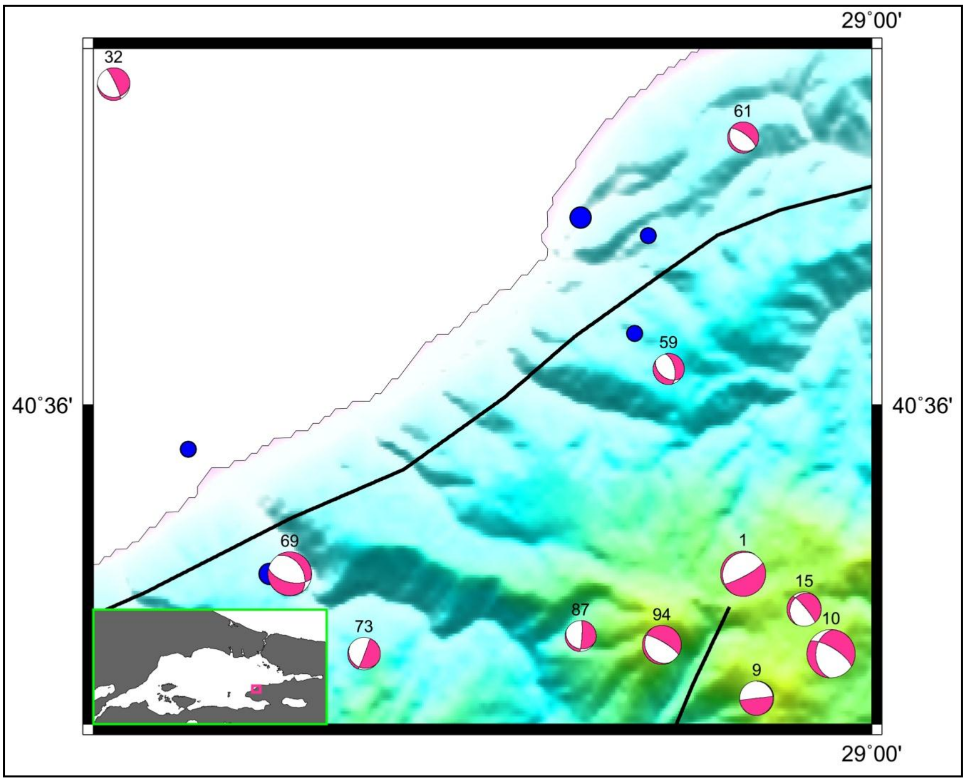

Figure 4.4.2. Focus of the 1st rectangle on the Yalova Cluster map

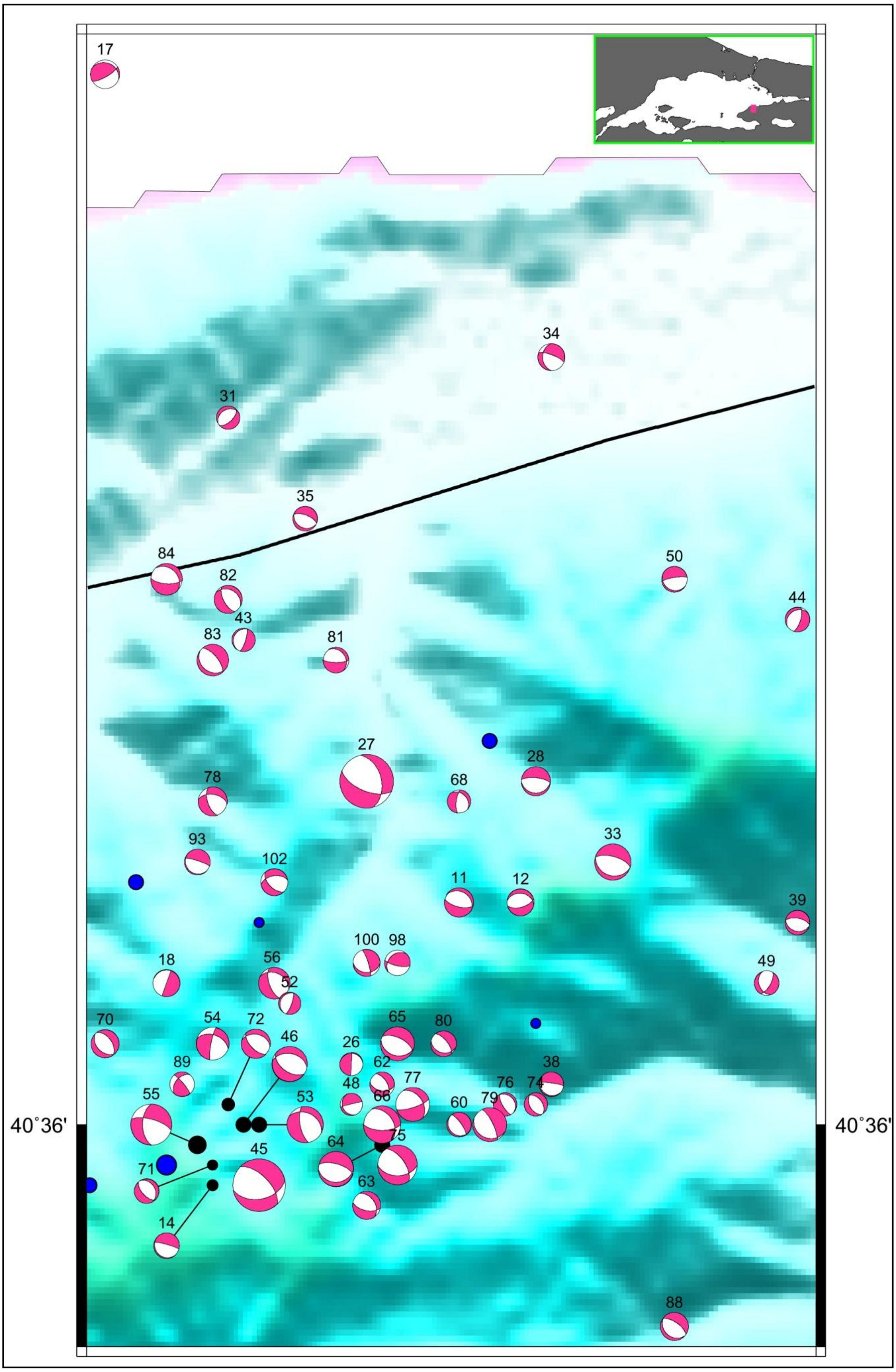

Figure 4.4.3. Focus of 2nd rectangle on the Yalova Cluster map

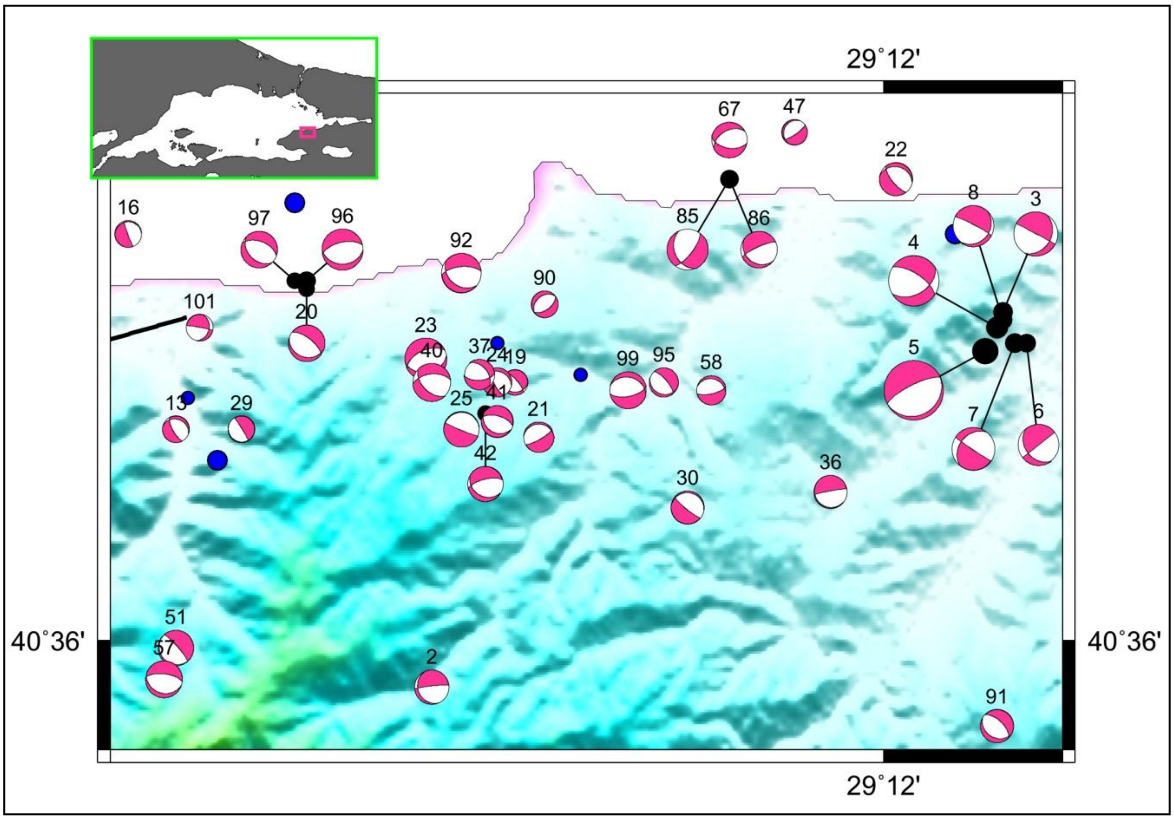

Figure 4.4.4. Focus of the 3rd rectangle on the Yalova Cluster map

Figure 4.4.2, Figure 4.4.3, and Figure 4.4.4 are three focus maps of Figure 4.4.1 in order to see fault plane solutions accurately. Earthquakes in these three maps are also designated time dependently. Their location and fault plane solution parameters including number of misfits can be seen from Table B4, in Appendix B. Details of these simultaneous fault plane solutions, determined through the program of Horiuchi *et al.* (1995), are also allowed to see under the Yalova Cluster title in Appendix C. Besides, individual fault plane solutions obtained by the use of FOCMEC software inside of SEISAN program are available under the Yalova Cluster title in Appendix D. Each earthquake has the same number in maps, and Appendix B, C and D.

As it can be seen from Figure 4.4.2, earthquakes of the Western Yalova cluster, have normal and oblique fault systems. In the middle of the cluster most of the events have nearly pure normal faulting mechanisms, but some oblique mechanisms also exist (Figure 4.4.3). What is more, 2 reverse faulting mechanisms are also observed, one is onshore and the other one is offshore. Moreover, eastern part of the cluster involves mostly normal faulting mechanisms and some oblique ones at the most eastern part.

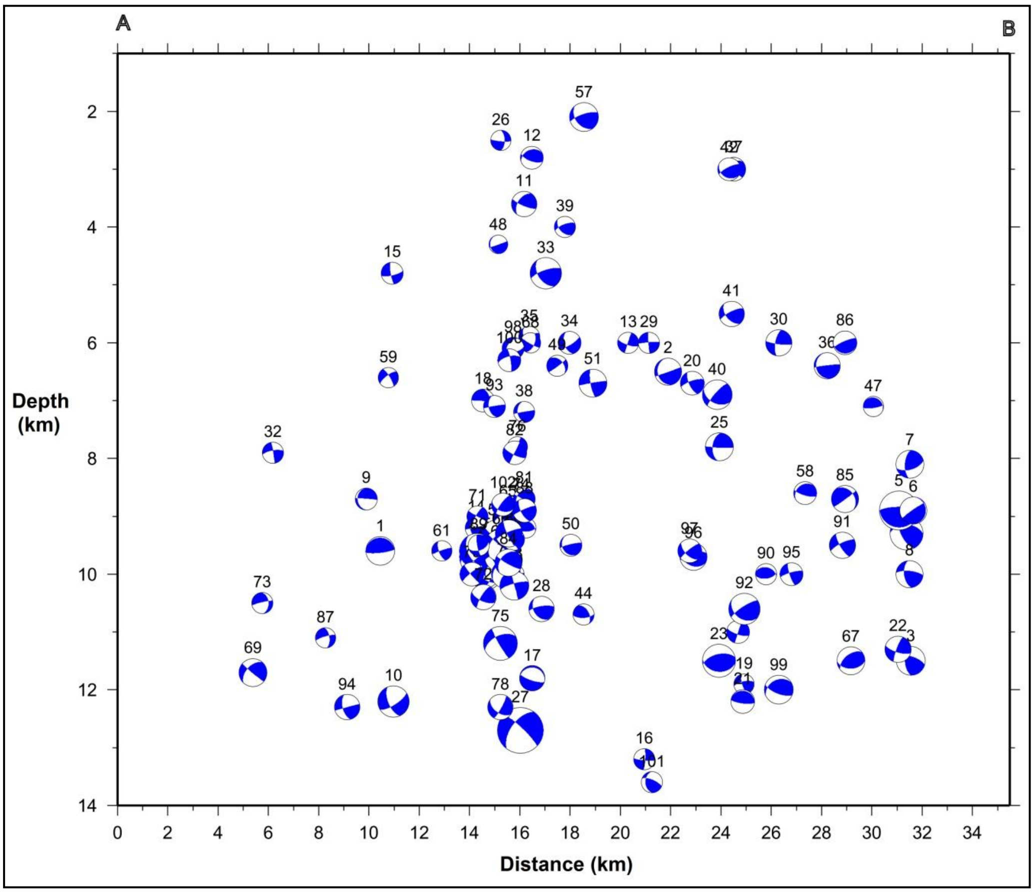

Figure 4.4.5. Depth distribution of fault plane solutions for Yalova Cluster

Figure 4.4.5 is the cross section of the AB profile, indicating a seismogenic zone between 5.5 km and 12.5 km depth. Orientations of maximum (σ_1), intermediate (σ_2) and minimum (σ_3) principal stress axes, and the graphic of number of inconsistency versus R-values are also seen in Figure 4.4.6. As it is clearly seen, the region has a transtensional stress regime, as a result of a WNW-ESE oriented maximum principal stress axis with 75° dipping. While the maximum principle stress axis is vertically oriented, minimum principle stress axis is horizontal. Moreover, the appropriate R-value of the Yalova Region is also equal to 0.32, but it has a wide range between 0.30 and 0.70. Besides, just 3 of the 102 fault plane solutions have thrust components.

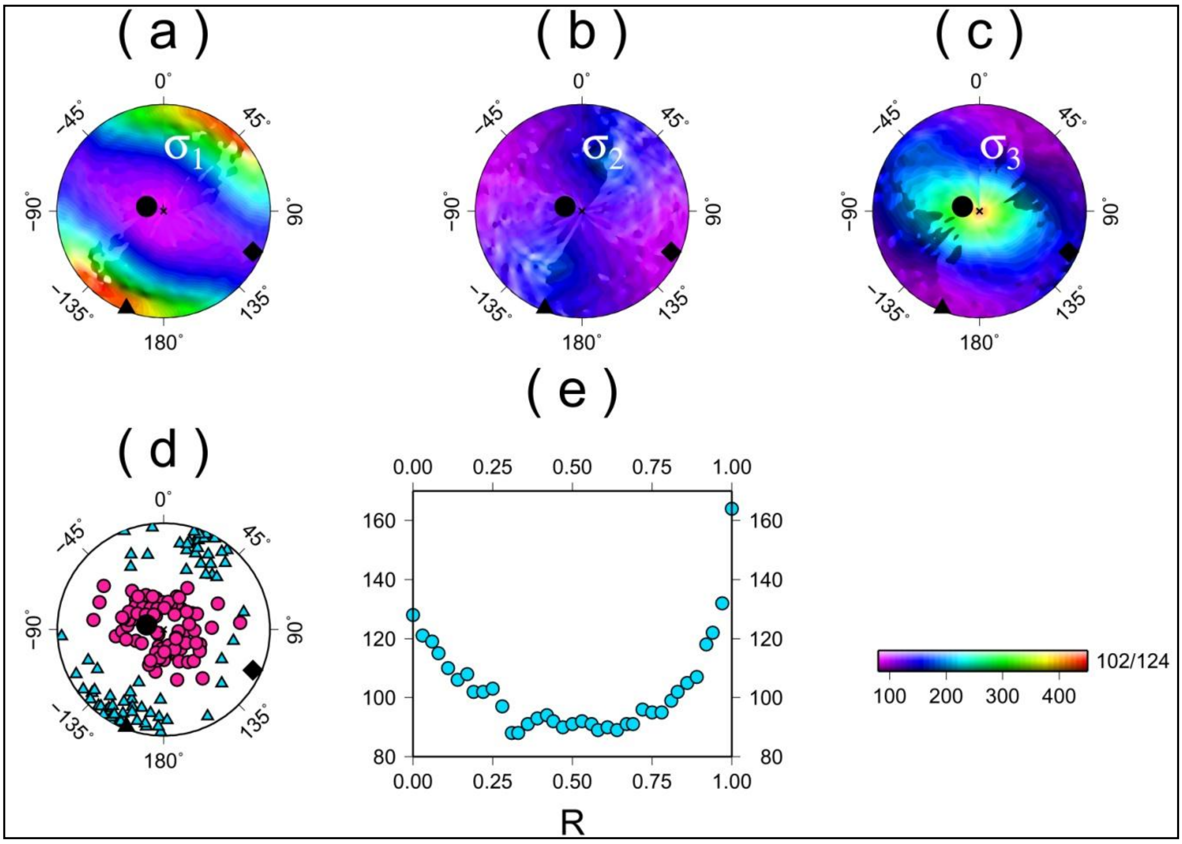

Figure 4.4.6. Stress orientations and R-value graphic of the Yalova Cluster

4.5. The Gemlik Cluster

Gemlik Region is located at the southern branch of the NAFZ in the North Western Turkey. In the study of the Gemlik Cluster, 63 out of 100 earthquakes have been relocated and data of SBO stations is used for the analysis of 10 events. Individual and simultaneous fault plane solutions, and stress tensor orientations of the principal stress axes have been obtained by the use of 1565 high quality P wave initial motion polarities. Hence, number of average polarity in the Gemlik Cluster is 25. Also, 19 of 63 selected earthquakes give one inconsistent station for 5˚ grid search through the method of Horiuchi *et al.* (1995), while 11 of 63 events depict one misfit for 1˚ grid search using the program of Focmec. Average error values of depth, latitude, longitude and azimuthal GAP are; 3.0 km, 1.1 km, 1.4 km and 75˚, respectively. Azimuth and plunge values of orientations of maximum, intermediate and minimum axes are; 90˚-65˚, 285˚-30˚, and 209˚-12˚, respectively.

Most of the selected earthquakes in the Gemlik Region occurred between the end of 2006 and the beginning of 2007 because an ML5.7 Earthquake occurred in 24.10.2006 in the Gemlik Gulf. Thus, many of the earthquakes in this cluster are the aftershocks of the 24.10.2006 event. This moderate size event is the largest earthquake of the south Marmara since 1999 with its 18 cm slip and 3.43E+15 Nm seismic moment value (Bekler *et al.*, unpublished). Besides, the data quality of KOERI stations was much better after the 6th month of 2008, and the number of stations of the TURDEP Project also increased in 2007. Namely, the data quality till the end of 2007 was not as good as the data quality after the middle of 2008. This is the reason of decrease in the number of selected earthquakes, as 47 events eliminated due to having not enough number of polarities.

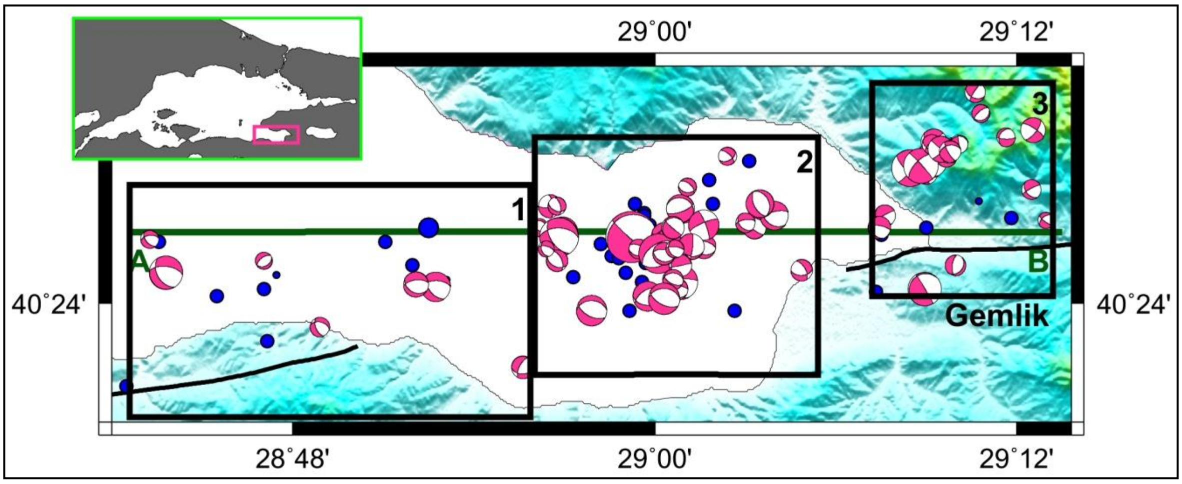

Figure 4.5.1. 63 fault plane solutions in Gemlik Cluster

In Figure 4.5.1 fault plane solutions of 63 earthquakes are characterized, and they have been simultaneously determined by the program of Horiuchi *et al.* (1995) after the determination of orientations of the principal stress axes. Three black rectangles indicate just focusing areas to see the fault plane solutions in detail (Figure 4.5.2, Figure 4.5.3, and Figure 4.5.4). The dark green AB profile shows the cross section which was analyzed to present depth distribution versus fault plane solutions (Figure 4.5.5). Earthquakes in the three focusing maps also designated time dependently. Their location and fault plane solution parameters including number of misfits can be seen from Table B5, in Appendix B. Details of these simultaneous fault plane solutions, determined through the program of Horiuchi *et al.* (1995), are also allowed to see under the Gemlik Cluster title in Appendix

C. Besides, individual fault plane solutions obtained by the use of FOCMEC software inside of SEISAN program are available under the Gemlik Cluster title in Appendix D. Each earthquake has the same number in maps, and Appendix B, C and D.

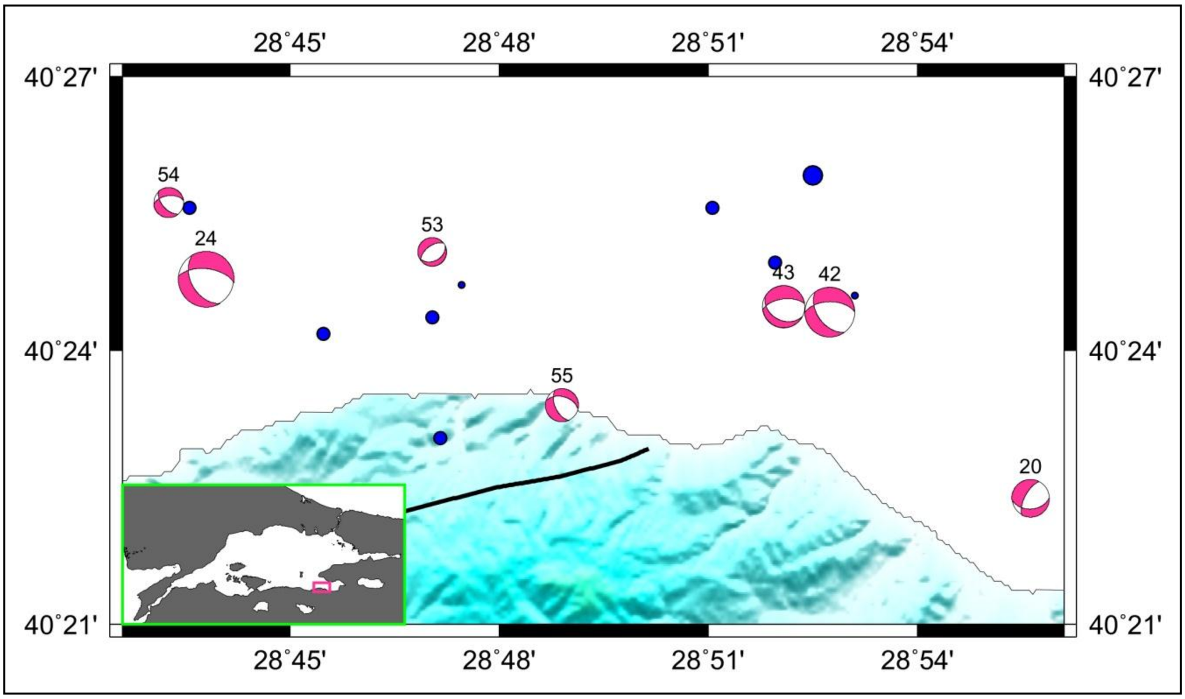

Figure 4.5.2. Focus of the 1st rectangle on the Gemlik Cluster map

As it can be stated from Figure 4.5.2, 6 oblique and 1 pure normal fault mechanisms are obtained in the western part of the Gemlik Cluster, and they are located in the Gemlik Gulf except for one. In the middle of the Gemlik Gulf, earthquakes are randomly distributed with nearly pure normal and some oblique mechanisms (Figure 4.5.3). In addition to these, one left lateral strike-slip faulting mechanism is obtained in the Gemlik Gulf (Earthquake with number 10). In the eastern part of the Gemlik Cluster, earthquakes are located on land, except for 2 events (Figure 4.5.4). Most of the earthquakes on the land have right lateral strike-slip mechanisms even though some a few normal faulting mechanisms also exist.

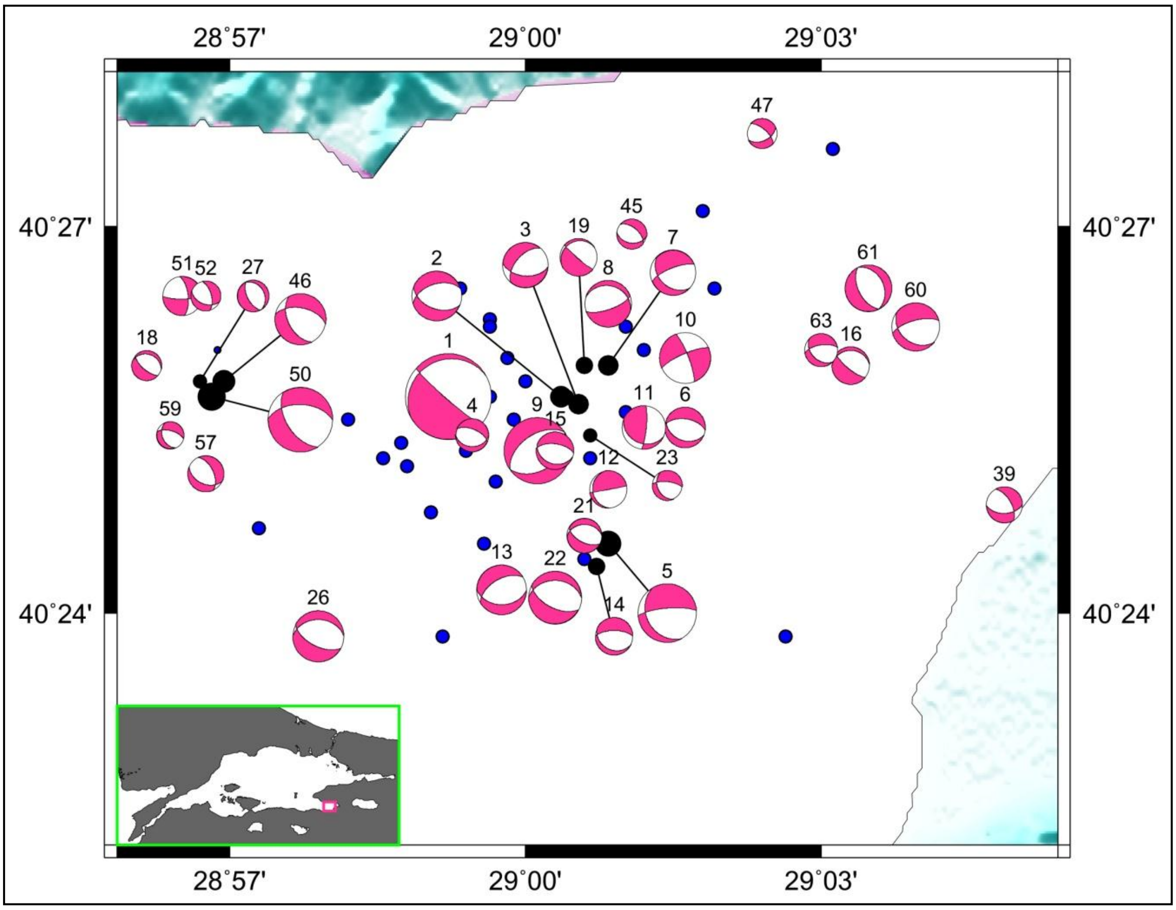

Figure 4.5.3. Focus of 2nd rectangle on the Gemlik Cluster map

Seismogenic zone of the Gemlik Region was found out between 4 km and 10.5 km depth (Figure 4.5.5). Orientations of maximum (σ_1), intermediate (σ_2) and minimum (σ_3) principal stress axes, and the graphic of number of misfits versus R-values are also seen in Figure 4.5.6, but it is doesn't indicate an exact R-value which corresponds to a minimum number of misfits. In other words, the R-value changes between 0.4 and 0.6. Nevertheless, the best value of R for the Gemlik Region equals to 0.54. Almost all the earthquakes occurred in the Gemlik Gulf have normal faulting mechanisms, but most of them have right lateral components. In addition, most of the land earthquakes of the Gemlik Cluster have right lateral strike-slip fault mechanisms consistent with the general structure of the NAFZ. Briefly, the Gemlik Region has a 0.54 value of R indicating a strike-slip regime.

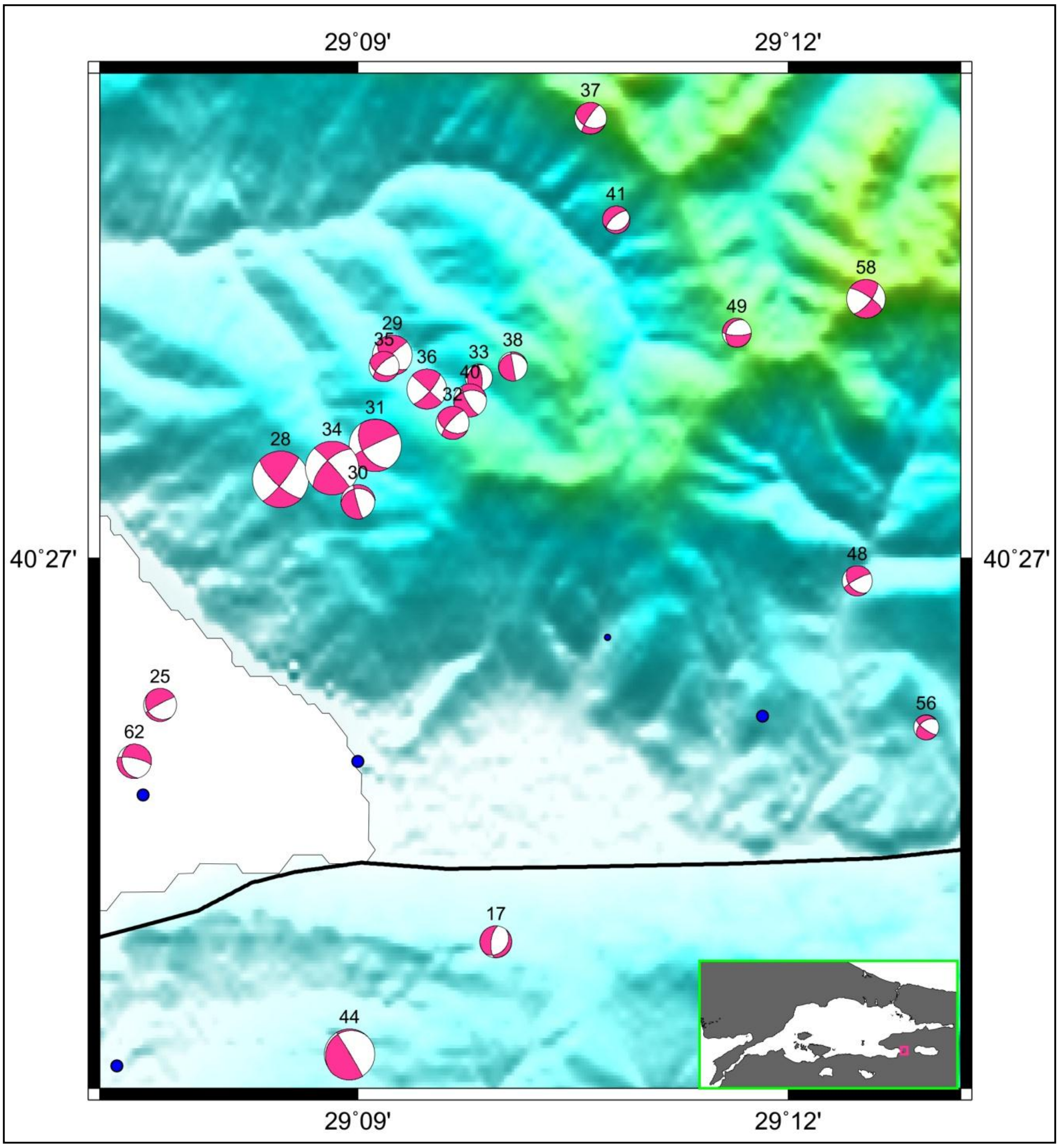

Figure 4.5.4. Focus of the 3rd rectangle on the Gemlik Cluster map

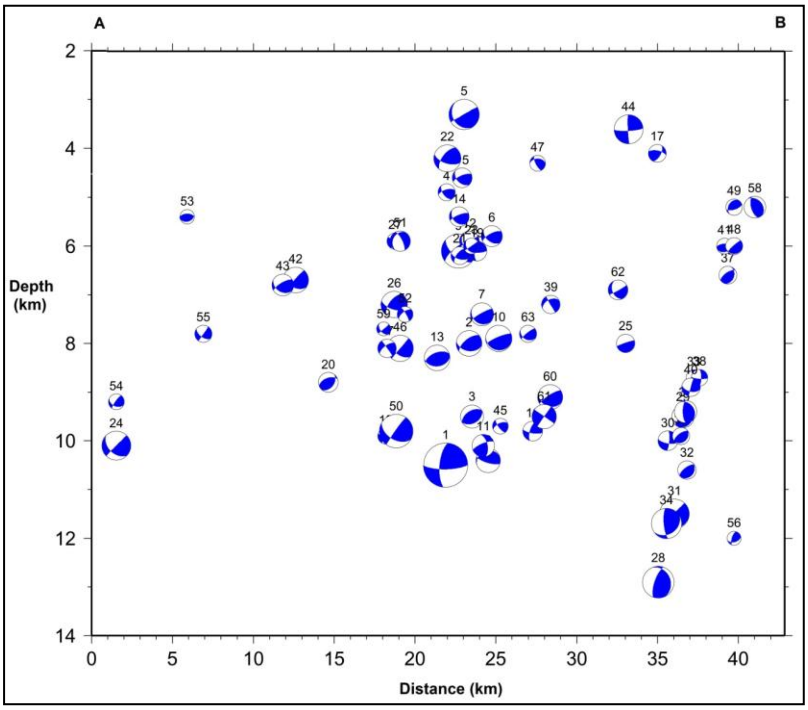

Figure 4.5.5. Depth distribution of fault plane solutions for Gemlik Cluster

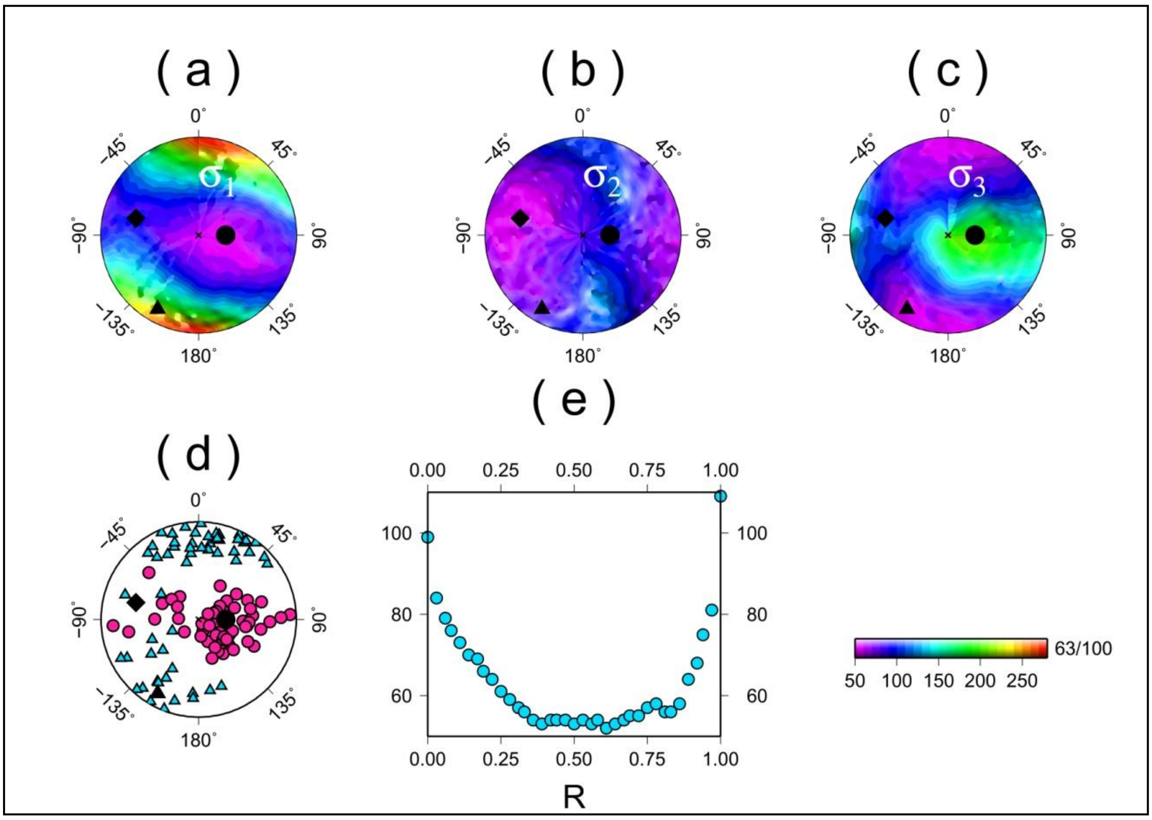

Figure 4.5.6. Stress orientations and R-value graphic of the Gemlik Cluster

4.5.1. 16 August 2011, ML4.0 Gemlik Gulf Earthquake

Epicentral location of the 16 August 2011, ML4.0 Gemlik Gulf Earthquake is very close to the 24 October 2006 ML5.7 Earthquake given with ML5.2 in the earthquake catalogue of KOERI. These two Gemlik Gulf earthquakes are located on the Northern Gemlik Fault (Tsukuda, 1988) and this part of the fault is too complex to understand (Bekler *et al.*, unpublished). The epicentral distance between these two earthquakes is about 6.5 km which means they are most probably located on the same fault plane. The 2011 Earthquake wasn't included in the stress tensor inversion process of the Gemlik Cluster which gave the opportunity of comparison whether stress tensor inversion results of the whole region are compatible with the fault parameters of this new earthquake or not.

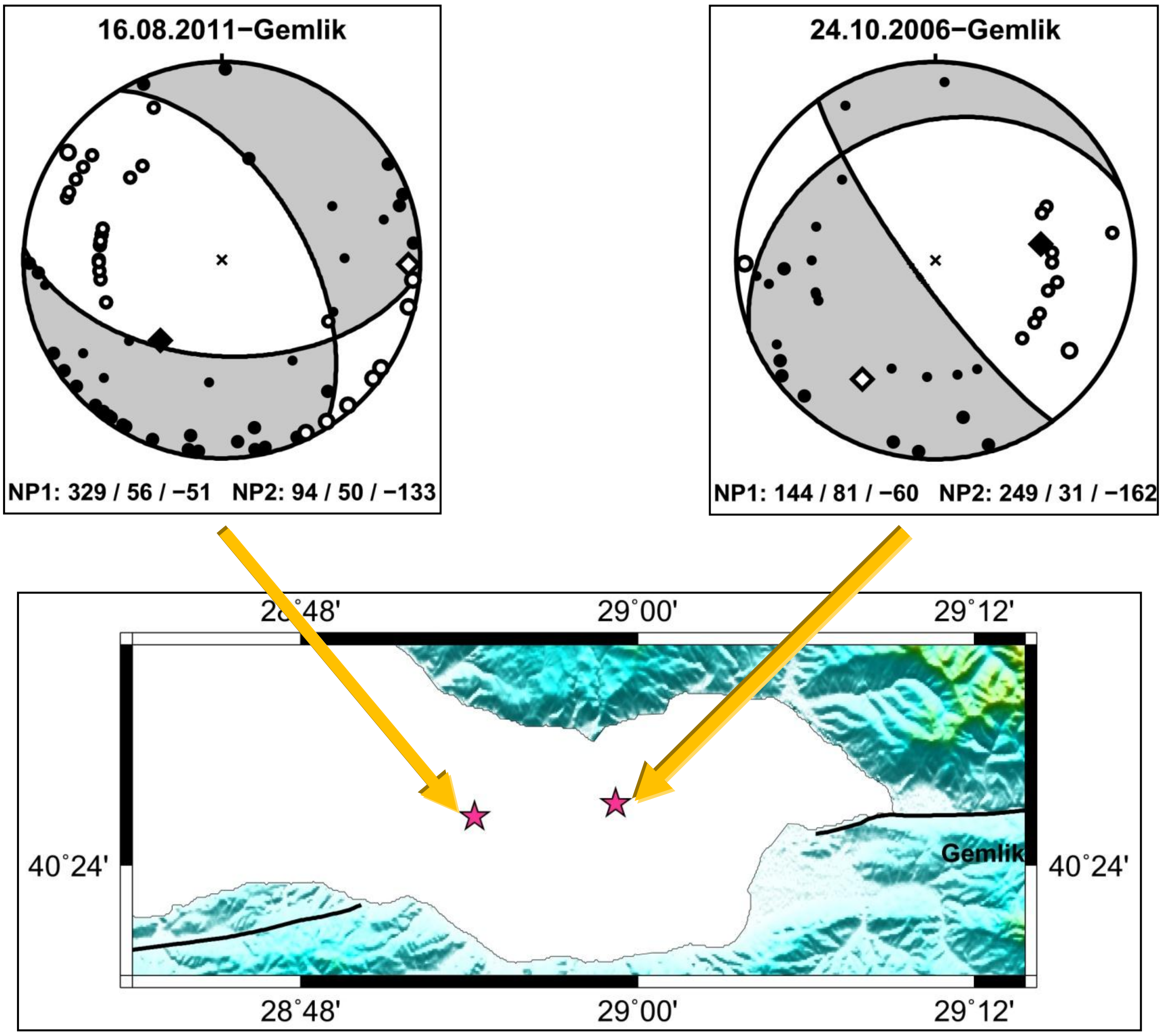

Figure 4.5.1.1. Relocations and fault plane solutions of the two Gemlik Gulf events

Furthermore, comparison of the two Gemlik Gulf earthquakes made possible the evaluation of change of data quality during this study. That is why 16 August 2011 event has also been analyzed despite the fact that it is out of the time interval of this study.

Epicenter locations and fault plane solutions with station distribution of 16.08.2011 (ML4.0 in KOERI catalogue) and 24.10.2006 (ML5.7 in KOERI catalogue ML5.2) Gemlik Gulf earthquakes are shown in Figure 4.5.1.1. As it can be understood from the figure they both have oblique faulting mechanisms, having normal and right lateral strike-slip components.

Table 4.5.1.1. Source parameters of the two moderate size Gemlik Gulf earthquakes

Quality	16.08.2011 ML4.0	24.10.2006 ML5.2
P (Trend, Plunge)	297, 59	85, 45
T (Trend, Plunge)	33, 3	210, 30
B (Trend, Plunge)	125, 31	319, 30
N1-Strike/Dip/Rake	329/56/-51	144/81/-60
N2-Strike/Dip/Rake	94/50/-133	249/31/-162

Azimuth and dip values of principal stress axes are shown on the Table 4.5.1.1, and their fault parameters indicate similar stress features. Dip values of maximum principal stress axes of the whole Gemlik Cluster and 2011 Gemlik Gulf earthquake, 65 and 59 respectively, are coincide each other. Besides, not only stress tensor inversion results of Gemlik Cluster but also fault plane solution of 16 August 2011 Earthquake point out a transtensional stress regime.

24.10.2006 ML5.2 Earthquake was solved with 37 P-wave first motion polarities (Table 5.5.1.2), whereas 16.08.2011 ML4.0 event was solved with 70 polarities although it is much smaller. Moreover, azimuthal GAP in station coverage, horizontal error values and vertical error values are also much smaller for the 2011 Gemlik Gulf earthquake. Therefore, it is clearly stated how the quality of the data set of this study has been enhanced.

Table 4.5.1.2. Detailed information of relocations and source mechanisms of the two moderate size Gemlik Gulf earthquakes

	16.08.2011 ML4.0 Earthquake	**24.10.2006 ML5.2 Earthquake**
Origin Time	17:30:6.7	14:00:21.6
Latitude	40.422	40.428
Longitude	28.903	28.987
Depth (km)	7.9	10.5
Error Latitude	0.8	1.9
Error Longitude	0.9	1.8
Error Depth	1.7	3.3
Azimuthal GAP in Station Coverage	57	153
Number of used Polarities	70	37
Number of Inconsistent Stations	1	0
Degree of Grid Search Interval	1	1
Number of Acceptable Solutions	14	1

5. DISCUSSION

5.1. The Ganos Offshore Cluster

Aksoy *et al.* (2010) obtained the fault plane solution of the 9 August 1912 M7.4 Ganos Earthquake with the use of P-wave first motion polarities from data of five stations. The fault mechanism has WNW-ESE oriented dilatational and NNE-SSW oriented compressional axis. Hence, their result appears to be compatible with the dextral strike-slip stress tensor alignments of the Ganos Offshore Cluster of this current thesis study and the NW-SE oriented maximum principle compressive stress axis. In addition to this, sub-5.5 m right lateral strike-slip offsets of this 1912 Earthquake between Gaziköy and Saros Gulf (obtained by Altunel *et al.* (2000) and Altınok *et al.* (2001)) are also consistent with the stress tensor inversion results of my study. Additionally, the focal mechanism solution of the 27 April 1985 Mürefte Earthquake on the Ganos Fault indicates a thrust fault mechanism which is consistent with the results of the western transpression of the Marmara Region (Kalafat, *et al.*, 2009). On the other hand, I discovered a 14.5 km depth limit for the Ganos Bend, although Meade *et al.* (2002) and Okay *et al.* (2004) proposed a seismogenic zone up to 8±1 km. Five of the 85 earthquakes in this cluster are even located between a depth interval of 14.5 km and 18 km.

Moreover, Gürbüz *et al.* (2000) obtained focal mechanisms of 23 microearthquakes in the Marmara Region, but just one of them is located in the Ganos Cluster, and it has a nearly reverse faulting mechanism which is a possible solution that would also fit the results of this thesis study. Polat *et al.* (2002) obtained a few fault plane solutions at the southeast of the Ganos Offshore Cluster, and their results resemble the findings of this study with normal and strike-slip faults (Figure 4.1.4). Furthermore, focal mechanism results of Pınar *et al.* (2003) also coincide with the results of the most western part of the Ganos Offshore Cluster (Figure 4.1.2), but they do not match in the eastern part of the cluster (Figure 4.1.4). Most of the solutions of their study are formed by oblique mechanisms including thrust components, but in this study most of the solutions have normal components in the Eastern Ganos Bend although some reverse components also exist with some oblique fault systems. Moreover, individual fault plane solutions of this thesis study perfectly coincide with the fault structure mentioned by Seeber *et al.* (2004). Nearly all the thrust faults are seen on the western section of the Ganos Bend which is consistent with the uplift of the Ganos Mountain. Also, nearly all the normal faulting mechanisms are observed at the eastern section of the cluster, compatible with the depression of the Tekirdağ Basin. Likewise, the study of Örgülü (2011) implies similar faulting systems and stress tensor orientations for the most Western Marmara Sea, so our studies support each other.

5.2. The Tekirdağ Basin Cluster

Armijo *et al.* (2005) characterized a large component of normal slip along the southern margin of the Tekirdağ Basin which corresponds to the large number of extensional focal mechanism solutions obtained by this current study. Moreover, Sato *et al.* (2004) obtained two composite fault plane solutions with the analysis of microearthquakes between the Tekirdağ and Central basins, namely in the Tekirdağ Basin Cluster of this study. Both of these have pure right lateral strike-slip systems. The results of this thesis study also actually include dextral strike-slip solutions for the related earthquake cluster, but normal faults are predominant. Pınar *et al.* (2003) obtained three fault plane solutions inside the borders of the Tekirdağ Basin Cluster. All three solutions obtained by their study have oblique fault systems, and two of them have normal components, whereas the other one has reverse components. Nevertheless, I obtained almost purely normal fault mechanisms with some right lateral strike-slip and a few oblique components.

5.3. The Çınarcık Basin Cluster

Two composite focal mechanisms inside of the Eastern Çınarcık Basin were completed by Sato *et al.* (2004), and one of them indicated a right lateral oblique fault system located at the northern part of the basin, while the other one, located at the southern part of the basin, was described as a normal fault mechanism. On the other hand, Pınar *et al.* (2009) found out a compressional stress state and 0.65 value of R for a cluster of events that occurred in the Çınarcık Basin and Yalova Onshore area through the analysis of the aftershock activity of the 1999 İzmit earthquake. Furthermore, composite focal mechanism solutions of Bulut *et al.* (2009) indicate NW-SE trending dextral strike-slip features, while most of the solutions of this thesis study suggest extensional structures. Additionally, fault plane results of Örgülü (2011) point to strike-slip and oblique fault mechanisms, whereas most of the results of this study indicate almost purely normal faulting systems with a few oblique and strike-slip mechanisms in the Çınarcık Basin.

Furthermore, Pınar *et al.* (2003) obtained strike-slip fault plane solutions in the Çınarcık Basin, while just five of 73 focal mechanism solutions in my study have strike-slip mechanisms, and all the others show normal faulting mechanisms. Additionally, three of these strike-slip solutions are located at the northern boundary of the Çınarcık Basin, one is located on the eastern edge of the basin and the last one is located in the southern section of the basin. Pınar *et al.* (2003) also proposed that extensional fault mechanisms should have existed in the region, but because they did not find any extensional mechanisms in the region, they compared the fault system of the Çınarcık Basin with the system stated by Zachariasen & Sieh (1995). Hence, they asserted that the NAFZ extends through the Southern Çınarcık Basin and that the Princes' Islands fault is a secondary fault.

Two fault plane solutions were also obtained by Gürbüz *et al.* (2000) in the Çınarcık Cluster. One of them has a right lateral oblique fault mechanism, whereas the other has a nearly reverse faulting mechanism. Thus, since they include many normal and some right lateral strike-slip solutions, the results of my thesis study are not very compatible with the results of their study. In addition, Okay *et al.* (2000) obtained that the Çınarcık triple junction (TTT) was originated by three dextral strike-slip faults. Specifically, they stated that the Çınarcık Basin was bounded by pure right lateral strike-slip faults without any requirement for N-S extension. Additionally, fault plane solutions of the study of Polat *et al.* (2002) mostly indicate oblique faulting systems, whereas most of the mechanisms of this current study point to normal faulting systems with the exception of a few strike-slip features. Özalaybey *et al.* (2002) also obtained a few focal mechanism solutions of the aftershocks of the 1999 İzmit Earthquake in the Çınarcık Basin. However, they also have strike-slip mechanisms. Özalaybey *et al.* (2002) actually suggested that extensional mechanisms might exit at shallower depths, but in this study the deepest events of the Çınarcık Basin Cluster have normal fault mechanisms.

18 September 1963 Çınarcık Basin Earthquake with M6.3 was the last destructive event of the Northern Çınarcık Basin. Possible fault plane solutions of this earthquake were obtained by Taymaz *et al.* (1991) and Başarır (2011), and they both imply WNW-ESE trending normal faulting mechanisms which exactly coincide with the stress tensor alignments of this cluster.

Moreover, the seismogenic zone of the 50 km Eastern Marmara Sea Fault (Island Fault) is given as being between 10 km and 12 km by Yaltırak *et al.* (2003), whereas it has been discovered to be between 4.5 km and 11 km for most of the eastern part of the Çınarcık Basin during this current thesis study (Figure 4.3.5).

5.4. The Yalova Cluster

The Yalova cluster involves earthquakes recorded in the Western Yalova and Çınarcık land areas (Figure 4.4.1). The western part of the cluster, Çınarcık, is famous for its geothermal springs which lead to a claim of a weak fault plane and also a low coefficient of friction that is proportional to the rate of the shear and normal stresses (Pınar *et al.,* 2009; Twiss and Moores, 1992). Additionally, seismologists still debate whether or not the Yalova segment was ruptured during the 17 August 1999 İzmit event (Cormier *et al.,* 2006). Pınar *et al.* (2009) asserted that the post-seismic displacement of the Yalova segment was most probably triggered by the Çınarcık segment because no co-seismic displacement was observed on the Yalova segment during the 17 August main shock, and aftershocks delayed for 63 hours.

Source mechanism results of the study of Polat *et al.* (2002) indicate strike-slip, oblique and normal faulting mechanisms, though in my study very few oblique fault mechanisms exist, and almost all the solutions have normal faulting mechanisms. Moreover, some fault plane solutions of the aftershock activity of the 1999 İzmit Earthquake were achieved by Özalaybey *et al.* (2002) in the Yalova land, and they mostly show NW-SE trended normal fault mechanisms which completely coincide with the results of this study. In addition to this, the study of Karabulut *et al.* (2002) indicates mostly NW-SE aligned normal faulting systems which are also quite compatible with the mechanisms of my study. On the other hand, they also obtained some right lateral strike-slip fault mechanisms which are E-W oriented, while in this study strike-slip solutions are mostly NW-SE oriented. Fault plane solutions of the investigation of Pınar *et al.* (2003) in the Yalova Region are also consistent with the results of this study as they reported normal fault mechanisms and very few strike-slip ones. Sato *et al.* (2004) obtained two composite focal mechanisms in the northern part of the Armutlu Peninsula, and they both have extensional features. Furthermore, Bohnhoff *et al.* (2006) analyzed not only strike-slip but also normal faulting mechanisms in the western ruptures of the 1999 İzmit Earthquake, especially in low slip barriers. Based on the analysis of the aftershocks though, the main shock had a pure right lateral strike-slip mechanism. In addition, even though the outputs of the study of Pınar *et al.* (2009) characterize an extensional stress regime, the R=0.5 value result implies a strike-slip regime in the analysis of the aftershocks of the 1999 İzmit earthquake. I also discovered a very clear extensional stress regime for Yalova, but the R=0.32 value corresponds to the related stress regime for the Yalova Region. Likewise, many extensional fault plane solutions were done by Bulut *et al.* (2009) with the analysis of composite focal mechanism solutions in the Yalova Region, so their work confirms the results of this current study. In addition, source mechanisms of the land events of the Yalova Cluster in this thesis study correspond to the individual fault plane solutions of the investigations of Örgülü (2011) and Karabulut *et al.* (2011) that observed earthquakes $M \geq 3.7$.

The depth distribution of the events in the Yalova Cluster points to a seismogenic zone from 5.5 to 12.5 km depth as it can be seen from Figure 4.4.5. The study of Ito *et al.* (2002) also implies a seismogenic zone between 5 and 12.5 km in this region, whereas the aftershock activity of the 17 August 1999 İzmit Earthquake was much more shallow, as hypocenters of those aftershocks are not deeper than 5 km according to CMT locations (Pınar *et al.,* 2001; 2003) and some other relocations (Pınar *et al.,* 2009).

5.5. The Gemlik Cluster

Pınar *et al.* (2003) obtained two right lateral strike-slip mechanisms in the Gemlik Gulf. One is in the western end of the gulf, and the other is in the south. On the other hand, my results suggest extensional source mechanisms even though they mostly have small right lateral components. Furthermore, source parameters of the 24.10.2006 ML5.2 (in our catalogue ML5.7) Earthquake obtained in this thesis study are consistent with the fault parameters of Harvard CMT, Örgülü (2011) and Karabulut *et al.* (2011) pointing to an extensional faulting system with right lateral components. Principal stress orientation results of Örgülü (2011) for the whole Southern Marmara Sea are also compatible with the stress tensor inversion results of the Gemlik Cluster.

5.6. General Discussion

The stress tensor orientation results of Örgülü (2011) indicate a right lateral strike-slip stress regime for the Eastern Marmara Sea, whereas orientations of principal stress of this thesis study point to extensional stress states concerning stress tensor alignments of the Çınarcık Basin, Gemlik and Yalova clusters.

According to the proposal of Laigle *et al.* (2008), the basins of the Sea of Marmara are bounded by N115˚-125˚E aligned extensional faults indicating a N75˚-80˚E aligned maximum shear stress on the Ganos Bend and southeastern Çınarcık Basin. Therefore, the proposed orientation interval for the maximum principal stress axis is compatible with the NW-SE oriented Sigma-1 values of this current thesis study.

Armijo *et al.* (1999; 2002), Seeber *et al.* (2004; 2010), and Sorlien *et al.* (2012) presented that the fault structure of the Sea of Marmara is in a steady-state mode, and Sorlien *et al.* (2012), citing their results of stratigraphic horizons along the Main Marmara Fault, also implied that the fault feature of the Marmara Sea cannot be easily understood as having dextral strike-slip motion with pull-apart basins.

Likewise to Armijo *et al.* (2005), I stated that Western Marmara Sea is dominated by transtensional, transpressional and right lateral strike-slip fault regimes between the Central Marmara Basin and the Ganos Bend in terms of the stress tensor outputs of the Tekirdağ Basin and the Ganos Offshore clusters. Stress tensor inversion results of the

Eastern Marmara are compatible with the results of Armijo *et al.* (2005), as they stated that the Eastern Marmara Sea has an extensional stress regime with 2-4 m slip.

Stress tensor inversion results of Pınar *et al.* (2003) imply right dextral strike-slip regimes for both the Eastern and Western Marmara Sea with 16˚ counter clockwise rotation in the strike of the maximum principal stress axes. Additionally, they found that the intermediate stress axis (σ_2) is nearly vertical with 69˚ of plunge in the Eastern Marmara Sea. On the other hand, stress tensor results of the Gemlik, Yalova and Çınarcık regions of my study, or the Eastern Marmara, have vertical maximum principal stress axes (σ_1) with plunge values of; 65˚, 75˚, 80˚, respectively. Stress tensor inversion results of the Tekirdağ Basin Cluster also yielded a vertical σ_1 with 70˚ plunge value. On the other hand, in the Ganos Offshore Cluster stress tensor results imply a right lateral strike-slip state with σ_2 close to vertical with a plunge of 50˚.

Flerit *et al.* (2003) suggested primarily strike-slip motions along the north Marmara Sea and extensional motions along the south Marmara Sea. They also claimed that the evolution of the NAFZ may have been affected by the stress field of the Aegean. The Gemlik Cluster showed extensional structure, which is consistent with their suggestion. Nevertheless, extensional motions, rather than strike-slip movements, are very active in the Tekirdağ and Çınarcık basins.

Kiratzi (2002) investigated stress tensor orientations of the Marmara Region with the use of 11 previous fault plane solutions in the Marmara Region. She obtained a NW-SE trended right lateral strike-slip regime with R=0.7. In the present study, the best values of R for the Tekirdağ Basin and the Çınarcık Basin clusters are 0.8 and 0.67, respectively, and the best R-values of other clusters have wide ranges.

Contrary to other authors of the Le Pichon *et al.* (2001), Armijo and Meyer argued that the North Anatolian Fault is not completely dominated by a purely strike-slip character, but rather by a transtensional tectonic regime owing to the observation of an existing pull-apart structure. As a result, their suggestion coincides with the stress tensor inversion orientations of this thesis study.

Gürbüz *et al.* (2000) achieved two right lateral strike-slip stress regimes for the whole Marmara Region with the use of the method of Rivera and Cisternas (1990). One is from the re-evaluation of M≥5.0 historical events and the other is from the obtained focal mechanisms of 23 micro-seismic events. Their results correspond to the local stress state of the Ganos Offshore Cluster of this current thesis study. Land earthquakes of the Gemlik Region in my study are actually also compatible with their results, but our stress tensor inversion results differed for the other four clusters the Gemlik Region, the Yalova Region, the Çınarcık Basin, and the Tekirdağ Basin.

Further, as is stated in this current thesis study, the Ganos Offshore has a dextral strike-slip stress state which is close to transpression in terms of stress tensor orientations. Nevertheless, located in the eastern part of the Ganos Offshore Cluster, the Tekirdağ Basin Cluster has a transtensional stress state. It involves numerous high quality purely normal fault mechanisms and some right lateral strike-slip mechanisms. As an aside, the Tekirdağ Basin Cluster has the highest quality of the number of average polarity (28) with average vertical error value of 3.1 km, horizontal error value of 1.8 km and azimuthal GAP in station coverage of 58˚. As was stated before, this cluster is located at the southern end of the Western High of the Marmara Sea which is between the Tekirdağ and Central basins, but closer to the Tekirdağ Basin. Therefore, concerning these two pull-apart structures, another area of opening may exist between them.

6. CONCLUSION

In this thesis study 398 of 600 ML≥2.0 earthquakes, recorded in the Marmara Region between 02.09.2006 and 31.03.2011, have been relocated, and their individual focal mechanism solutions and stress tensor orientations have been obtained with the use of data from 105 seismic stations for the five apparent earthquake clusters. Eliminations of the earthquakes have been done with the following criteria: a minimum of 10 P-wave high quality first motion polarities and no more than one misfit must be observed for every selected event. The number of earthquakes decreased from 144 to 85, 105 to 75, 116 to 73, 124 to 102, 100 to 63 in the Ganos Offshore, Tekirdağ Basin, Çınarcık Basin, Yalova and Gemlik clusters, respectively. Events of the Ganos Offshore Cluster have been relatively small in magnitude which resulted in a significant decrease in the number of selected earthquakes. In addition, most of the earthquakes of the Gemlik Cluster were originated from the aftershock activity of the 24.10.2006 ML5.7 Gemlik Gulf Earthquake and, at that time, the quality of KOERI stations was not as high as it has been since 2008. Consequently, 37 earthquakes have been eliminated from this cluster. Considering all of the 9226 polarities, the average polarity number for the five examined earthquake clusters were 21, 28, 20, 23, and 25, respectively, using the same order as above. Average horizontal and vertical errors are, 1.6-2.6 km, 1.8-3.1 km, 1.4-2.8 km, 1.5-2.5 km and 1.8-3.0 km for Ganos Offshore, Tekirdağ Basin, Çınarcık Basin, Yalova and Gemlik clusters, respectively. Also, average azimuthal GAP in station coverage is 63˚ for the five selected clusters.

During this study, individual fault planes solutions of selected earthquakes have been obtained using Focmec software in order to observe the best-fit focal mechanism solutions with mostly 1˚ of grid search interval sensitivity. Fault plane solutions were then simultaneously determined by the implementation of the method of Horiuchi *et al.* (1995) with 5˚ of grid search which is the highest degree of sensitivity for this program. Stress tensor alignments of the earthquake clusters have also been achieved by use of the program of Horiuchi *et al.* (1995). NW-SE trended transtensional stress states in the Tekirdağ Basin, Çınarcık Basin, and Yalova clusters, W-E trended extensional state in the Gemlik Cluster and dextral strike-slip state in the Ganos Cluster were obtained. The present-day stress states derived from the method of Horiuchi *et al.* (1995) are also presented in Figure 5.1 using red arrows on the orientations of the maximum principal stress axes (Sigma-1). Pink dots characterize orientations of the maximum principal stress axes, whereas blue triangles indicate orientations of the minimum principal stress axes.

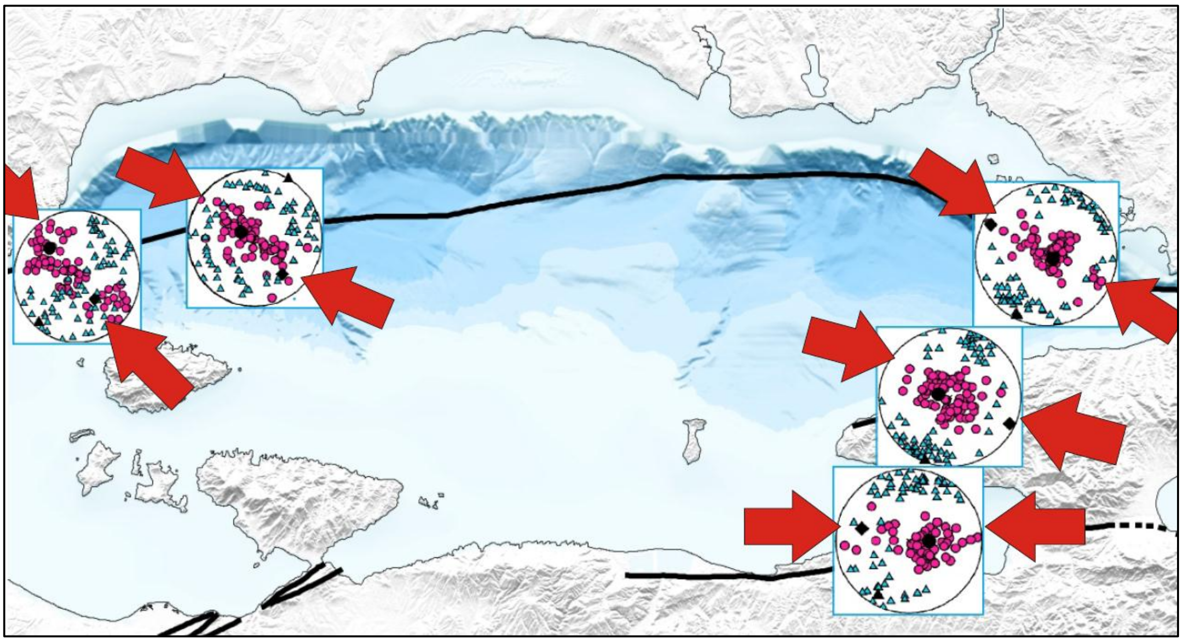

Figure 5.1. The present day stress states in the Marmara Region

Furthermore, two moderate-size earthquakes have been also analyzed though they do not fall between the time span of the mentioned cluster studies. The 25 July 2011 Marmara Sea Earthquake with ML5.2 is located in the middle of the Tekirdağ Basin Cluster, and its obtained source mechanism solution shows a nearly normal fault mechanism with right lateral components. Hence, the focal mechanism solution of this event is consistent with the stress tensor inversion results of the Tekirdağ Basin Cluster. In addition, when I have compared with the earthquake activities of other clusters, I observed a seven-month-seismic-sleep process, since only seven microearthquakes were recorded during the last seven months prior to the 25 July main shock. Additionally, the survey of this earthquake made possible the evaluation of the contribution of the data of SBO stations. This data may have leaded to an increase in the horizontal and vertical error values, although the use of their P-wave first motion polarities was helpful.

The second individually analyzed moderate size event of this study is the 16 August 2011 ML4.0 Gemlik Gulf earthquake. The epicenter of this earthquake was located about 6.5 km west of the epicenter of the 24.10.2006 ML5.2 Gemlik Gulf earthquake. They both have oblique fault mechanisms, having normal and dextral faulting components, but the maximum principal stress axis of the new event is closer to vertical as compared with the old one. Nevertheless, orientations of their minimum principle stress axes are almost the same. Additionally, plunge values of the intermediate principal stress axes are perfectly compatible. What is more, the focal mechanism solution of the 16 August 2011 Earthquake exactly coincides with the stress tensor orientations of the whole Gemlik Cluster (Table4.5.1.1 and Table 4.1).

Furthermore, plunge values of maximum principal stress axes decrease from north to south with a counter-clockwise rotation in the Eastern Marmara according to stress tensor orientation results of the Çınarcık Basin, Yalova and Gemlik clusters. Moreover, earthquake clustering of the Gemlik Region is located at the northern part of the known fault trace of Şaroğlu *et al.* (1992) (Figures 4.1.1, 4.2.1, 4.3.1, 4.4.1, 4.5.1), while for the Ganos Offshore, Tekirdağ Basin, and Yalova clusters, earthquakes were mostly located at the southern parts of the known faults. In addition, earthquake activity of the Çınarcık Basin has been mostly concentrated in the central section of the Çınarcık Basin. Likewise, NW-SE oriented extensional faulting mechanisms of the Çınarcık Basin are consistent with the NW-SE oriented pull-apart structure of the northeast Marmara Sea.

Polat *et al.* (2002) identified a stress regime between extension and strike-slip for the Marmara Region and nearly pure right lateral strike-slip regimes for the earthquake activities of the years of 1995 and 1942-1997. Further, according to their findings, dipping angles of σ_1 and σ_2 were 45˚ and σ_3 was 35˚. Though they did not state any vertical findings, in this current study, with the exception of the Ganos Offshore Cluster, the other four clusters have σ_1 close to vertical. This may indicate a change in the stress regime of the Marmara Region from nearly pure right lateral to an extension feature.

Results of this thesis study agree with the findings of Armijo *et al.* (2005), since nearly all the individual fault plane solutions have normal mechanisms which are consistent with the mentioned pull-apart structure. Many reverse fault mechanisms were also observed in the Ganos Offshore which is under a transpressional stress state. Moreover, stress tensor inversion results of the Western Marmara, namely the Ganos Bend and the Eastern Tekirdağ Basin, are consistent with the proposal of Okay *et al.* (2004) as they stated that a transpressional stress state is dominant in the Ganos area and it becomes transtensional from west to east. Additionally, as is proposed by Le Pichon *et al.* (2001) the Marmara Region is dominated not only by the NAFZ but also by extensional features (Smith *et al.*, 1995; Parke *et al.*, 1999), which is associated with strain partitioning. As a result, this current thesis study supports this proposal as well.

REFERENCES

Aki, K., and P. G. Richards, 1980, *Quantitative Seismology, Theory and Methods*, H. Freeman and Co., San Francisco, California. Vol. 1.

Aksoy, M.E., M. Meghraoui, M. Vallée, and Z. Çakır, 2010, "Rupture Characteristics of the A.D. 1912 Mürefte (Ganos) Earthquake Segment of the North Anatolian Fault (Western Turkey)", *Geological Society of America*, Vol. 38, pp. 37-57.

Aksu, A.E., T. J. Calon, R. N. Hiscott, and D. Yaşar, 2000, “Anatomy of the North Anatolian Fault Zone in the Marmara Sea Western Turkey: Extensional Basins above a Continental Transform”, *GSA Today*, Vol. 10, pp. 1-2.

Akyol, N., L. Zhu, B. J. Mitchell, H. Sözbilir, and K. Kekovalı, 2006, “Crustal Structure and Local Seismicity in Western Anatolia”, *Geophysical Journal International*, pp. 1259-1269.

Altınok, Y., B. Alpar, and C. Yaltırak, 2001, “Tsunami of the 1912 Earthquake (Ms=7.4), Extension of the Associated Faulting in the Marmara Sea”, *NATO Advanced Research Workshop On ‘Underwater Ground Failures on Tsunami Generation, Modeling, Risk and Mitigation’,* İstanbul, May 23-25, 2001.

Altunel, E., A. A.Barka, and H. S. Akyüz, 2000, “Slip Distribution along the 1912 Mürefte-Şarköy Earthquake, North Anatolian Fault, Western Turkey” in: A. A. Barka, Ö. Kozacı, S. H. Akyüz, and E. Altunel, (Eds.), *1999 İzmit-Düzce Earthquakes: Preliminary Results. İstanbul Technical University Publ.*, pp. 341-349.

Altunel, E., M. Meghraoui, H. S. Akyüz, and A. Dikbas, 2004, “Characteristics of the 1912 Coseismic Rupture along the North Anatolian Fault Zone (Turkey): Implications for the Expected Marmara Earthquake”, *Terra Nova*, 16, DOI:10.1111/j.1365-3121.2004.00552, pp. 198–204.

Ambraseys, N., 2002, “The Seismic Activity of the Marmara Sea Region over the Last 2000 Years”, *Bulletin of the Seismological Society of America,* pp. 1-18.

Ambraseys, N.N., and C.F. Finkel, 1987, "The Saros-Marmara Earthquake of 9 August 1912", *Earthquake Engineering and Structural Dynamics, Vol.* 15, pp. 189–211.

Armijo, R., B. Meyer, A. Hubert, and A. Barka, 1999, “Westward Propagation of the North Anatolian Fault into the Northern Aegean: Timing and Kinematics”, *Geology,* Vol. 27, pp. 267–270.

Armijo, R., B. Meyer, S. Navarro, G. King, and A. Barka, 2002, “Asymmetric Slip Partitioning in the Sea of Marmara Pull-Apart: A Clue to Propagation Processes of the North Anatolian Fault?”, *Terra Nova,* Vol. 14, pp. 80–86.

Armijo, R., N. Pondard, B. Meyer, G. Uçarkus, B. M. de Lepinay, J. Malavieille , S. Dominguez, M. Gustcher, S. Schmidt, C. Beck, N. Çagatay, Z. Çakir, C. Imren, K. Eris, B. Natalin, S. Özalaybey, L. Tolun, I. Lefevre, L. Seeber, L. Gasperini, C. Rangin, O. Emre, and K. Sarikavak, 2005, “Submarine Fault Scarps in the Sea of Marmara Pull-Apart (North Anatolian Fault): Implications for Seismic Hazard in İstanbul”, *AGU and the Geochemical Society,* ISSN: 1525-2027.

Avşar, Ü. and T. İşseven, 2009, “Regional Clockwise Rotation of the Armutlu Peninsula, Western Turkey, Resolved from Palaeomagnetic Study of Eocene Volcanics”, *Tectonophysics,* pp. 415-422.

Barış, S., A. Ito, S. Balamir Üçer, Y. Honkura, N. Kafadar, R. Pektaş, T. Komut and A. M. Işıkara, 2002, “Microearthquake Activity before the İzmit Earthquake in the Eastern Marmara Region, Turkey (1 January 1993–17 August 1999*)”, Bulletin of the Seismological Society of America,* pp. 394-405.

Barka, A. A., and K. Kadinsky-Cade, 1988, “Strike-Slip Fault Geometry in Turkey and its Influence on Earthquake Activity”, *Tectonics,* Vol. 7, pp. 663-684.

Barka, A. A., 1992, “The North Anatolian Fault Zone”, *Ann. Tectonophysics,* Vol. 6, pp. 164-195.

Başarır, N., 2011, *Reassessment of the Seismic Parameters from Historical Seismograms of 1912- Murefte-Sarkoy, 1935-Erdek-Marmara Island and 1963-Cinarcik Earthquakes,* M. S. Thesis, Boğaziçi University.

Becel, A., M. Laigle, B. de Voogd, A. Hirn, T. Taymaz, S. Yolsal-Cevikbilen, and H. Shimamura, 2010, “North Marmara Trough Architecture of Basin Infill, Basement and Faults, from PSDM Reflection and OBS Refraction Seismics”, *Tectonophysics,* pp. 1-14.

Bekler, T., and C. Gurbuz, 2008, “Insight into the Crustal Structure of the Eastern Marmara Region, NW Turkey”, *Pure and Applied Geophysics,* DOI 10.1007/s00024-008-0302-3.

Bekler F. N., N. Meral Özel and G. Birgören Tanırcan, unpublished, “Rupture Process of two Small Earthquakes in the Southern Marmara Region”.

Bohnhoff, M., H. Grosser, and G. Dresen, 2006, “Strain Partitioning and Stress Rotation at the North Anatolian Fault Zone from Aftershock Focal Mechanisms of the 1999 İzmit *M*w = 7.4 Earthquake”, *Geophysical Journal International*, Vol. 160, pp. 373-385.

Bohnhoff, M., F. Bulut, E. Görgün, C. Milkereit, and G. Dresen, 2007, “Seismotectonic Setting at the North Anatolian Fault Zone after the 1999 Mw=7.4 İzmit Earthquake based on High-Resolution Aftershock Locations”, *Advances in Geosciences,* pp. 1-8.

Bormann, P., 2002, New Manual of Seismological Observatory Practice (NMSOP), IASPEI, GeoForchungsZentrum Potsdam.

Bouchon, M., M. N. Toksöz, H. Karabulut, M.-P. Bouin, M. Dietrich, M. Aktar, and M. Edie, 2002, “Space and Time Evolution of Rupture and Faulting during the 1999

İzmit (Turkey) Earthquake", *Bulletin of the Seismological Society of America,* Vol. 92, pp. 256–266 DOI:10.1785/0120000845.

Bulut, F., M. Bohnhoff, W. L. Ellsworth, M. Aktar, and G. Dresen, 2009, "Microseismicity at the North Anatolian Fault in the Sea of Marmara Offshore İstanbul, NW Turkey", *Journal of Geophysical Research,* DOI:10.1029/2008JB006244.

Bulut, F., Y. Ben-Zion, M. Bohnhoff, 2012, "Evidence for a Biomaterial Interface along the Mudurnu Segment of the North Anatolian Fault Zone from Polarization Analysis of P Waves", *Earth and Planetary Science Letters*, pp. 17-22.

Carton, H., S. C. Singh, A. Hirn, S. Bazin, B. de Voogd, A. Vigner, A. Ricolleau, S. Cetin, N. Oçakoğlu, F. Karakoç, and V. Sevilgen, 2007, "Seismic Imaging of the Three-Dimensional Architecture of the Çınarcık Basin along the North Anatolian Fault", *Journal of Geophysical Research,* DOI:10.1029/2006JB004548.

Cormier, M. H., L. Seeber, C. M. G. McHugh, A. Polonia, N. Cagatay, O. Emre, L. Gasperini, N. Gorur, G. Bortoluzzi, E. Bonatti,W. B. F. Ryan, and K. R. Newman, 2006, "North Anatolian Fault in the Gulf of İzmit (Turkey): Rapid Vertical Motion in Response to Minor Bends of a Nonvertical Continental Transform", *Journal of Geophyical. Research,* Vol. 111, B04102, DOI:10.1029/2005JB003633.

Deniz, P., 2010, *Deprem ve Patlatma Verilerinin Birbirinden Ayırt Edilmesi,* M. S. Thesis, University of Sakarya, Institute of Science and Technology (In Turkish).

Dewey, J. F., and A. M. C. Şengör, 1979, "Aegean and Surrounding Regions: Complex Multiplate and Continuum Mechanics in a Convergence Zone", *Bulletin of the Geological Society of America,* Vol. 84, pp. 3137-3180.

Dewey, J. F., R. E. Holdswoth and R. A. Strachan, 2012, "Transpression and Transtension Zones", *http://sp.lyellcollection.org.*

Dreger, D.S. and D. V. Helmberger, 1991, “Source Parameters of the Sierra Madre Earthquake from Regional and Local Body Waves”, *Geophysical Research Letters,* Vol. 18, pp. 2015–2018.

Dreger, D.S. and D. V. Helmberger, 1993, “Determination of Source at Regional Distances with Single Stations or Sparse Network Data”, *Journal of Geophyical. Research,* Vol. 98, pp. 8107–8125.

Dreger, D.S. and C. Langston, 1995, “Moment Tensor InversionWorkshop”, *an IRIS DMS Short Course, Seattle, Washington*.

Dresen, G., M. Bohnhoff, M. Aktar, and H. Eyidogan, 2008, “Drilling the North Anatolian Fault”, *Workshop Reports,* DOI:10.2204/iodp.sd.6.10.2008.

Durand, V., M. Bouchon, H. Karabulut, D. Marsan, J. Schmittbuhl, M. P. Bouin, M. Aktar, and G. Daniel, 2010, “Seismic Interaction and Delayed Triggering Along the North Anatolian Fault”, *Geophysical Research Letters,* VOL. 37, L18310, DOI:10.1029/2010GL044688.

Elmas, A., and A. Gürer, 2004, “A Comparison of the Geological and Geoelectrical Structures in the Eastern Marmara Region (NW Turkey)”, *Journal of Asian Earth Sciences,* pp. 153-162.

Ergün, M. and E. Özel, 1995, “Structural Relationship between the Sea of Marmara Basin and the North Anatolian Fault”, *Terra Nova,* Vol. 7, pp. 278-288.

Eyidoğan, H., 1988, “Rates of Crustal Deformation in Western Turkey as Deduced from Major Earthquakes”, *Tectonophysics,* Vol. 148, pp. 83-92.

Eyidoğan, H., U. Guclu, Z. Utku, and E. Degirmenci, 1991, “A Macro-Seismic Guide Book for the Large Turkish Earthquakes (in Turkish)”, *İstanbul Technical University*.

Flerit, F., R. Armijo, G. C. P. King, B. Meyer, and A. Barka, 2003, "Slip Partitioning in the Sea of Marmara Pull-Apart Determined from GPS Velocity Vectors", *Geophysical Journal International,* pp. 1-7.

Gephart, J. W., and D. W. Forsyth 1984, "An Improved Method for Determining the Regional Stress Tensor Using Earthquake Focal Mechanism Data: Application to the San Fernando Earthquake Sequence", *Journal of Geophysical Research,* pp. 9305-9320.

Gephart, J.W., 1985, "Principal Stress Directions and the Ambiguity in Fault Plane Identification from Focal Mechanisms", *Bulletin of the Seismological Society of America*, Vol. 75, pp. 621–625.

Gephart, J.W., "FMSI: A Fortran Program for Inverting Fault/Slickenside and Earthquake Focal Mechanism Data to Obtain the Regional Stress Tensor", *Comprehensive Geoscience,* Vol. 16, pp. 953–989.

Görgün, E., 2008, *Analysis of the 17 August 1999 Mw 7.4 İzmit Earthquake Aftershocks and Monitoring of the Ganos Segment of the North Anatolian Fault Zone, NW Turkey,* Ph.D. Thesis, University of Potsdam,

Görgün, E., M. Bohnhoff, F. Bulut, and G. Dresen, 2010, "Seismotectonic Setting of the Karadere–Düzce Branch of the North Anatolian Fault Zone between the 1999 İzmit and Düzce Ruptures from Analysis of İzmit Aftershock Focal Mechanisms", *Tectonophysics,* pp. 170-181.

Gürbüz, C., M. Aktar, H. Eyidogan, A. Cisternas, H. Haessler, A. Barka, M. Ergin, N. Türkelli, O. Polat, S. B. Üçer, S. Kuleli, S. Baris, B. Kaypak, T. Bekler, E. Zor, F. Bicmen, and A. Yoruk, 2000, "The Seismotectonics of the Marmara Region (Turkey): Results from a Microseismic Experiment", *Tectonophysics,* pp. 1-17.

Hardebeck, J. L., and E. Hauksson, "Stress Orientations Obtained from Earthquake Focal Mechanisms: What Are Appropriate Uncertainty Estimates?", *Bulletin of the Seismological Society of America,* pp. 250-262.

Heidbach, O., A. Barth, P. Connolly, F. Fuchs, B. Müller, J. Reinecker, B. Sperner, M. Tingay, and F. Wenzel, 2004, "Stress Maps in a Minute: The 2004 Stress Map Release", *EOS,* Vol. 85(49), pp. 521-529.

Horiuchi S., K. Emura and T. Hirasawa, 1972, "Reliability of Pressure and Tension Axes Determined by Initial Motion of P-Waves from Deep Earthquakes in and near Japan", *the use of J.M.A. network (in Japanese with English abstract), Journal of the Seismological Society of Japan.,* Vol. 2, 25, pp. 92-104.

Horiuchi, S., G. Rocco, and A. Hasegawa, 1995, "Discrimination of Fault Planes from Auxiliary Planes Based on Simultaneous Determination of Stress Tensor and a Large Number of Fault Plane Solutions", *Journal of Geophysical Research,* pp. 8327-8338.

Ito, A., S. B. Ucer, S. Baris, Y. Honkura, A. Nakamura, T. Kono, R. Pektas, T. Komut, A. Hasegawa, and A. M. Isikara, 2002, "Aftershock Activity of 1999 İzmit Earthquake, Turkey, Revealed from Microearthquake Observations", *Bulletin of the Seismological Society of America,* pp. 418–427.

İmren, C., Le Pichon, X., C. Rangin, E. Demirbağ, B. Ecevitoğlu, and N. Görür, 2000, "The North Anatolian Fault within the Sea of Marmara: A New Interpretation Based on Multichannel Seismic and Multi-Beam Bathymetry Data", *Earth Planetary Science Letters,* Vol. 186, pp. 143-158.

Janssen, C., M. Bohnhoff, Y. Vapnik, E. Görgün, F. Bulut, B. Plessen, D. Pohl, M. Aktar, A. I. Okay, and G. Dressen, 2009, "Tectonic Evolution of the Ganos Segment of the North Anatolian Fault (NW Turkey)", *Journal of Structural Geology,* pp. 11-28.

Kahle, H.-G., M. Cocard, Y. Peter, A. Geiger, R. Reilinger, A. Barka, and G. Veis, 2000, "GPS-Derived Strain Rate Field within the Boundary Zones of the Eurasian, African, and Arabian Plates", *Journal of Geophysical Research*, Vol. 105, 23 353, pp. 23-370.

Kalafat, D., K. Kekovalı, Y. Güneş, M. Yılmazer, M. Kara, P. Deniz, M. Berberoğlu, 2009, "Türkiye ve Çevresi Faylanma-Kaynak Parametreleri (MT) Kataloğu", *(In Turkish) Boğaziçi University, Kandilli Observatory and Earthquake Research Institute.*

Karabulut, H., M. Bouin, M. Bouchon, M. Dietrich, C. Cornou, and M. Aktar, 2002, "The Seismicity in the Eastern Marmara Sea after the 17 August 1999 İzmit Earthquake", *Bulletin of the Seismological Society of America*, pp. 387-393.

Karabulut, H., S. Özalaybey, T. Taymaz, M. Aktar, O. Selvi, and A. Kocaoğlu, 2003, "A Tomographic Image of the Shallow Crustal Structure in the Eastern Marmara", *Geophysical Research Letters*, DOI:10.1029/2003GL018074.

Karabulut, H., J. Schmittbuhl, S. Özalaybey, O. Lengline, A. Kömeç-Mutlu, V. Durand, M. Bouchon, G. Daniel, and M. P. Bouin, 2011, "Evolution of the Seismicity in the Eastern Marmara Sea a Decade before and after the 17 August 1999 İzmit Earthquake", *Tectonophysics*, pp. 17-27.

Ketin, I., 1996, "6 Ekim 1964 Manyas Depremi Esnasında Zeminde Meydana Gelen Tansiyon Çatlakları", *Türkiye Jeoloji Kurumu Bülteni*, Vol. 10, pp. 1-2.

King, G. C. P., A. Hubert-Ferrari, S. S. Nalbant, B. Meyer, R. Armijo, and D. Bowman, 2001, "Coulomb Interactions and the 17 August İzmit, Turkey Earthquake", *Earth and Planetary Sciences*, pp. 557-569.

Kiratzi, A. A., 2002, "Stress Tensor Inversions along the Westernmost North Anatolian Fault Zone and Its Continuation into the North Aegean Sea", *Geophysical Journal International*, pp. 360-376.

Kostrov, B. V., and S. Das, 2005, *Principles of Earthquake Source Mechanics*, Chambridge Monographs on Mechanics and Applied Mathematics, USA.

Laigle, M., A. Becel, B. Voogd, A. Hirn, T. Taymaz and S. Özalaybey, 2008, “A First Deep Seismic Survey in the Sea of Marmara: Deep Basins and Whole Crust Architecture and Evolution”, *Earth and Planetary Science Letters,* Vol. 270, pp. 168–179.

Lay, T., and T. Wallace, 1995, *Modern Global Seismology*, USA.

Le Pichon, X., T. Taymaz, and A. M. C. Şengör, 1999, “The Marmara Fault and the Future İstanbul Earthquake”, *Proc. ITUIAHS International Conference on the Kocaeli Earthquake, İstanbul,* pp. 41-54.

Le Pichon, X., A.M.C. Şengör, E. Demirbağ, C. Rangın, C. İmren, R. Armıjo, N. Görür, N. Çağatay, B. Mercıer De Lepınay, B. Meyer, R. Saatçiler and B. Tok, 2001, “The Active Main Marmara Fault”, *Earth and Planetary Science Letters,* Vol. 192, pp. 595–616.

Lisle, R., T. Orife, and L. Arlegui, 2001, “A Stress Inversion Method Requiring only Fault Slip Sense”, *Journal of Geophysical Research, Solid Earth,* Vol. 106, pp. 2281–2289.

McClusky, S., R. Reilinger, S. Mahmoud, D. Ben Sari, and A. Tealeb, 2003, “GPS Constraints on Africa (Nubia) and Arabia Plate Motions”, *Geophysical Journal International,* pp. 126-138.

McKenzie, D., 1972, “Active Tectonics of the Mediterranean Region” *Geophysical Journal of the Royal Astronomical Society,* Vol. 30, pp. 109-185.

McKenzie, D., 1978, “Active Tectonics of the Alpine-Himalayan Belt: the Aegean Sea and Surrounding Regions”, *Geophysical Journal of the Royal Astronomical Society,* Vol. 55, pp. 217-254.

Meade, B. J., B. H. Hager, S. C. McClusky, R. E. Reilinger, S. Ergintav, L. Onur, A. Barka, and H. Özener, 2002, “Estimates of Seismic Potential in the Marmara Sea

Region from Block Models of Secular Deformation Constrained by Global Positioning System Measurements”, *Bulletin of the Seismological Society of America*, Vol. 92, pp. 208–215.

Michael, A. J., 1984, “Determination of Stress from Slip Data: Faults and Folds”, *Journal of Geophysical Research*, pp. 11,517-11.526.

Michael, A. J., 1987, “Use of Focal Mechanisms to Determine Stress: A Control Study”, *Journal of Geophysical Research*, Vol. 92, pp. 357–368.

Michael, A. J., 1987b, “Stress Rotation during the Coalinga Aftershock Sequence”, *Journal of Geophysical Research*, Vol. 92, pp. 7963–7979.

Motagh M., J. Hoffmann, B. Kampes, M. Baes, J. Zschau, 2007, “Strain Accumulation across the Gazikoy-Saros Segment of the North Anatolian Fault Inferred from Persistent Scatterer Interferometry and GPS Measurements”, *Earth Planet Science Letters*, Vol. 255, pp. 432-444.

Nowack, R. L., *Seismic Locations and Focal Mechanisms, Introduction to Seismology*, Purdue University, EAS 557, Lecture 17.

Okay, A., E. Demirbağ, H. Kurt, N. Okay, and I. Kuşçu, 1999, “An Active, Deep Marine Strike-Slip Basin along the North Anatolian Fault in Turkey”, *Tectonics*, Vol. 18, pp. 129-147.

Okay, A. I., A. Kaşlılar-Özcan, C. İmren, A. Boztepe-Güney, E. Demirbağ, and İ. Kuşçu, 2000, “Active Faults and Evolving Strike-Slip Basins in the Marmara Sea, Northwest Turkey: A Multichannel Seismic Reflection Study”, *Tectonophysics*, pp. 189-218.

Okay, A. I., O. Tüysüz, and Ş. Kaya, 2004, “From Transpression to Transtension: Changes in Morphology and Structure around a Bend on the North Anatolian Fault in the Marmara Region”, *Tectonophysics*, pp. 259-282.

Oncel, A. O., and T. Wilson, 2006, “Evaluation of Earthquake Potential along the Northern Anatolian Fault Zone in the Marmara Sea Using Comparisons of GPS Strain and Seismotectonic Parameters”, *Tectonophysics,* pp. 205-218.

Örgülü, G. and M. Aktar, 2001, “Regional Moment Tensor Inversion for Strong Aftershocks of the August 17, 1999 İzmit Earthquake (Mw = 7.4)”, *Geophysical Research Letters,* Vol. 28(2), pp. 371–374.

Örgülü, G., 2011, “Seismicity and Source Parameters for Small-Scale Earthquakes along the Splays of the North Anatolian Fault (NAF) in the Marmara Sea”, *Geophysical Journal International,* pp. 385-404.

Otsubo, M., A. Yamaji, and A. Kubo, 2008, “Determination of Stresses from Heterogeneous Focal Mechanism Data: An Adaptation of the Multiple Inverse Method”, *Tectonophysics,* pp. 150-160.

Özalaybey, S., M. Ergin, M. Aktar, C. Tapırdamaz, F. Biçmen, and A. Yörük, 2002, “The 1999 İzmit Earthquake Sequence in Turkey: Seismological and Tectonic Aspects”, *Bulletin of the Seismological Society of America,* pp. 376-386.

Parejas E., I. H. Akyol, and E. Altinli, 1942, “Le Tremblement de Terre d’Erzincan du 17 Decembre 1939”, *Rev. Fac. Sci. Univ. NVI,* pp. 177-222.

Parke, J.R., T. A. Minshull, G. Anderson, R. S. White, D. McKenzie, I. Kuşçu, J. M. Bull, N. Görür, and C. Şengör, 1999, “Active Faults in the Sea of Marmara, Western Turkey, Imaged by Seismic Refection Profiles”, *Terra Nova,* Vol. 11, pp. 223-227.

Pınar, A., Y. Honkura, and K. Kuge, 2001, “Seismic Activity Triggered by the 1999 İzmit Earthquake and Its Implications for the Assessment of Future Seismic Risk”, *Geophysical Journal International,* Vol. 146, F1–F7.

Pinar, A., K. Kuge, and Yoshimori Honkura, 2003, “Moment Tensor Inversion of Recent Small to Moderate Sized Earthquakes: Implications for Seismic Hazard and Active

Tectonics beneath the Sea of Marmara”, *Geophysical Journal International*, pp. 133-145.

Pinar, A., S. B. Ucer, Y. Honkura, N. Sezgin, A. Ito, S. Baris, D. Kalafat, M. Matsushima, and S. Horiuchi, 2009, “Spatial Variation of Stress Field Along the Fault Rupture Zone of the 1999 İzmit Earthquake”, *Earth Planets Space*, pp. 1-14.

Polat, O., H. Haessler, A. Cisternas, H. Philip, H. Eyidogan, M. Aktar, M. Frogneux, D. Comte, and C. Gürbüz, 2002, “The İzmit (Kocaeli), Turkey Earthquake of 17 August 1999: Previous Seismicity, Aftershocks, and Seismotectonics”, *Bulletin of the Seismological Society of America,* pp. 361-375.

Reasenberg, P.A. & D. Oppenheimer, 1985, “FPFIT, FPPLOT, and FPPAGE: Fortran Computer Programs for Calculating and Displaying Earthquake Fault Plane Solutions”, *Depth of Interior, US Geological Survey, Open-file report,* Vol. 109, pp. 85–739.

Reilinger, R., S. McClusky and P. Vernant, 2006, “GPS Constraints on Continental Deformation in the Africa–Arabia–Eurasia Continental Collision Zone and Implications for the Dynamics of Plate Interactions”, *Journal of Geophysical Reseach,* BO5411. DOI:10.1029/2005JB004051.

Reilinger, R., S. McClusky, D. Paradissis, S. Ergintav, and P. Vernant, 2010, “Geodetic Constraints on the Tectonic Evolution of the Aegean Region and Strain Accumulation along the Hellenic Subduction Zone “, *Tectonophysics,* pp. 22-30.

Rivera L. and A. Cisternas, 1990, “Stress Tensor and Fault Plane Solutions for a Population of Earthquakes”, *Bulletin of the Seismological Society of America,* Vol. 80 (3), pp. 600-614.

Robertson, A. H. F. and T. Ustaömer, 2004, “Tectonic Evolution of the Intra-Pontide Suture Zone in the Armutlu Peninsula, NW Turkey”, *Tectonophysics,* pp. 175-209.

Sato, T., J. Kasahara, T. Taymaz, M. Ito, A. Kamimura, T. Hayakawa, and O. Tan, 2004, "A Study of Microearthquake Seismicity and Focal Mechanisms within the Sea of Marmara (NW Turkey) Using Ocean Bottom Seismometers (OBSs)", *Tectonophysics*, pp. 303-314.

Sato, K., 2006, "Incorporation of Incomplete Fault-Slip Data into Stress Tensor Inversion", *Tectonophysics*, pp. 319-330.

Seeber, L., O. Emre, M.-H. Cormier, C. C. Sorlien, C. M. G. McHugh, A. Polonia, N. Ozer, and N. Cagatay, 2004, "Uplift and Subsidence from Oblique Slip: the Ganos–Marmara Bend of the North Anatolian Transform, Western Turkey", *Tectonophysics*, pp. 239-258.

Seeber, L., C. Sorlien, M. Steckler, and M.-H. Cormier, 2010, "Continental Transform Basins: Why Are They Asymmetric?", *EOS, Transactions of the American Geophysical Union*, Vol. 91, pp. 29–31.

Shan, Y.H., G. Lin, and Z. Li, 2004, "An Inverse Method to Determine the Optimal Stress from Imperfect Fault Data" *Tectonophysics*, Vol. 387, pp. 205–215.

Siyako, M., T. Tanş, and F. Şaroğlu, 2000, "Marmara Denizi Aktif Fay Geometrisi", *TUBITAK, Bilim Teknik Dergisi*, Vol. 388, pp. 66-71.

Smith, A. D., , T. Taymaz, F. Y. Oktay, H. Yüce, B. Alpar, H. Basaran, J. Jackson, S. Kara, and M. Şimşek, 1995, "High-Resolution Seismic Profiling in the Sea of Marmara (Northwest Turkey): Late Quaternary Sedimentation and Sea-Level Changes", *Bulletin of the Geological Society of America*, Vol. 107, pp. 923-936.

Snoke, J. A., 2003, "FOCMEC: Focal Mechanism Determinations, in International Handbook of Earthquake and Engineering Seismology", *Academic, San Diego, California*, Vol. 85, 12.

Sorlien, C., S. D. Akhun, L. Seeber, M. S. Steckler, D. J. Shillington, H. Kurt, G. Çiftçi, D. T. Poyraz, S. Gürçay, D. Dondurur, C. İmren, E. Perinçek, S. Okay, H. M. Küçük, and J. B. Diebold, 2012, "Uniform Basin Growth over the Last 500 ka, North Anatolian Fault, Marmara Sea, Turkey", *Tectonophysics,* Vol. 518-521, pp. 1-16.

Straub, C., H. G. Kahle, and C. Schindler, 1997, "GPS and Geological Estimates of the Tectonic Activity in the Marmara Sea Region, NW Anatolia", *Journal of Geophysical Research,* Vol. 102-27, pp. 587–601.

Suetsugu, D., 1996, "Source Mechanism Practice. In: Training Course in Seismology and Earthquake Engineering II". *Japan International Cooperation Agency (JICA), Ibaraki-ken 305 Japan*, pp. 13-48.

Şaroğlu, F., M. Emre, and M. Kuşçu, 1992, "Active Fault Map of Turkey", *General Directorate of Mineral Research.*

Taymaz, T., 1990, *Earthquake Source Parameters in the Eastern Mediterranean Region*, Ph.D. Thesis, Cambridge University.

Taymaz, T., J. Jackson, and D. McKenzie, 1991, "Active Tectonics of the North and Central Aegean Sea", *Geophysical Journal International,* pp. 433-490.

Taymaz, T., 2000, "Seismotectonics of the Marmara region: Source Characteristics of 1999 Gölcük-Sapanca-Düzce Earthquakes", in: A. Barka, Ö. Kozacı, S. H. Akyüz, E. Altunel, (Eds), 1999 İzmit-Düzce Earthquakes: Preliminary Results, *İstanbul Technical University Publ.,* pp. 79-97.

Tsukuda, E,, E. Herece, and I. Kuşçu, 1988, "Some Geological Evidence on Activity of the Western North Anatolian Fault, Geyve, İznik, Gemlik Area", *ITIT Project 8513,* pp. 68-91.

Tunç, B., D. Çaka, T. S. Irmak, H. Woith, S. Tunç, Ş. Bariş, M. F. Özer, B. G. Lühr, E. Günther, H. Grosser, and J. Zschau, 2011, "The Armutlu Network: An Investigation into the Seismotectonic Setting of Armutlu-Yalova-Gemlik and the Surrounding Regions", *Annals of Geophysics, 2011*. DOI: 10.4401/ag-4877.

Tüysüz, O., A. Barka, and E. Yiğitbaş, 1998, "Geology of the Saros Graben and its Implications for the Evolution of the North Anatolian Fault in the Ganos–Saros Region, Northwestern Turkey", *Tectonophysics,* pp. 105-126.

Twiss, R. J., and E. M. Moores, 1992, "Structural Geology", *W.H. Freeman and Company, New Yor*k.

Üçer, B., 2011, *SEISAN*, Oral Communication.

Wong, H. K., T. Lüdmann, A. Ulug, and N. Görür, 1995, "The Sea of Marmara: A Plate Boundary Sea in an Escape Tectonic Regime", *Tectonophysics,* pp. 231-250.

Wright, T., E. Fielding, and B. Parsons, 2001, "Triggered Slip: Observations of the 17 August 1999 İzmit (Turkey) Earthquake Using Radar Interferometry", *Geophysical Research Letters,* Vol. 28, pp. 1079– 1082, DOI:10.1029/2000GL011776.

Yaltırak, C., 1996, "Tectonic History of the Ganos Fault System" *(in Turkish with English abstract), Bulletin of the Turk Association Petroleum Geology,* Vol. 8, pp. 137-156.

Yaltırak, C., 2002, "Tectonic Evolution of the Marmara Sea and Its Surroundings", *Marine Geology*, pp. 493-529.

Yaltırak, C., and B. Alpar, 2002, "Evolution of the Middle Strand of North Anatolian Fault and Shallow Seismic Investigation of the Southeastern Marmara Sea (Gemlik Bay)", *Marine Geology,* pp. 307-327.

Yaltırak, C., M. K. Erturaç, O. Tüysüz, and K. Saki-Yaltırak, 2003, "Marmara Denizi'nde Tarihsel Depremler: Yerleri, Büyüklükleri, Etki Alanları ve Güncel Kırılma Olasılıkları", *Kuvaterner Çalıştayı (Turkish),* pp. 174-180.

Yılmaz, Y., E. Gökaşan, and A. Y. Erbay, 2010, "Morphotectonic Development of the Marmara Region", *Tectonophysics*, pp. 51-70.

Zachariasen, J. and K. Sieh, 1995, "The Transfer of Slip between, En Echelon Strike-Slip Faults: A Case Study from the 1992 Landers Earthquake, Southern California", *Journal of Geophysical Research*, Vol. 100-15, pp. 281-301.

APPENDIX A. LIST OF STATIONS

Table A1. List of 40 BB stations of Kandilli Observatory & Earthquake Research Institute

No	Station Name	Seismometer Type	Lat.	Lon.	Elevation	Starting Date	Org. Name
1	ADVT	CMG-3T	40.4332	29.7383	193	05.19.2006	KOERI
2	ALT	CMG-3T	39.0552	30.1103	1060	03.31.2007	KOERI
3	ARMT	CMG-3ESP	40.5683	28.866	320	12.17.2007	KOERI
4	BALB	CMG-3T	39.64	27.88	120	06.05.2007	KOERI
5	BGKT	CMG-3ESP	41.181	28.773	80	05.29.2007	KOERI
6	CANB	CMG-6TD	40.0167	2703.75	229	2004	KOERI
7	CAVI	CMG-3ESP	40.2018	29.8377	670	09.27.2007	KOERI
8	CRLT	CMG-3ESP	41.129	27.736	230	05.16.2007	KOERI
9	CTKS	CMG-3ESP	41.2373	28.5072	47	09.28.2007	KOERI
10	CTYL	CMG-3T	41.476	28.2897	77	09.29.2007	KOERI
11	EDC	CMG-3T	40.3468	27.8633	269	11.27.2008	KOERI
12	EDRB	CMG-3T	41.847	26.7437	209	04.18.2007	KOERI
13	ENEZ	CMG-3T	40.7362	26.153	100	06.21.2006	KOERI
14	ERIK	CMG-3ESP	40.6708	26.5132	35	07.02.2008	KOERI
15	EZN	CMG-3ESP	39.8267	26.3258	48	11.09.2007	KOERI
16	GADA	CMG-3T	40.1908	25.8987	130	07.06.2006	KOERI
17	GELI	CMG-3ESP	40.398	26.4742	130	07.05.2008	KOERI
18	GEMT	CMG-3T	40.435	29.189	220	07.07.2006	KOERI
19	GONE	CMG-3ESP	40.0467	27.686	140	06.27.2008	KOERI
20	GULT	CMG-3ESP	40.432	30.515	930	09.15.2007	KOERI
21	HRTX	CMG-3ESP	40.8217	29.668	645	06.25.2008	KOERI
22	ISK	CMG-3T	41.0657	29.0592	132	01.25.2007	KOERI
23	KCTX	CMG-3ESP	40.2625	28.3353	445	07.11.2008	KOERI
24	KDZE	CMG-3T	41.3132	31.443	410	07.01.2006	KOERI
25	KLYT	CMG-3T	41.253	29.042	30	05.18.2006	KOERI
26	KRBG	CMG-3ESP	40.3932	27.2977	75	06.27.2008	KOERI
27	LAP	CMG-3ESP	40.3727	26.7602	200	12.27.2007	KOERI

28	MDNY	CMG-3ESP	40.3708	28.8847	115	07.09.2008	KOERI
29	MDUB	CMG-3T	40.4712	31.1978	1108	05.22.2008	KOERI
30	MFTX	CMG-40T	40.7867	27.2812	924	10.10.1998	KOERI
31	MRMT	CMG-3T	40.6058	27.5837	702	10.09.2008	KOERI
32	PHSR	CMG-40T	41.6308	27.5238	263	07.09.2009	KOERI
33	RKY	CMG-3ESP	40.6875	27.1777	687	05.16.2006	KOERI
34	SILT	CMG-3ESP	41.153	29.643	100	05.31.2007	KOERI
35	SLVT	CMG-3ESP	41.23	28.21	180	06.01.2007	KOERI
36	SPNC	CMG-3ESP	40.686	30.3083	190	06.27.2008	KOERI
37	SVRH	CMG-3T	39.447	31.5232	1000	12.27.2007	KOERI
38	TKR	CMG-3ESP	40.9902	27.5357	140	05.18.2007	KOERI
39	TVSB	CMG-3ESP	39.4497	29.4615	1090	02.12.2009	KOERI
40	YLVX	CMG-40T	40.5667	29.3728	829	10.21.1998	KOERI

Table A2. List of 50 Stations of the TURDEP Project

No	**Station Name**	**Seismometer Type**	**Lat.**	**Lon.**	**Elevation**	**Starting Date**	**Org. Name**
1	ALET	CMG-LE3D	41.06624	28.60557	91	10.20.2009	TUBITAK
2	ALTM	CMG-3ESPC	41.08800	28.74000	18	07.25.2006	TUBITAK
3	ARCE	CMG-J	40.82616	29.36025	45	07.09.2009	TUBITAK
4	ATIM	CMG-3T	40.08300	27.56333	230	01.24.2008	TUBITAK
5	BAHT	CMG-LE3D	41.08783	28.69179	142	10.12.2009	TUBITAK
6	BEY2	CMG-LE3D	41.00294	28.64531	170	03.18.2010	TUBITAK
7	BEYT	CMG-LE3D	41.00459	28.63510	214	10.07.2009	TUBITAK
8	BOZM	CMG-40T	40.53400	28.78200	119	04.28. 2007	TUBITAK
9	BUYM	CMG-3T	40.85233	29.11800	231	11.30.2006	TUBITAK
10	BZGM	CMG-40T	40.17267	26.9865	180	07.11.2008	TUBITAK
11	CAN	CMG- ---	40.0275	2703.77	200	---	TUBITAK
12	CALI	CMG-L4C	40.16519	28.92000	179	02.10.2011	TUBITAK
13	CMHM	CMG-3ESPC	40.01200	27.97000	205	09.05.2006	TUBITAK
14	EREM	CMG-3ESPC	40.04533	28.89117	657	03.29.2007	TUBITAK
15	ESKM	CMG-40T	40.60683	28.94533	20	08.31.2006	TUBITAK
16	GBZM	CMG-3ESPC	40.78600	29.45000	270	07.08.2005	TUBITAK

17	GOZT	CMG-J	40.89078	29.25363	213	07.13.2009	TUBITAK
18	IBBT	CMG-J	40.86608	29.32315	115	07.09.2009	TUBITAK
19	IGDM	CMG-3ESPC	40.26400	29.20133	165	03.27.2007	TUBITAK
20	ISU2	CMG-LE3D	40.99775	28.72363	96	03.23.2010	TUBITAK
21	ISUT	CMG-LE3D	40.98875	28.72382	85	10.08.2009	TUBITAK
22	KLCM	CMG-3ESPC	40.63300	29.39800	138	09.01.2006	TUBITAK
23	KKZM	CMG-40T	41.11600	27.34400	150	07.28.2006	TUBITAK
24	KMRM	CMG-3ESPC	40.41800	27.06900	40	09.09.2006	TUBITAK
25	KNLM	CMG-40T	40.27000	27.52600	178	09.05.2006	TUBITAK
26	KRCM	CMG-3ESPC	40.26517	28.33233	443	03.30.2007	TUBITAK
27	KURN	CMG-J	40.95496	29.33150	210	16.07.2009	TUBITAK
28	KVKM	CMG-3ESPC	40.60400	26.88767	75	07.03.2007	TUBITAK
29	MADM	CMG-40T	40.65367	27.66467	40	09 06.2006	TUBITAK
30	MARM	CMG-40T	40.96700	27.96100	43	07.27 2006	TUBITAK
31	MSDM	CMG-40T	40.34950	28.60033	201	04.01.2007	TUBITAK
32	MYCM	CMG-40T	41.03250	27.71333	99	07.03.2008	TUBITAK
33	NEVM	CMG-3T	39.95400	27.26300	329	10.17.2006	TUBITAK
34	NUKT	CMG-LE3D	41.02651	28.75885	56	10.07.2009	TUBITAK
35	OMRT	CMG-LE3D	40.97066	28.60385	56	10.09.2009	TUBITAK
36	SABA	CMG-J	40.89365	29.38134	161	07.13.2009	TUBITAK
37	SAKI	CMG-J	40.83204	29.27543	50	16.07.2009	TUBITAK
38	SGTM	CMG-40T	40.76683	27.10783	295	---	TUBITAK
39	SLVM	CMG-3T	41.07312	28.14034	30	05.05.2008	TUBITAK
40	SNLM	CMG-3ESPC	41.22800	28.20900	173	07.26.2006	TUBITAK
41	TEPT	CMG-LE3D	41.06394	28.50939	91	10.13.2009	TUBITAK
42	TRNM	CMG-40T	40.50500	27.77800	80	01.00.2006	TUBITAK
43	YNKM	CMG-3ESPC	40.82567	27.39667	370	03.27.2007	TUBITAK
44	BALY	CMG-3T	39.74033	27.61933	645	05.24.2007	AFAD
45	BOZC	CMG-3T	39.84190	26.0528	195	10.18.2006	AFAD
46	DURS	CMG-3T	39.60100	28.47000	960	06.06.2007	AFAD
47	ELBA	CMG-3T	41.14667	28.43050	331	09.29.2005	AFAD
48	SART	CMG-3T	40.68883	27.18000	679	09.11.2007	AFAD
49	EADA	CMG-6T	40.82117	29.29050	6	02.19.2009	SENTEZ
50	SYY1	CMG-6T	40.94417	29.12667	30	05.05.2008	SENTEZ

Table A3. List of 10 Short-period stations of Kandilli Observatory & Earthquake Research Institute

No	Station Name	Seismometer Type	Latitude	Longitude	Elevation	Organization Name
1	BADT	-	4051.14	2907.05	175	KOERI
2	BNT	SS-1	40.3542	27.8950	353	KOERI
3	DST	L4-C	39.6040	28.6192	625	KOERI
4	ESKT	CMG-40V	39.5222	30.8497	1289	KOERI
5	EYL	Willmor	40.5658	30.1250	1160	KOERI
6	GPA	CMG-40V	40.2863	30.3183	560	KOERI
7	HRT	-	4049.30	2940.08	645	KOERI
8	IZI	Willmor	40.3368	29.4728	910	KOERI
9	ORLT	Mark	40.0462	28.8958	649	KOERI
10	OSM	-	4036.12	2942.00	820	KOERI

Table A4. List of 5 SBO stations of Kandilli Observatory & Earthquake Research Institute

No	Station Name	Latitude	Longitude	Elevation	Starting Date	Organization
1	SBO1	40.705638	29.149183	-1260	31.12.2010	KOERI
2	SBO2	40.878619	28.514247	-810	03.11.2010	KOERI
3	SBO3	40.884783	27.975100	-1204	21.01.2011	KOERI
4	SBO4	40.828184	27.535460	-1114	22.12.2010	KOERI
5	SBO5	40.631132	28.880385	-368	09.06.2010	KOERI

APPENDIX B. LIST OF EARTHQUAKES

Table B 1. Relocations and fault plane solutions of 85 earthquakes in the Ganos Offshore

No	Date	Time	Lat.	Lon.	Dep.	ML	Erlt	Erln	Erdp	GAP	P(Az)	P(Pl)	T(Az)	T(Pl)	Strike	Dip	Rake	Pl	In	H.In
1	24.10.2006	09:22	40.776	27.501	8.0	2.0	1.9	1.9	5.0	90	11.2	84.9	81.0	5	355.94	46.84	-83.41	12	0	0
2	15.11.2006	15:51	40.727	27.472	9.1	2.2	1.0	1.4	5.3	62	142.6	7.3	43.3	51.5	81.95	62.39	133.45	11	0	0
3	20.11.2006	01:36	40.765	27.464	10.0	2.7	1.3	1.4	3.6	132	283.8	20	44.7	54.7	171.95	70.41	60.36	16	0	0
4	14.01.2007	16:35	40.771	27.454	15.5	3.8	1.2	1.6	1.7	65	105.1	30.2	214.6	29.8	159.77	89.76	-45.01	31	0	0
5	22.01.2007	01:07	40.703	27.409	2.0	2.2	1.2	1.4	1.8	67	355.1	27.3	253.9	20.6	125.72	85.67	-144.9	12	0	0
6	05.02.2007	11:44	40.732	27.417	13.5	3.6	1.3	1.6	2.1	65	316.8	9.8	204.1	66	244.98	58.28	115.8	21	0	0
7	08.05.2007	04:30	40.759	27.511	14.1	3.5	1.8	2.3	3.0	86	291.6	32.1	178.4	32.1	55.00	90.00	-131.3	20	0	1
8	26.05.2007	22:41	40.666	27.493	3.7	2.2	1.5	2.1	4.2	56	175.0	79.1	380.4	9.8	286.39	54.99	-95.60	14	0	1
9	27.05.2007	19:43	40.735	27.347	12.3	3.4	1.4	2.2	2.5	46	121.5	7.4	224.8	60.7	8.17	58.28	56.27	20	0	0
10	02.06.2007	17:10	40.789	27.508	12.4	2.1	1.1	1.8	2.9	73	147.6	85.2	55.2	0.2	320.44	45.40	-96.74	12	0	0
11	16.06.2007	23:47	40.710	27.370	8.7	2.5	1.3	1.5	2.9	65	320.9	2.9	60.7	73.6	216.02	50.00	68.73	17	0	1
12	24.06.2007	12:44	40.759	27.398	9.9	2.2	1.2	1.5	2.0	50	319.8	36.7	205.3	29.1	84.13	85.49	-129.8	14	0	1
13	03.08.2007	04:18	40.795	27.501	12.1	2.2	1.1	1.6	2.6	77	314.1	76.9	170.5	10.6	73.92	56.04	-99.17	13	0	0
14	27.08.2007	18:59	40.767	27.434	2.0	3.0	0.8	1.2	2.8	54	282.4	28.7	23.5	19.3	331.22	83.93	-35.22	19	0	0
15	08.09.2007	21:16	40.701	27.474	4.9	2.4	0.9	1.6	4.1	62	147.6	85.2	55.2	0.2	320.44	45.40	-96.74	16	0	0
16	17.09.2007	18:02	40.676	27.486	0.7	2.5	0.8	1.1	1.2	57	118.9	14.5	219.0	34.1	352.69	77.33	36.01	12	0	0
17	08.10.2007	14:06	40.711	27.411	7.6	3.7	0.9	1.0	2.2	53	307.1	24.9	215.6	3.2	84.03	75.04	-159.6	34	0	1
18	12.01.2008	17:43	40.788	27.497	15.7	3.0	1.0	1.1	1.4	72	322.3	66	63.5	5	353.86	54.22	-60.67	32	0	0

No	Date	Time	Lat.	Lon.	Dep.	ML	Erlt	Erln	Erdp	GAP	P(Az)	P(Pl)	T(Az)	T(Pl)	Strike	Dip	Rake	Pl	In	H.In
19	12.01.2008	17:49	40.787	27.499	15.4	2.6	0.9	1.0	1.4	46	339.0	36.8	244.4	6.2	117.38	69.67	-147.8	26	0	0
20	28.03.2008	01:04	40.787	27.552	14.5	3.1	0.9	1.0	1.8	65	47.6	85	34.6	5	303.37	45.08	-91.60	36	0	1
21	19.05.2008	20:31	40.804	27.568	13.0	2.5	0.9	1.0	2.0	52	333.0	8.4	233.0	49.7	273.04	64.15	134.44	29	0	1
22	21.05.2008	12:52	40.687	27.447	2.0	2.0	0.9	1.0	1.2	70	139.5	13.7	231.3	7.4	184.83	85.62	-15.03	12	0	0
23	05.07.2008	11:23	40.703	27.449	7.5	2.3	0.9	1.0	3.5	58	297.8	42.8	137.3	45.5	217.32	88.63	99.89	14	0	0
24	14.07.2008	16:02	40.740	27.353	13.5	3.7	1.1	1.1	1.6	60	136.9	32.4	32.1	21.9	266.58	83.39	-139.7	30	0	0
25	14.07.2008	21:05	40.716	27.397	2.1	2.2	0.7	1.0	2.8	51	325.3	48.2	59.6	3.8	1.99	61.30	-40.88	20	0	0
26	26.07.2008	04:33	40.745	27.315	3.8	2.3	1.0	1.1	2.9	120	160.6	34.9	46.1	30.7	284.22	87.50	-130.0	20	0	1
27	07.08.2008	21:44	40.679	27.478	1.5	2.2	0.9	1.0	1.2	50	329.3	14.5	222.2	48.6	267.83	69.31	130.85	12	0	0
28	17.09.2008	12:51	40.728	27.359	6.5	2.1	1.3	2.0	4.9	92	288.9	50.1	73.2	34.2	358.72	81.66	-71.77	12	0	0
29	20.09.2008	22:54	40.721	27.400	3.0	2.5	1.0	1.1	2.8	31	291.2	41.3	58.1	34.4	353.31	86.15	-60.21	20	0	1
30	05.10.2008	22:25	40.796	27.565	2.6	2.0	0.9	1.3	3.2	86	209.1	67.5	69.5	17.5	328.23	63.86	-105.3	12	0	0
31	07.10.2008	04:36	40.762	27.537	7.2	2.0	0.8	1.1	3.5	71	294.8	72.9	67.0	11.7	347.49	57.82	-75.40	15	0	1
32	16.11.2008	15:12	40.755	27.399	11.7	2.8	0.9	1.1	1.5	47	304.3	21.3	149.3	66.7	221.68	66.89	99.75	27	0	0
33	19.11.2008	10:48	40.699	27.409	3.3	2.0	1.3	1.6	4.4	64	221.8	69.2	382.4	19.7	297.68	65.00	-82.96	15	0	0
34	06.12.2008	06:19	40.764	27.540	8.5	2.0	1.0	1.4	4.5	60	347.9	29.4	246.9	18.7	119.37	83.08	-144.7	14	0	0
35	30.01.2009	14:29	40.722	27.368	3.6	2.5	1.0	1.3	3.1	75	316.8	9.8	204.1	66	244.98	58.28	115.77	16	1	1
36	30.01.2009	15:40	40.742	27.384	3.5	2.3	0.9	1.2	2.6	79	288.2	26.1	68.0	57.3	183.30	73.51	70.94	19	0	1
37	03.02.2009	21:06	40.772	27.405	4.4	2.5	0.9	1.3	2.7	73	124.3	46	28.8	5.3	265.74	63.68	-140.2	24	0	1
38	01.03.2009	01:11	40.833	27.563	11.5	2.9	0.8	1.0	1.6	62	292.8	69.4	489.0	19.8	34.61	65.03	-95.85	34	0	0
39	01.03.2009	01:12	40.821	27.570	4.1	2.4	0.7	1.0	2.5	60	241.0	61.1	97.3	24	354.92	70.64	-106.1	19	0	0
40	01.03.2009	01:22	40.834	27.566	11.7	2.9	0.9	1.0	1.6	63	244.8	76.1	375.5	9.2	294.55	55.00	-77.32	34	0	1
41	01.03.2009	03:03	40.825	27.568	5.2	2.0	0.7	1.0	2.5	60	231.8	63.6	84.4	22.7	343.94	68.87	-103.7	19	0	0

No	Date	Time	Lat.	Lon.	Dep.	ML	Erlt	Erln	Erdp	GAP	P(Az)	P(Pl)	T(Az)	T(Pl)	Strike	Dip	Rake	Pl	In	H.In
42	01.03.2009	06:58	40.833	27.565	8.1	2.5	0.8	0.8	3.6	123	278.6	59.6	504.4	22.3	38.55	70.02	-110.9	16	0	0
43	01.03.2009	21:40	40.827	27.560	10.0	2.2	0.8	1.3	3.4	60	303.0	57.6	162.9	25.9	58.21	73.26	-108.8	18	0	0
44	25.03.2009	01:46	40.788	27.559	14.5	2.4	1.1	1.4	2.6	59	295.4	41.4	514.6	41.4	45.00	90.00	-110.8	17	1	1
45	05.04.2009	13:41	40.737	27.402	4.7	2.3	0.9	1.1	2.8	62	120.6	5.6	218.5	54.2	2.29	59.72	48.10	16	0	0
46	20.04.2009	10:44	40.706	27.496	11.6	3.4	0.8	1.0	1.7	37	126.5	34.2	222.2	8.3	169.72	72.82	-31.53	46	0	0
47	27.04.2009	19:03	40.728	27.537	14.5	4.4	0.9	1.1	1.5	55	96.7	76.6	193.3	1.6	115.94	48.06	-71.98	58	0	0
48	27.04.2009	19:34	40.730	27.539	11.6	2.7	0.8	0.9	1.4	35	100.1	25.6	8.7	2.9	237.25	74.35	-159.2	33	0	0
49	25.06.2009	04:36	40.729	27.367	8.8	2.4	0.7	0.9	2.0	47	304.3	21.3	149.3	66.7	221.68	66.89	99.75	21	0	0
50	25.06.2009	04:38	40.719	27.372	4.1	2.3	0.8	0.8	2.1	46	306.1	10.7	164.3	76.4	223.20	56.24	99.90	19	0	0
51	25.06.2009	04:47	40.722	27.370	8.1	2.6	0.7	0.8	2.4	43	7.2	69.6	37.7	13.3	322.43	44.53	-73.44	22	0	1
52	25.06.2009	04:49	40.724	27.372	6.9	2.5	0.7	0.8	2.7	58	310.6	18.9	175.4	64.3	234.30	65.90	108.46	16	0	0
53	17.08.2009	23:46	40.757	27.426	2.1	2.3	0.7	0.9	0.9	63	301.1	25.6	209.3	3.8	78.00	75.01	-158.6	17	0	0
54	25.08.2009	05:34	40.698	27.524	9.4	3.2	0.7	1.0	1.8	27	193.7	64.3	391.4	24.7	295.70	70.01	-97.32	34	0	0
55	24.09.2009	11:46	40.752	27.384	7.9	2.5	0.8	1.1	3.1	63	310.4	14.8	151.6	74.2	225.01	60.01	96.31	18	0	0
56	04.11.2009	01:30	40.734	27.376	9.3	2.5	0.9	1.3	2.8	58	123.6	20.3	221.8	21.1	352.83	89.47	29.99	14	0	0
57	04.11.2009	17:46	40.723	27.432	11.7	2.8	1.1	1.3	2.2	65	121.5	7.4	224.8	60.7	8.17	58.28	56.27	22	0	0
58	07.11.2009	05:10	40.786	27.506	17.4	2.9	1.0	1.2	1.8	37	339.0	36.8	244.4	6.2	117.38	69.67	-147.8	34	0	1
59	26.11.2009	16:44	40.724	27.354	11.8	2.4	1.0	1.3	1.8	55	316.8	9.8	204.1	66	244.98	58.28	115.77	28	0	0
60	04.12.2009	07:58	40.698	27.419	2.1	2.1	1.2	1.0	3.7	111	315.7	27.3	187.8	50	247.26	77.44	117.50	19	0	0
61	04.12.2009	20:36	40.711	27.427	2.5	2.0	1.0	1.0	3.2	66	338.0	23.4	233.0	30.8	284.05	85.34	139.82	17	0	0
62	14.12.2009	18:20	40.698	27.490	7.2	2.6	0.7	0.8	3.8	47	298.2	47.6	58.7	24.9	353.64	77.03	-57.26	29	0	1
63	24.12.2009	04:23	40.675	27.523	7.6	2.2	1.0	1.2	3.6	41	319.8	36.7	205.3	29.1	84.13	85.49	-129.8	22	0	0
64	25.12.2009	06:36	40.739	27.396	4.0	2.2	1.0	1.1	2.8	113	287.5	33.7	62.4	46.6	177.22	83.03	65.93	11	0	0

No	Date	Time	Lat.	Lon.	Dep.	ML	Erlt	Erln	Erdp	GAP	P(Az)	P(Pl)	T(Az)	T(Pl)	Strike	Dip	Rake	Pl	In	H.In
65	04.01.2010	15:08	40.802	27.557	11.4	2.3	0.9	1.1	2.2	107	300.3	47.1	148.5	39.3	45.32	85.98	-104.5	14	0	1
66	19.01.2010	17:36	40.808	27.556	14.1	3.0	0.8	1.0	1.5	58	311.0	79.3	150.0	10.1	57.02	55.20	-94.16	25	0	0
67	28.01.2010	03:05	40.804	27.557	11.5	2.0	0.7	1.1	2.0	103	311.0	79.3	150.0	10.1	57.02	55.20	-94.16	18	0	1
68	26.02.2010	10:55	40.726	27.424	2.2	2.1	0.8	0.9	2.7	56	232.3	62.8	382.2	23.9	302.13	69.99	-77.11	15	0	0
69	03.03.2010	13:13	40.720	27.383	10.0	3.0	1.1	1.3	2.6	79	300.3	47.1	148.5	39.3	45.32	85.98	-104.5	18	0	0
70	20.03.2010	07:24	40.775	27.535	13.9	2.0	1.0	1.0	2.6	119	297.1	36.3	127.9	53.3	211.70	81.46	95.24	15	0	0
71	20.04.2010	15:30	40.742	27.344	2.2	3.1	0.8	1.0	2.8	60	110.8	19.5	15.2	15.3	243.60	87.17	-155.0	27	0	0
72	09.06.2010	16:57	40.693	27.384	3.6	3.0	0.8	1.0	2.7	67	133.9	6.2	252.5	77.2	33.87	52.18	75.83	23	0	0
73	01.07.2010	00:57	40.709	27.497	12.1	2.5	1.3	1.2	2.5	69	68.0	74.7	183.9	6.8	105.99	53.26	-72.89	21	0	1
74	15.08.2010	12:11	40.783	27.509	11.4	3.3	0.8	0.9	1.7	43	160.8	47.4	47.1	20.3	289.98	74.03	-127.2	29	0	0
75	26.08.2010	05:24	40.675	27.530	5.6	2.0	0.7	0.9	1.5	55	334.8	79.8	164.9	10	73.37	55.05	-92.14	10	0	0
76	22.09.2010	03:34	40.751	27.474	9.1	2.2	0.9	1.0	2.8	67	325.9	78.3	61.7	1.2	342.89	47.34	-74.08	13	0	0
77	03.10.2010	13:55	40.747	27.434	13.1	2.6	0.8	1.1	2.0	75	276.2	18.3	24.4	43.3	155.76	74.76	47.13	19	0	0
78	24.10.2010	15:20	40.715	27.530	8.5	2.2	0.8	0.8	2.8	66	110.7	40.8	213.8	14.8	156.73	73.65	-42.02	23	1	1
79	11.12.2010	07:39	40.740	27.418	8.1	2.8	0.9	1.2	2.9	59	304.3	21.3	149.3	66.7	221.68	66.89	99.75	14	0	0
80	23.12.2010	13:04	40.748	27.370	3.7	2.7	0.9	0.9	2.6	62	277.5	30.8	382.1	22.9	328.25	85.01	-39.77	22	0	0
81	24.12.2010	09:54	40.730	27.395	2.3	2.2	0.7	0.9	2.6	71	314.1	17.8	68.6	52.2	199.29	69.97	55.58	17	0	0
82	18.02.2011	00:52	40.787	27.502	11.9	3.2	1.0	1.3	1.5	45	118.5	29.2	219.5	18.8	167.09	83.28	-35.24	31	0	0
83	03.03.2011	11:07	40.666	27.533	6.9	2.7	0.7	0.8	3.2	40	288.6	41.8	70.8	41.5	359.65	89.84	-69.99	16	0	0
84	07.03.2011	14:48	40.716	27.513	10.3	2.5	1.0	1.4	2.7	54	293.2	40.9	53.5	30.3	351.17	83.90	-55.48	11	0	0
85	23.03.2011	23:12	40.667	27.489	16.5	2.9	0.9	1.0	1.6	46	114.5	11.1	19.5	23.9	65.14	81.35	154.69	35	0	0

“ML” values are determined by TUBITAK. Erlt, Erln, Erdp values indicate latitude, longitude, and depth errors, respectively. The given P(Az, Pl), T(Az, Pl) and Strike/Dip/Rake values are obtained by the stress tensor inversion approach of the Horiuchi *et al.* (1995). “Pl” indicates the value of the polarity used for each event, and “In” shows the value of the inconsistency obtained using Focmec software with 1 degree of grid search for each source mechanism. “H.In” signifies the value of the inconsistency obtained by the program of Horiuchi *et al.* (1995) with five-degree grid search interval for each source mechanism.

Table B 2. Relocations and fault plane solutions of 75 earthquakes in the Tekirdağ Basin

No	Date	Time	Lat.	Lon.	Dep.	ML	Erlt	Erln	Erdp	GAP	P(Az)	P(Pl)	T(Az)	T(Pl)	Strike	Dip	Rake	Pl	In	H.In
1	23.12.2006	07:48	40.800	27.783	13.5	2.5	1.1	1.7	2.7	73	271.9	80	90.3	10	0.54	55.00	-89.67	14	0	1
2	10.07.2007	20:35	40.826	27.744	13.6	2.2	1.3	1.5	2.3	77	144.3	68	354.7	19.2	256.19	64.97	-101.4	19	0	0
3	10.01.2008	16:35	40.814	27.744	13.1	1.9	0.9	1.3	2.6	82	127.7	47.5	243.6	21.8	180.01	75.01	-54.26	15	0	0
4	10.01.2008	16:39	40.822	27.740	14.5	2.3	0.9	1.2	1.9	68	106.8	48	349.9	22.2	233.99	75.03	-124.9	30	0	1
5	27.01.2008	13:40	40.812	27.724	9.6	2.9	1.1	1.1	2.1	44	313.1	20.4	54.6	28.2	185.29	84.97	35.65	32	1	1
6	27.01.2008	18:55	40.807	27.725	9.9	3.2	1.0	1.2	2.0	43	141.4	17.2	232.3	2.9	185.60	80.02	-14.40	47	1	1
7	29.01.2008	19:05	40.787	27.726	10.0	2.0	1.2	1.8	3.9	127	162.5	38.3	405.7	29.7	285.89	84.96	-127.7	10	0	0
8	07.02.2008	04:02	40.804	27.735	10.7	2.3	1.2	1.4	3.0	75	305.4	55.9	525.3	27.5	60.03	74.98	-109.3	27	0	0
9	21.02.2008	08:45	40.810	27.735	7.4	3.6	0.9	1.1	2.6	49	8.3	69.9	223.7	16.6	124.57	62.48	-102.4	37	0	0
10	01.07.2008	22:51	40.798	27.764	6.4	2.3	0.9	1.2	4.1	50	305.4	55.9	525.3	27.5	60.03	74.98	-109.3	13	0	0
11	05.07.2008	20:45	40.812	27.768	9.8	2.0	1.1	1.2	5.0	126	94.8	64.4	284.2	25.3	191.16	70.40	-93.88	10	0	0
12	18.08.2008	00:27	40.804	27.732	6.3	2.0	0.8	0.9	3.2	44	313.1	20.4	54.6	28.2	185.29	84.97	35.65	32	0	1
13	27.08.2008	21:02	40.827	27.689	4.2	2.6	1.0	1.2	3.4	55	271.9	80	90.3	10	0.54	55.00	-89.67	33	0	0
14	13.09.2008	02:20	40.796	27.727	3.0	2.2	1.5	1.8	4.6	43	144.3	68	354.7	19.2	256.19	64.97	-101.4	17	0	0
15	30.09.2008	12:40	40.794	27.712	3.0	2.2	1.4	1.9	4.8	83	127.7	47.5	243.6	21.8	180.01	75.01	-54.26	20	0	0

No	Date	Time	Lat.	Lon.	Dep.	ML	Erlt	Erln	Erdp	GAP	P(Az)	P(Pl)	T(Az)	T(Pl)	Strike	Dip	Rake	Pl	In	H.In
16	01.10.2008	23:47	40.791	27.724	2.8	2.5	1.5	1.9	4.6	80	106.8	48	349.9	22.2	233.99	75.03	-124.9	25	1	1
17	02.10.2008	00:22	40.794	27.712	2.3	2.0	1.2	1.4	3.3	83	313.1	20.4	54.6	28.2	185.29	84.97	35.65	15	0	0
18	02.10.2008	05:41	40.806	27.781	11.1	2.5	1.3	1.5	2.5	50	141.4	17.2	232.3	2.9	185.60	80.02	-14.40	21	1	1
19	16.01.2009	19:13	40.781	27.740	4.5	2.0	1.3	1.5	4.6	52	162.5	38.3	405.7	29.7	285.89	84.96	-127.7	21	0	1
20	23.01.2009	16:34	40.796	27.752	14.1	3.7	1.3	1.5	2.5	40	305.4	55.9	525.3	27.5	60.03	74.98	-109.3	65	0	0
21	23.01.2009	17:58	40.786	27.749	14.7	2.2	1.6	1.9	3.6	43	8.3	69.9	223.7	16.6	124.57	62.48	-102.4	21	0	0
22	23.01.2009	19:51	40.790	27.744	13.1	2.6	1.3	1.8	3.7	44	305.4	55.9	525.3	27.5	60.03	74.98	-109.3	35	1	1
23	24.01.2009	15:50	40.782	27.742	12.5	2.3	1.1	1.3	3.0	44	94.8	64.4	284.2	25.3	191.16	70.40	-93.88	32	0	1
24	24.01.2009	15:58	40.793	27.763	14.6	4.3	1.4	1.6	2.5	39	313.1	20.4	54.6	28.2	185.29	84.97	35.65	63	0	1
25	24.01.2009	23:59	40.797	27.770	12.7	2.8	1.5	1.8	3.0	39	260.1	74.3	65.5	15.2	338.68	60.31	-85.65	60	0	1
26	25.01.2009	02:54	40.793	27.752	12.3	3.0	1.2	1.3	2.7	39	269.5	23.6	10.5	23.6	320.00	90.00	-34.48	54	0	1
27	25.01.2009	03:26	40.791	27.753	14.0	3.8	1.2	1.4	2.5	39	340.0	90	70.0	0	340.00	45.00	-90.00	57	1	1
28	25.01.2009	04:19	40.776	27.758	13.7	2.0	1.4	1.9	3.8	63	260.1	74.3	65.5	15.2	338.68	60.31	-85.65	21	0	0
29	25.01.2009	08:08	40.796	27.758	13.1	3.0	1.2	1.4	2.7	40	266.4	74.8	78.1	15.1	349.87	60.11	-87.58	41	0	1
30	25.01.2009	08:28	40.791	27.755	12.0	2.9	1.4	1.5	2.6	39	100.5	18.2	369.3	3.8	236.28	79.98	-164.2	46	0	1
31	25.01.2009	12:34	40.792	27.757	15.0	3.6	1.4	1.5	2.5	39	107.4	57.8	317.2	28.7	216.02	75.00	-103.9	49	0	1
32	25.01.2009	14:26	40.789	27.761	11.6	2.4	1.7	2.4	4.9	42	323.9	76.3	428.8	3.6	351.00	50.01	-72.65	27	0	0
33	26.01.2009	15:48	40.776	27.748	10.2	2.5	1.3	2.1	3.9	46	315.6	75.7	419.2	3.4	342.00	49.98	-71.76	27	0	0
34	27.01.2009	05:21	40.783	27.730	10.0	2.0	1.5	1.6	4.9	78	120.0	75	300.0	15	210.00	60.00	-90.00	14	0	1
35	27.01.2009	09:58	40.795	27.736	11.1	2.0	1.3	1.7	4.5	79	189.7	76.5	331.7	10.7	248.72	56.21	-80.22	14	0	1
36	27.01.2009	11:13	40.790	27.740	7.8	2.2	1.0	1.5	4.8	45	302.3	72.9	420.8	8.3	343.68	55.00	-71.81	17	0	0
37	29.01.2009	22:21	40.794	27.737	12.0	2.0	1.2	1.3	2.6	44	260.1	74.3	65.5	15.2	338.68	60.31	-85.65	26	1	1
38	01.02.2009	06:20	40.786	27.753	11.1	2.5	1.1	1.5	2.8	39	269.5	23.6	10.5	23.6	320.00	90.00	-34.48	18	0	0
39	01.02.2009	12:26	40.788	27.749	15.4	2.1	1.4	1.8	3.3	76	340.0	90	70.0	0	340.00	45.00	-90.00	10	0	0
40	02.02.2009	16:19	40.805	27.750	16.5	2.9	1.3	1.4	2.6	41	260.1	74.3	65.5	15.2	338.68	60.31	-85.65	45	0	1

No	Date	Time	Lat.	Lon.	Dep.	ML	Erlt	Erln	Erdp	GAP	P(Az)	P(Pl)	T(Az)	T(Pl)	Strike	Dip	Rake	Pl	In	H.In
41	18.02.2009	14:24	40.796	27.755	14.8	2.0	1.3	1.7	3.6	46	266.4	74.8	78.1	15.1	349.87	60.11	-87.58	21	0	0
42	27.02.2009	15:08	40.779	27.747	14.8	2.1	1.3	1.4	2.6	44	100.5	18.2	369.3	3.8	236.28	79.98	-164.2	17	0	0
43	03.03.2009	21:49	40.782	27.753	12.3	1.9	1.1	1.4	3.5	43	107.4	57.8	317.2	28.7	216.02	75.00	-103.9	23	0	1
44	18.03.2009	03:23	40.807	27.746	13.3	2.5	1.1	1.1	2.4	45	323.9	76.3	428.8	3.6	351.00	50.01	-72.65	37	0	0
45	18.03.2009	09:47	40.803	27.739	12.1	2.6	1.1	1.1	2.8	46	315.6	75.7	419.2	3.4	342.00	49.98	-71.76	24	0	0
46	18.03.2009	09:55	40.800	27.747	8.2	2.1	1.2	1.3	4.5	44	120.0	75	300.0	15	210.00	60.00	-90.00	25	0	1
47	18.03.2009	10:03	40.801	27.735	13.0	2.1	1.3	1.2	3.8	52	189.7	76.5	331.7	10.7	248.72	56.21	-80.22	12	0	0
48	18.03.2009	16:33	40.803	27.739	11.8	3.8	1.0	1.1	2.3	41	302.3	72.9	420.8	8.3	343.68	55.00	-71.81	63	0	1
49	18.03.2009	17:48	40.807	27.737	11.8	2.0	1.2	1.5	3.4	42	179.2	88.3	88.3	0	356.60	45.04	-92.40	19	0	0
50	18.03.2009	22:32	40.808	27.752	15.5	2.1	1.3	1.5	3.0	47	2.9	76.3	245.4	6.4	144.62	52.55	-105.3	24	0	1
51	13.04.2009	02:27	40.804	27.741	11.0	2.1	0.9	1.5	2.6	60	249.0	68	48.6	20.8	324.40	66.13	-82.33	17	0	1
52	16.04.2009	21:57	40.803	27.747	10.0	2.0	0.9	1.3	2.3	41	323.7	59.6	189.4	22.3	83.59	70.02	-110.9	33	0	1
53	25.04.2009	05:28	40.810	27.758	12.0	2.0	1.0	1.5	3.0	87	260.5	85	78.9	5	349.03	50.00	-89.82	17	0	0
54	25.04.2009	05:29	40.807	27.761	13.5	2.2	1.1	1.3	3.3	57	5.8	81.7	271.7	0.6	173.59	46.19	-101.5	18	0	0
55	05.05.2009	18:07	40.801	27.751	9.9	2.1	1.0	1.3	2.8	46	312.9	84.1	45.8	0.3	321.63	45.60	-81.74	25	0	0
56	21.05.2009	03:33	40.801	27.732	11.7	2.5	0.8	1.0	2.0	42	188.9	64.9	374.7	25	282.85	70.03	-92.37	34	0	0
57	27.05.2009	22:52	40.776	27.799	11.6	1.8	1.4	1.3	3.2	115	297.6	51.3	439.6	32.3	5.65	79.98	-70.71	19	0	0
58	02.07.2009	11:57	40.795	27.690	7.5	2.5	0.9	1.1	2.7	51	120.0	60	300.0	30	210.00	75.00	-90.00	22	0	0
59	02.07.2009	12:10	40.798	27.700	6.4	3.1	0.8	1.0	2.5	50	226.4	45.7	26.8	42.7	306.35	88.48	-80.08	36	0	0
60	02.07.2009	12:19	40.792	27.691	9.1	2.3	0.9	1.2	3.6	60	119.0	79.2	274.3	9.8	188.18	54.97	-84.59	18	0	0
61	04.07.2009	12:36	40.794	27.701	6.4	3.0	0.7	0.9	2.2	42	179.2	88.3	88.3	0	356.60	45.04	-92.40	39	0	0
62	13.07.2009	18:49	40.793	27.707	13.7	2.2	0.9	1.1	2.1	42	2.9	76.3	245.4	6.4	144.62	52.55	-105.3	28	0	0
63	03.09.2009	12:28	40.802	27.733	8.7	2.5	0.9	1.0	2.2	75	249.0	68	48.6	20.8	324.40	66.13	-82.33	32	0	0
64	27.09.2009	20:33	40.811	27.756	10.8	2.2	1.0	1.5	2.8	75	323.7	59.6	189.4	22.3	83.59	70.02	-110.9	13	0	0
65	22.10.2009	05:24	40.810	27.749	11.5	2.9	1.1	1.1	2.1	67	260.5	85	78.9	5	349.03	50.00	-89.82	34	0	0

No	Date	Time	Lat.	Lon.	Dep.	ML	Erlt	Erln	Erdp	GAP	P(Az)	P(Pl)	T(Az)	T(Pl)	Strike	Dip	Rake	Pl	In	H.In
66	09.12.2009	16:05	40.801	27.746	4.0	2.0	1.2	1.3	3.8	129	5.8	81.7	271.7	0.6	173.59	46.19	-101.5	16	0	0
67	14.02.2010	18:44	40.809	27.809	14.1	3.4	1.0	1.4	1.9	55	312.9	84.1	45.8	0.3	321.63	45.60	-81.74	44	0	0
68	18.02.2010	04:56	40.804	27.754	11.3	2.3	1.1	1.9	2.5	69	188.9	64.9	374.7	25	282.85	70.03	-92.37	25	0	1
69	09.06.2010	17:48	40.787	27.742	11.1	2.2	1.4	1.5	3.3	101	297.6	51.3	439.6	32.3	5.65	79.98	-70.71	12	0	0
70	14.08.2010	00:36	40.819	27.715	4.4	2.3	0.9	1.2	2.6	45	120.0	60	300.0	30	210.00	75.00	-90.00	30	0	0
71	07.09.2010	00:05	40.794	27.722	10.0	3.1	0.9	1.7	3.1	98	226.4	45.7	26.8	42.7	306.35	88.48	-80.08	14	0	0
72	17.09.2010	05:24	40.814	27.747	15.3	2.7	1.1	1.4	2.5	45	119.0	79.2	274.3	9.8	188.18	54.97	-84.59	25	0	0
73	09.12.2010	12:46	40.806	27.765	16.9	2.6	1.1	1.3	2.1	42	135.3	73.5	343.9	14.6	247.53	60.01	-98.74	22	0	0
74	09.12.2010	13:00	40.812	27.760	15.8	2.5	1.2	1.3	2.1	42	300.9	46.4	443.1	36.9	10.55	84.98	-70.17	24	0	0
75	23.12.2010	02:22	40.807	27.706	17.8	2.0	1.0	1.2	1.7	87	123.5	64.7	292.0	24.9	205.68	70.02	-85.28	21	0	0

Table B 3. Relocations and fault plane solutions of 73 earthquakes in the Çınarcık Basin

No	Date	Time	Lat.	Lon.	Dep.	ML	Erlt	Erln	Erdp	GAP	P(Az)	P(Pl)	T(Az)	T(Pl)	Strike	Dip	Rake	Pl	In	H.In
1	16.11.2006	23:49	40.743	29.069	11.1	2.7	0.8	1.1	1.9	61	55.3	83.6	94.1	4.9	8.49	45.12	-84.28	22	0	0
2	16.11.2006	23:51	40.742	29.071	11.1	2.8	0.9	1.2	2.1	62	47.3	74.7	236.6	15.1	144.61	60.15	-92.72	24	1	1
3	19.02.2007	23:05	40.712	29.164	8.9	2.0	1.1	1.5	4.0	81	130.6	72.9	248.9	8.3	171.82	54.99	-71.77	12	0	0
4	29.03.2007	23:18	40.767	29.192	8.4	2.5	1.0	1.2	3.4	100	151.8	48.7	349.6	39.9	251.37	85.55	-98.93	15	0	0
5	20.05.2007	04:14	40.696	29.240	10.6	1.9	1.0	1.4	4.0	97	323.8	64.7	456.6	17.8	20.76	64.97	-70.76	12	0	0
6	07.07.2007	12:18	40.770	29.093	14.2	2.0	1.1	1.8	2.9	70	56.5	73.8	217.4	15.3	131.65	60.51	-84.19	12	0	0
7	16.07.2007	12:00	40.761	29.210	6.0	2.6	1.0	1.3	3.4	95	61.0	47.6	232.7	42.1	146.65	87.24	-85.85	14	0	1
8	17.07.2007	03:55	40.699	29.205	6.7	2.6	1.0	1.3	2.9	83	151.8	48.7	349.6	39.9	251.37	85.55	-98.93	13	0	0
9	06.01.2008	12:51	40.729	29.080	10.0	2.7	0.9	1.6	2.6	44	148.3	61.8	384.8	16.5	276.89	65.01	-114.6	23	0	1

No	Date	Time	Lat.	Lon.	Dep.	ML	Erlt	Erln	Erdp	GAP	P(Az)	P(Pl)	T(Az)	T(Pl)	Strike	Dip	Rake	Pl	In	H.In
10	17.01.2008	02:23	40.723	29.038	10.0	2.9	0.9	1.2	2.3	37	286.0	56.6	521.4	20.6	51.45	70.02	-116.8	30	0	0
11	21.01.2008	13:27	40.758	29.205	6.6	2.3	0.8	1.1	3.9	65	101.5	67.9	225.2	12.7	150.00	60.02	-69.36	21	0	0
12	21.01.2008	18:57	40.757	29.201	6.0	2.0	0.9	1.2	3.0	59	280.4	75.2	407.1	9	327.28	55.03	-75.71	21	0	0
13	08.02.2008	13:26	40.755	29.207	7.3	2.4	0.7	1.0	2.8	54	480.7	13.5	216.0	20.9	349.40	85.00	24.77	15	0	0
14	08.02.2008	13:52	40.759	29.206	6.0	2.2	0.9	1.2	3.1	54	322.3	44.3	424.7	12.4	6.43	70.00	-43.41	18	0	0
15	17.07.2008	06:11	40.718	29.137	12.0	2.3	0.8	1.2	2.1	57	327.6	67.2	183.2	18.9	83.06	64.98	-103.6	18	0	0
16	19.07.2008	18:12	40.713	29.158	7.5	2.4	0.7	1.1	2.0	49	260.3	78	402.8	9.6	319.08	54.98	-81.23	22	0	0
17	18.08.2008	11:06	40.706	29.127	6.1	2.9	0.9	1.1	2.1	41	296.6	45.7	184.2	20.4	65.98	74.95	-128.8	33	0	0
18	18.08.2008	11:08	40.700	29.123	3.7	3.0	0.8	1.1	2.8	40	298.6	28.2	391.9	6.1	341.99	74.99	-25.07	29	0	0
19	18.08.2008	15:52	40.709	29.129	5.8	2.2	0.9	1.1	2.9	48	53.6	69.4	222.5	20.2	135.52	65.32	-85.99	19	0	0
20	21.09.2008	20:24	40.705	29.230	9.6	2.1	0.9	1.4	2.0	82	70.5	69.3	170.4	3.7	98.61	51.99	-63.83	18	0	0
21	09.10.2008	16:36	40.699	29.218	10.0	2.6	0.8	1.1	2.0	49	475.9	12.4	210.4	19.7	344.12	85.04	23.06	24	0	0
22	22.10.2008	01:00	40.731	29.193	8.1	3.9	1.1	1.3	2.1	64	143.2	76.4	46.5	1.6	303.69	48.13	-108.2	41	0	1
23	22.10.2008	01:19	40.737	29.194	5.6	2.3	1.1	1.2	3.0	66	306.4	70.3	418.0	7.5	343.69	55.01	-67.71	16	0	0
24	30.11.2008	13:55	40.719	29.151	5.3	2.3	0.9	1.3	3.2	82	222.3	74.9	396.2	15	307.49	60.03	-88.23	18	0	0
25	12.12.2008	06:59	40.748	29.197	4.8	2.6	0.8	1.2	2.0	53	296.9	59.9	481.8	30	30.00	75.04	-92.20	18	0	0
26	14.01.2009	06:30	40.718	29.135	6.3	2.3	0.7	0.9	4.3	49	73.6	83.7	17.8	5.1	282.25	46.05	-97.30	19	0	0
27	15.01.2009	20:53	40.704	29.179	7.4	2.6	0.7	1.0	2.4	47	116.1	23.2	379.2	15.7	248.83	85.00	-151.9	23	0	1
28	21.02.2009	22:29	40.731	29.035	9.1	3.1	0.8	1.0	2.2	34	163.8	77.6	67.7	1.3	325.91	47.60	-106.8	27	0	0
29	21.02.2009	22:31	40.731	29.036	12.9	1.9	1.0	1.6	2.8	108	302.9	63.4	415.2	10.8	344.98	60.00	-61.97	11	0	0
30	21.02.2009	23:03	40.732	29.030	8.2	3.3	0.8	1.2	3.6	52	138.3	78.5	387.9	4.1	287.97	50.01	-104.1	22	0	0
31	21.02.2009	23:04	40.732	29.029	6.0	3.4	0.7	1.0	2.1	52	172.2	74.1	37.5	11.4	298.07	57.27	-103.1	28	0	0
32	04.03.2009	12:04	40.728	29.022	6.9	2.3	0.8	1.1	2.7	42	333.8	55.2	196.4	27.1	89.97	75.02	-110.9	21	0	0

No	Date	Time	Lat.	Lon.	Dep.	ML	Erlt	Erln	Erdp	GAP	P(Az)	P(Pl)	T(Az)	T(Pl)	Strike	Dip	Rake	Pl	In	H.In
33	04.03.2009	22:09	40.733	29.027	6.0	2.1	0.7	1.0	2.2	43	266.7	46.4	380.5	21	318.00	75.01	-52.42	23	0	0
34	13.05.2009	05:00	40.731	29.136	7.8	2.2	0.8	1.0	3.0	49	55.3	64.8	229.8	25.1	141.56	70.13	-87.75	17	0	0
35	01.10.2009	23:28	40.679	29.239	8.7	2.0	0.5	0.8	2.6	61	302.9	63.4	415.2	10.8	344.98	60.00	-61.97	23	0	0
36	26.02.2010	23:06	40.763	29.224	13.3	2.3	0.8	1.0	1.6	52	146.4	17.5	413.1	10.2	280.60	84.99	-160.2	27	0	0
37	28.02.2010	19:43	40.730	29.153	17.9	1.8	1.0	1.5	2.8	71	46.9	56.4	208.5	32.2	125.76	77.75	-81.30	15	0	0
38	04.04.2010	07:17	40.724	29.247	12.6	2.0	0.8	1.3	2.4	80	107.8	26.4	212.2	26.4	160.00	90.00	-39.00	15	0	0
39	26.04.2010	20:47	40.764	29.144	7.9	2.0	0.9	1.0	3.4	72	318.7	62.6	429.4	10.4	359.98	59.99	-60.73	16	0	0
40	07.05.2010	00:24	40.700	29.229	10.8	3.0	0.9	1.6	2.0	55	92.0	68.9	218.9	13.1	142.50	60.02	-71.11	28	1	1
41	07.05.2010	02:34	40.697	29.237	10.2	1.9	0.8	1.4	2.9	48	37.1	58.2	188.7	28.6	109.28	74.78	-76.82	22	0	0
42	09.05.2010	03:34	40.691	29.260	10.9	2.3	0.7	1.0	1.8	42	107.2	72.2	223.6	8.1	147.27	55.00	-70.68	25	0	0
43	11.05.2010	14:38	40.699	29.224	9.3	2.0	0.8	1.2	4.1	88	49.8	65.1	200.3	22	119.41	67.88	-78.02	17	0	0
44	11.05.2010	19:04	40.699	29.228	8.8	2.4	0.7	1.0	3.7	57	169.8	72.1	18.1	15.8	281.36	61.31	-99.20	27	0	0
45	11.05.2010	22:07	40.698	29.227	8.9	3.1	0.6	0.9	1.7	29	41.6	79.9	229.7	10	138.48	55.02	-91.70	44	0	1
46	23.06.2010	11:28	40.749	29.250	7.1	2.0	0.9	1.3	4.5	63	51.0	51.9	217.1	37.3	133.17	82.65	-83.17	14	0	0
47	30.06.2010	17:39	40.720	29.166	9.5	2.5	1.0	1.7	3.7	46	40.0	85	24.6	5	293.15	45.11	-91.89	24	0	0
48	17.07.2010	01:33	40.708	29.161	7.6	2.3	0.6	0.8	2.7	40	81.1	70.2	213.2	13.5	135.03	60.00	-73.61	32	0	0
49	17.07.2010	04:27	40.710	29.159	9.0	1.8	0.6	0.9	3.5	78	107.5	61	359.6	9.7	247.47	60.04	-121.7	17	0	0
50	17.07.2010	19:39	40.709	29.163	8.9	2.6	0.5	0.7	2.0	39	53.3	67.7	211.6	20.9	127.82	66.29	-81.77	31	0	0
51	19.07.2010	00:39	40.706	29.162	9.2	1.6	0.7	1.0	3.4	108	21.3	65.8	158.3	18.2	80.91	64.90	-72.95	13	0	0
52	25.07.2010	04:26	40.708	29.164	9.1	1.6	0.6	0.9	3.7	107	56.3	68.8	198.3	17	118.47	63.09	-76.19	16	0	0
53	14.08.2010	23:54	40.707	29.172	8.6	2.4	0.9	1.1	3.0	31	81.0	68.7	277.8	20.5	183.13	65.71	-96.19	21	0	0
54	15.08.2010	01:15	40.709	29.177	9.8	2.1	0.8	1.1	3.3	50	55.4	79.6	221.6	10.1	133.73	55.15	-87.04	19	0	0
55	11.09.2010	21:39	40.708	29.283	8.6	1.9	0.7	1.2	3.3	60	328.4	29.6	422.6	7.3	12.00	74.97	-27.05	17	0	0

No	Date	Time	Lat.	Lon.	Dep.	ML	Erlt	Erln	Erdp	GAP	P(Az)	P(Pl)	T(Az)	T(Pl)	Strike	Dip	Rake	Pl	In	H.In
56	15.09.2010	19:27	40.765	29.208	5.4	1.4	1.2	1.4	3.1	97	155.5	79.8	345.1	10	253.64	55.05	-92.03	10	0	0
57	19.09.2010	15:05	40.735	29.160	6.5	1.9	0.9	1.0	2.9	103	318.2	86.5	26.5	0.1	299.82	44.50	-85.36	15	0	0
58	26.10.2010	15:16	40.762	29.208	6.0	1.4	1.2	1.4	2.2	98	56.5	73.8	217.4	15.3	131.65	60.51	-84.19	10	0	0
59	04.11.2010	23:57	40.733	29.161	8.3	2.7	0.6	0.9	2.9	57	53.4	70	233.8	20	143.69	65.00	-90.14	22	1	1
60	05.11.2010	00:02	40.738	29.161	5.9	1.7	0.9	1.1	2.3	60	199.3	74.4	63.7	11.3	324.59	57.14	-102.7	20	0	0
61	11.11.2010	17:36	40.704	29.210	7.4	2.6	0.8	1.1	3.2	29	322.3	44.3	424.7	12.4	6.43	70.00	-43.41	24	0	0
62	12.11.2010	04:00	40.725	28.997	6.0	2.4	0.5	0.8	2.3	44	50.6	67.8	176.5	13.5	100.88	60.67	-70.04	31	0	1
63	21.12.2010	16:12	40.681	29.210	9.0	1.8	0.6	1.0	3.4	51	251.2	87.6	42.4	0	313.51	46.06	-88.39	18	0	0
64	07.01.2011	01:28	40.707	29.131	11.7	1.8	1.1	1.4	1.8	108	285.0	81.5	07.4	4.6	285.93	47.39	-78.50	16	0	0
65	07.01.2011	02:17	40.708	29.131	10.4	1.5	0.8	1.1	2.6	103	298.6	7.3	207.7	6.8	73.18	89.65	-170.0	14	0	0
66	16.01.2011	08:56	40.715	29.205	9.6	1.9	0.8	1.2	2.9	77	74.8	59.6	261.2	30.2	168.84	75.28	-92.89	10	0	1
67	16.01.2011	17:33	40.713	29.211	10.7	2.1	0.9	1.1	3.1	72	302.9	63.4	415.2	10.8	344.98	60.00	-61.97	14	0	0
68	06.02.2011	12:17	40.728	29.150	5.9	2.2	0.7	1.0	1.5	72	165.8	68.1	5.7	20.7	270.06	66.04	-97.47	14	0	0
69	06.02.2011	14:15	40.721	29.157	7.1	2.3	0.6	1.0	2.6	74	155.8	68.9	351.0	20.4	256.80	65.60	-95.57	19	0	0
70	06.02.2011	14:16	40.726	29.148	7.2	2.2	0.7	1.1	3.0	84	61.5	54.7	236.6	35.2	148.63	80.24	-87.65	17	0	0
71	06.02.2011	14:52	40.746	29.248	6.0	2.9	0.7	1.1	2.0	36	317.1	62.5	465.1	23.8	25.71	70.01	-76.22	25	0	1
72	12.03.2011	14:34	40.732	29.146	8.0	3.0	0.6	0.9	2.4	36	56.5	73.8	217.4	15.3	131.65	60.51	-84.19	41	0	1
73	28.03.2011	07:38	40.728	29.030	8.6	1.7	1.0	1.5	3.3	100	107.5	61	359.6	9.7	247.47	60.04	-121.7	12	0	0

Table B 4. Relocations and fault plane solutions of 102 earthquakes in the Yalova Region

No	Date	Time	Lat.	Lon.	Dep.	ML	Erlt	Erln	Erdp	GAP	P(Az)	P(Pl)	T(Az)	T(Pl)	Strike	Dip	Rake	Pl	In	H.In
1	12.09.2006	07:25	40.581	28.981	9.6	2.9	1.4	1.4	4.8	120	202.9	61.3	45.3	26.9	61.86	79.99	-83.99	13	0	0
2	16.09.2006	23:10	40.594	29.124	6.5	2.7	1.5	1.3	4.7	74	228.2	83.9	14.9	5.1	263.88	84.10	-109.1	11	0	0
3	28.10.2006	11:36	40.642	29.220	11.5	2.8	1.2	1.5	3.1	68	85.1	25	353.6	3.2	298.06	88.88	-60.06	13	0	0
4	28.10.2006	12:01	40.640	29.219	9.3	3.2	0.9	1.2	3.0	64	261.8	49.1	370.8	15.8	303.15	65.70	-50.90	18	1	1
5	28.10.2006	15:28	40.637	29.217	8.9	3.9	1.0	1.2	2.7	65	153.8	60	332.2	30	243.30	75.00	-89.15	19	1	1
6	28.10.2006	16:53	40.638	29.224	8.9	2.7	0.8	1.1	2.6	65	87.9	49.3	181.5	3.1	231.45	90.00	-125.0	15	0	0
7	28.10.2006	20:35	40.638	29.222	8.1	2.7	0.9	1.1	3.0	65	64.4	39	182.7	30.4	123.64	86.60	-55.13	18	0	0
8	16.11.2006	16:08	40.641	29.220	10.0	2.7	0.8	1.1	2.1	63	85.1	25	353.6	3.2	297.64	83.79	-70.98	18	0	0
9	11.01.2007	04:16	40.567	28.983	8.7	2.3	1.4	1.5	3.7	105	357.6	67	218.7	17.7	263.80	89.45	94.97	18	1	1
10	11.01.2007	20:04	40.572	28.994	12.2	3.0	1.3	1.3	2.1	64	164.9	45.8	401.6	28.1	302.15	69.98	-121.6	20	0	0
11	13.01.2007	00:54	40.611	29.037	3.6	2.5	1.0	1.0	2.0	90	40.0	66.9	195.6	21.2	103.85	65.00	-97.00	15	0	0
12	13.01.2007	01:11	40.611	29.041	2.8	2.3	1.2	1.2	2.4	51	247.6	64.7	338.2	0.3	74.96	60.04	-101.6	14	0	0
13	27.01.2007	03:28	40.627	29.081	6.0	2.1	0.6	0.8	3.6	88	202.9	61.3	45.3	26.9	151.00	71.16	-73.30	13	0	0
14	05.02.2007	21:04	40.597	29.021	9.2	2.1	1.5	1.4	2.5	123	228.2	83.9	14.9	5.1	285.62	81.27	-94.89	11	0	0
15	20.02.2007	02:47	40.577	28.990	4.8	2.3	1.0	1.0	3.4	90	85.1	25	353.6	3.2	320.20	80.37	-107.6	14	0	0
16	03.04.2007	14:03	40.652	29.073	13.2	2.1	1.0	1.3	2.7	69	261.8	49.1	370.8	15.8	159.65	86.50	-80.63	10	0	0
17	10.05.2007	12:01	40.652	29.014	11.8	2.5	1.1	1.4	2.2	69	153.8	60	332.2	30	60.02	75.04	72.18	15	1	1
18	28.09.2007	03:35	40.607	29.018	7.0	2.3	1.0	1.2	2.8	32	87.9	49.3	181.5	3.1	20.00	90.00	-92.41	18	0	1
19	31.10.2007	16:47	40.633	29.138	11.9	1.9	1.3	2.0	3.7	64	64.4	39	182.7	30.4	318.83	72.97	-71.48	12	0	0

No	Date	Time	Lat.	Lon.	Dep.	ML	Erlt	Erln	Erdp	GAP	P(Az)	P(Pl)	T(Az)	T(Pl)	Strike	Dip	Rake	Pl	In	H.In
20	01.11.2007	03:49	40.645	29.103	6.7	2.4	0.9	1.3	4.2	37	85.1	25	353.6	3.2	307.97	66.34	-81.70	18	0	0
21	03.11.2007	10:21	40.626	29.142	12.2	2.5	1.0	1.6	3.2	57	357.6	67	218.7	17.7	60.34	76.89	-97.31	15	1	1
22	02.12.2007	05:39	40.659	29.202	11.3	2.6	0.8	1.5	2.6	47	164.9	45.8	401.6	28.1	141.44	70.00	-74.44	32	0	0
23	14.12.2007	19:51	40.636	29.123	11.5	3.3	0.8	1.2	1.9	38	40.0	66.9	195.6	21.2	245.47	54.99	-98.43	27	0	1
24	15.12.2007	04:38	40.633	29.135	11.0	2.5	0.9	1.7	2.9	64	247.6	64.7	338.2	0.3	152.64	71.65	-72.74	14	0	0
25	23.12.2007	09:46	40.627	29.129	7.8	2.9	1.3	1.6	4.5	39	143.0	55.5	242.9	6.7	112.49	85.35	-88.07	26	0	0
26	10.03.2008	15:14	40.603	29.030	2.5	1.8	1.3	1.6	4.3	113	191.1	53.6	20.8	36	3.14	89.44	80.01	13	0	0
27	12.03.2008	18:53	40.617	29.031	12.7	4.6	0.9	1.3	2.2	29	296.4	67.6	190.2	6.5	112.47	60.01	-124.2	63	0	1
28	12.03.2008	19:33	40.617	29.042	10.6	2.6	0.9	1.4	2.2	30	138.9	68.2	38.6	4.1	276.16	70.13	-87.87	23	0	1
29	01.04.2008	08:38	40.627	29.092	6.0	2.2	1.1	1.3	2.4	61	202.9	61.3	45.3	26.9	328.25	84.99	-86.58	12	0	0
30	07.04.2008	09:37	40.617	29.167	6.0	2.6	0.7	0.9	1.8	46	267.6	54.9	376.4	12.8	129.39	80.00	-84.44	21	0	0
31	11.04.2008	15:25	40.635	29.022	9.2	1.9	0.6	0.8	2.7	99	326.2	74.9	210.1	6.8	46.45	60.69	-96.77	15	0	0
32	18.04.2008	20:18	40.636	28.888	7.9	2.1	0.7	1.1	1.7	97	303.5	77	207.1	1.5	334.62	81.09	-72.00	19	0	0
33	18.04.2008	21:12	40.613	29.047	4.8	3.1	0.8	1.0	2.0	40	169.4	68.5	42.9	13.2	285.55	64.99	-90.99	32	0	0
34	11.05.2008	17:26	40.638	29.043	6.0	2.4	0.7	1.0	2.5	53	119.2	54.8	380.2	6.3	290.87	76.02	-122.4	16	1	1
35	15.05.2008	16:32	40.630	29.027	5.9	2.2	0.8	1.2	4.5	66	60.2	62.4	183.0	15.8	290.75	65.02	-92.59	15	0	0
36	28.05.2008	14:02	40.619	29.191	6.4	2.7	0.8	1.1	2.9	58	138.9	68.2	38.6	4.1	259.42	85.03	-95.41	14	0	0
37	02.06.2008	10:36	40.634	29.132	3.0	2.4	1.0	1.4	3.0	70	143.0	55.5	242.9	6.7	86.40	59.31	-124.7	15	0	0
38	03.06.2008	19:56	40.602	29.043	7.2	2.2	1.0	1.2	4.1	46	191.1	53.6	20.8	36	277.56	82.00	-96.06	15	0	0
39	03.06.2008	20:27	40.610	29.059	4.0	2.0	1.4	1.5	3.2	74	296.4	67.6	190.2	6.5	280.39	60.11	-92.33	12	0	0
40	11.06.2008	15:38	40.633	29.124	6.9	3.1	0.9	1.1	2.4	37	138.9	68.2	38.6	4.1	264.00	53.11	-126.5	30	0	0

No	Date	Time	Lat.	Lon.	Dep.	ML	Erlt	Erln	Erdp	GAP	P(Az)	P(Pl)	T(Az)	T(Pl)	Strike	Dip	Rake	Pl	In	H.In
41	11.06.2008	16:52	40.628	29.135	5.5	2.5	0.8	1.0	2.3	55	202.9	61.3	45.3	26.9	285.29	60.79	-97.25	24	1	1
42	11.06.2008	16:57	40.629	29.133	3.0	2.4	0.9	1.1	2.4	55	267.6	54.9	376.4	12.8	255.48	67.65	-110.5	24	0	0
43	19.09.2008	23:59	40.624	29.023	10.0	2.1	0.9	1.2	2.6	62	326.2	74.9	210.1	6.8	16.96	75.37	-93.34	20	0	1
44	28.09.2008	13:33	40.625	29.059	10.7	2.0	1.0	1.3	3.2	68	303.5	77	207.1	1.5	17.57	69.42	-104.6	15	0	0
45	05.10.2008	06:04	40.597	29.024	9.7	4.5	1.1	1.2	1.7	33	169.4	68.5	42.9	13.2	315.02	60.00	-54.15	60	0	0
46	06.10.2008	17:10	40.600	29.023	9.8	3.1	0.8	1.0	1.5	32	119.2	54.8	380.2	6.3	124.72	52.41	-75.11	43	0	1
47	09.10.2008	16:33	40.665	29.185	7.1	2.1	0.9	1.2	3.7	58	60.2	62.4	183.0	15.8	55.11	76.36	-83.69	20	0	0
48	14.10.2008	06:40	40.601	29.030	4.3	2.1	1.3	1.7	4.3	105	138.9	68.2	38.6	4.1	255.60	87.04	-109.8	14	0	0
49	16.10.2008	08:26	40.607	29.057	6.4	2.2	1.2	1.2	3.0	71	29.8	49.4	205.2	40.5	30.15	64.39	-62.00	16	0	0
50	31.10.2008	00:59	40.627	29.051	9.5	2.1	1.0	1.4	2.7	74	112.5	56.7	214.0	7.4	261.04	78.24	-99.38	11	0	0
51	23.11.2008	18:09	40.599	29.081	6.7	2.9	1.3	1.5	2.9	31	332.9	57.3	228.5	9.1	318.44	80.00	-89.38	31	0	0
52	30.11.2008	13:58	40.606	29.026	9.8	1.9	1.3	1.3	2.5	50	190.4	64.8	4.9	25.1	19.45	75.23	-92.75	19	0	1
53	08.01.2009	23:07	40.600	29.024	10.0	3.1	0.8	1.1	1.9	32	202.4	57.7	37.6	31.4	169.10	67.35	-62.60	32	0	1
54	11.01.2009	06:06	40.604	29.021	10.0	2.7	0.9	1.1	1.8	32	92.8	71	205.9	7.7	191.03	81.14	-45.70	28	0	0
55	11.01.2009	06:07	40.599	29.020	9.6	3.5	1.0	1.2	1.6	35	176.9	68	336.6	20.8	285.65	68.91	-142.1	28	0	0
56	12.01.2009	20:45	40.607	29.025	9.3	2.7	0.9	1.1	1.9	39	317.8	55.3	220.6	5	160.83	63.69	-66.03	23	0	0
57	10.02.2009	00:35	40.595	29.079	2.1	3.0	0.9	0.9	2.4	42	193.0	70	16.2	20	276.74	65.44	-94.72	24	0	0
58	06.03.2009	23:48	40.632	29.171	8.6	2.2	0.9	1.1	2.8	61	238.1	68.1	77.8	20.7	77.11	70.01	-100.6	19	0	0
59	17.04.2009	18:39	40.604	28.970	6.6	1.8	0.9	1.3	1.9	47	195.7	69.9	382.6	20	347.08	58.62	-63.81	20	0	0
60	21.04.2009	18:28	40.600	29.037	9.5	2.2	0.9	1.0	1.9	41	202.9	61.3	45.3	26.9	324.02	74.99	-88.39	21	0	0
61	09.05.2009	17:31	40.630	28.981	9.6	2.0	1.2	1.7	2.5	83	29.8	49.4	205.2	40.5	306.53	70.17	-92.91	18	0	0

No	Date	Time	Lat.	Lon.	Dep.	ML	Erlt	Erln	Erdp	GAP	P(Az)	P(Pl)	T(Az)	T(Pl)	Strike	Dip	Rake	Pl	In	H.In
62	10.05.2009	17:01	40.602	29.032	10.0	1.9	0.8	1.0	1.8	27	112.5	56.7	214.0	7.4	328.71	56.56	-57.89	26	0	0
63	02.06.2009	02:34	40.596	29.031	9.9	2.4	0.9	1.1	1.8	37	332.9	57.3	228.5	9.1	101.71	59.11	-116.8	22	0	0
64	02.06.2009	03:33	40.599	29.032	9.7	3.0	0.9	1.1	1.8	37	190.4	64.8	4.9	25.1	285.63	65.85	-83.47	37	0	0
65	02.06.2009	03:34	40.604	29.033	9.0	3.0	0.9	1.1	1.7	33	202.4	57.7	37.6	31.4	295.58	60.45	-84.70	31	0	0
66	02.06.2009	21:10	40.600	29.032	9.5	3.3	0.8	1.0	1.7	27	92.8	71	205.9	7.7	90.44	64.76	-122.1	45	0	0
67	12.07.2009	06:59	40.664	29.174	11.5	2.8	0.6	0.8	1.5	41	176.9	68	336.6	20.8	99.69	52.40	-63.11	33	0	0
68	16.09.2009	01:02	40.616	29.037	6.0	2.1	0.9	1.1	1.7	77	317.8	55.3	220.6	5	187.03	70.46	-66.77	19	0	0
69	27.09.2009	01:19	40.581	28.914	11.7	2.8	0.8	1.0	1.1	42	193.0	70	16.2	20	104.40	58.01	-115.4	34	0	0
70	05.10.2009	10:51	40.604	29.014	10.0	2.4	0.7	1.0	1.4	42	238.1	68.1	77.8	20.7	324.60	50.40	-83.79	26	0	0
71	11.10.2009	20:16	40.598	29.021	9.0	2.2	0.8	1.1	2.3	42	195.7	69.9	382.6	20	137.38	60.62	-96.31	24	0	0
72	25.10.2009	04:21	40.601	29.022	10.4	2.6	0.7	1.0	1.7	41	202.9	61.3	45.3	26.9	135.89	59.59	-71.80	29	0	0
73	29.10.2009	19:36	40.572	28.925	10.5	2.2	0.9	1.3	1.8	62	287.5	62.3	385.7	4.3	21.10	87.63	-75.20	14	0	1
74	15.11.2009	23:28	40.601	29.042	8.8	2.1	0.7	1.1	2.4	42	121.2	67.9	213.7	1	322.42	45.24	-95.35	26	0	0
75	16.11.2009	18:47	40.598	29.033	11.2	3.5	0.7	0.9	1.4	27	196.8	75	15.5	15	324.92	60.10	-54.68	47	0	0
76	16.11.2009	22:32	40.601	29.040	7.8	2.2	0.6	0.9	2.1	42	92.2	64	205.9	11.1	150.69	70.70	-84.65	25	0	0
77	02.12.2009	13:12	40.601	29.034	10.0	2.7	0.7	0.9	1.5	45	184.3	73.9	22.8	15.3	72.04	75.00	-129.6	30	0	0
78	06.01.2010	19:16	40.616	29.021	12.3	2.4	0.6	0.9	1.4	43	78.2	67.8	191.2	9.1	161.65	61.28	-47.15	18	0	0
79	12.01.2010	22:46	40.600	29.039	10.2	2.8	0.6	0.9	1.8	32	178.2	71	30.7	16.2	333.63	74.64	-77.00	33	0	1
80	13.01.2010	01:06	40.604	29.036	9.4	2.2	0.6	0.9	1.6	43	192.4	63.1	29.3	25.9	321.24	65.04	-72.77	33	0	0
81	25.01.2010	07:41	40.623	29.029	8.7	2.2	1.1	1.7	2.3	59	276.2	59.3	381.2	8.8	90.49	74.51	-109.8	11	0	0
82	25.01.2010	08:30	40.626	29.022	7.9	2.5	0.8	1.0	2.5	63	97.4	77.4	205.0	3.8	151.31	63.72	-74.92	20	0	0

No	Date	Time	Lat.	Lon.	Dep.	ML	Erlt	Erln	Erdp	GAP	P(Az)	P(Pl)	T(Az)	T(Pl)	Strike	Dip	Rake	Pl	In	H.In
83	25.01.2010	15:33	40.623	29.021	9.3	2.4	0.6	0.9	1.8	36	346.6	63	132.9	23	320.29	65.68	-84.05	27	0	1
84	27.01.2010	06:25	40.627	29.018	9.8	2.5	0.7	1.1	1.8	35	179.6	64.1	348.0	25.4	93.79	66.51	-109.3	24	0	0
85	26.03.2010	14:39	40.659	29.174	8.7	2.7	0.5	0.8	3.8	45	287.5	62.3	385.7	4.3	37.80	70.58	-58.58	28	0	0
86	29.03.2010	02:55	40.659	29.174	6.0	2.4	0.6	0.9	1.8	58	121.2	67.9	213.7	1	245.14	77.22	-111.6	29	0	0
87	25.05.2010	09:34	40.574	28.957	11.1	1.9	0.7	1.1	1.3	59	196.8	75	15.5	15	3.43	83.22	-71.11	17	0	0
88	30.06.2010	19:42	40.590	29.051	8.9	2.5	0.8	1.0	2.8	34	92.2	64	205.9	11.1	304.61	65.01	-92.77	26	0	0
89	09.07.2010	19:12	40.602	29.019	9.5	2.0	0.8	1.1	3.2	61	184.3	73.9	22.8	15.3	319.84	80.28	45.89	18	0	0
90	10.07.2010	19:57	40.643	29.143	10.0	2.1	0.8	1.3	3.2	78	78.2	67.8	191.2	9.1	53.90	55.03	-88.61	18	0	0
91	06.08.2010	02:43	40.589	29.219	9.5	2.5	0.6	0.9	2.4	71	178.2	71	30.7	16.2	314.01	60.77	-83.03	28	0	1
92	07.08.2010	14:57	40.647	29.129	10.6	3.0	0.8	1.0	1.9	39	192.4	63.1	29.3	25.9	264.94	63.10	-113.4	38	0	1
93	26.08.2010	20:51	40.613	29.020	7.1	2.1	0.9	1.0	2.5	44	276.2	59.3	381.2	8.8	288.07	81.07	-94.50	22	0	0
94	30.08.2010	06:35	40.573	28.969	12.3	2.5	0.8	1.2	1.9	36	97.4	77.4	205.0	3.8	300.79	76.84	-97.25	23	0	0
95	15.09.2010	15:07	40.633	29.163	10.0	2.4	1.0	1.4	4.3	80	346.6	63	132.9	23	319.29	72.01	-81.14	15	0	0
96	01.10.2010	13:18	40.646	29.103	9.7	2.6	0.6	0.9	2.3	39	179.6	64.1	348.0	25.4	257.38	60.62	-96.31	30	0	0
97	01.10.2010	23:11	40.646	29.101	9.6	2.3	0.7	0.9	2.5	48	26.8	65	204.5	25	290.27	52.70	-105.6	32	0	0
98	10.12.2010	02:59	40.608	29.033	6.1	2.2	0.8	1.4	2.9	81	179.6	64.1	348.0	25.4	102.41	72.72	114.95	21	0	0
99	10.01.2011	17:30	40.632	29.157	12.0	2.9	0.6	0.8	1.2	28	285.7	59.6	99.1	30.2	78.87	62.61	-102.7	37	0	1
100	13.01.2011	05:50	40.608	29.031	6.3	2.3	0.7	1.2	2.1	38	285.7	54.7	477.3	34.8	342.46	80.11	-61.53	21	0	0
101	09.02.2011	03:13	40.640	29.085	13.6	2.1	0.8	1.2	2.1	45	136.3	52.9	233.3	5.2	279.94	87.09	-60.11	21	0	1
102	05.03.2011	23:37	40.612	29.025	8.8	2.4	0.6	0.8	1.8	39	141.3	37	247.9	20.9	135.48	55.31	-51.45	36	0	1

Table B 5. Relocations and fault plane solutions of the 63 earthquakes in the Gemlik Region

No	Date	Time	Lat.	Lon.	Dep.	ML	Erlt	Erln	Erdp	GAP	P(Az)	P(Pl)	T(Az)	T(Pl)	Strike	Dip	Rake	Pl	In	H.In
1	24.10.2006	14:00	40.428	28.987	10.5	5.7	1.9	1.8	3.3	153	56.1	48.1	208.3	38.5	130.95	84.59	-76.08	37	0	0
2	24.10.2006	14:52	40.428	29.006	8.0	3.3	1.5	1.5	3.1	153	94.9	68.9	361.4	1.4	252.02	50.01	-118.0	25	0	1
3	24.10.2006	18:00	40.427	29.009	9.5	3.0	1.6	1.4	4.6	145	71.7	59.4	336.9	2.8	220.93	54.97	-128.2	19	0	0
4	25.10.2006	00:24	40.423	28.991	4.9	2.2	2.0	1.9	4.4	154	229.2	72.7	374.6	14.3	292.49	59.94	-79.16	14	0	0
5	25.10.2006	00:56	40.409	29.014	3.3	3.9	1.2	1.2	3.0	122	144.3	51.3	16.0	26.4	265.07	76.26	-116.9	29	0	0
6	25.10.2006	01:01	40.424	29.027	5.8	2.7	1.6	1.6	4.0	155	160.4	78.5	373.6	9.7	278.19	54.97	-97.55	15	0	0
7	25.10.2006	03:41	40.432	29.014	7.4	3.0	1.0	1.0	3.6	145	133.9	54.1	4.9	24.5	248.17	72.22	-122.5	20	0	0
8	25.10.2006	11:12	40.440	29.014	10.4	3.1	1.2	1.2	3.2	120	320.1	62.7	530.9	23.9	70.72	70.01	-103.2	17	0	0
9	25.10.2006	11:56	40.421	29.002	6.1	4.4	1.5	1.4	4.3	121	141.1	85	25.8	5	235.42	49.99	-90.53	25	0	0
10	03.11.2006	00:20	40.433	29.027	7.9	3.4	1.7	1.4	3.8	140	130.6	53.4	353.4	28.6	246.28	76.75	-11.43	22	0	0
11	16.11.2006	06:17	40.424	29.020	10.1	2.9	2.0	1.9	4.4	139	434.3	30	303.9	48.3	5.63	79.96	116.46	18	1	1
12	08.01.2007	23:33	40.416	29.014	5.9	2.5	1.6	1.6	4.2	98	144.3	51.3	16.0	26.4	79.49	88.83	108.58	23	0	1
13	15.01.2007	05:09	40.403	28.996	8.3	3.3	0.9	1.0	2.1	100	97.5	72.8	342.9	7.3	239.34	54.17	-109.2	24	0	1
14	18.05.2007	01:30	40.406	29.012	5.4	2.5	1.3	1.1	3.5	53	157.9	67.9	368.6	19.2	269.99	65.01	-101.5	14	0	0
15	14.07.2007	04:46	40.421	29.005	4.6	2.5	1.4	1.4	4.2	57	172.6	74.4	371.6	14.8	277.50	59.97	-95.61	14	1	1
16	21.08.2007	17:17	40.432	29.055	9.8	2.5	1.2	1.8	3.2	57	56.4	58.9	209.2	28.2	129.19	74.26	-77.51	13	1	1
17	30.09.2007	00:09	40.416	29.166	4.1	2.3	1.2	1.9	2.7	62	68.5	66.3	288.6	18.5	186.95	64.98	-105.7	20	0	1
18	23.11.2007	06:10	40.432	28.936	9.9	2.0	1.1	1.2	4.3	55	58.0	66.9	213.7	21.2	130.83	66.76	-80.57	18	0	0
19	18.02.2008	16:37	40.432	29.010	6.1	2.5	1.2	1.3	4.2	54	56.1	48.1	208.3	38.5	131.08	85.06	-75.84	19	0	0
20	24.02.2008	14:57	40.373	28.927	8.8	2.5	1.1	1.1	3.3	87	71.8	55.2	322.5	12.9	207.66	65.0	-125.4	22	0	0

No	Date	Time	Lat.	Lon.	Dep.	ML	Erlt	Erln	Erdp	GAP	P(Az)	P(Pl)	T(Az)	T(Pl)	Strike	Dip	Rake	Pl	In	H.In
21	27.04.2008	06:15	40.410	29.010	6.2	2.3	0.9	1.1	3.4	59	65.2	72.3	196.4	11.9	117.38	58.13	-74.72	20	0	0
22	29.06.2008	08:28	40.402	29.005	4.2	3.5	0.8	1.0	2.8	57	65.2	72.3	196.4	11.9	117.38	58.13	-74.72	38	0	0
23	07.07.2008	03:37	40.423	29.011	6.0	2.0	1.2	1.4	3.1	56	148.7	55.6	27.6	19.5	276.20	69.67	-119.1	12	0	0
24	09.07.2008	04:54	40.413	28.730	10.1	3.7	0.9	1.1	2.1	38	134.3	59.7	30.6	7.9	276.79	58.94	-124.6	38	0	1
25	09.11.2008	10:51	40.437	29.127	8.0	2.4	1.1	1.3	3.2	49	131.0	47.3	347.9	36.4	241.08	84.26	-109.2	17	0	0
26	06.12.2008	07:51	40.397	28.965	7.2	3.4	0.9	1.0	1.8	43	65.2	72.3	196.4	11.9	117.38	58.13	-74.72	53	1	1
27	15.12.2008	15:44	40.430	28.945	5.9	2.1	1.3	1.4	3.4	56	66.6	74.9	241.8	15	152.82	60.04	-88.61	11	0	0
28	23.05.2009	21:57	40.457	29.141	12.9	4.1	1.0	1.9	2.0	131	446.9	5.5	355.0	19.9	39.37	80.03	161.76	44	1	1
29	25.05.2009	22:50	40.468	29.154	9.5	2.9	1.0	1.2	1.8	36	99.0	31.9	353.1	23.9	227.65	84.99	-138.5	50	0	0
30	29.05.2009	06:31	40.455	29.150	10.0	2.5	1.4	2.0	2.8	122	97.6	45.1	233.9	35.8	164.16	84.99	-66.61	12	0	0
31	31.05.2009	15:25	40.460	29.152	11.5	3.8	0.9	1.3	2.0	36	115.8	33.2	368.0	25.1	243.55	84.99	-136.4	48	0	1
32	04.06.2009	09:38	40.462	29.161	10.6	2.4	1.0	1.3	1.8	42	91.6	44.4	341.4	19.5	221.99	75.0	-130.9	25	0	0
33	04.06.2009	13:35	40.466	29.164	8.7	2.0	1.6	1.8	3.2	43	451.8	24.3	246.5	63.5	353.55	70.01	79.34	15	0	0
34	22.06.2009	09:29	40.458	29.147	11.7	3.9	0.8	1.3	1.5	121	448.7	14.2	184.5	21.7	317.63	85.36	26.28	36	0	0
35	22.06.2009	19:10	40.467	29.153	9.9	2.2	1.3	1.6	2.2	58	91.9	49.2	342.6	15.9	224.96	70.03	-129.1	16	0	0
36	23.06.2009	01:51	40.465	29.158	9.4	2.9	1.1	1.3	2.1	35	265.9	10.9	357.9	10.2	311.84	89.51	-15.01	38	0	0
37	08.07.2009	09:26	40.489	29.177	6.6	2.3	0.9	1.3	3.3	71	85.9	40.1	334.5	23.5	213.73	80.0	-131.5	19	0	0
38	28.08.2009	20:07	40.467	29.168	8.7	2.1	0.9	1.1	2.4	36	93.3	43.4	246.7	43.4	170.0	90.0	-76.33	22	0	0
39	09.10.2009	11:33	40.414	29.081	7.2	2.4	0.9	1.2	4.2	39	293.7	53.2	391.0	5.4	330.01	60.03	-46.93	18	0	0
40	01.01.2010	17:27	40.464	29.163	8.9	2.4	0.9	1.1	2.3	36	98.7	46.4	212.5	21	150.0	75.01	-52.42	21	0	0
41	12.01.2010	02:51	40.480	29.180	6.0	2.0	0.8	1.4	1.9	124	121.7	66.9	326.2	21.2	229.01	66.76	-99.50	12	0	0
42	03.02.2010	21:57	40.407	28.879	6.7	3.3	1.3	1.9	3.0	52	120.6	58.8	25.5	3.1	269.21	55.48	-128.7	43	0	1
43	04.02.2010	16:05	40.408	28.868	6.8	2.8	1.0	1.2	3.2	46	132.1	68.5	366.6	12.9	262.50	59.99	-109.6	31	0	0

No	Date	Time	Lat.	Lon.	Dep.	ML	Erlt	Erln	Erdp	GAP	P(Az)	P(Pl)	T(Az)	T(Pl)	Strike	Dip	Rake	Pl	In	H.In
44	08.03.2010	16:07	40.406	29.149	3.6	3.7	1.1	1.4	2.6	66	68.4	41.7	229.3	46.6	329.25	87.52	80.33	53	1	1
45	29.03.2010	15:22	40.449	29.018	9.7	2.0	1.0	1.2	3.3	50	272.3	71.3	386.2	7.8	310.86	54.99	-69.23	12	0	0
46	09.04.2010	11:27	40.430	28.949	8.1	3.4	0.9	1.1	2.2	29	130.1	61.1	36.6	1.9	281.48	53.45	-126.9	61	0	1
47	16.04.2010	22:16	40.462	29.040	4.3	2.0	0.8	1.0	2.7	37	270.6	49.4	371.6	9.3	311.50	65.0	-45.92	20	0	0
48	01.05.2010	20:51	40.448	29.208	6.0	2.2	0.8	1.3	1.9	47	114.3	40.4	362.3	23.8	241.83	80.04	-131.0	28	1	1
49	16.05.2010	09:58	40.470	29.194	5.2	2.1	1.1	1.4	2.3	57	32.5	53.3	161.2	25	91.22	74.45	-63.97	11	0	0
50	11.06.2010	10:56	40.428	28.947	9.8	4.3	1.3	1.8	3.0	71	116.7	58.3	210.4	2.3	147.31	55.02	-50.25	51	0	0
51	05.09.2010	00:44	40.441	28.942	5.9	2.6	0.8	1.1	2.9	54	313.4	27	219.2	8.2	89.09	77.28	-154.4	38	1	1
52	05.09.2010	14:48	40.441	28.946	7.4	2.0	0.9	1.1	4.0	81	306.4	58.9	410.9	8.6	345.00	60.01	-55.19	17	0	0
53	04.10.2010	13:29	40.418	28.784	5.4	1.9	1.1	1.6	2.6	121	120.1	78.4	327.7	10.3	233.12	55.52	-96.38	13	0	0
54	26.10.2010	01:54	40.427	28.721	9.2	2.0	1.1	1.6	3.3	58	108.6	57	201.1	1.6	139.10	55.03	-48.41	14	1	1
55	01.12.2010	11:25	40.390	28.815	7.8	2.2	0.8	1.4	2.6	94	124.1	61.7	221.5	4	155.51	56.12	-55.70	13	0	0
56	06.01.2011	17:33	40.435	29.216	12.0	1.8	1.0	1.5	2.9	67	78.3	41.4	184.1	17.2	126.0	75.01	-44.46	15	0	0
57	13.01.2011	10:33	40.418	28.946	8.1	2.4	0.7	1.1	2.2	58	301.3	67.2	406.6	6.4	335.43	55.01	-63.04	14	0	0
58	13.01.2011	12:57	40.473	29.209	5.2	2.8	0.8	1.1	3.3	45	259.9	24.6	351.7	3.9	303.23	75.74	-20.69	31	0	0
59	13.01.2011	18:08	40.423	28.940	7.7	1.8	0.8	1.4	2.3	70	149.9	60.2	37.2	12.5	285.77	62.57	-120.3	11	0	0
60	03.02.2011	14:05	40.437	29.066	9.1	3.2	0.8	1.1	2.7	38	126.3	58.1	4.8	18	254.64	67.56	-117.6	28	0	0
61	14.03.2011	19:42	40.442	29.058	9.5	3.1	0.9	1.2	2.2	37	59.7	80	243.5	10	152.93	54.99	-90.79	44	1	1
62	20.03.2011	20:56	40.432	29.124	6.9	2.5	0.8	1.0	2.5	51	161.0	52.4	32.5	25.6	282.07	75.25	-116.4	26	0	0
63	26.03.2011	08:57	40.434	29.050	7.8	2.2	0.8	0.9	3.6	43	125.6	58.4	12.9	13.4	260.54	63.99	-121.6	18	1	1

APPENDIX C. DISCRIMINATION OF FAULT PLANES FROM AUXILIARY PLANES BY THE METHOD OF HORUICHI et al. (1995)

1. The Ganos Offshore Cluster

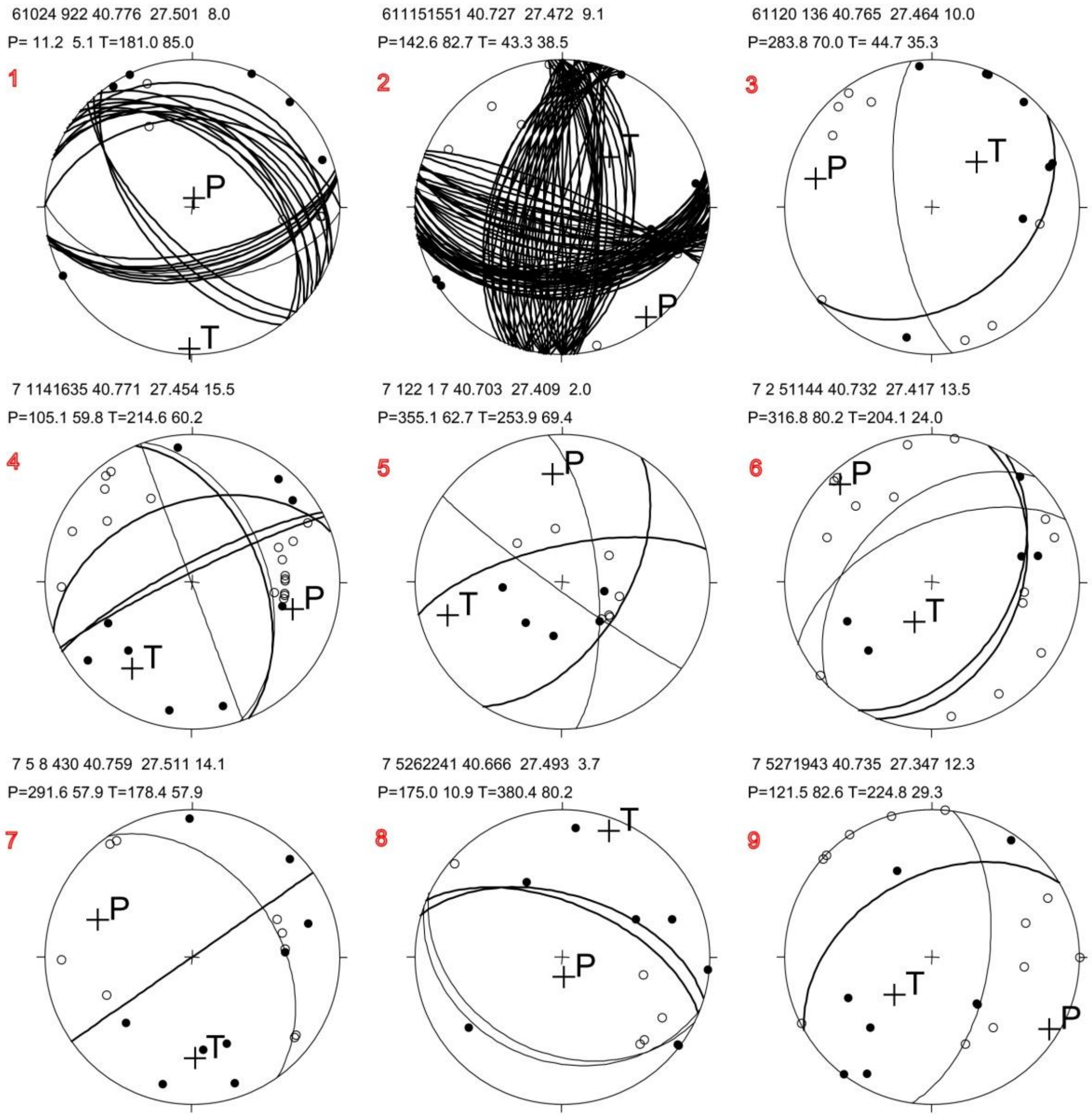

Figure C.1.1. Lower hemisphere projection of fault plane solutions obtained through the program of Horiuchi *et al.* (1995). Solutions are given time dependently for Ganos offshore, and bold lines show fault planes

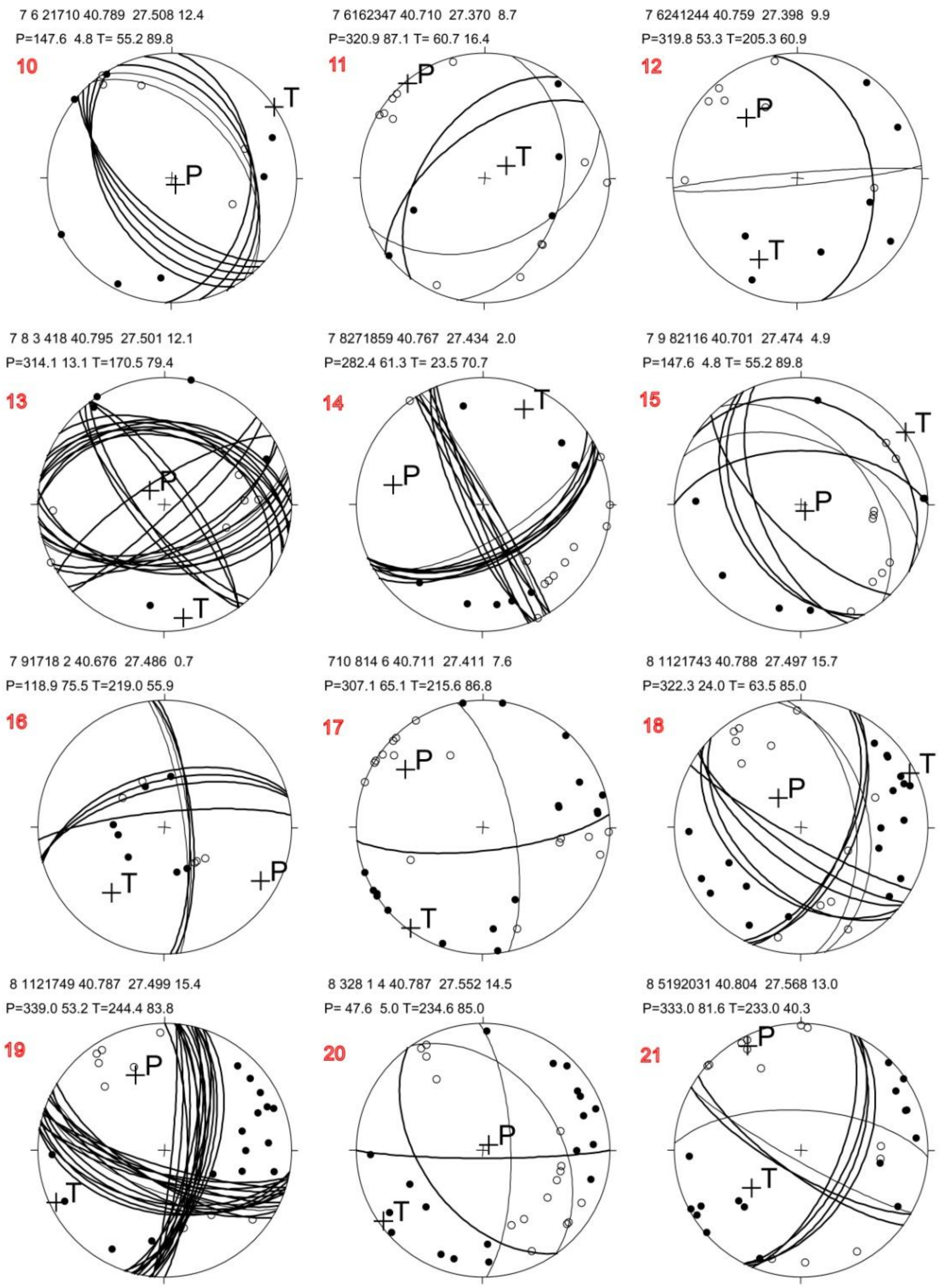

Figure C.1.2. Fault plane solutions obtained through the program of Horiuchi *et al.* (1995). Solutions are given time dependently for Ganos offshore, and bold lines show fault planes

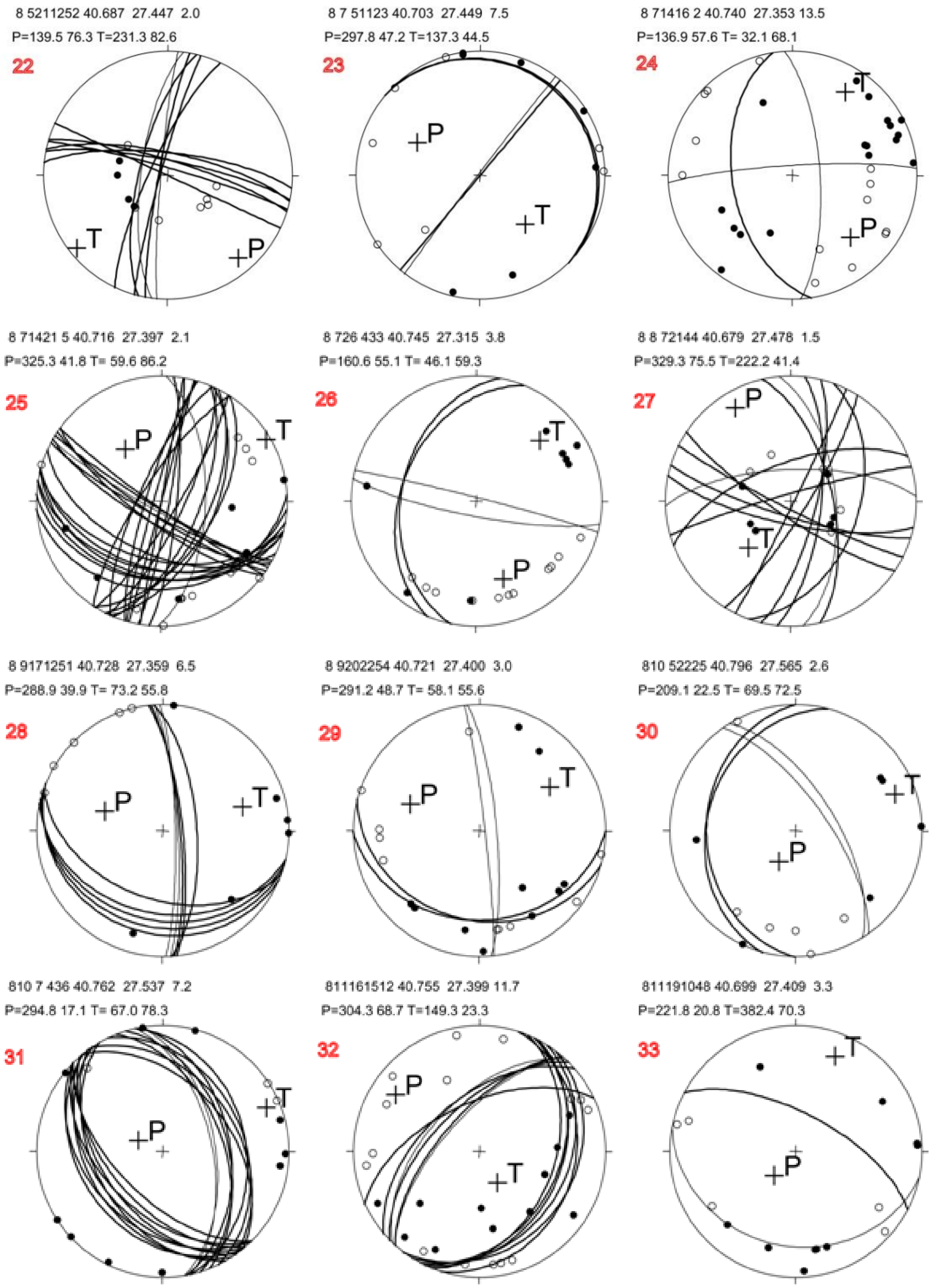

Figure C.1.3. Fault plane solutions obtained through the program of Horiuchi *et al.* (1995). Solutions are given time dependently for Ganos offshore, and bold lines show fault planes

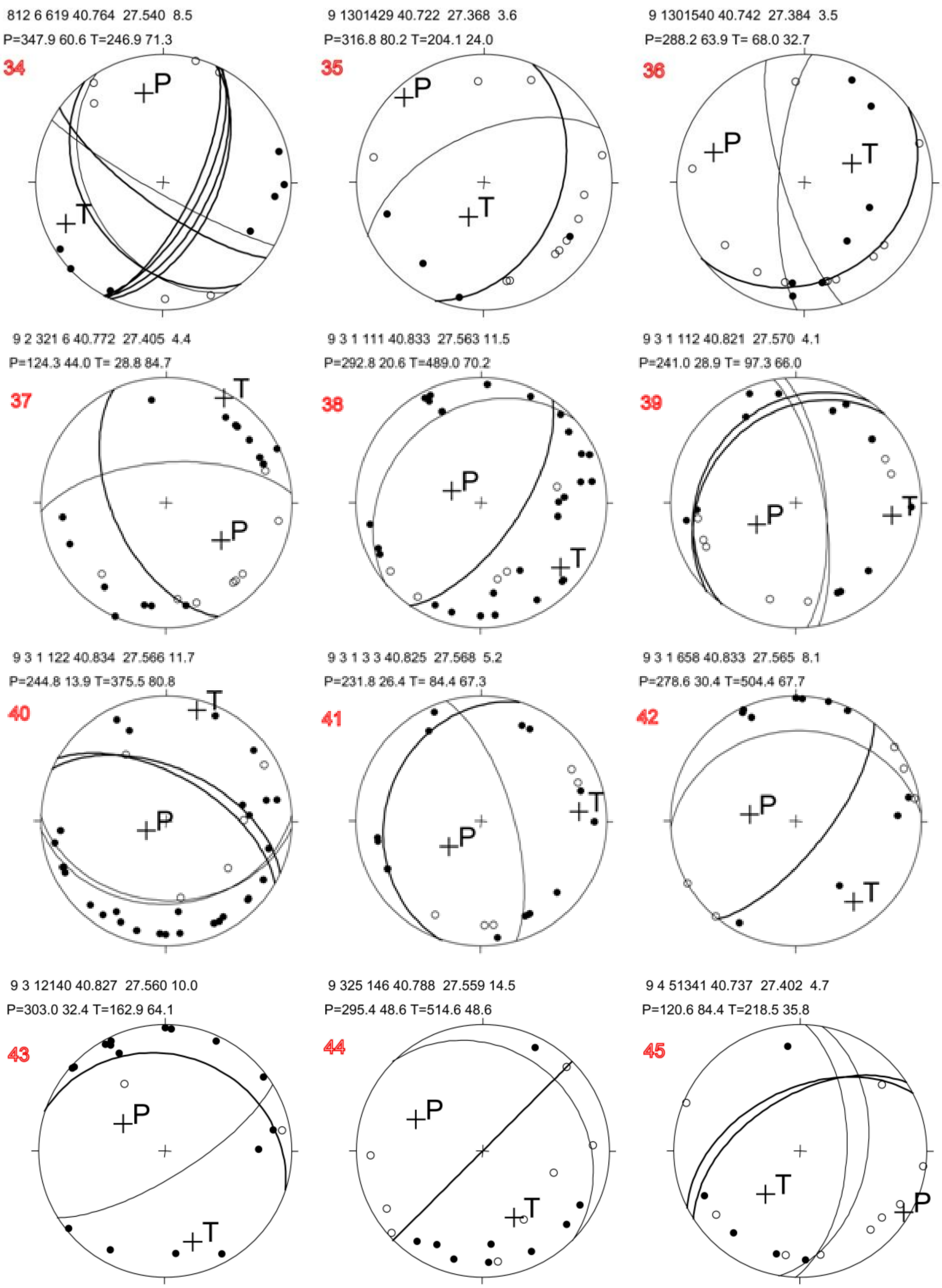

Figure C.1.4. Fault plane solutions obtained through the program of Horiuchi *et al.* (1995). Solutions are given time dependently for Ganos offshore, and bold lines show fault planes

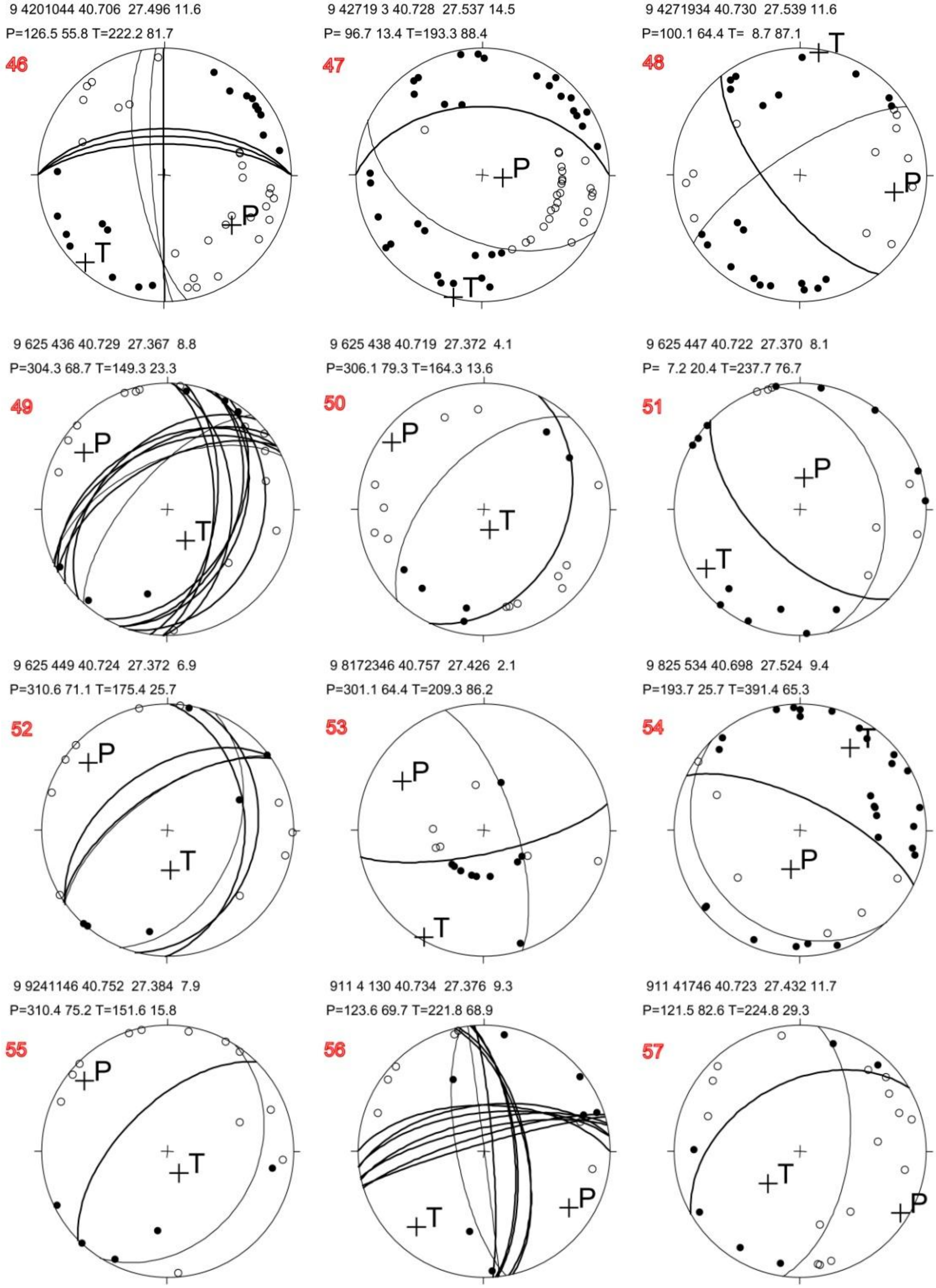

Figure C.1.5. Fault plane solutions obtained through the program of Horiuchi *et al.* (1995). Solutions are given time dependently for Ganos offshore, and bold lines show fault planes

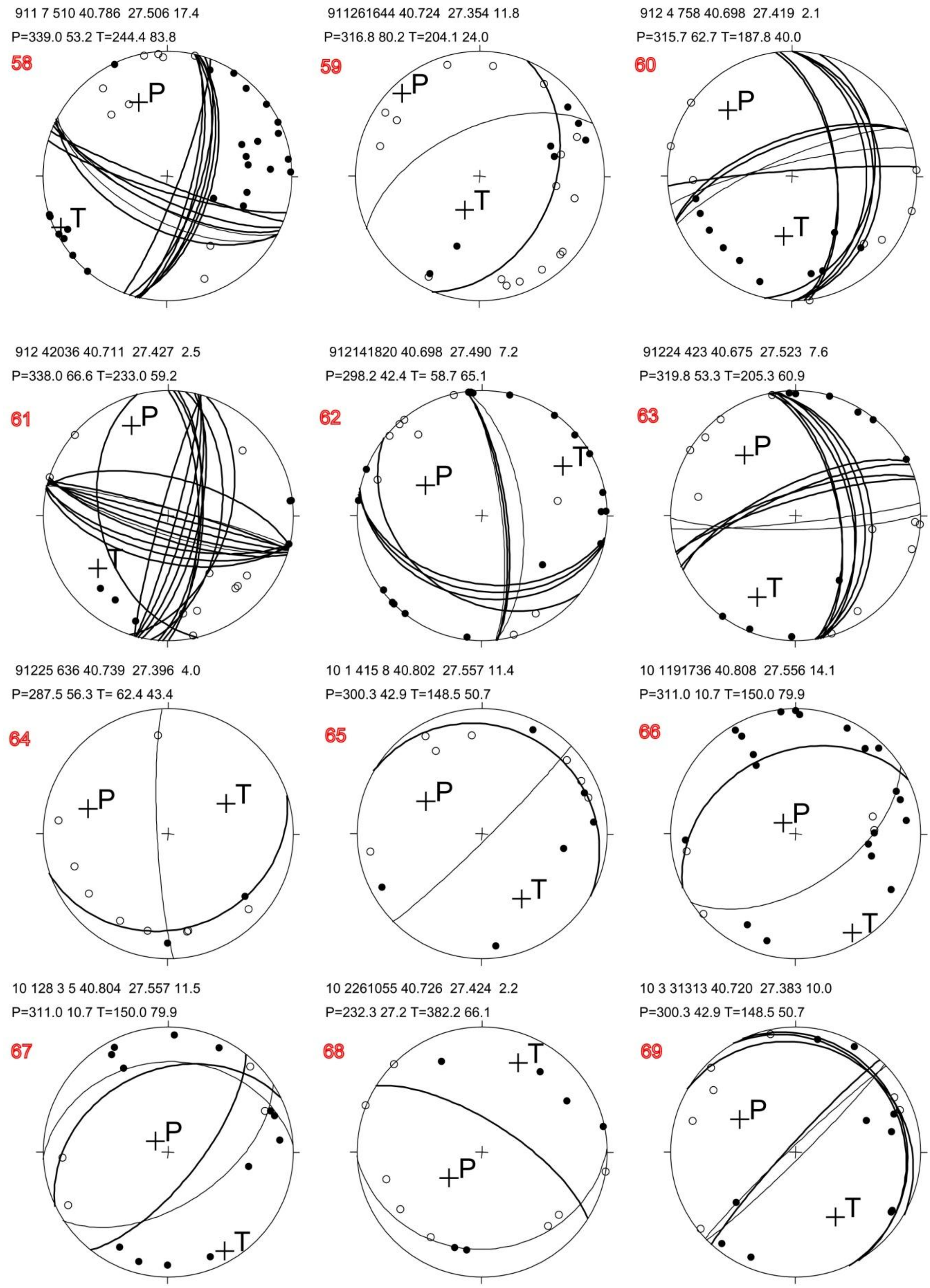

Figure C.1.6. Fault plane solutions obtained through the program of Horiuchi *et al.* (1995). Solutions are given time dependently for Ganos offshore, and bold lines show fault planes

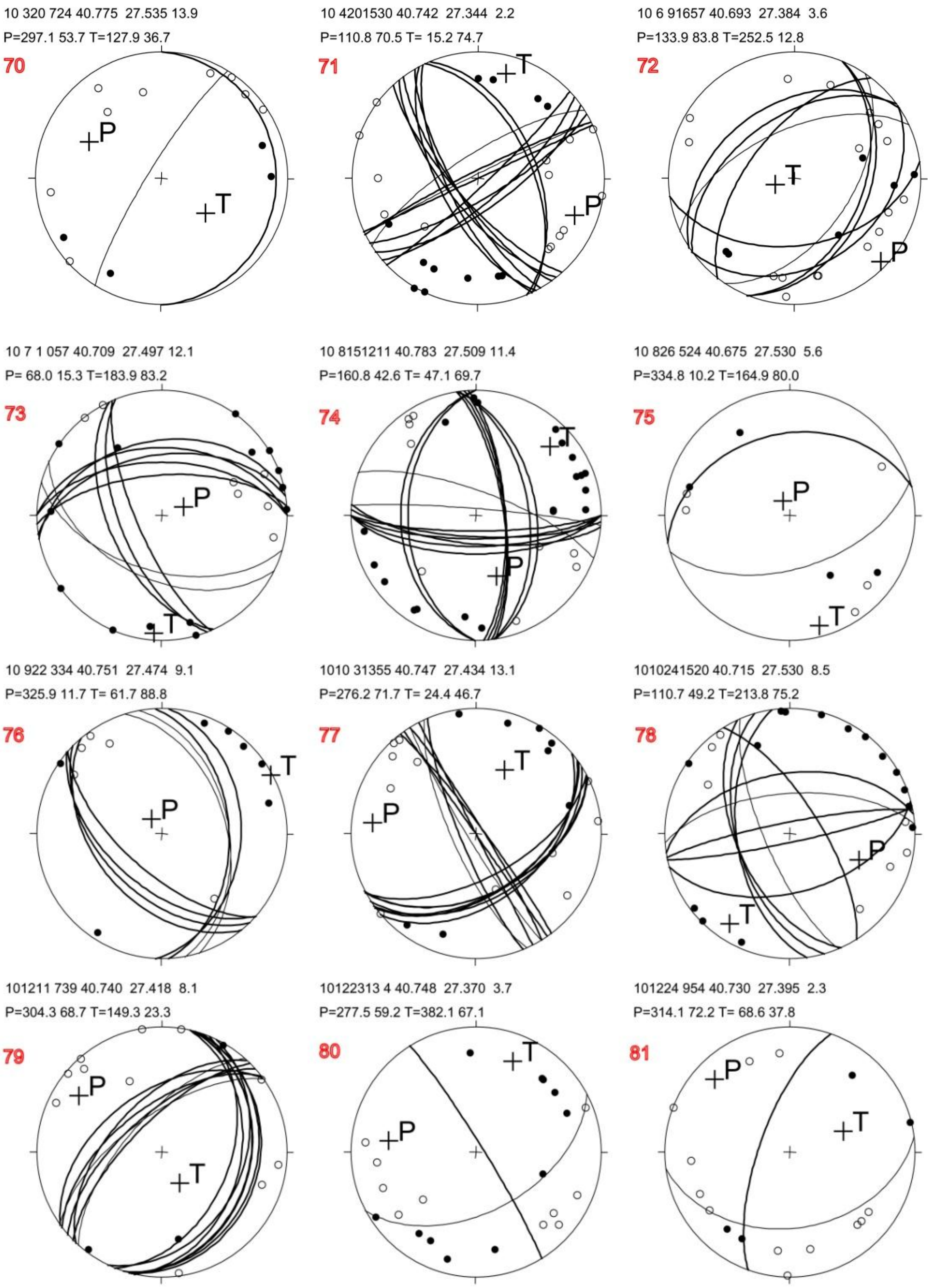

Figure C.1.7. Fault plane solutions obtained through the program of Horiuchi *et al.* (1995). Solutions are given time dependently for Ganos offshore, and bold lines show fault planes

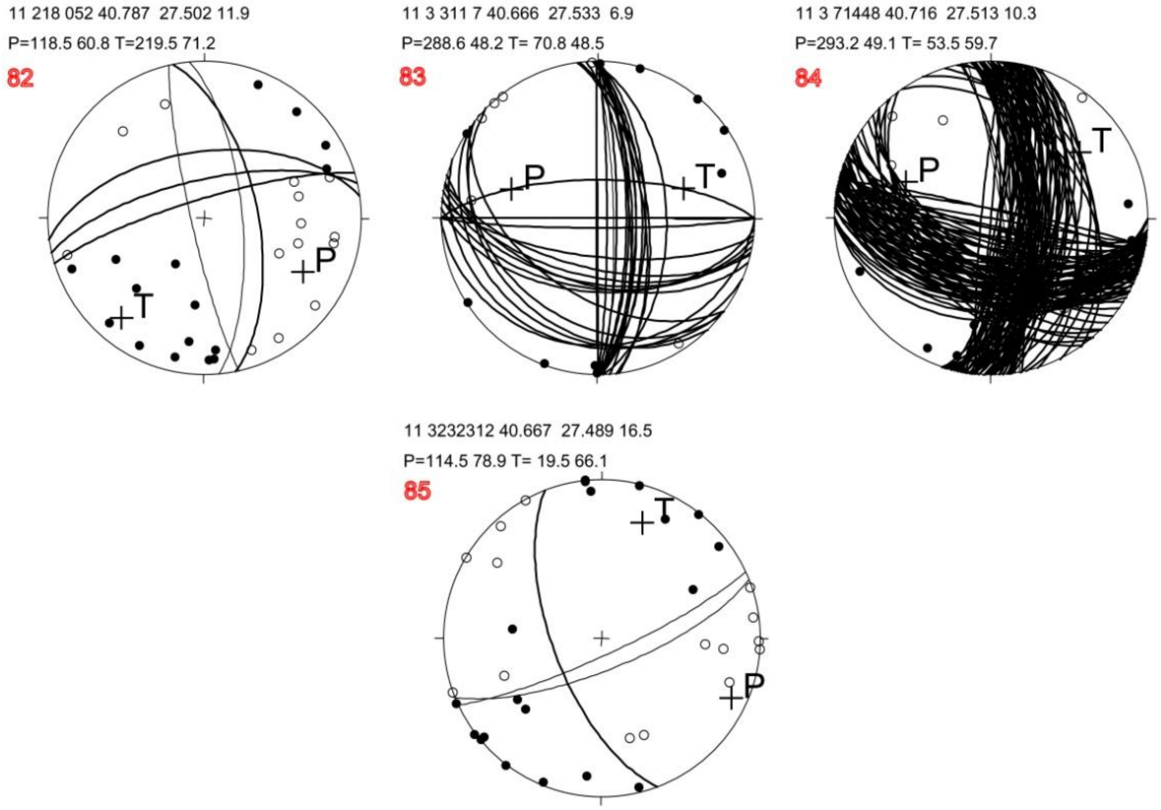

Figure C.1.8. Fault plane solutions obtained through the program of Horiuchi *et al.* (1995). Solutions are given time dependently for Ganos offshore, and bold lines show fault planes

2. The Tekirdağ Basin Cluster

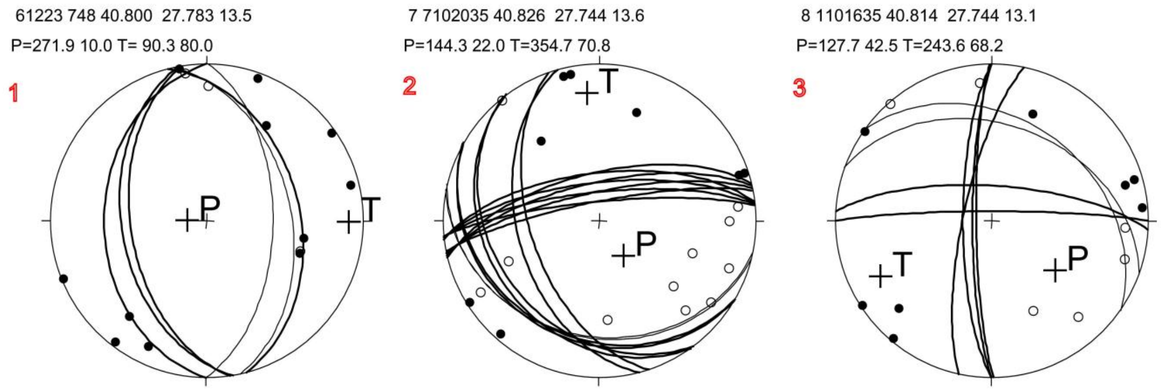

Figure C.2.1. Fault plane solutions obtained through the program of Horiuchi *et al.* (1995). Solutions are given time dependently for Tekirdağ Basin, and bold lines show fault planes

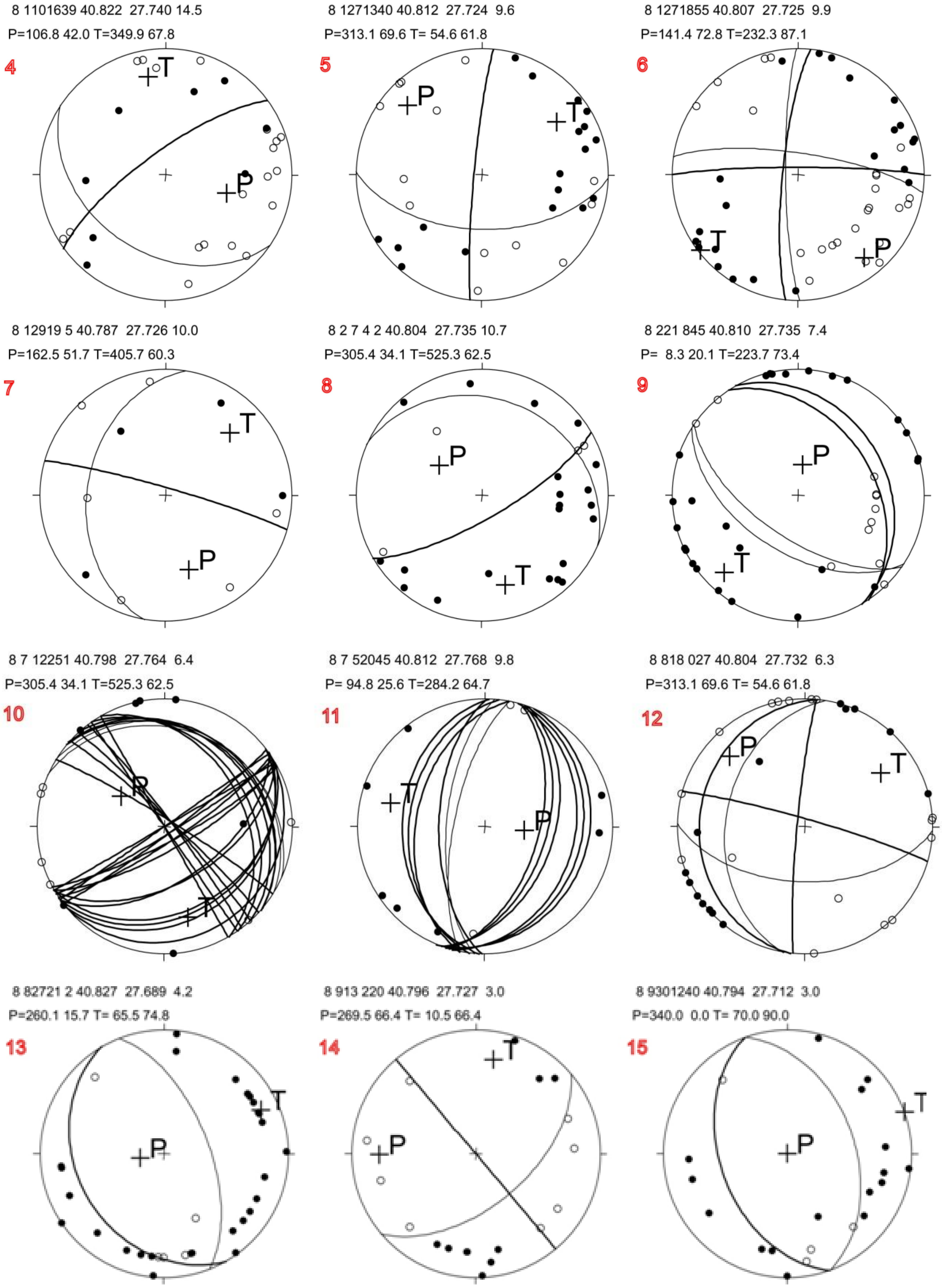

Figure C.2.2. Fault plane solutions obtained through the program of Horiuchi *et al.* (1995). Solutions are given time dependently for Tekirdağ Basin, and bold lines show fault planes

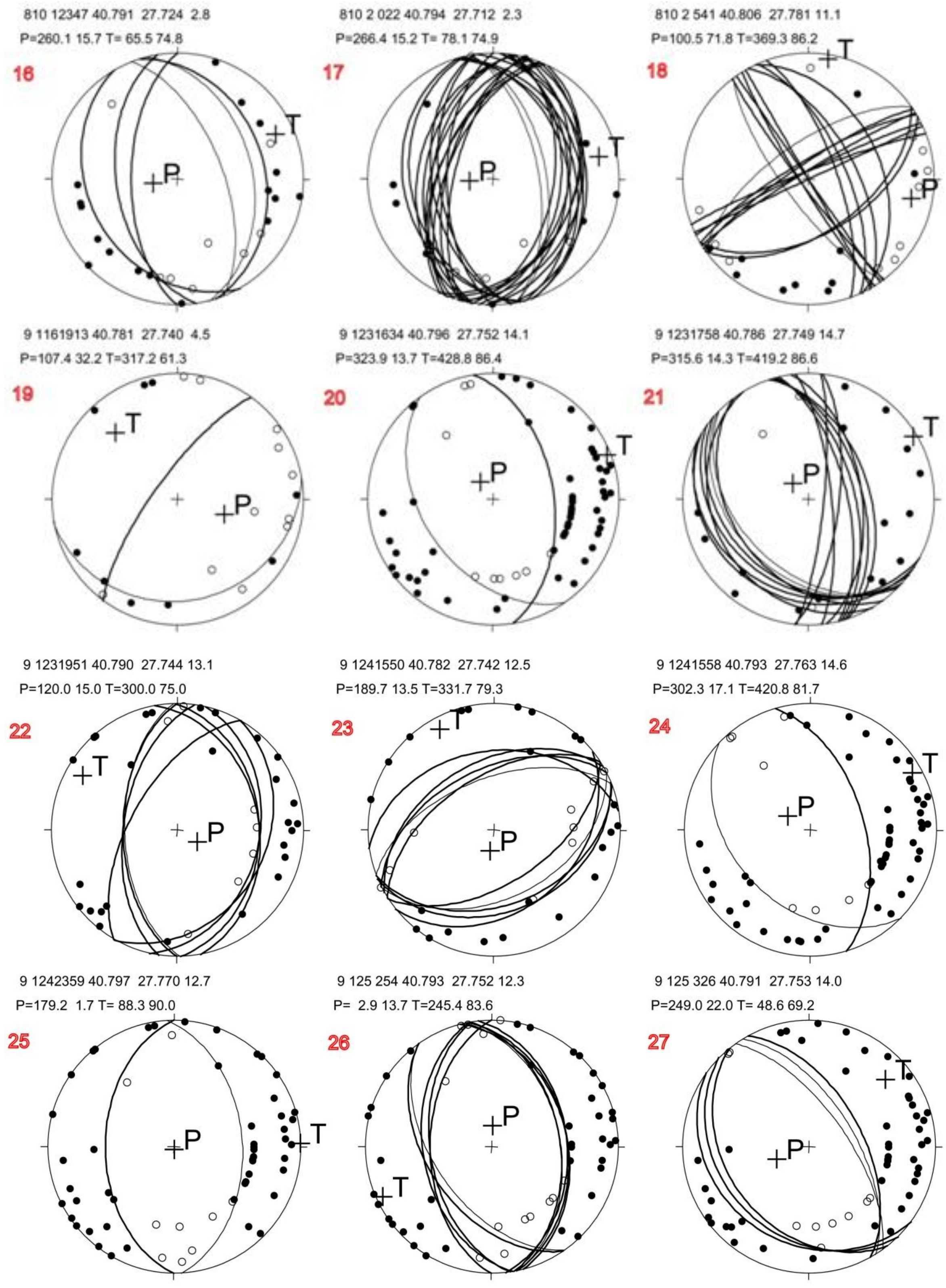

Figure C.2.3. Fault plane solutions obtained through the program of Horiuchi *et al.* (1995). Solutions are given time dependently for Tekirdağ Basin, and bold lines show fault planes

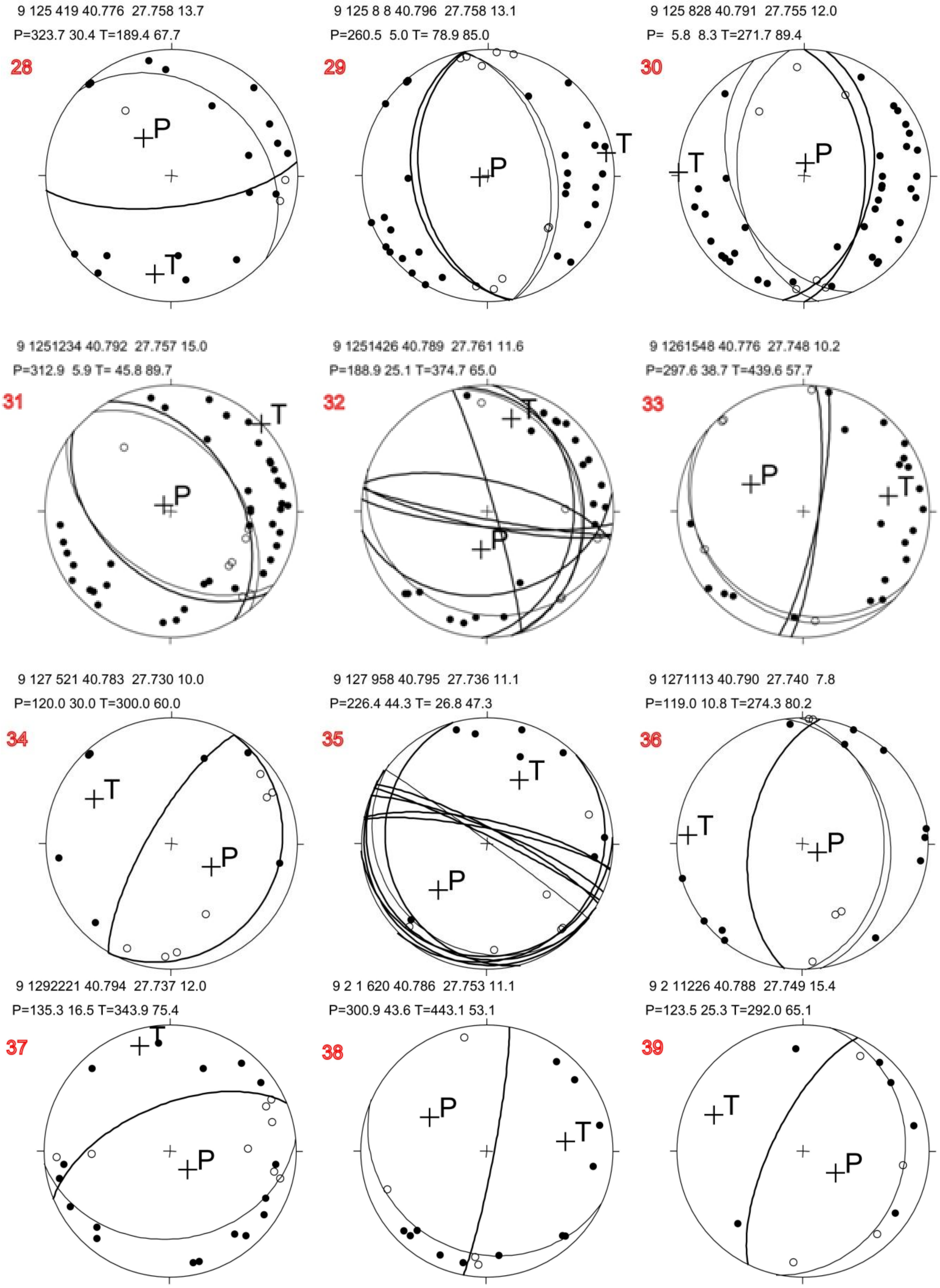

Figure C.2.4. Fault plane solutions obtained through the program of Horiuchi *et al.* (1995). Solutions are given time dependently for Tekirdağ Basin, and bold lines show fault planes

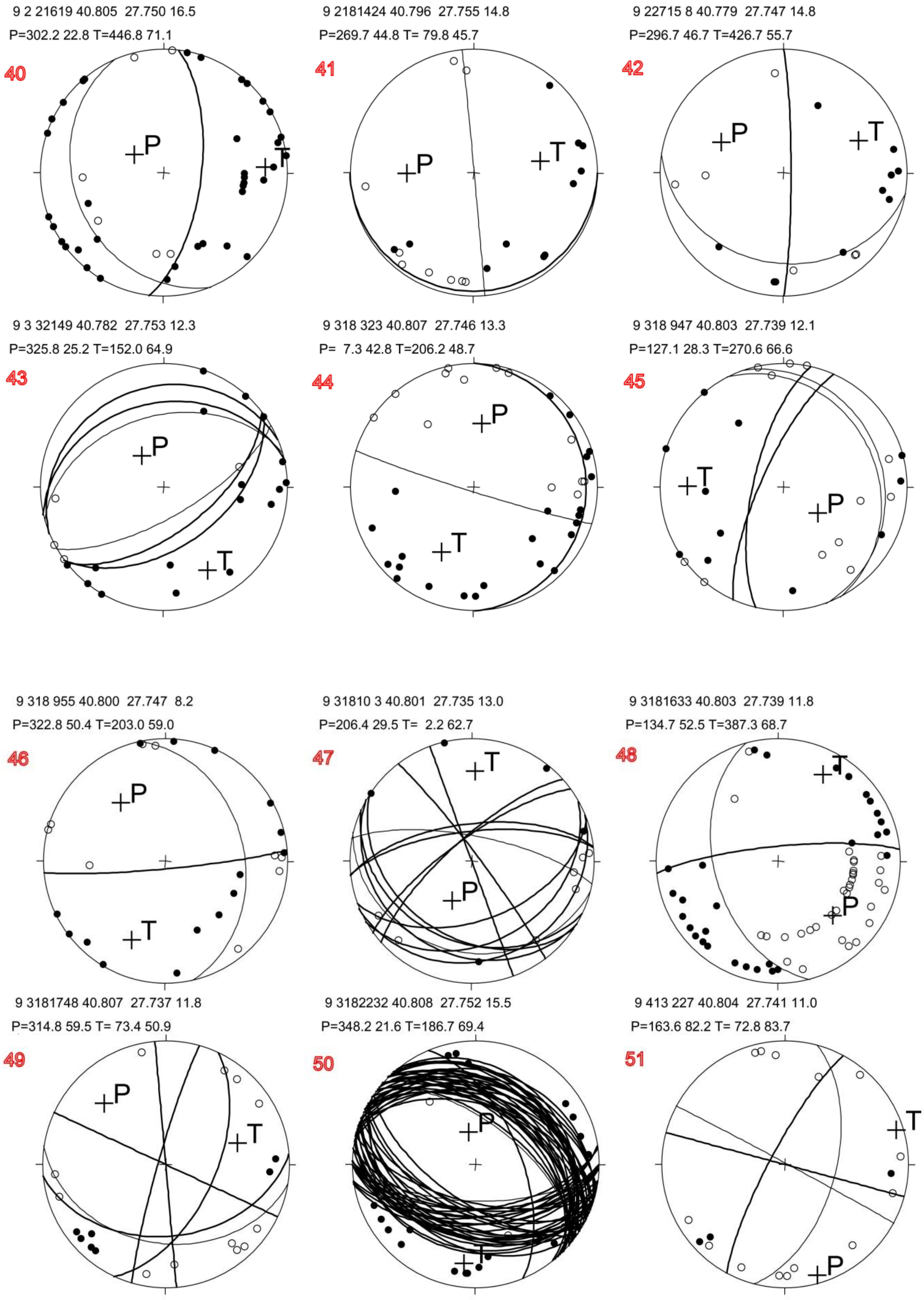

Figure C.2.5. Fault plane solutions obtained through the program of Horiuchi *et al.* (1995). Solutions are given time dependently for Tekirdağ Basin, and bold lines show fault planes

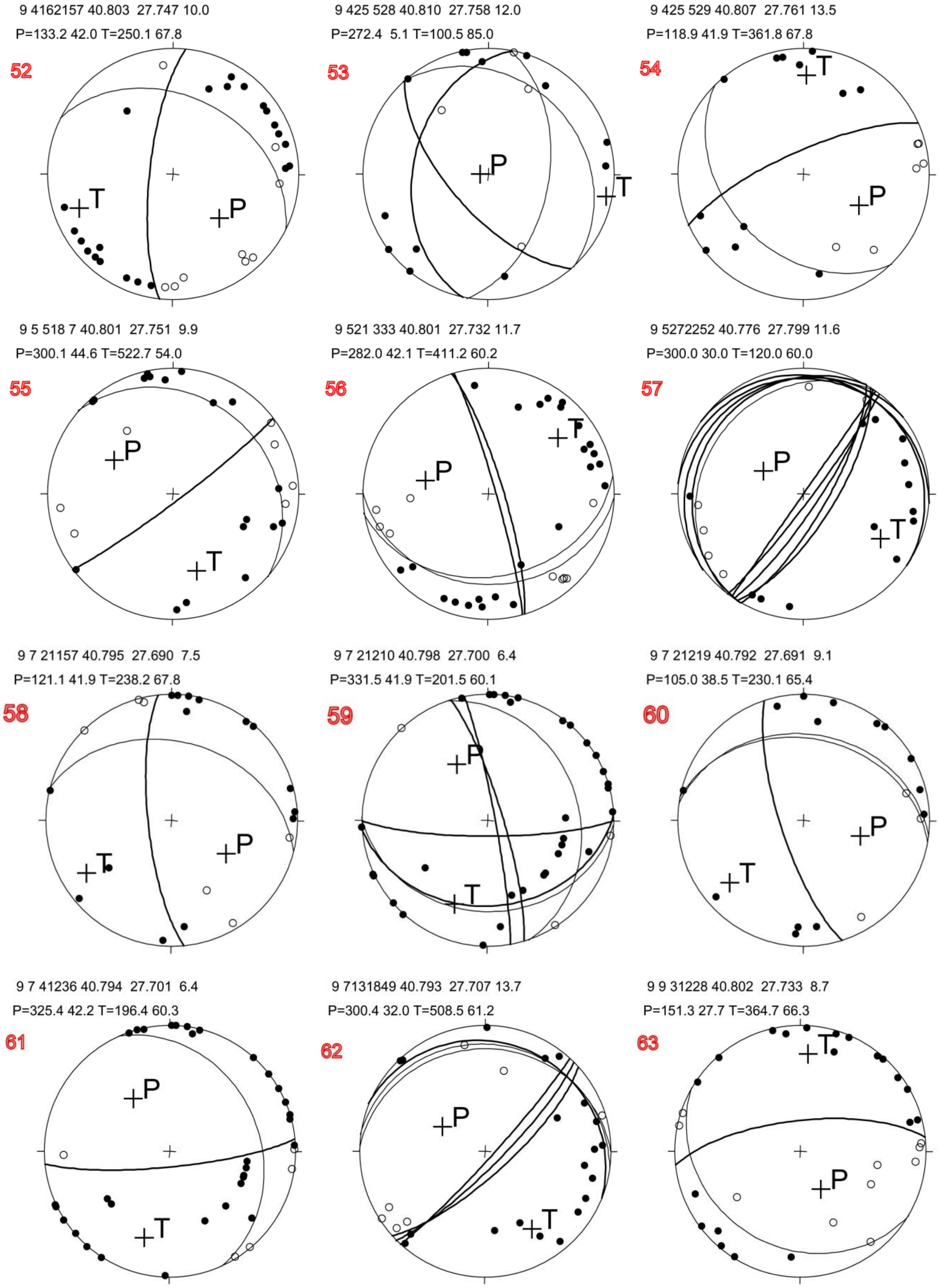

Figure C.2.6. Fault plane solutions obtained through the program of Horiuchi *et al.* (1995). Solutions are given time dependently for Tekirdağ Basin, and bold lines show fault planes

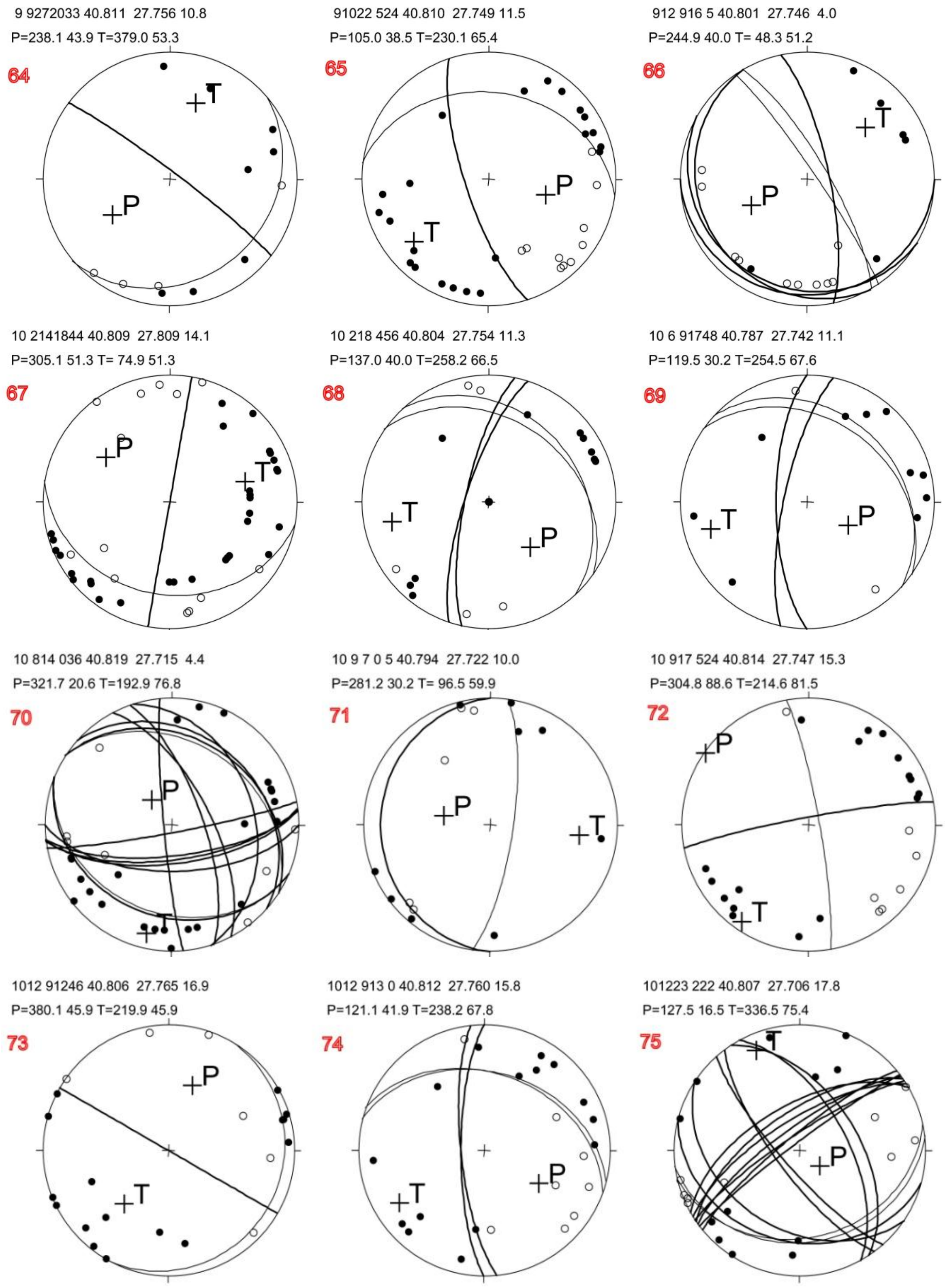

Figure C.2.7. Fault plane solutions obtained through the program of Horiuchi *et al.* (1995). Solutions are given time dependently for Tekirdağ Basin, and bold lines show fault planes

3. The Çınarcık Basin Cluster

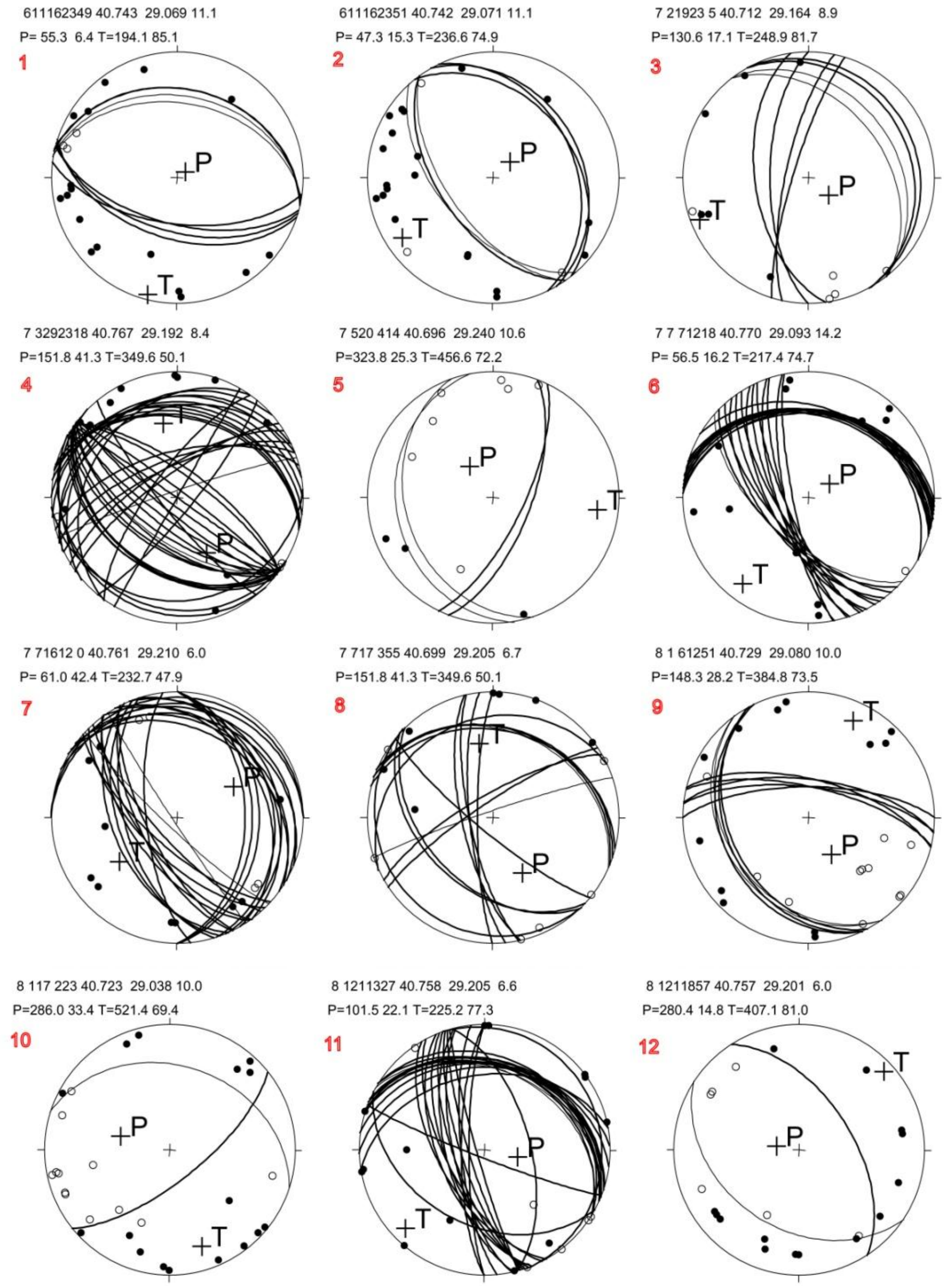

Figure C.3.1. Fault plane solutions obtained through the program of Horiuchi *et al.* (1995). Solutions are given time dependently for Çınarcık Basin, and bold lines show fault planes

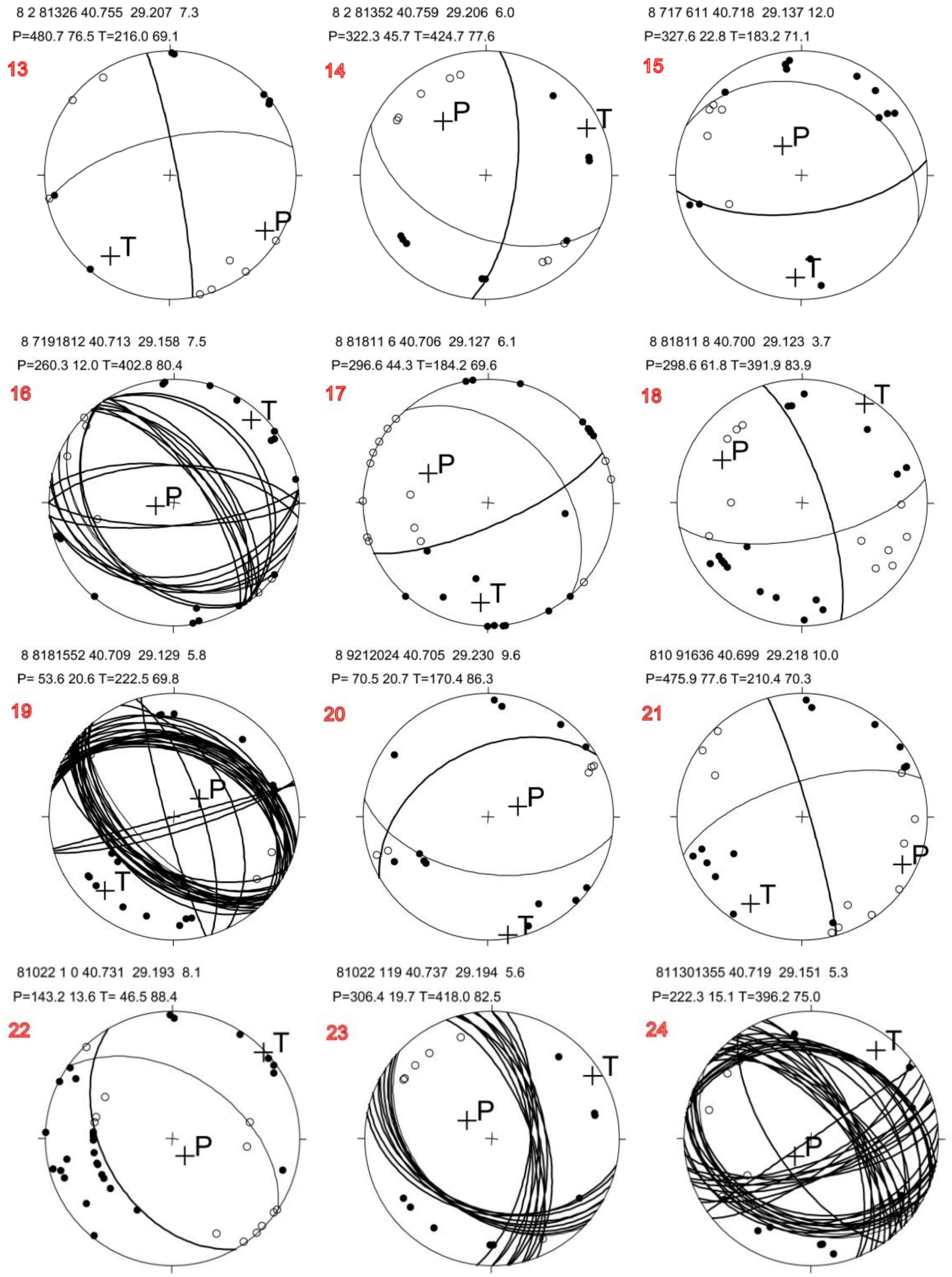

Figure C.3.2. Fault plane solutions obtained through the program of Horiuchi et al. (1995). Solutions are given time dependently for Çınarcık Basin, and bold lines show fault planes

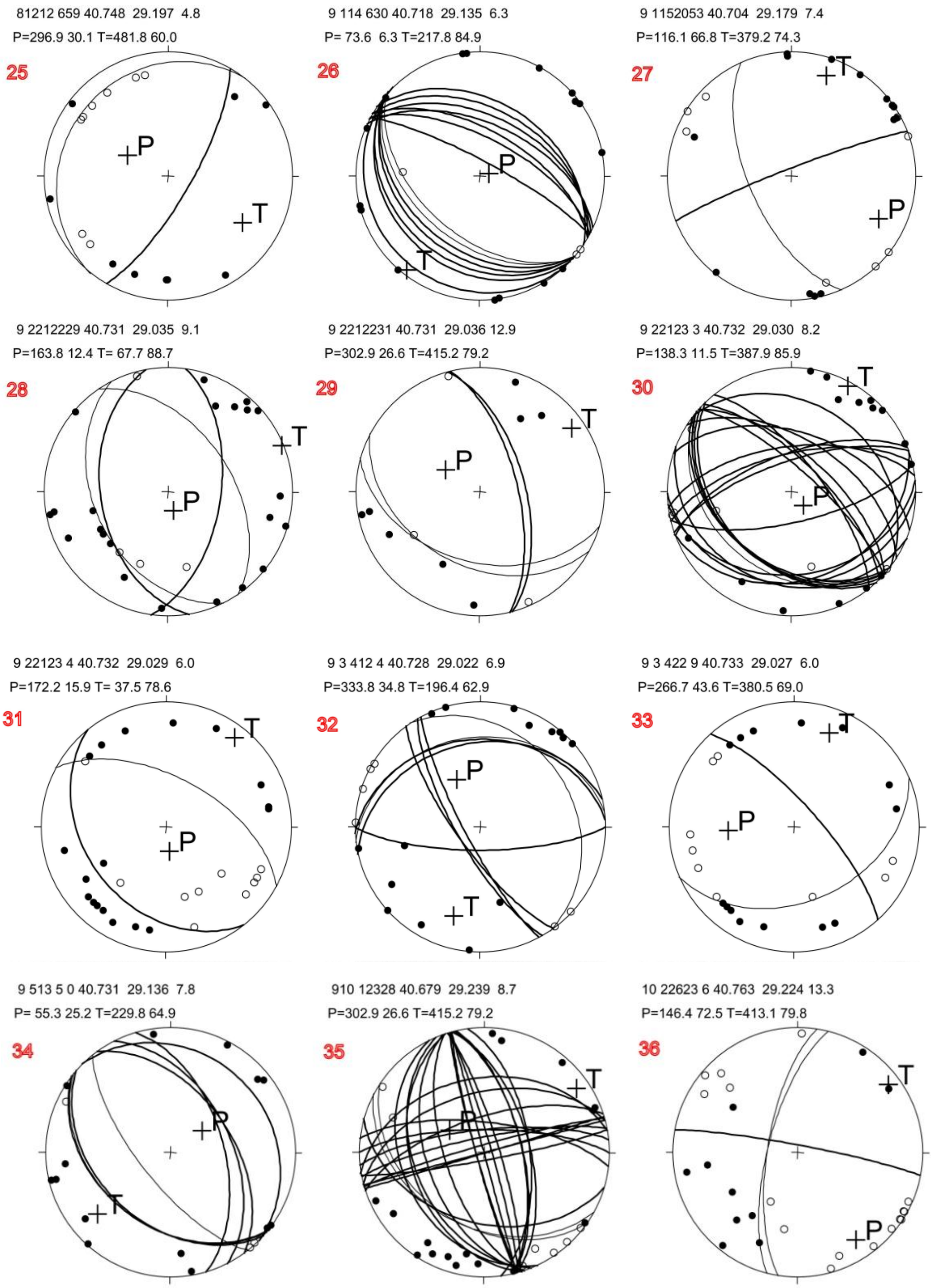

Figure C.3.3. Fault plane solutions obtained through the program of Horiuchi *et al.* (1995). Solutions are given time dependently for Çınarcık Basin, and bold lines show fault planes

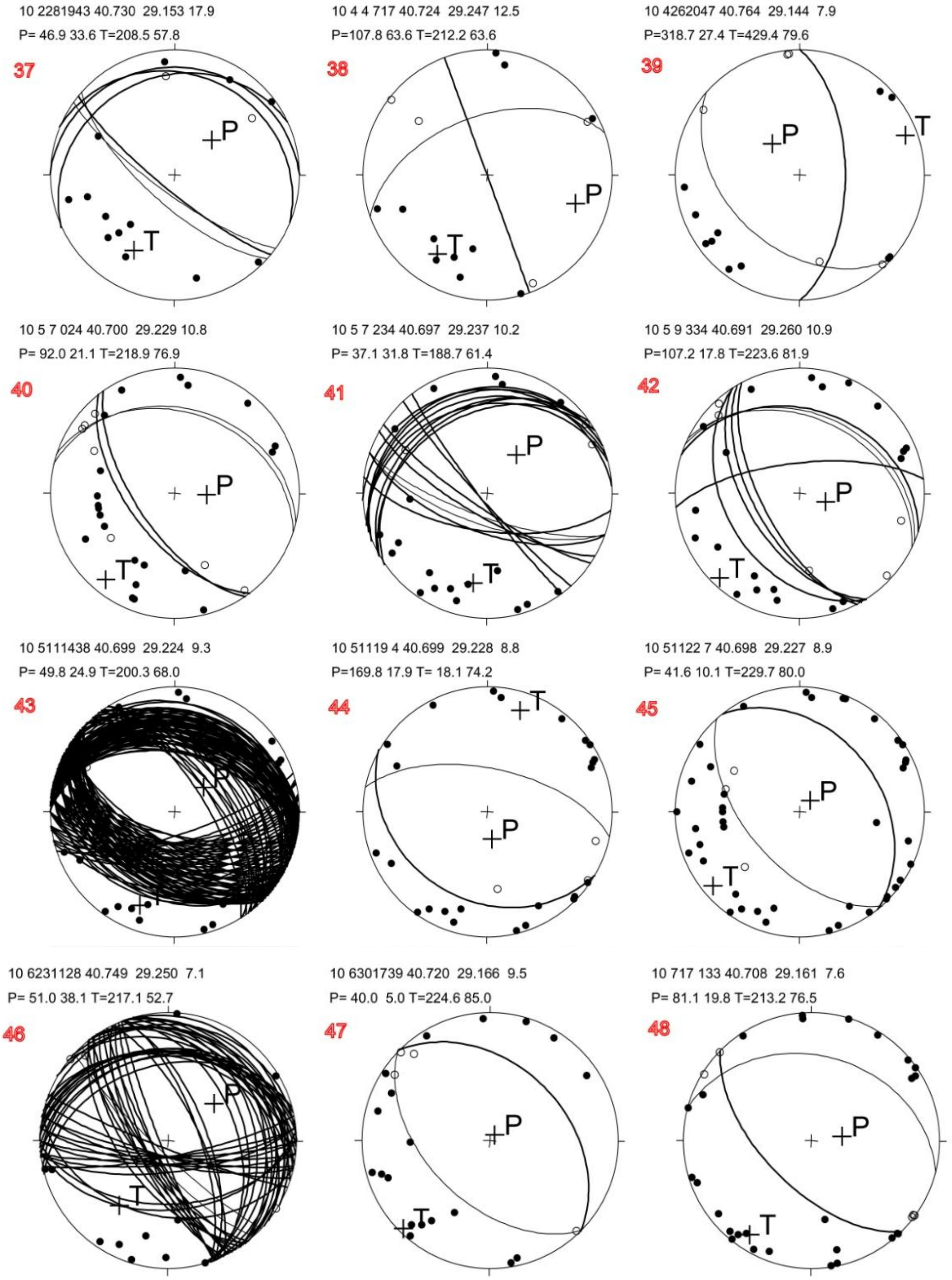

Figure C.3.4. Fault plane solutions obtained through the program of Horiuchi *et al.* (1995). Solutions are given time dependently for Çınarcık Basin, and bold lines show fault planes

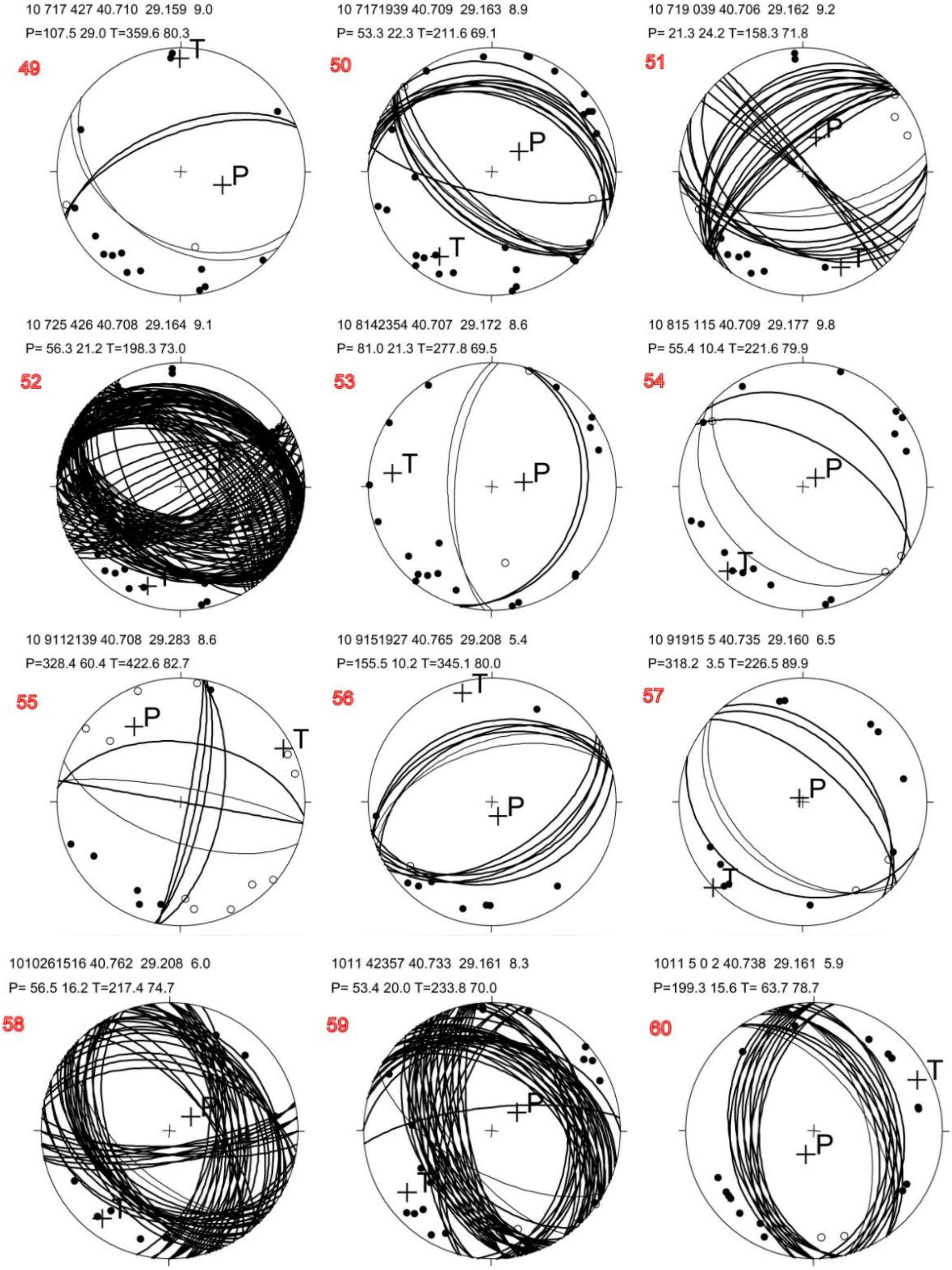

Figure C.3.5. Fault plane solutions obtained through the program of Horiuchi *et al.* (1995). Solutions are given time dependently for Çınarcık Basin, and bold lines show fault planes

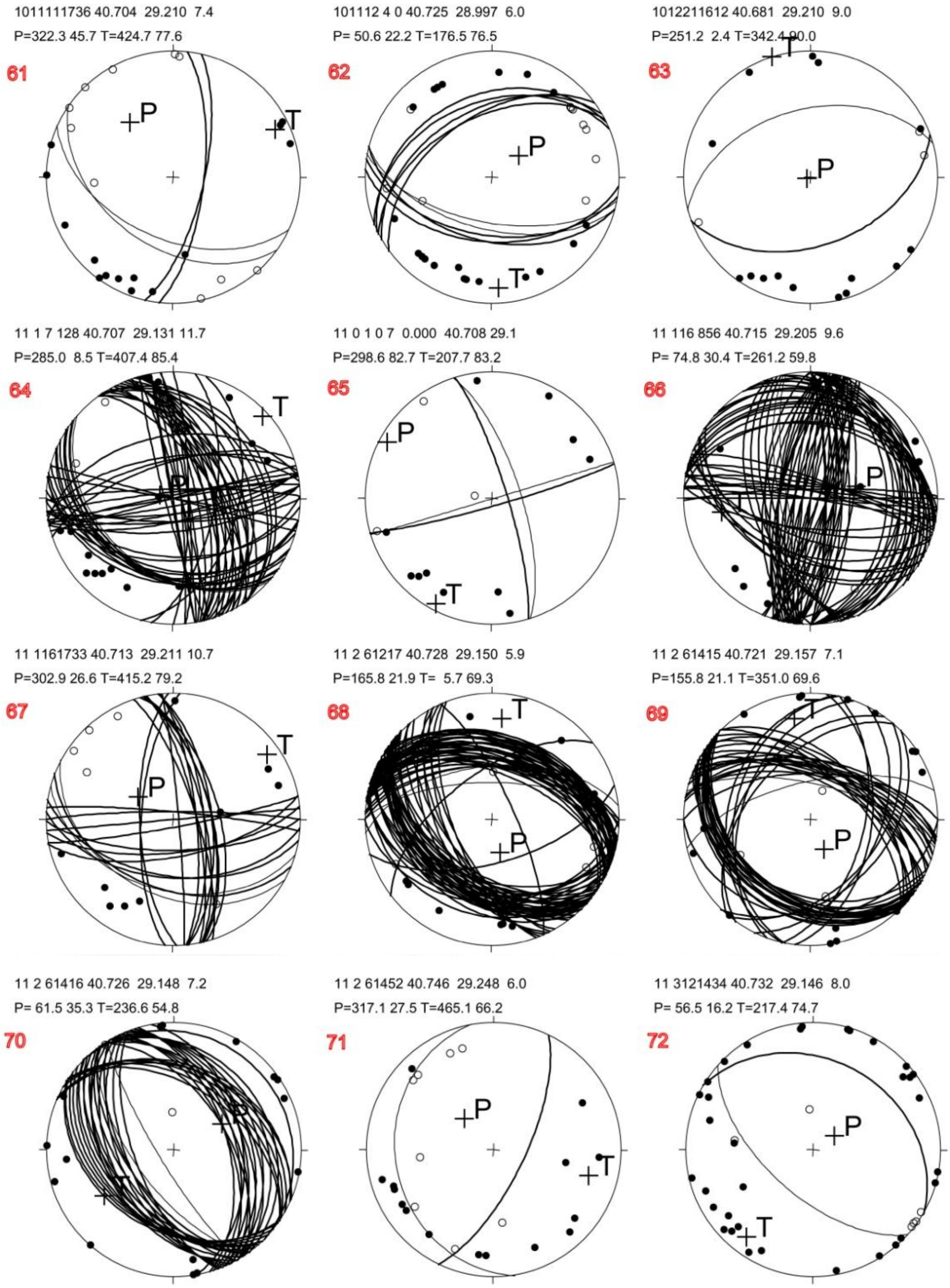

Figure C.3.6. Fault plane solutions obtained through the program of Horiuchi *et al.* (1995). Solutions are given time dependently for Çınarcık Basin, and bold lines show fault planes

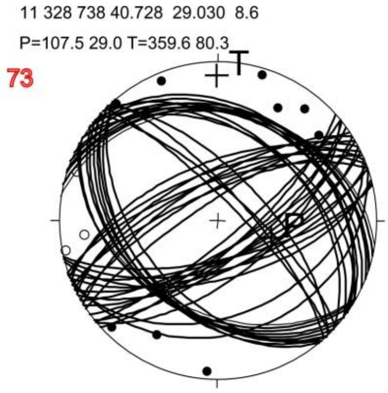

Figure C.3.7. Fault plane solutions obtained through the program of Horiuchi *et al.* (1995). Solutions are given time dependently for Çınarcık Basin, and bold lines show fault planes

4. The Yalova Cluster

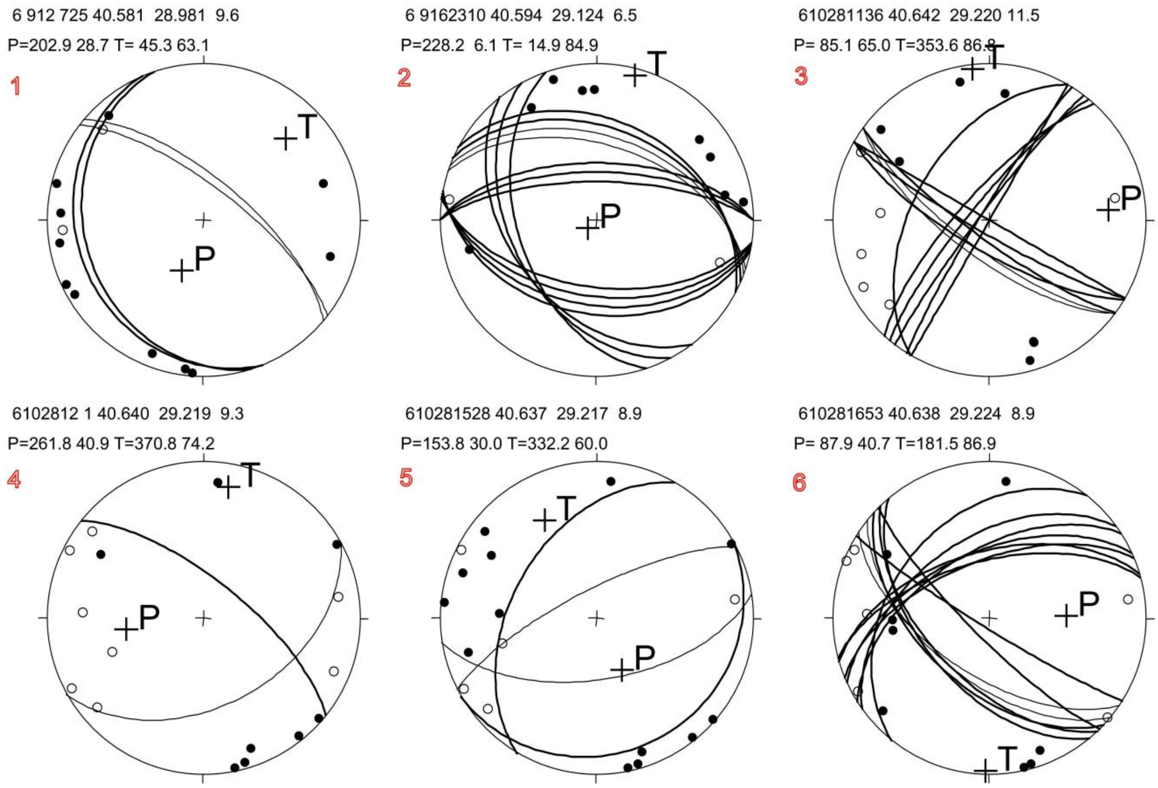

Figure C.4.1. Fault plane solutions obtained through the program of Horiuchi *et al.* (1995). Solutions are given time dependently for Yalova Region, and bold lines show fault planes

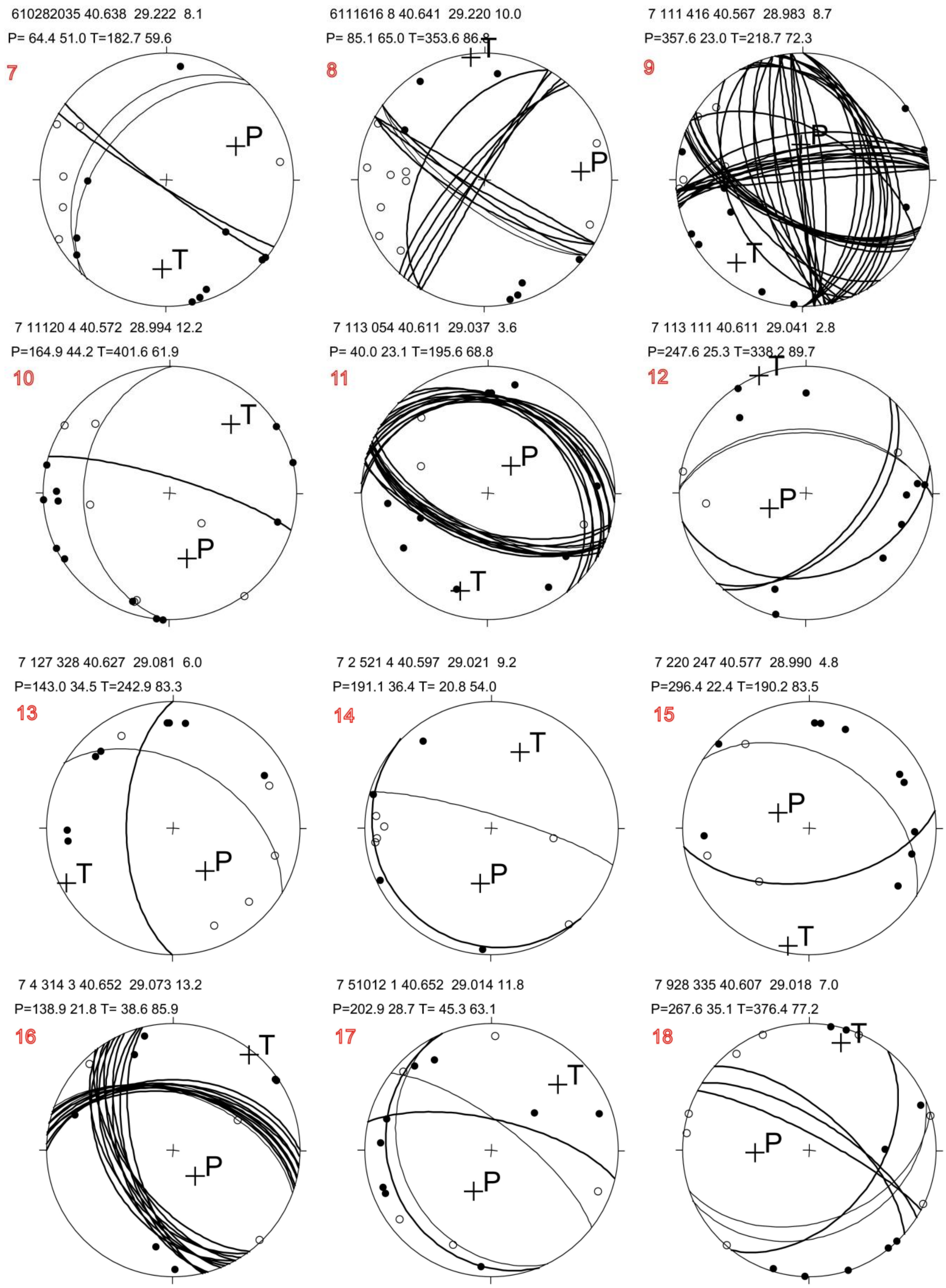

Figure C.4.2. Fault plane solutions obtained through the program of Horiuchi *et al.* (1995). Solutions are given time dependently for Yalova Region, and bold lines show fault planes

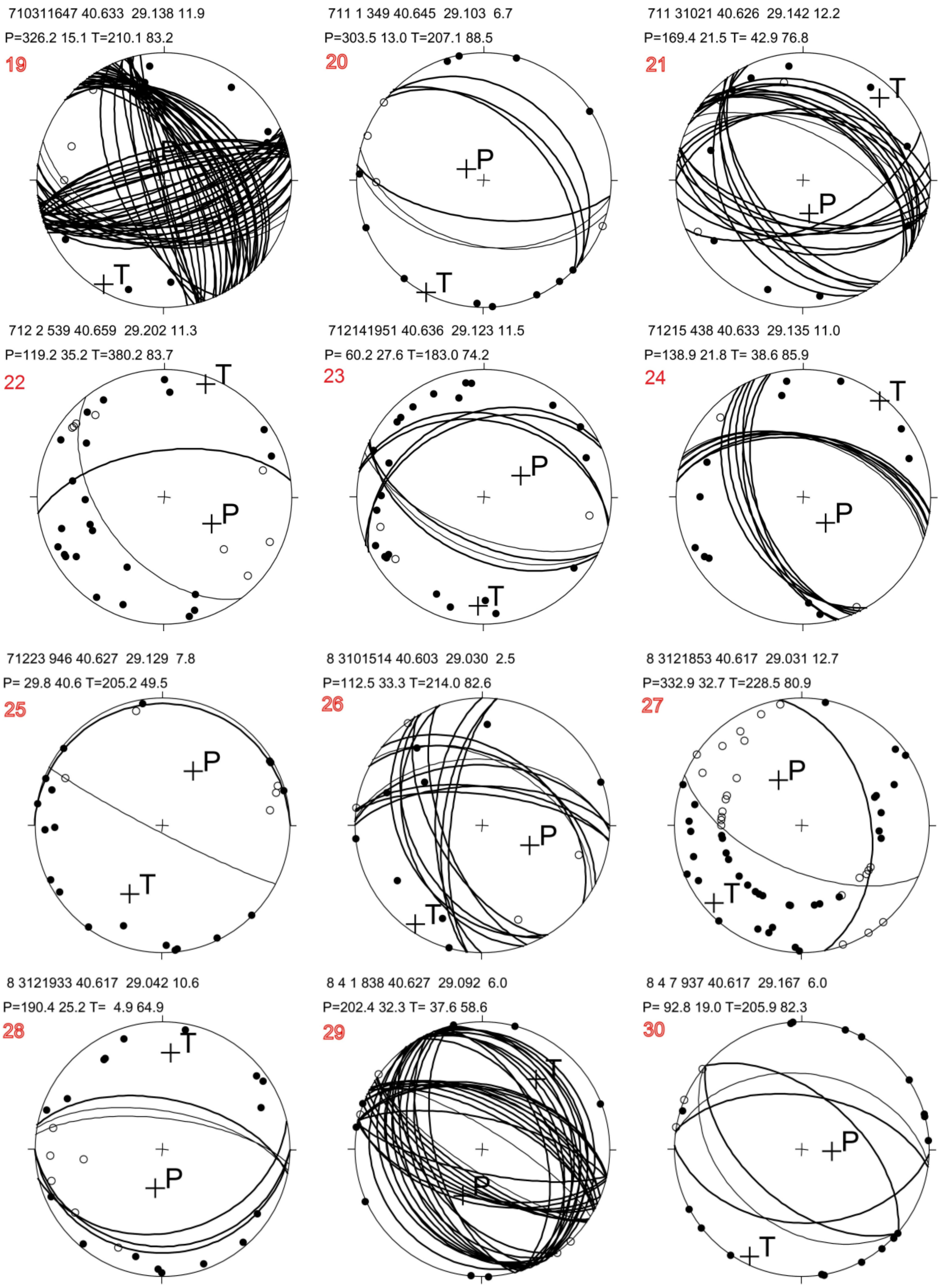

Figure C.4.3. Fault plane solutions obtained through the program of Horiuchi *et al.* (1995). Solutions are given time dependently for Yalova Region, and bold lines show fault planes

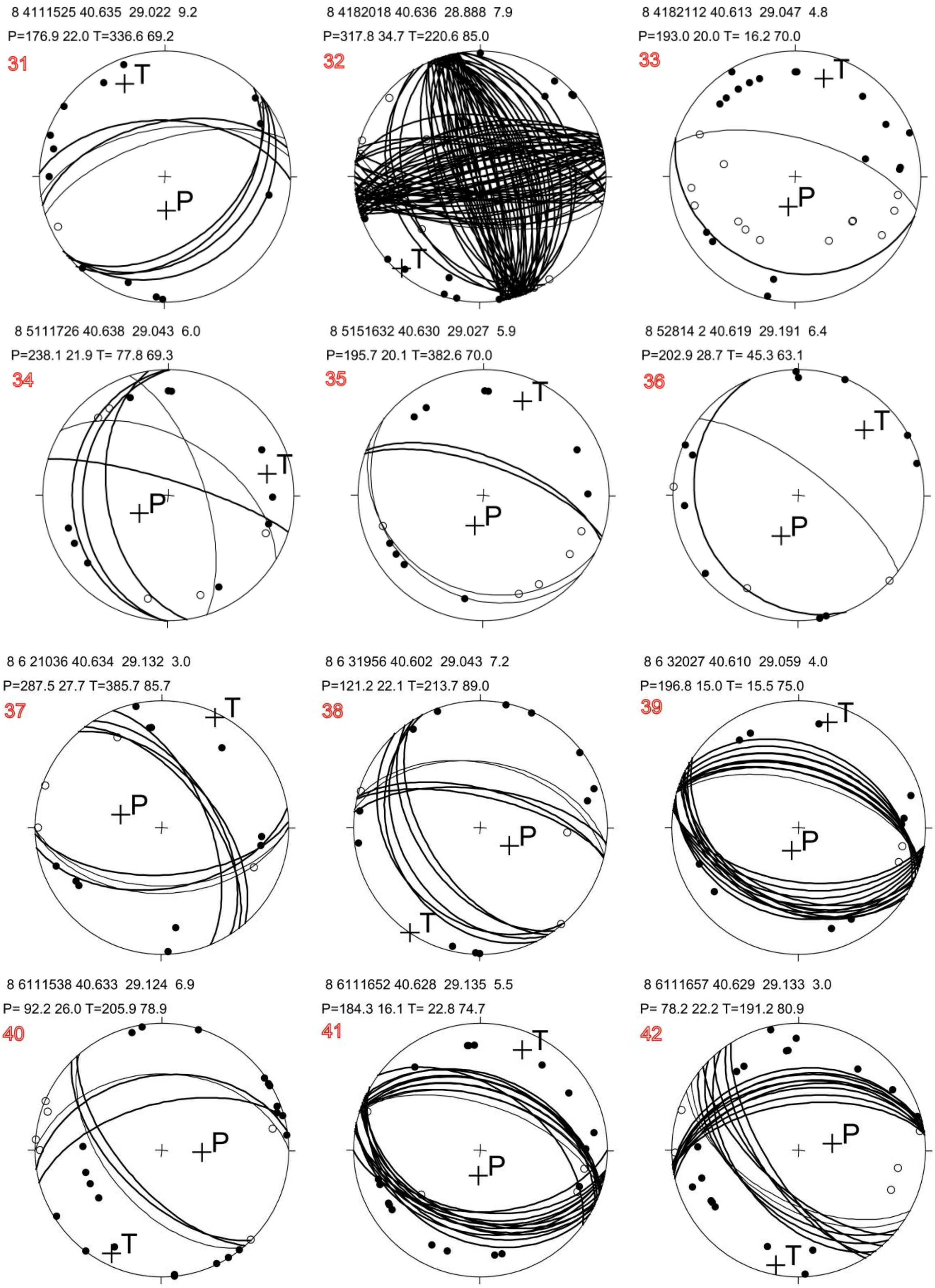

Figure C.4.4. Fault plane solutions obtained through the program of Horiuchi *et al.* (1995). Solutions are given time dependently for Yalova Region, and bold lines show fault planes

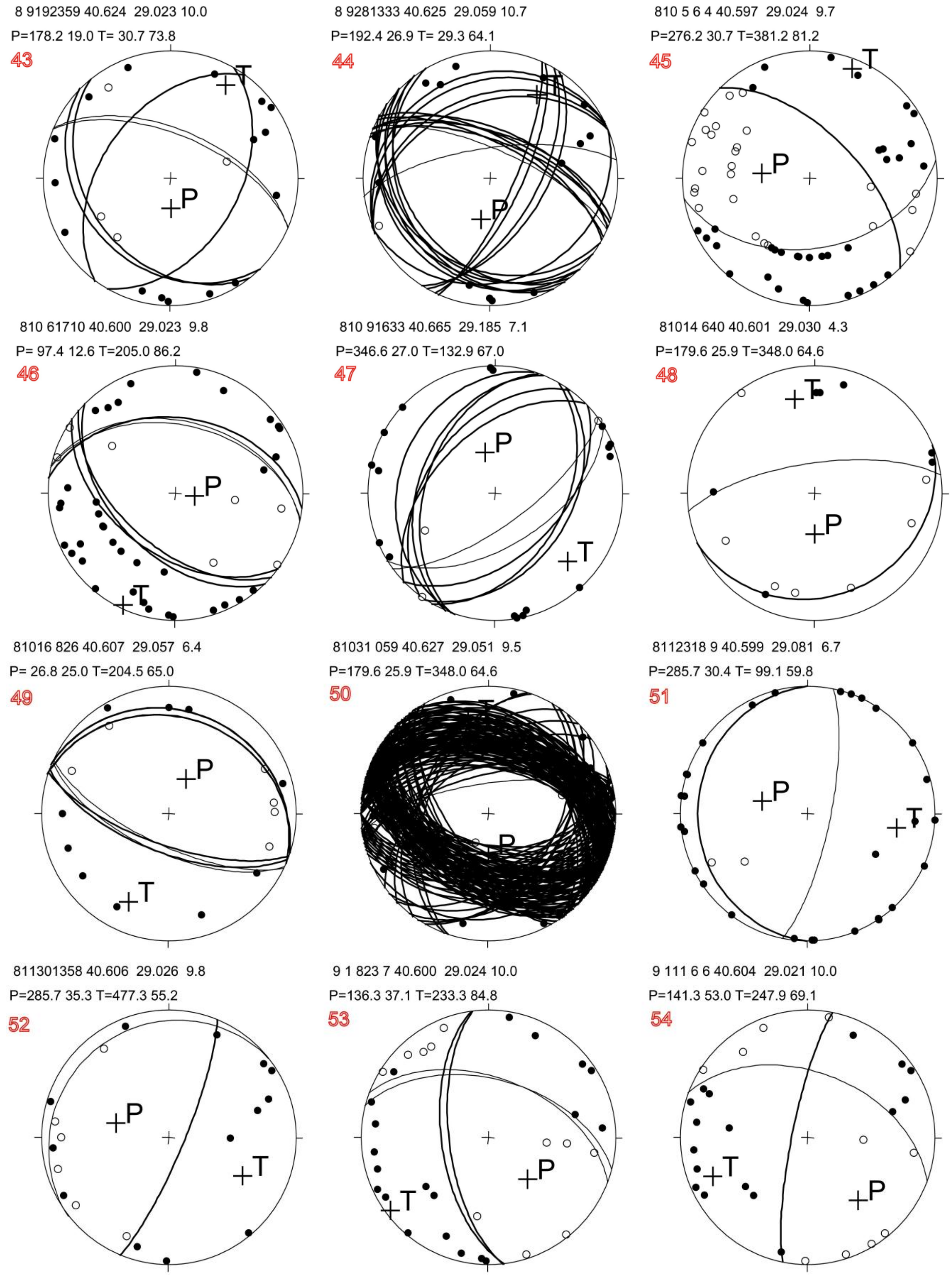

Figure C.4.5. Fault plane solutions obtained through the program of Horiuchi *et al.* (1995). Solutions are given time dependently for Yalova Region, and bold lines show fault planes

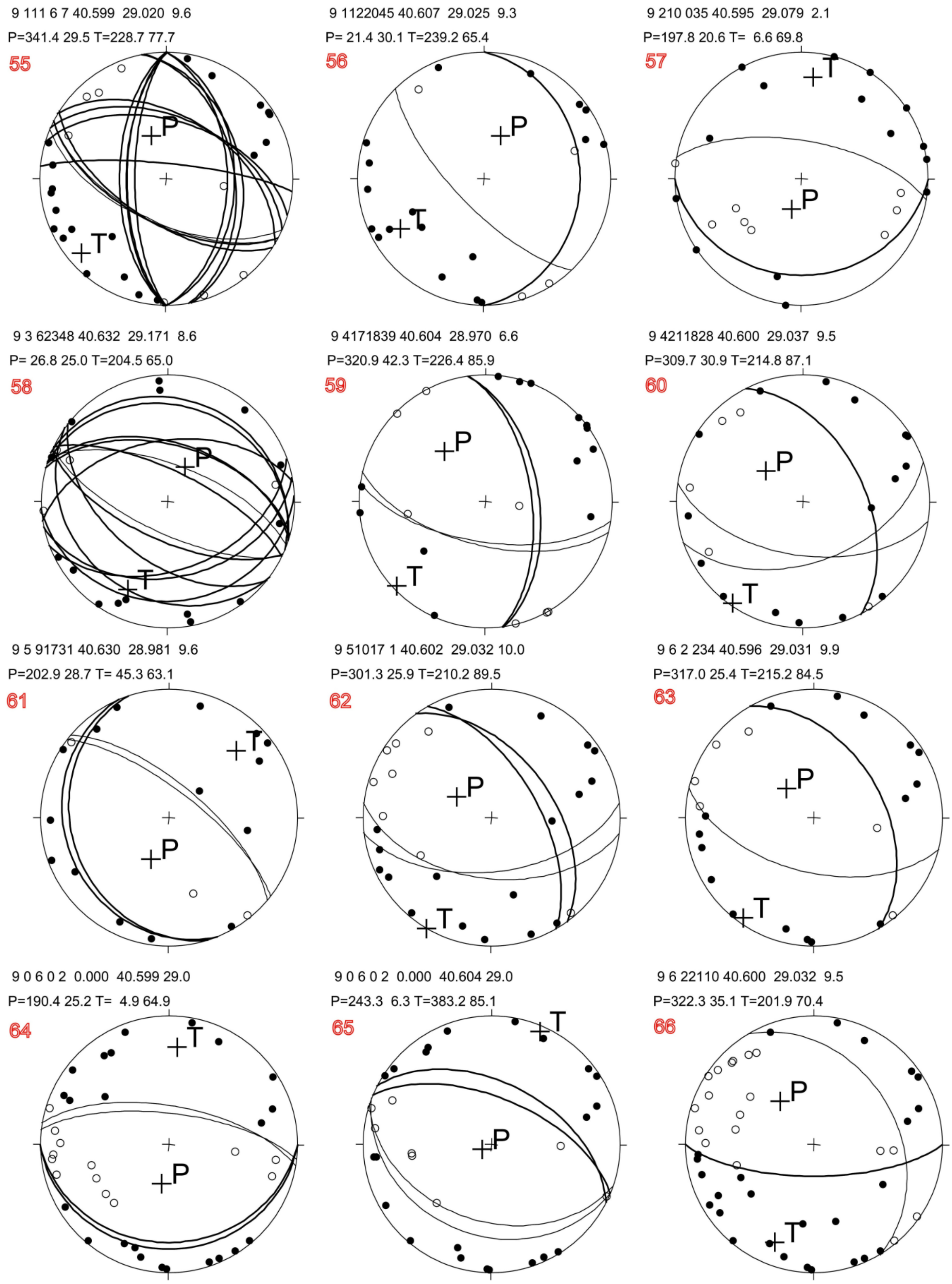

Figure C.4.6. Fault plane solutions obtained through the program of Horiuchi *et al.* (1995). Solutions are given time dependently for Yalova Region, and bold lines show fault planes

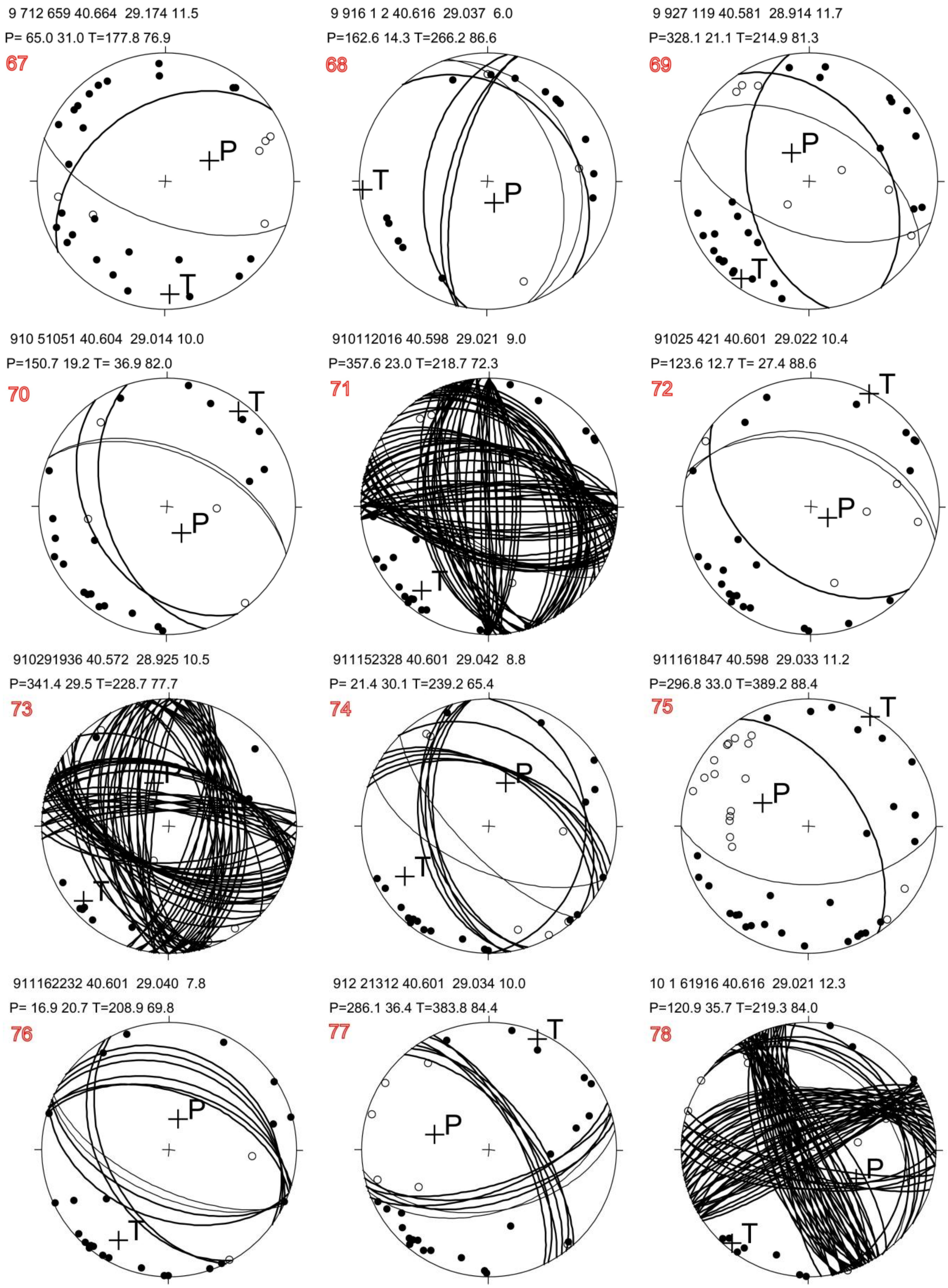

Figure C.4.7. Fault plane solutions obtained through the program of Horiuchi *et al.* (1995). Solutions are given time dependently for Yalova Region, and bold lines show fault planes

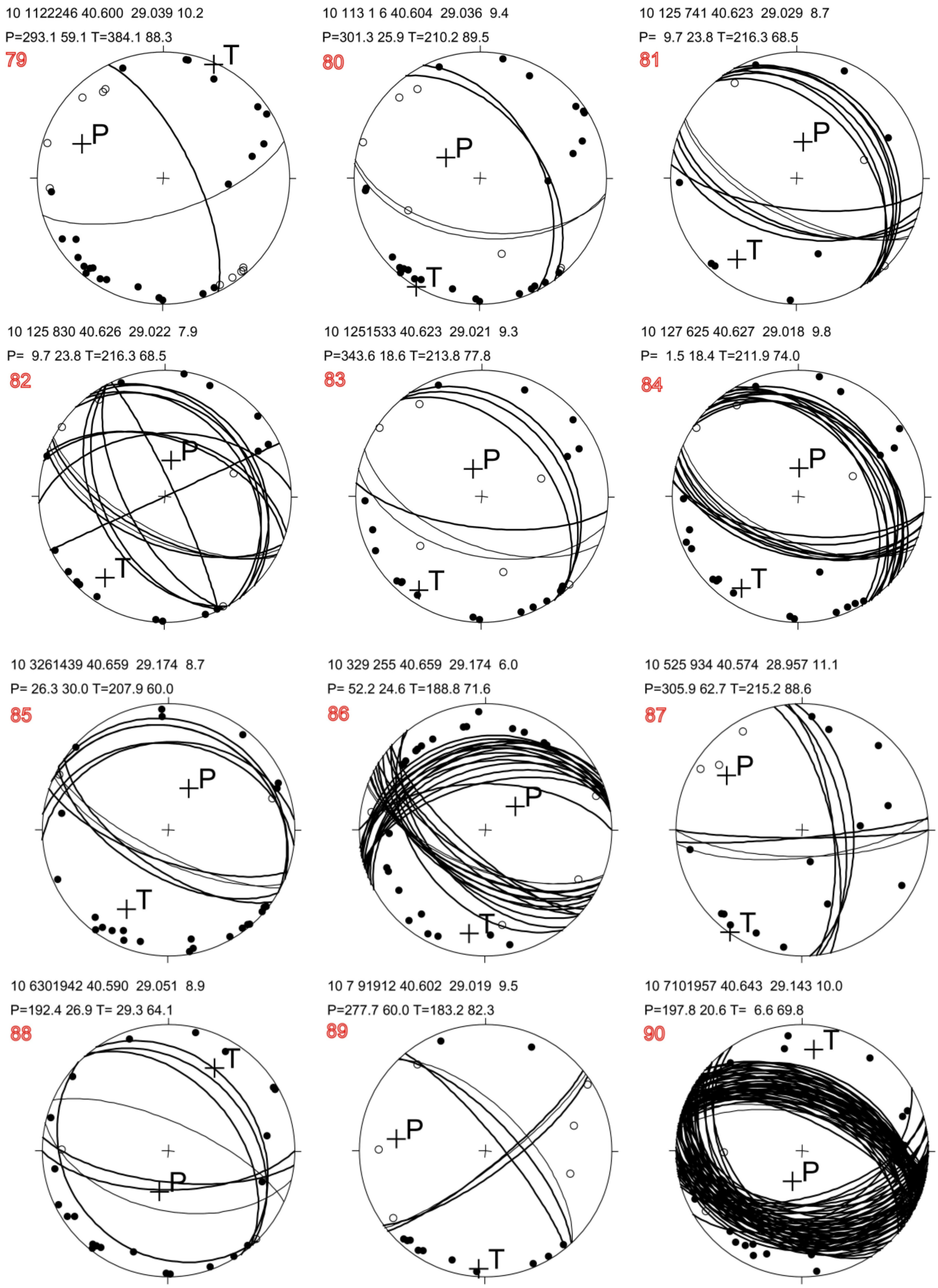

Figure C.4.8. Fault plane solutions obtained through the program of Horiuchi *et al.* (1995). Solutions are given time dependently for Yalova Region, and bold lines show fault planes

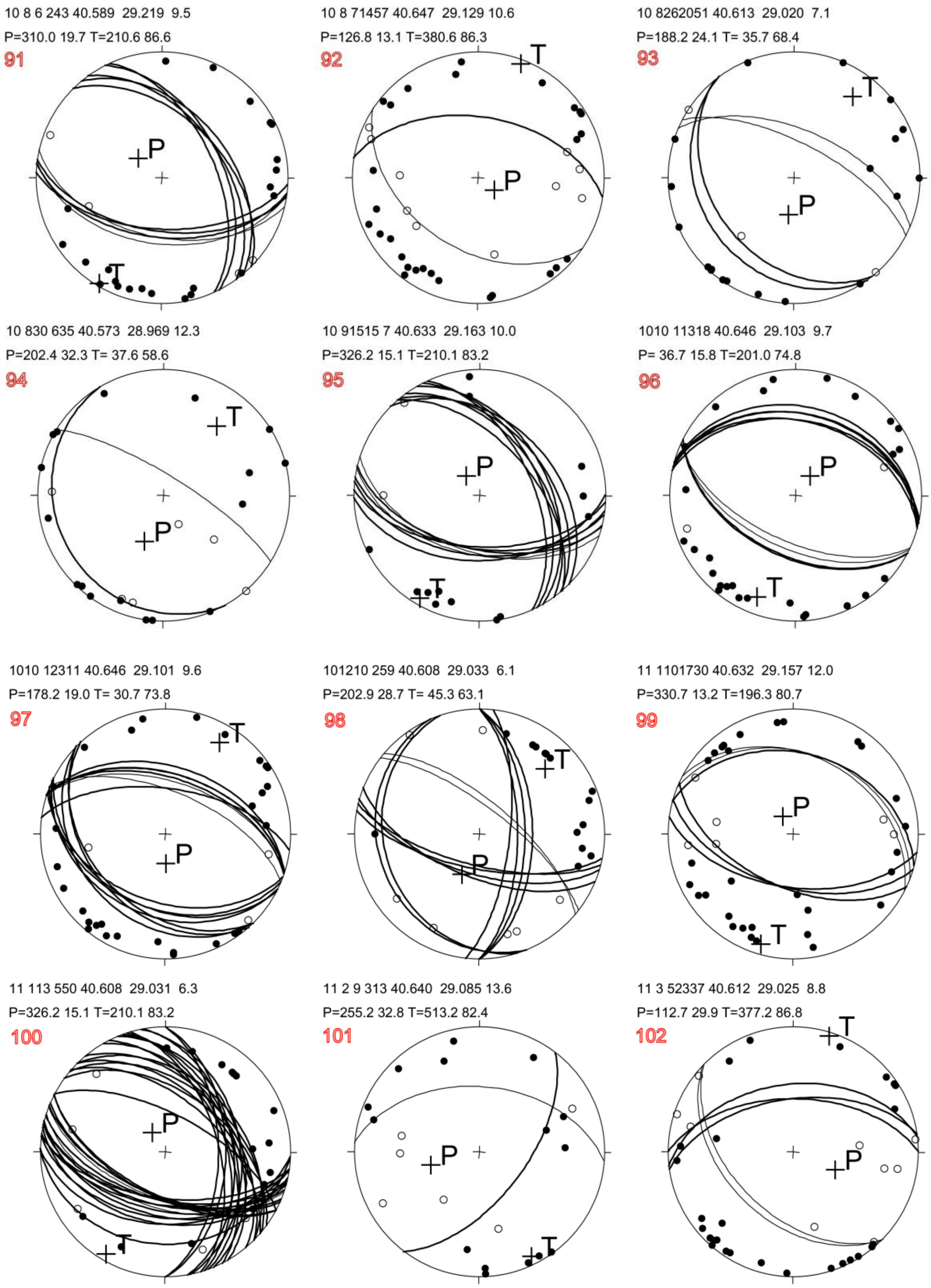

Figure C.4.9. Fault plane solutions obtained through the program of Horiuchi *et al.* (1995). Solutions are given time dependently for Yalova Region, and bold lines show fault planes

5. The Gemlik Cluster

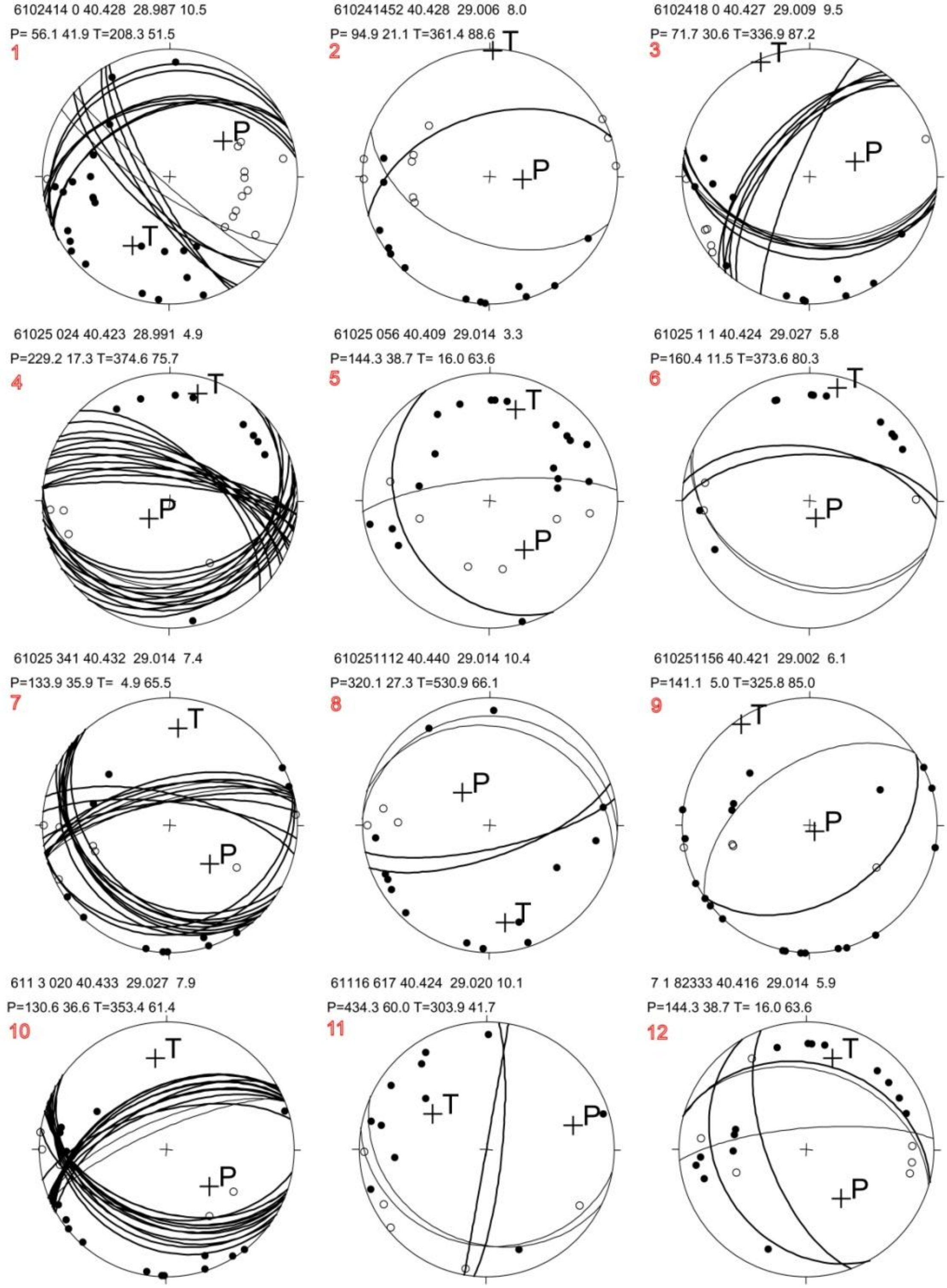

Figure C.5.1. Fault plane solutions obtained through the program of Horiuchi *et al.* (1995). Solutions are given time dependently for Gemlik Region, and bold lines show fault planes

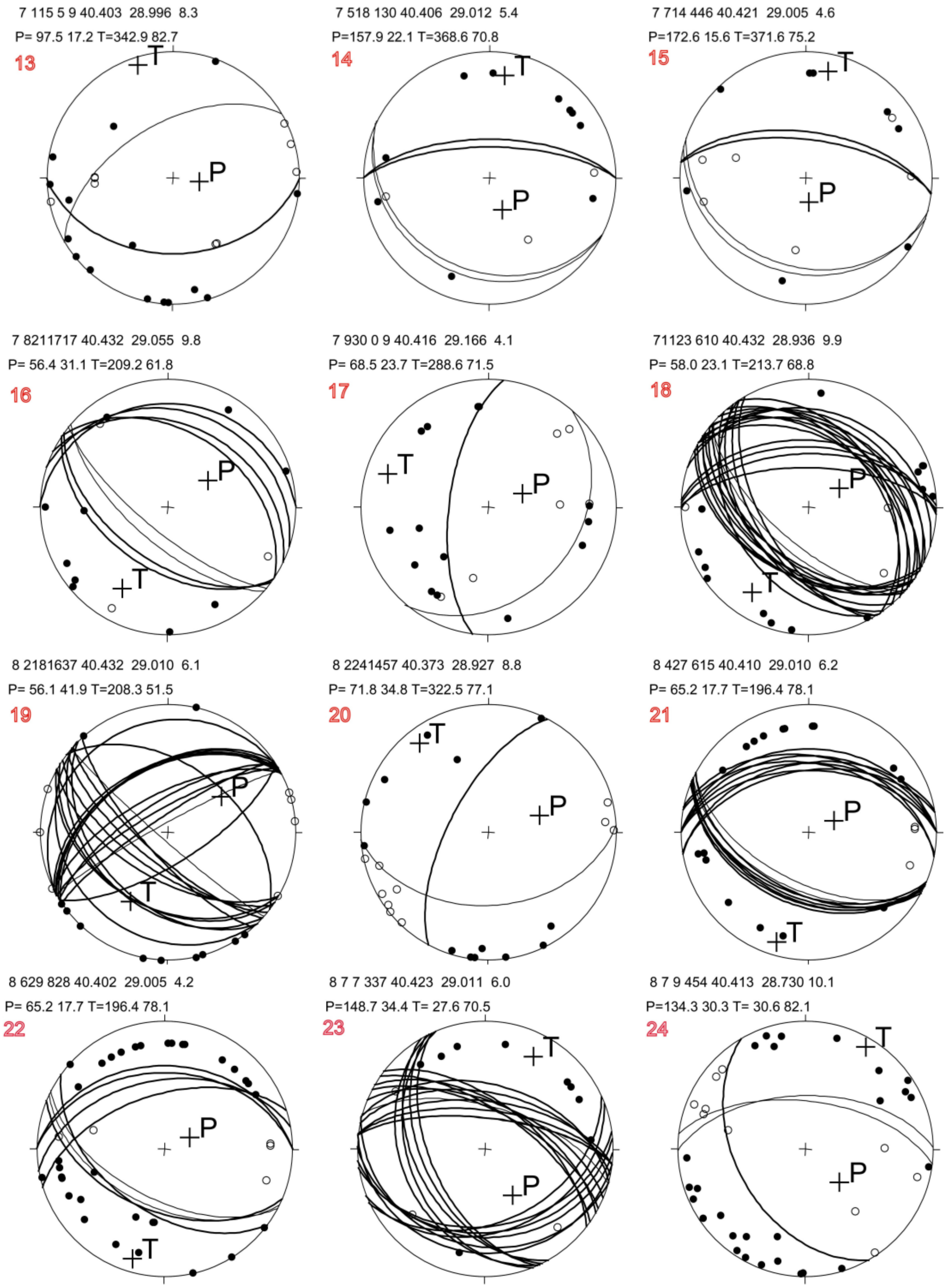

Figure C.5.2. Fault plane solutions obtained through the program of Horiuchi *et al.* (1995). Solutions are given time dependently for Gemlik Region, and bold lines show fault planes

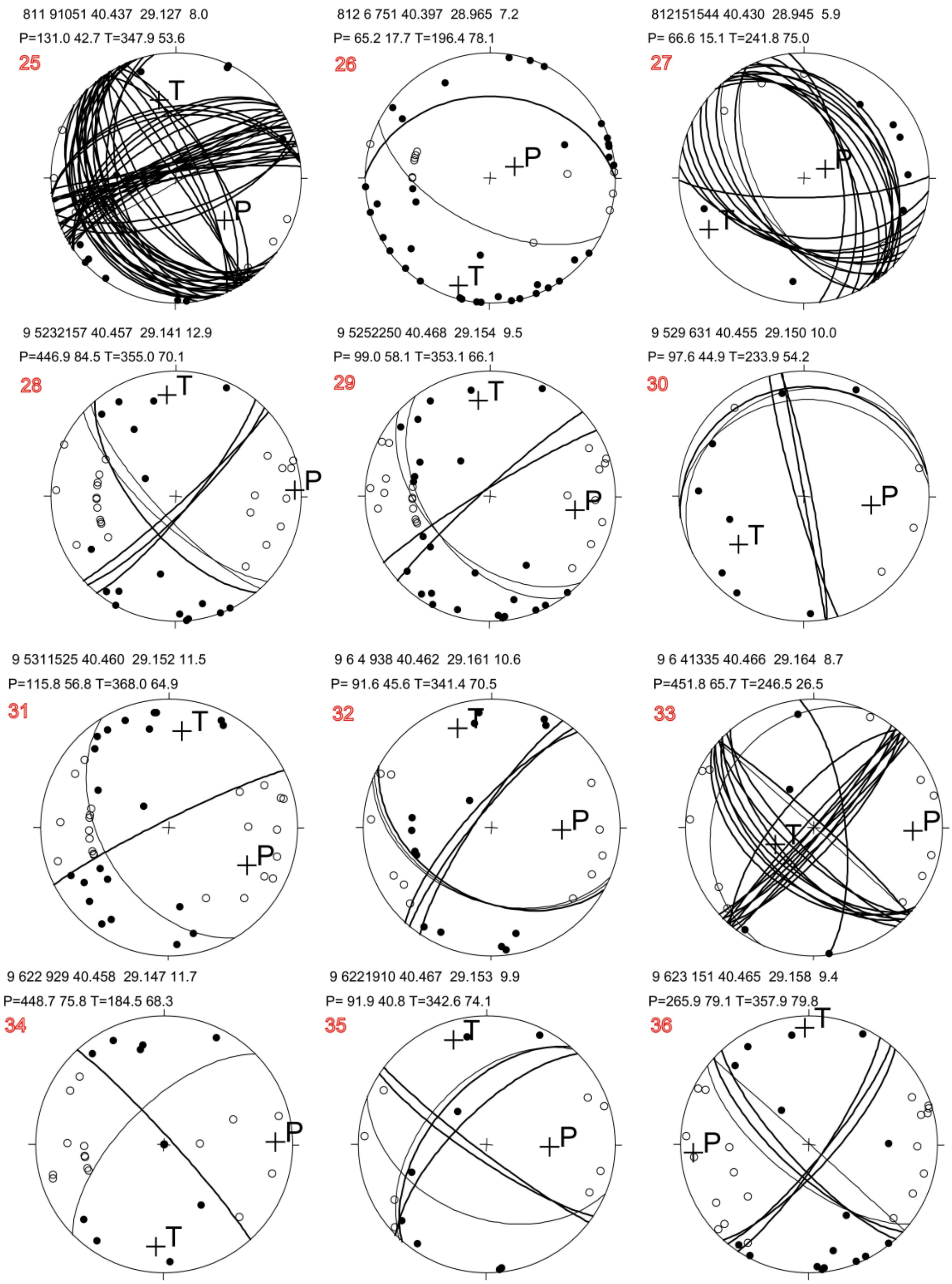

Figure C.5.3. Fault plane solutions obtained through the program of Horiuchi *et al.* (1995). Solutions are given time dependently for Gemlik Region, and bold lines show fault planes

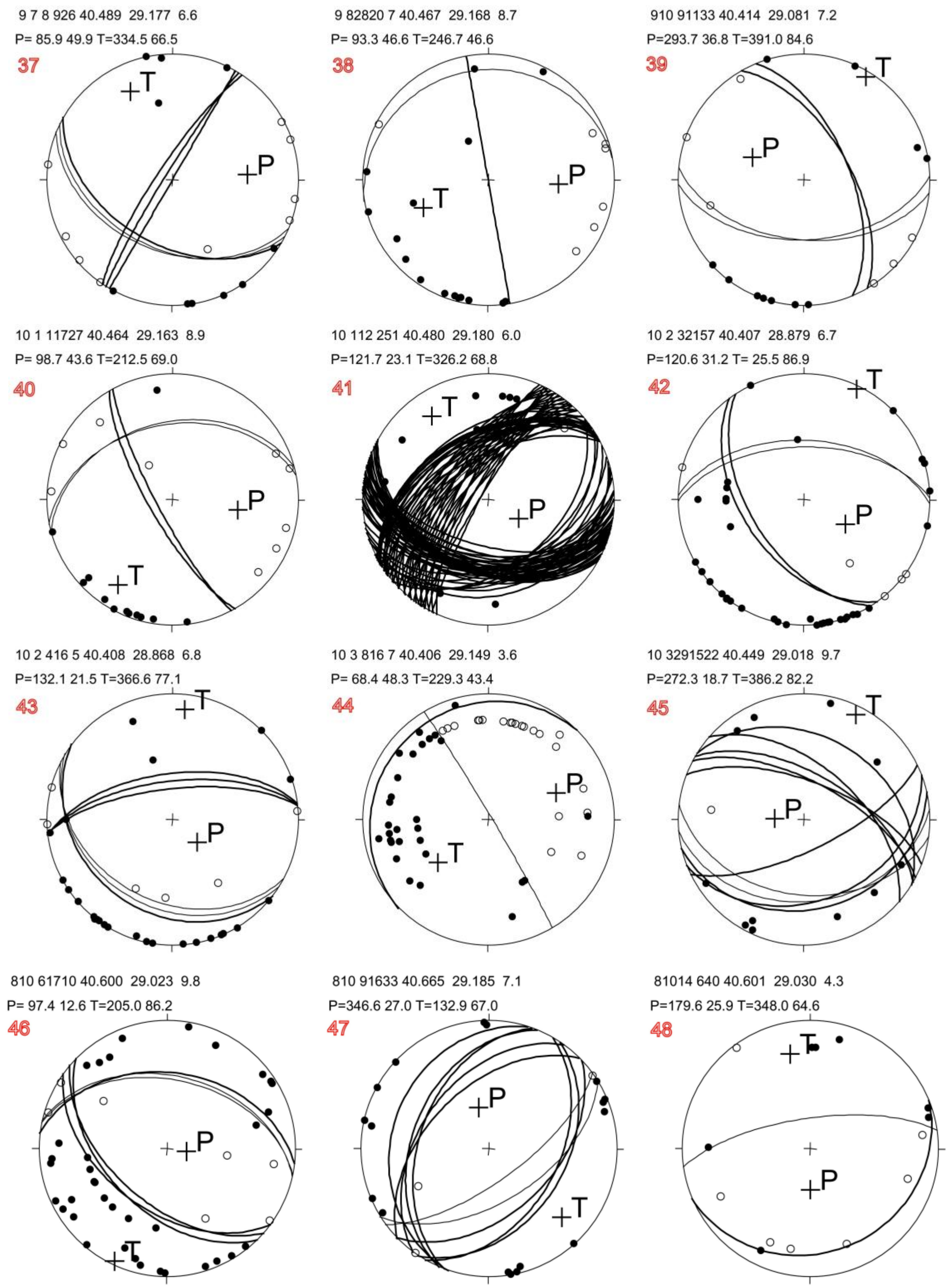

Figure C.5.4. Fault plane solutions obtained through the program of Horiuchi *et al.* (1995). Solutions are given time dependently for Gemlik Region, and bold lines show fault planes

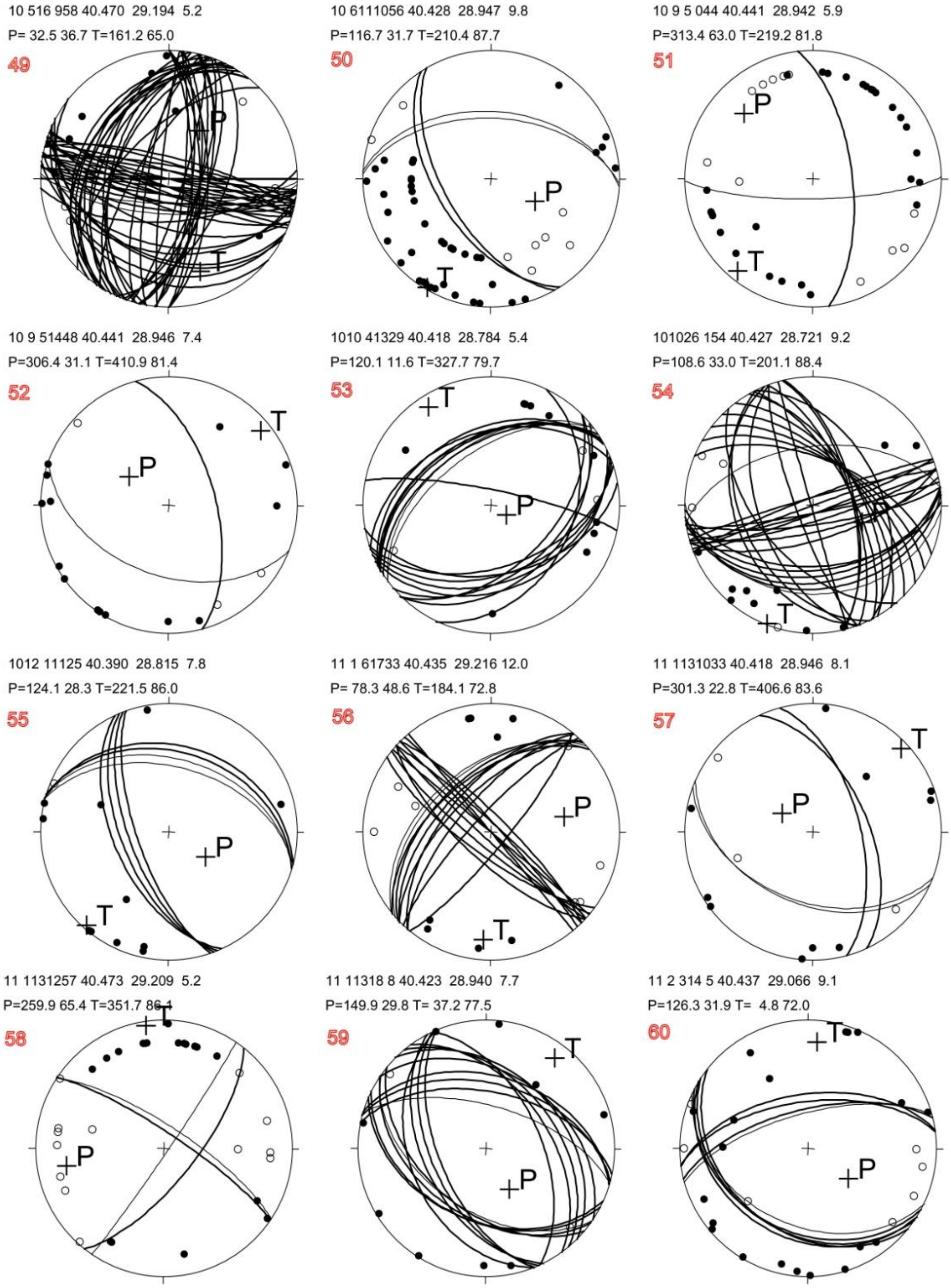

Figure C.5.5. Fault plane solutions obtained through the program of Horiuchi *et al.* (1995). Solutions are given time dependently for Gemlik Region, and bold lines show fault planes

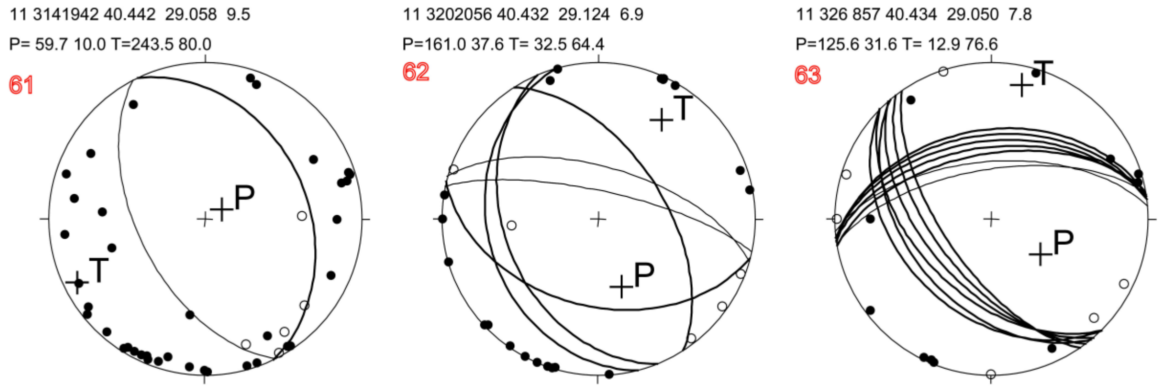

Figure C.5.6. Fault plane solutions obtained through the program of Horiuchi *et al.* (1995). Solutions are given time dependently for Gemlik Region, and bold lines show fault planes

APPENDIX D. FAULT PLANE SOLUTIONS OBTAINED BY THE FOCMEC PROGRAM

1. The Ganos Offshore Cluster

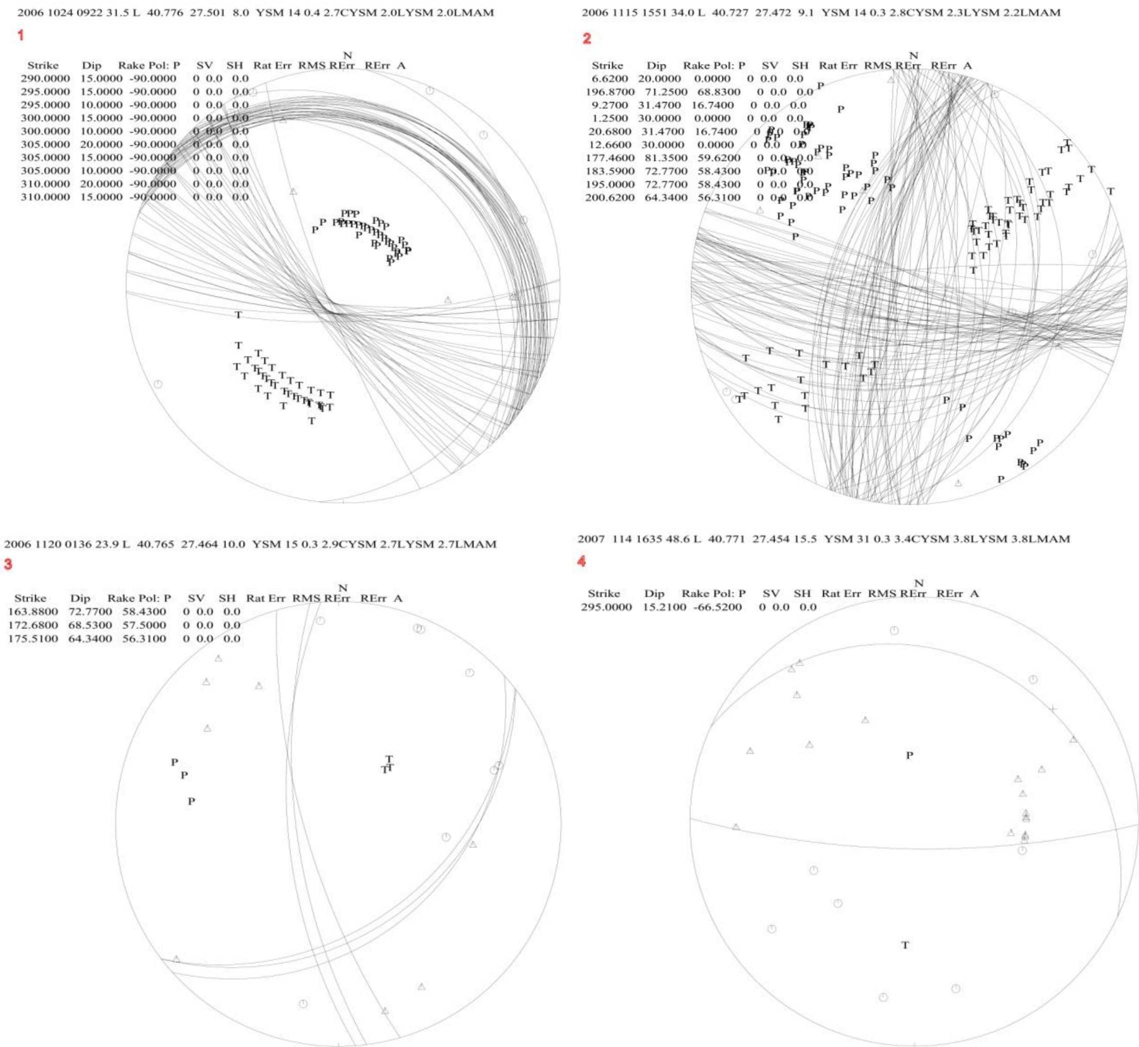

Figure D.1.1. Lower hemisphere projections of fault plane solutions obtained through the program of FOCMEC. Black circles indicate compressional P-wave first motion polarities, while black triangles show dilatational ones. Solutions are given time dependently for the Ganos Offshore Cluster

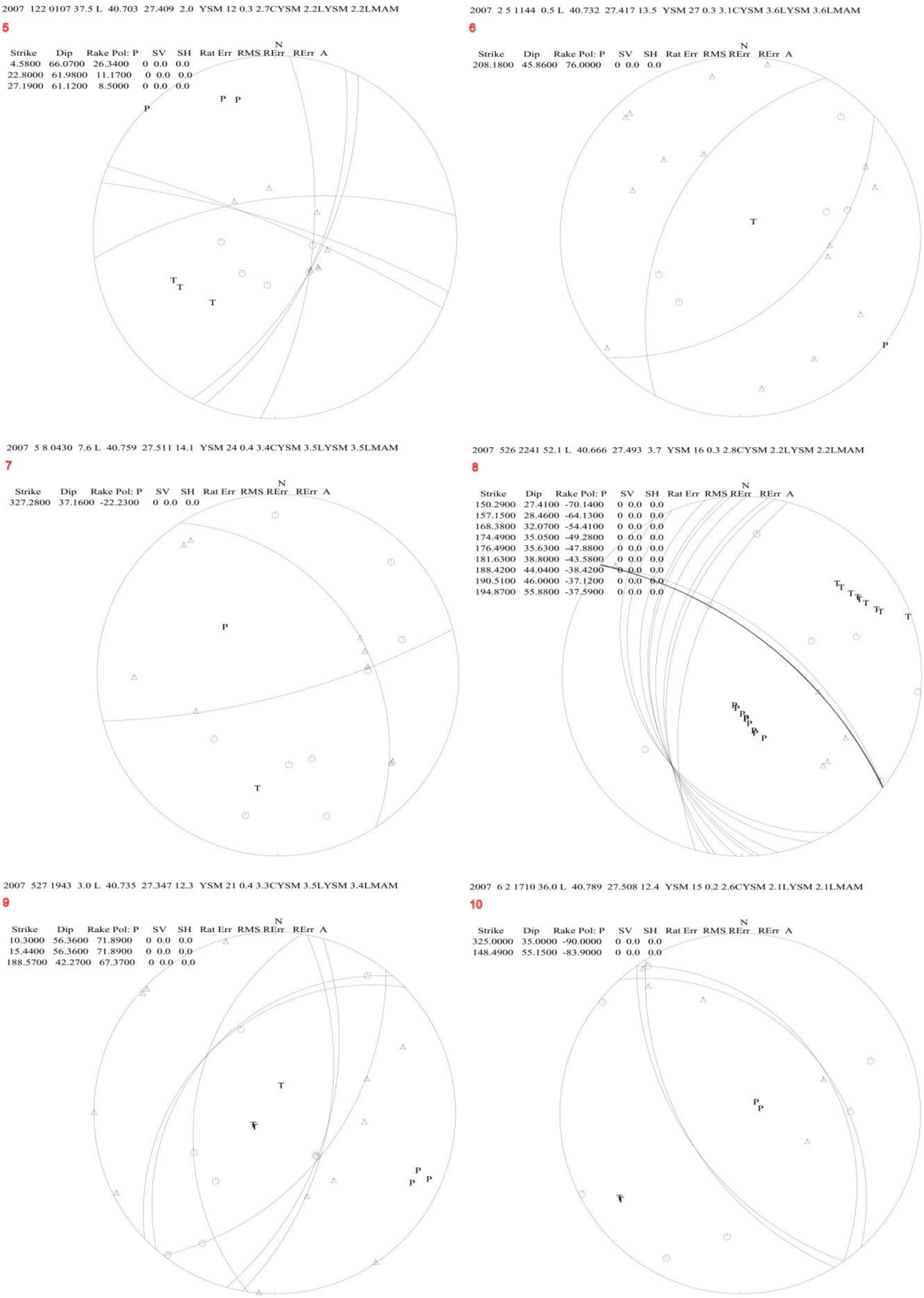

Figure D.1.2. Fault plane solutions obtained through the program of FOCMEC. Solutions are given time dependently for the Ganos Offshore Cluster

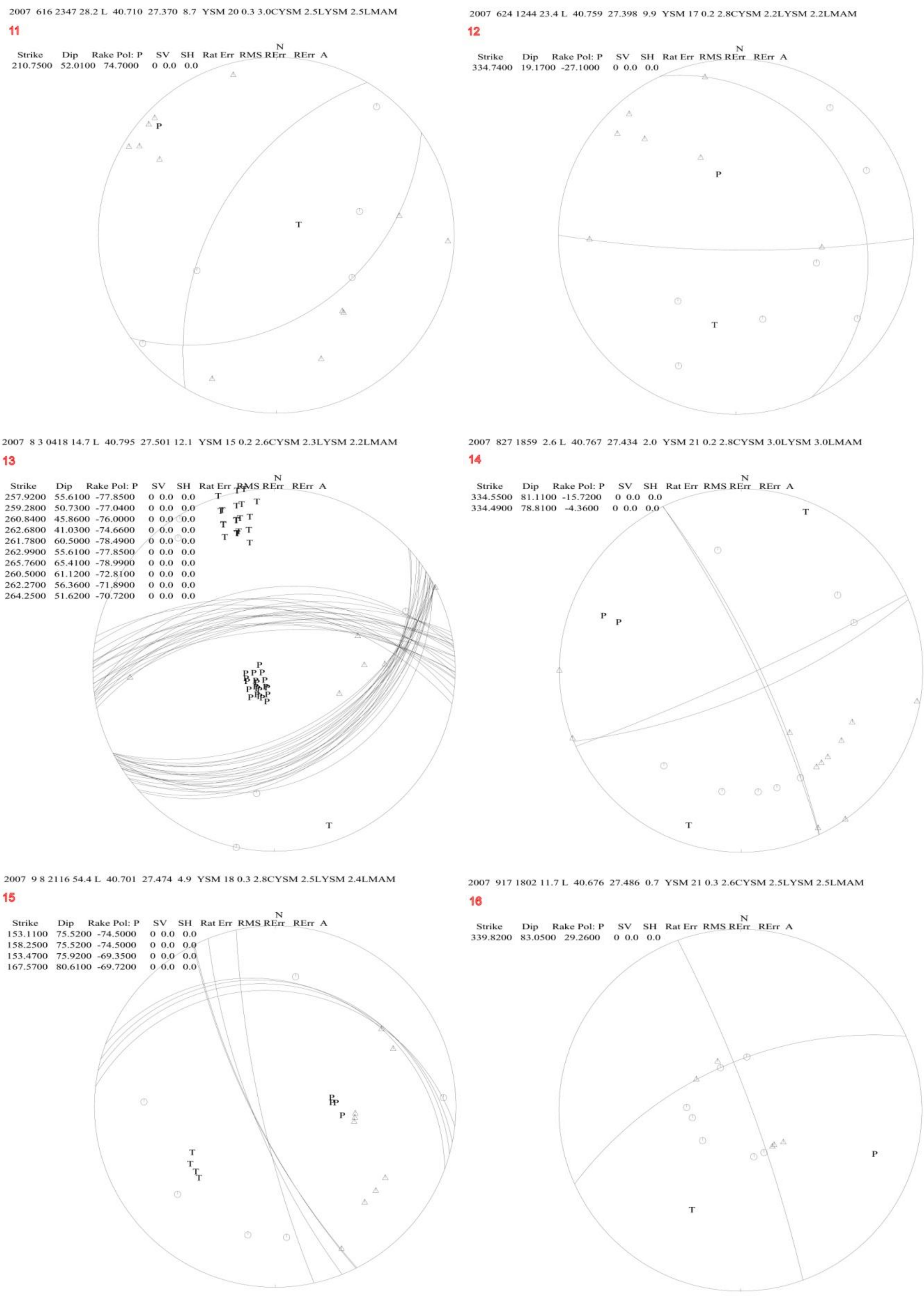

Figure D.1.3. Fault plane solutions obtained through the program of FOCMEC. Solutions are given time dependently for the Ganos Offshore Cluster

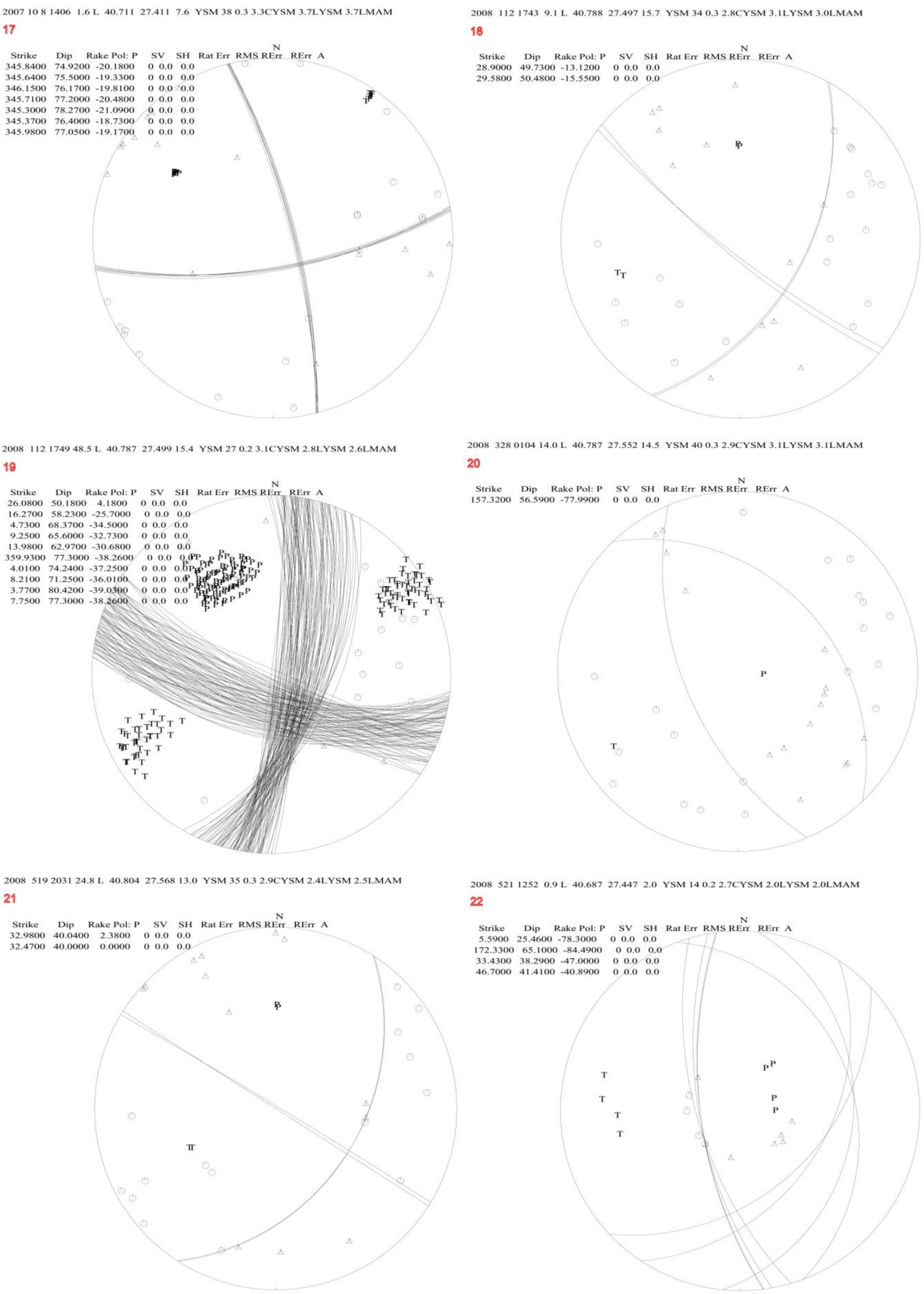

Figure D.1.4. Fault plane solutions obtained through the program of FOCMEC. Solutions are given time dependently for the Ganos Offshore Cluster

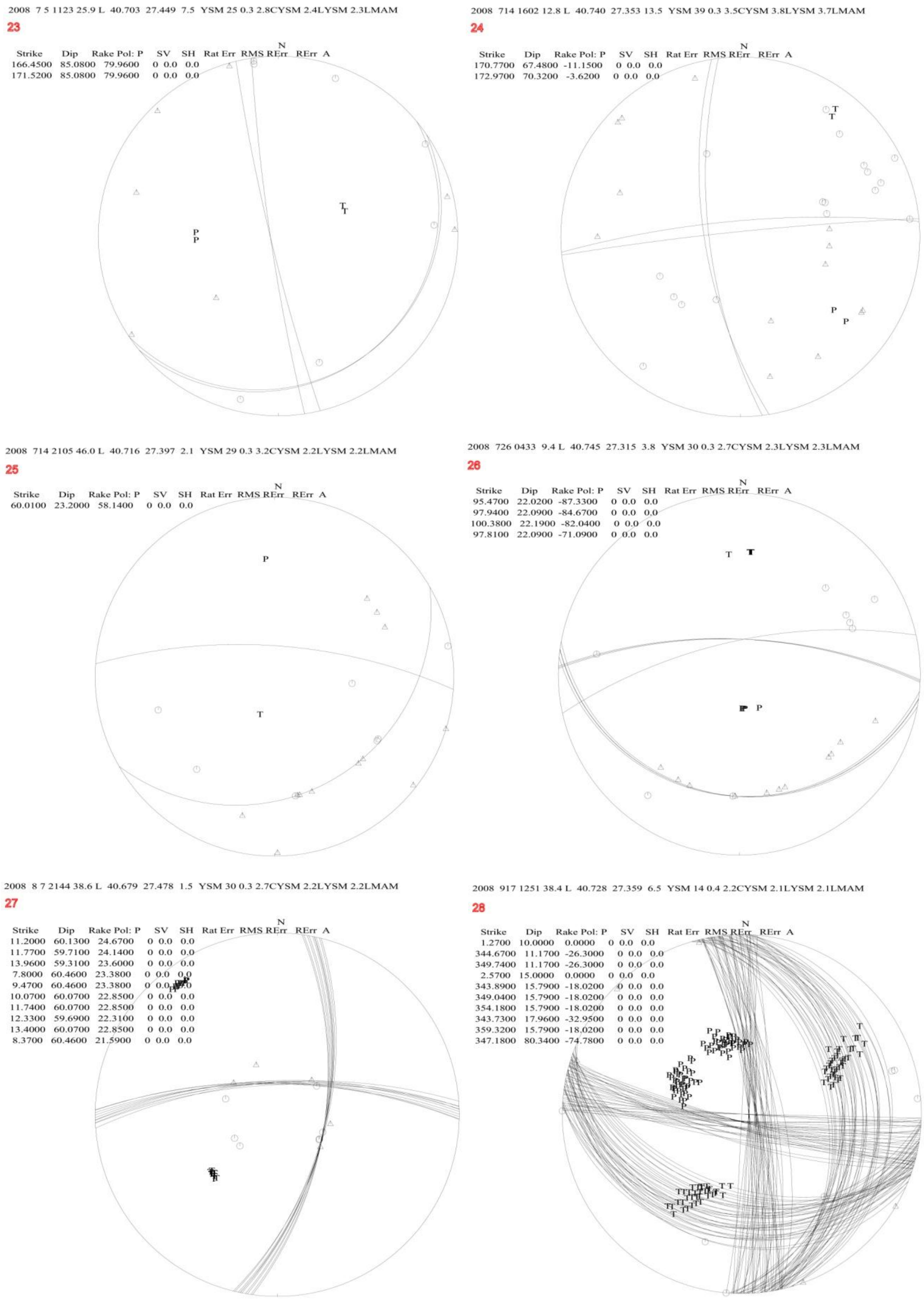

Figure D.1.5. Fault plane solutions obtained through the program of FOCMEC. Solutions are given time dependently for the Ganos Offshore Cluster

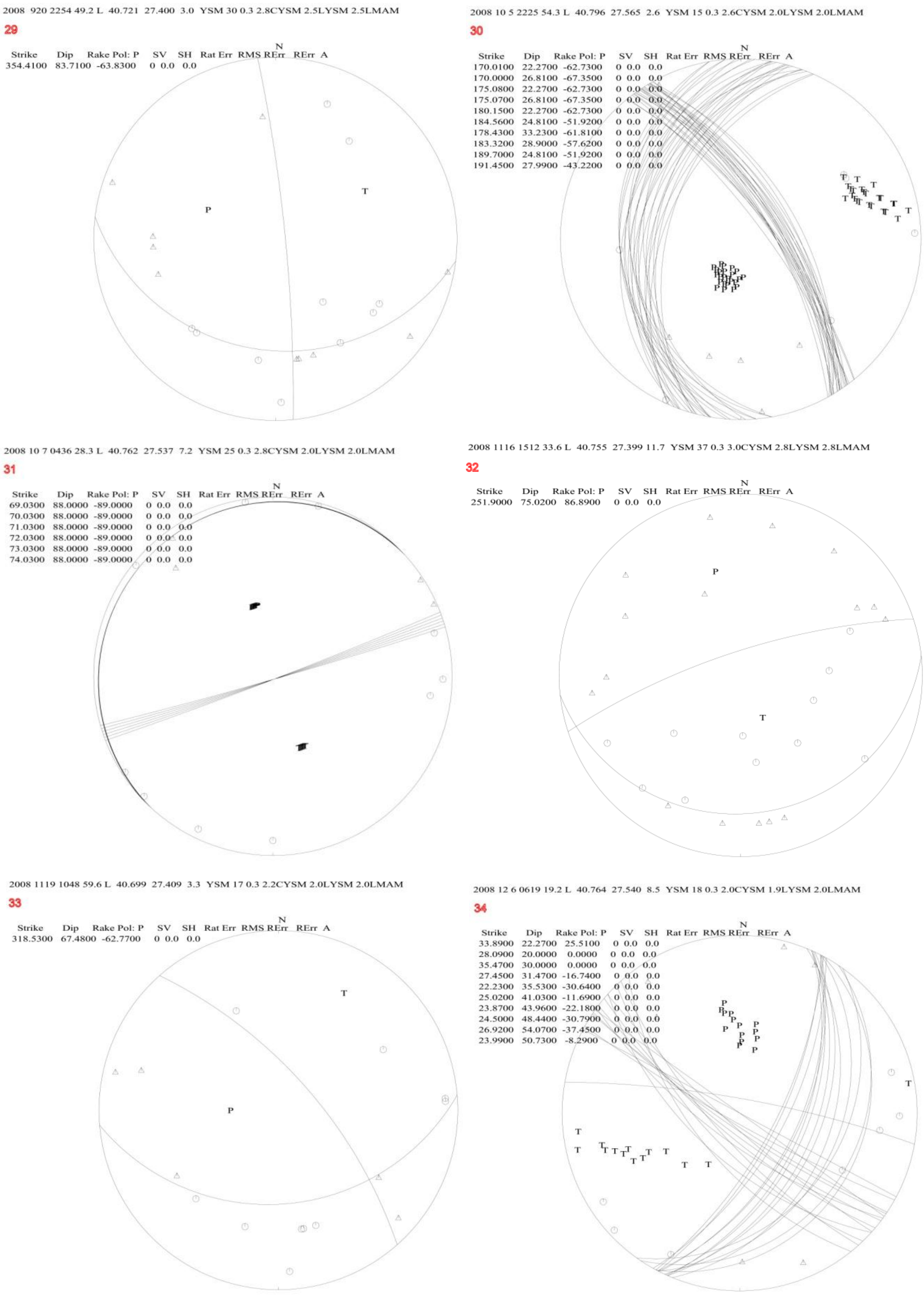

Figure D.1.6. Fault plane solutions obtained through the program of FOCMEC. Solutions are given time dependently for the Ganos Offshore Cluster

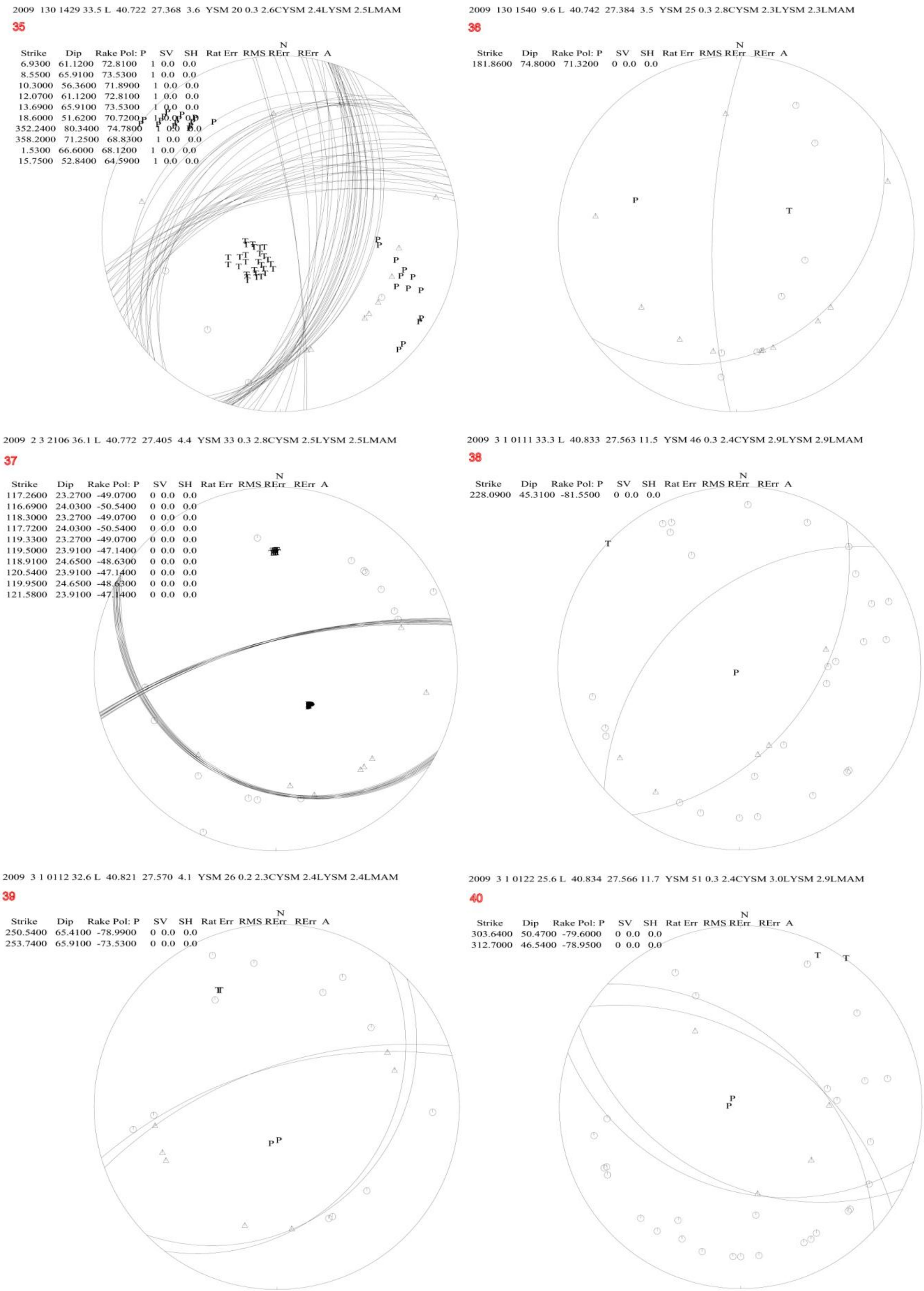

Figure D.1.7. Fault plane solutions obtained through the program of FOCMEC. Solutions are given time dependently for the Ganos Offshore Cluster

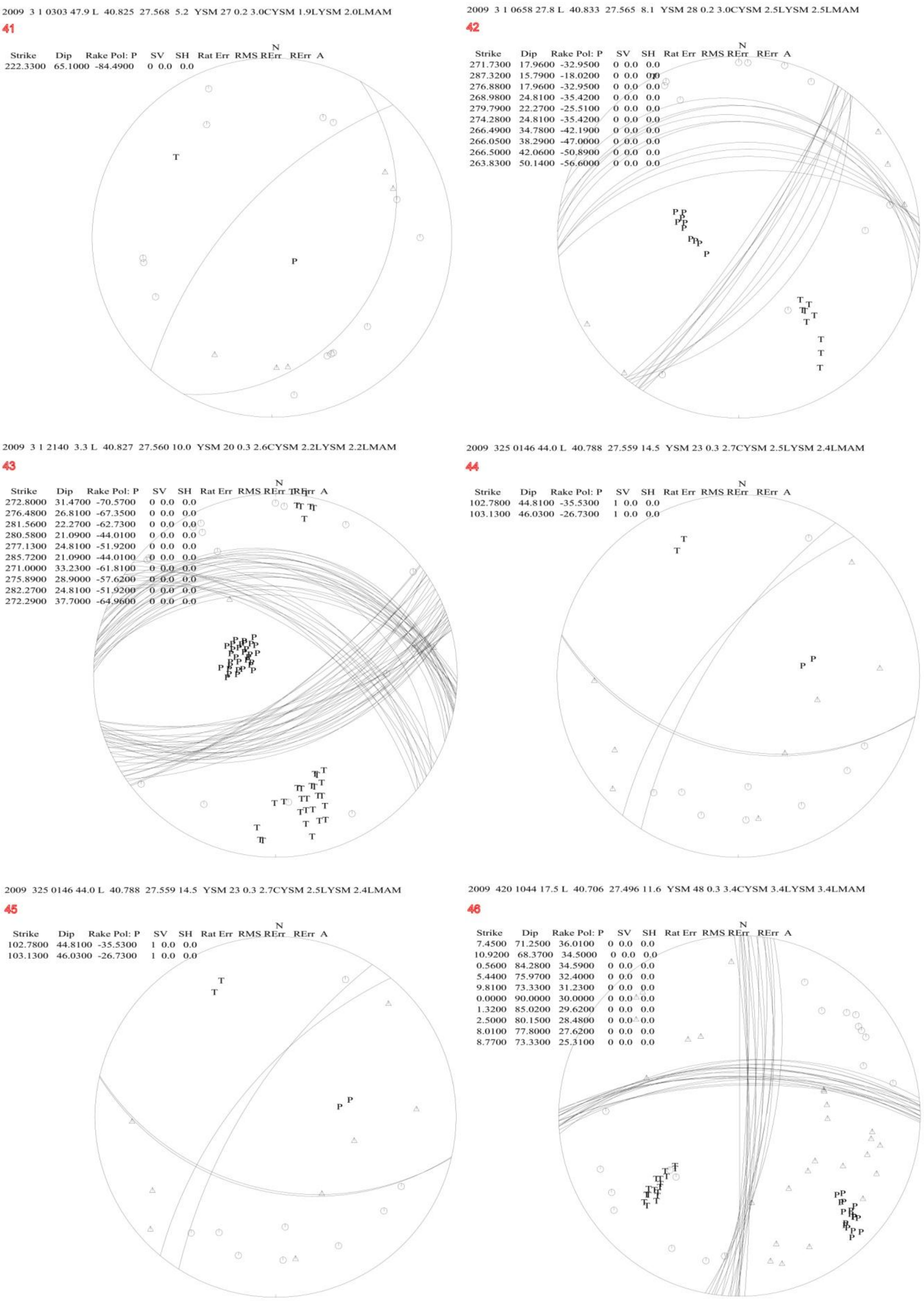

Figure D.1.8. Fault plane solutions obtained through the program of FOCMEC. Solutions are given time dependently for the Ganos Offshore Cluster

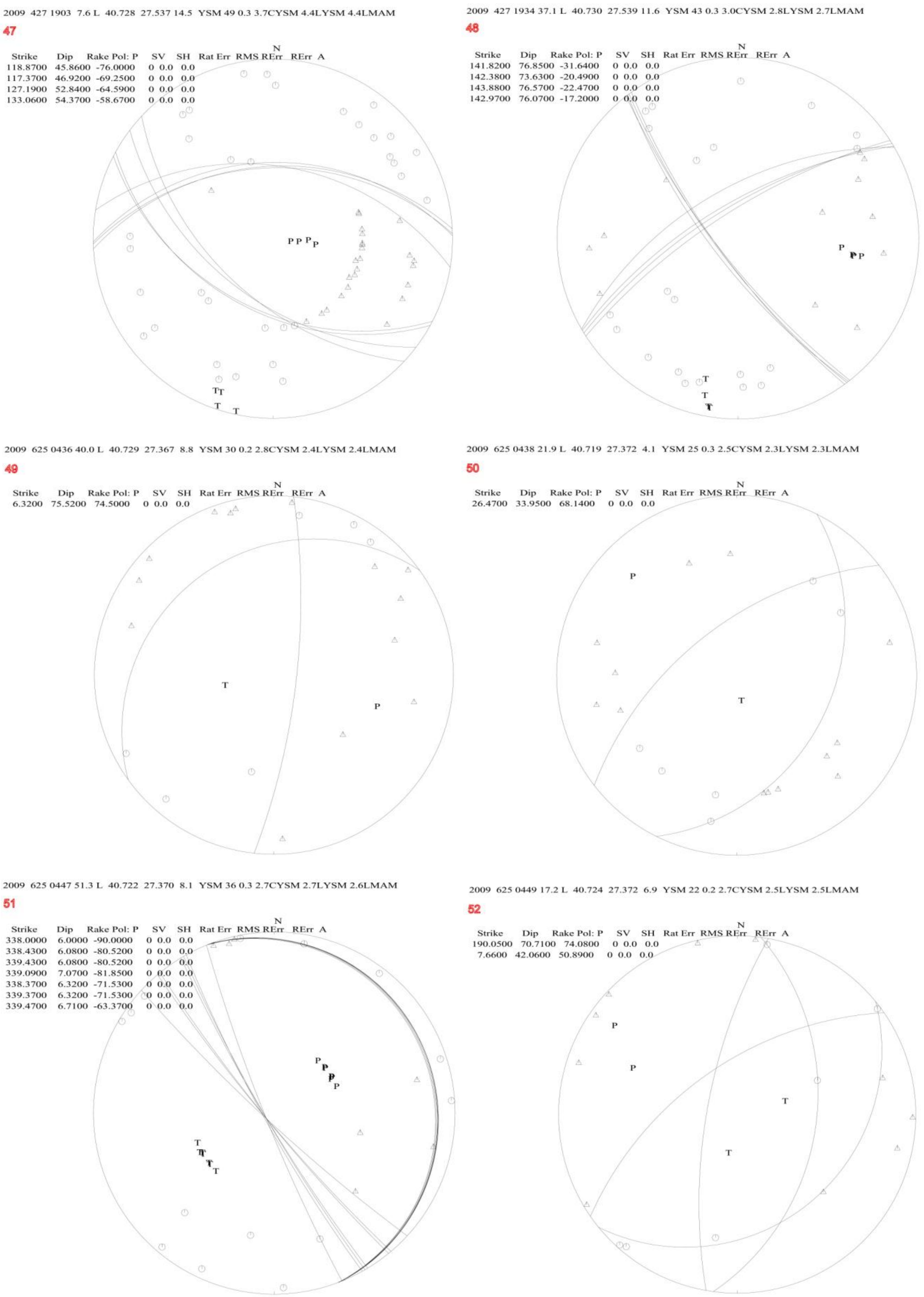

Figure D.1.9. Fault plane solutions obtained through the program of FOCMEC. Solutions are given time dependently for the Ganos Offshore Cluster

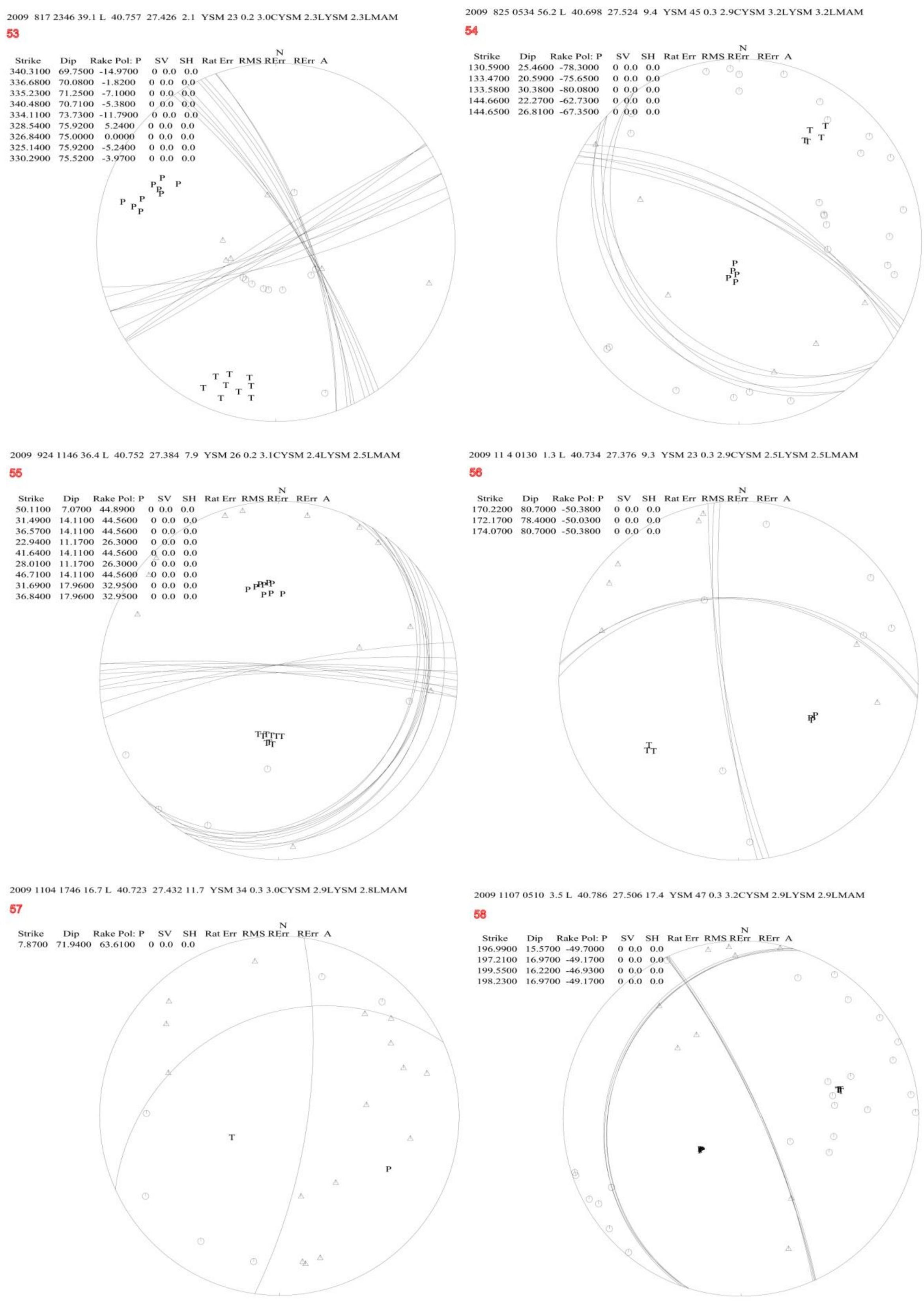

Figure D.1.10. Fault plane solutions obtained through the program of FOCMEC. Solutions are given time dependently for the Ganos Offshore Cluster

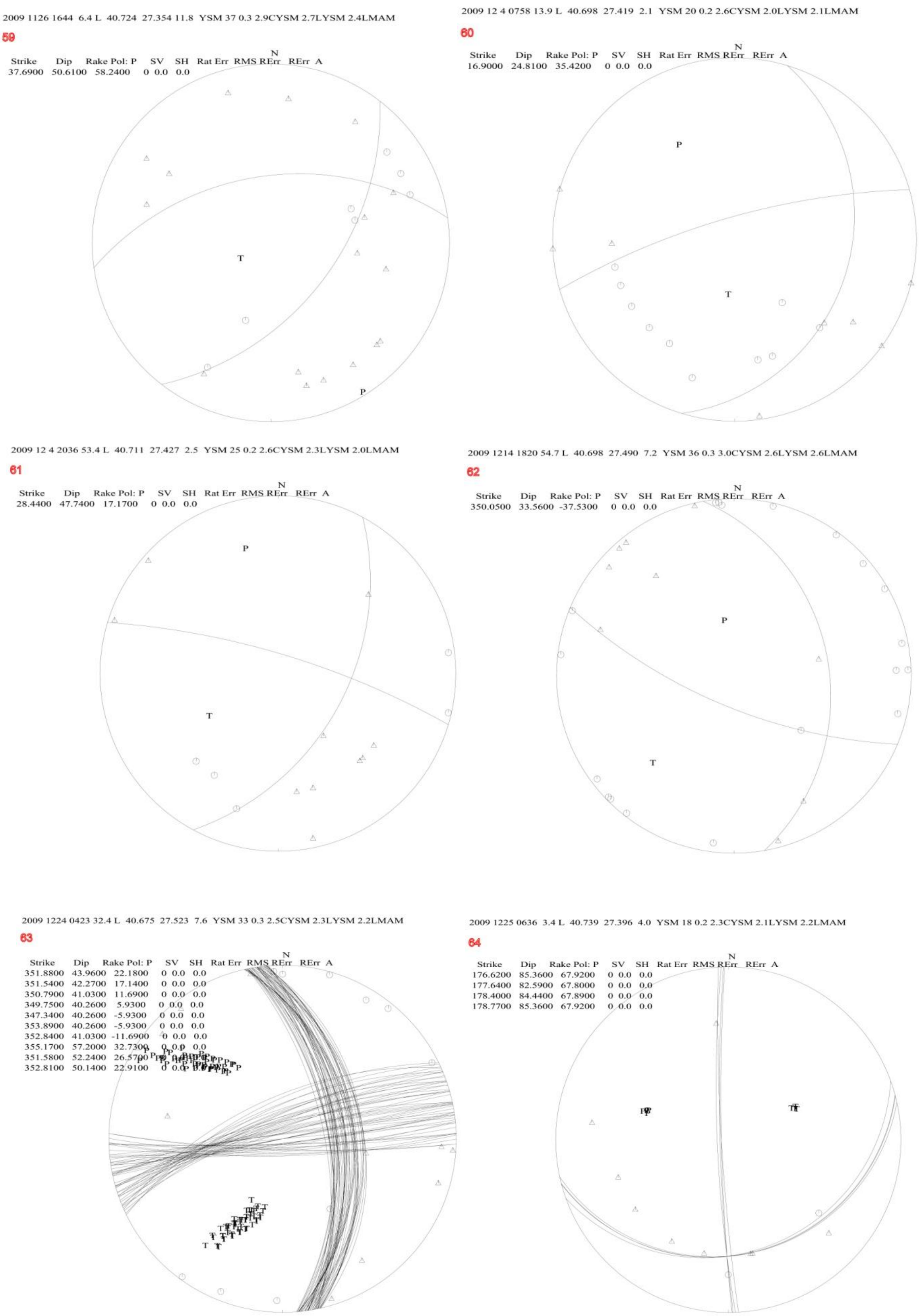

Figure D.1.11. Fault plane solutions obtained through the program of FOCMEC. Solutions are given time dependently for the Ganos Offshore Cluster

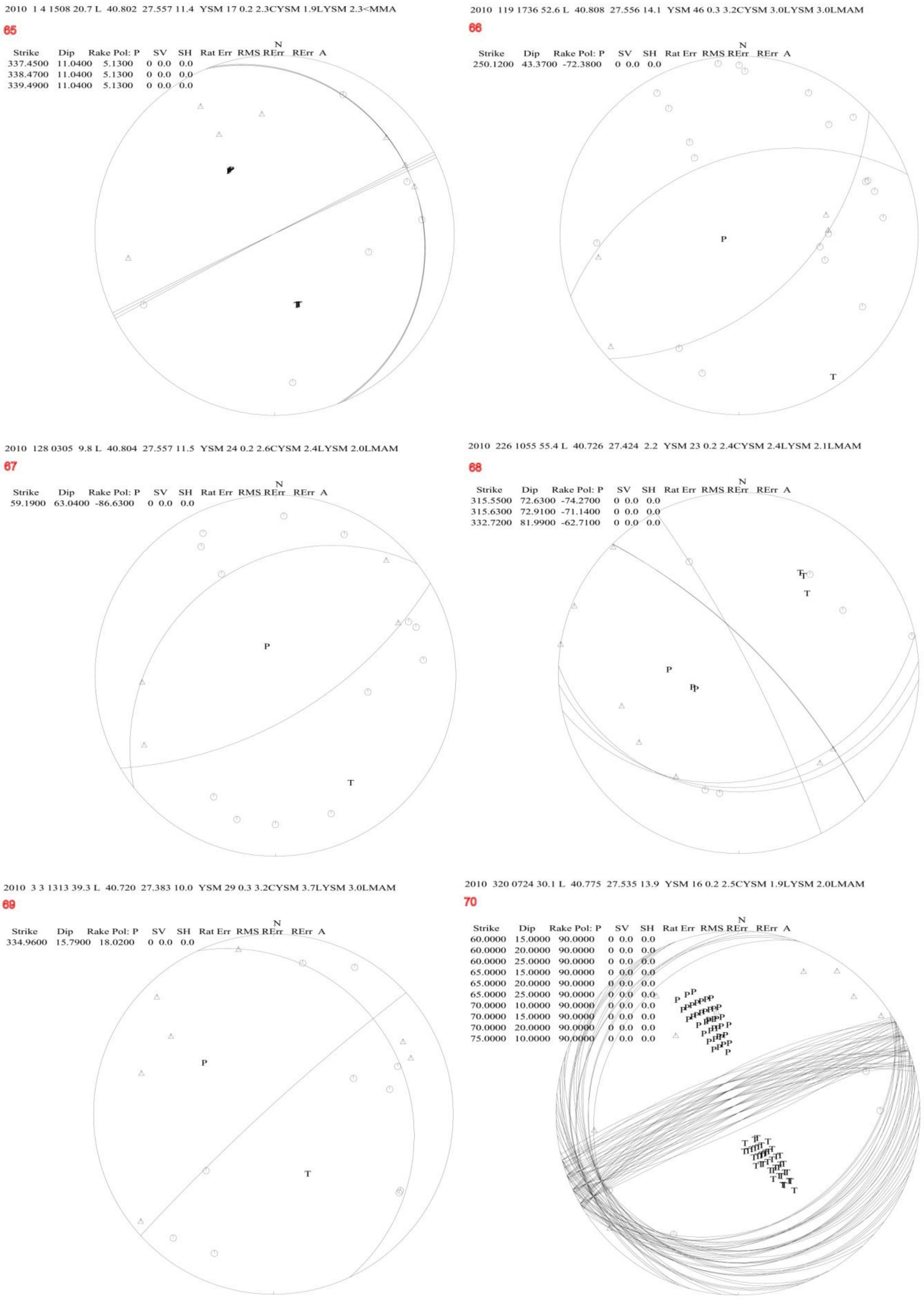

Figure D.1.12. Fault plane solutions obtained through the program of FOCMEC. Solutions are given time dependently for the Ganos Offshore Cluster

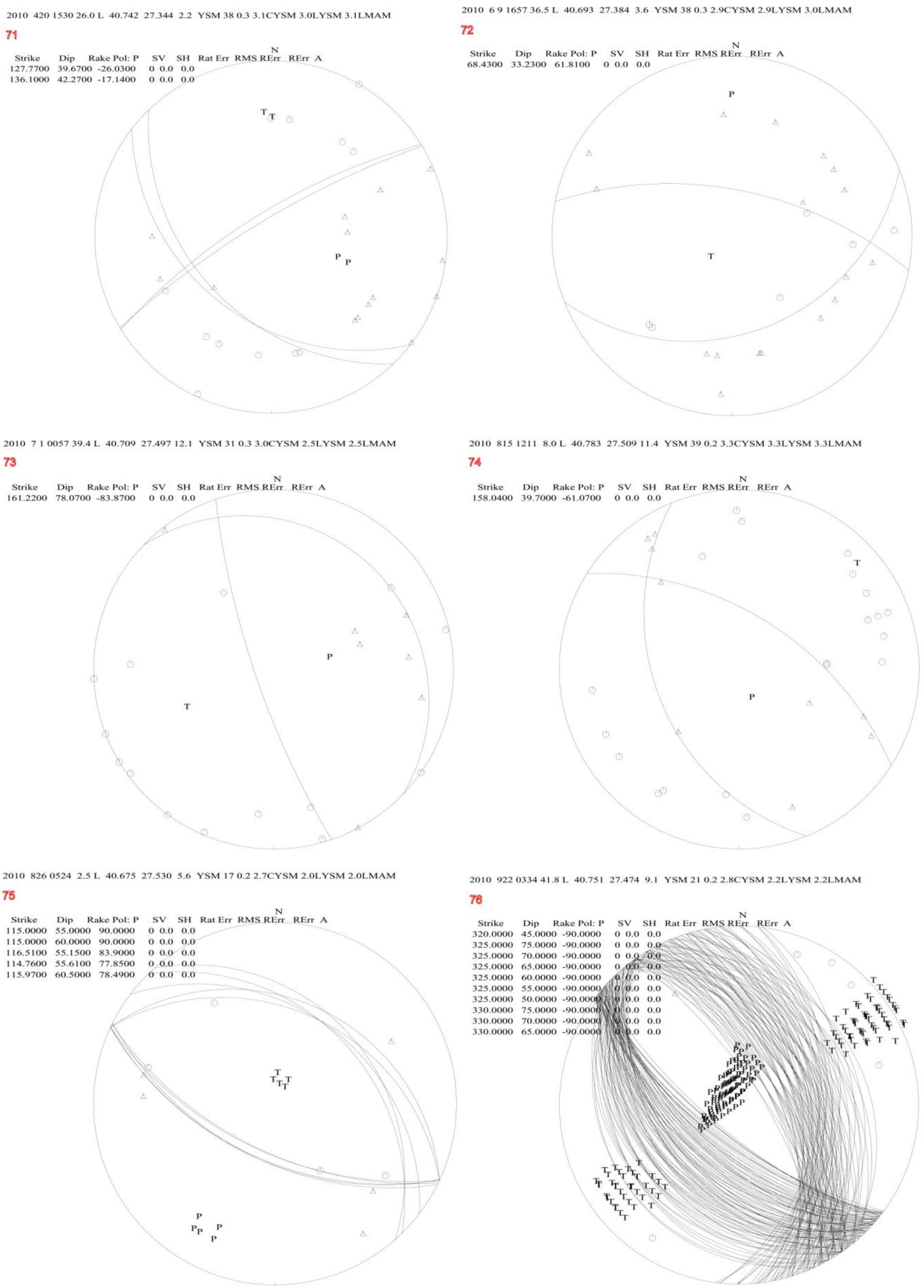

Figure D.1.13. Fault plane solutions obtained through the program of FOCMEC. Solutions are given time dependently for the Ganos Offshore Cluster

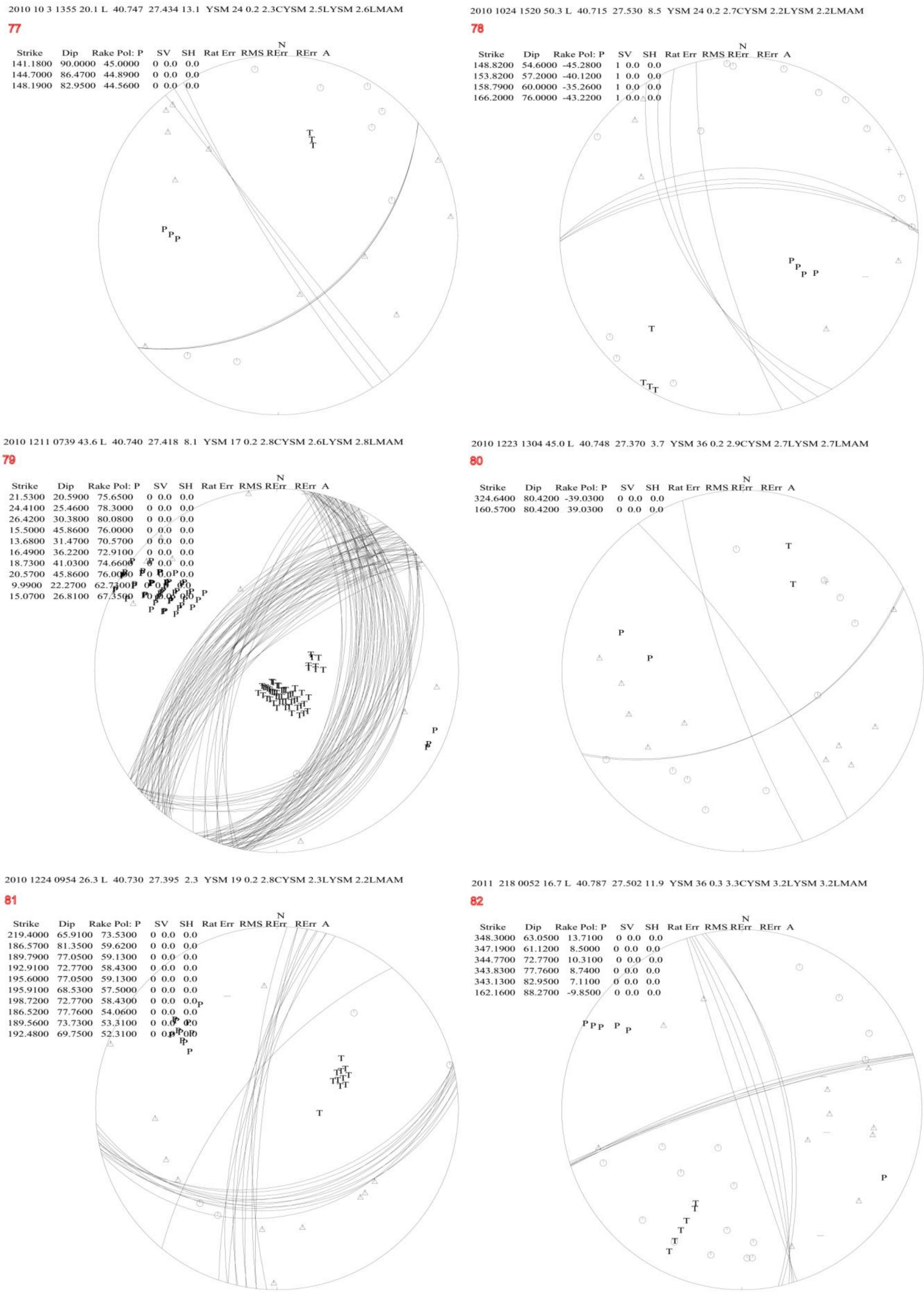

Figure D.1.14. Fault plane solutions obtained through the program of FOCMEC. Solutions are given time dependently for the Ganos Offshore Cluster

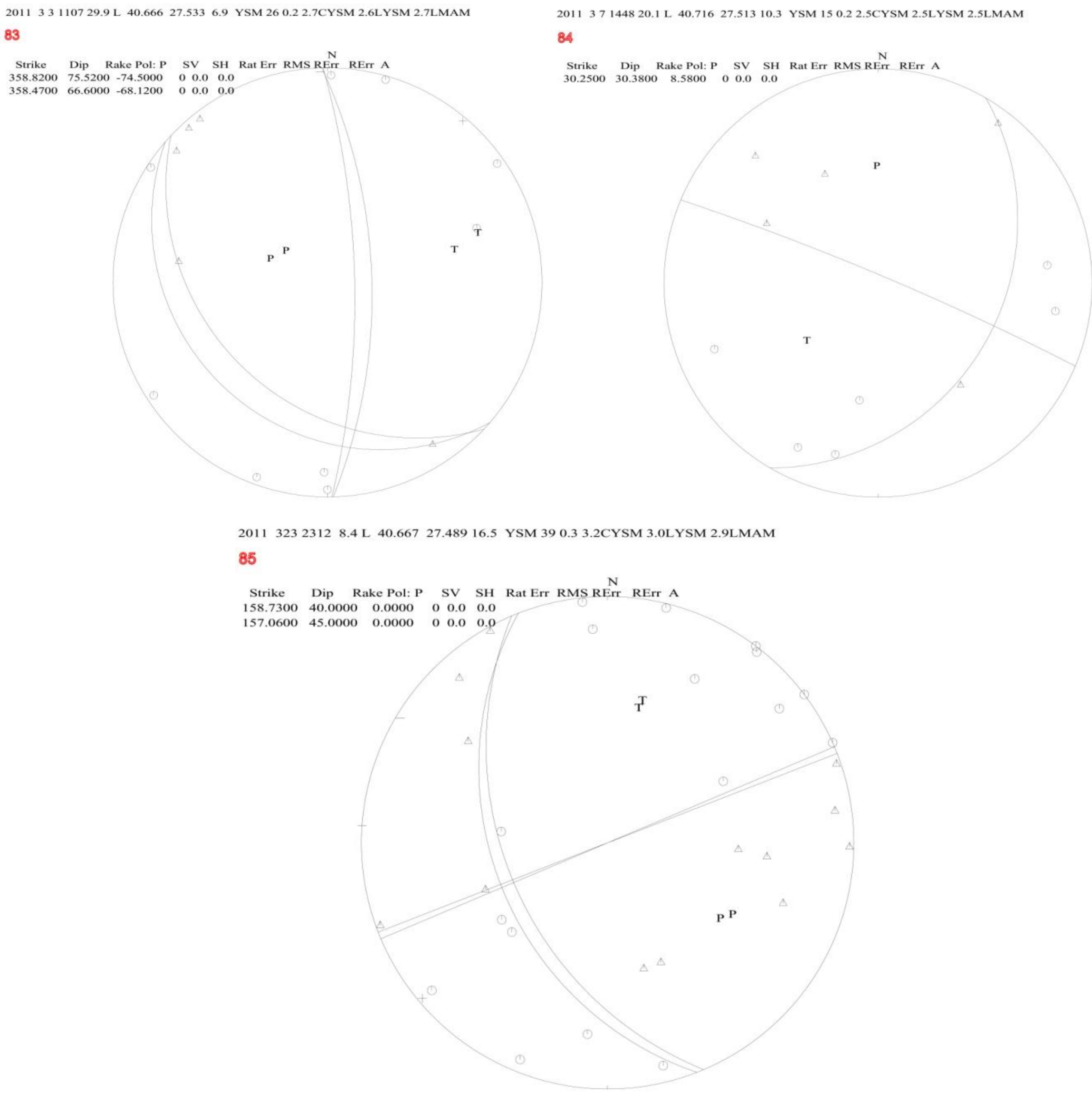

Figure D.1.15. Fault plane solutions obtained through the program of FOCMEC. Solutions are given time dependently for the Ganos Offshore Cluster

2. The Tekirdağ Basin Cluster

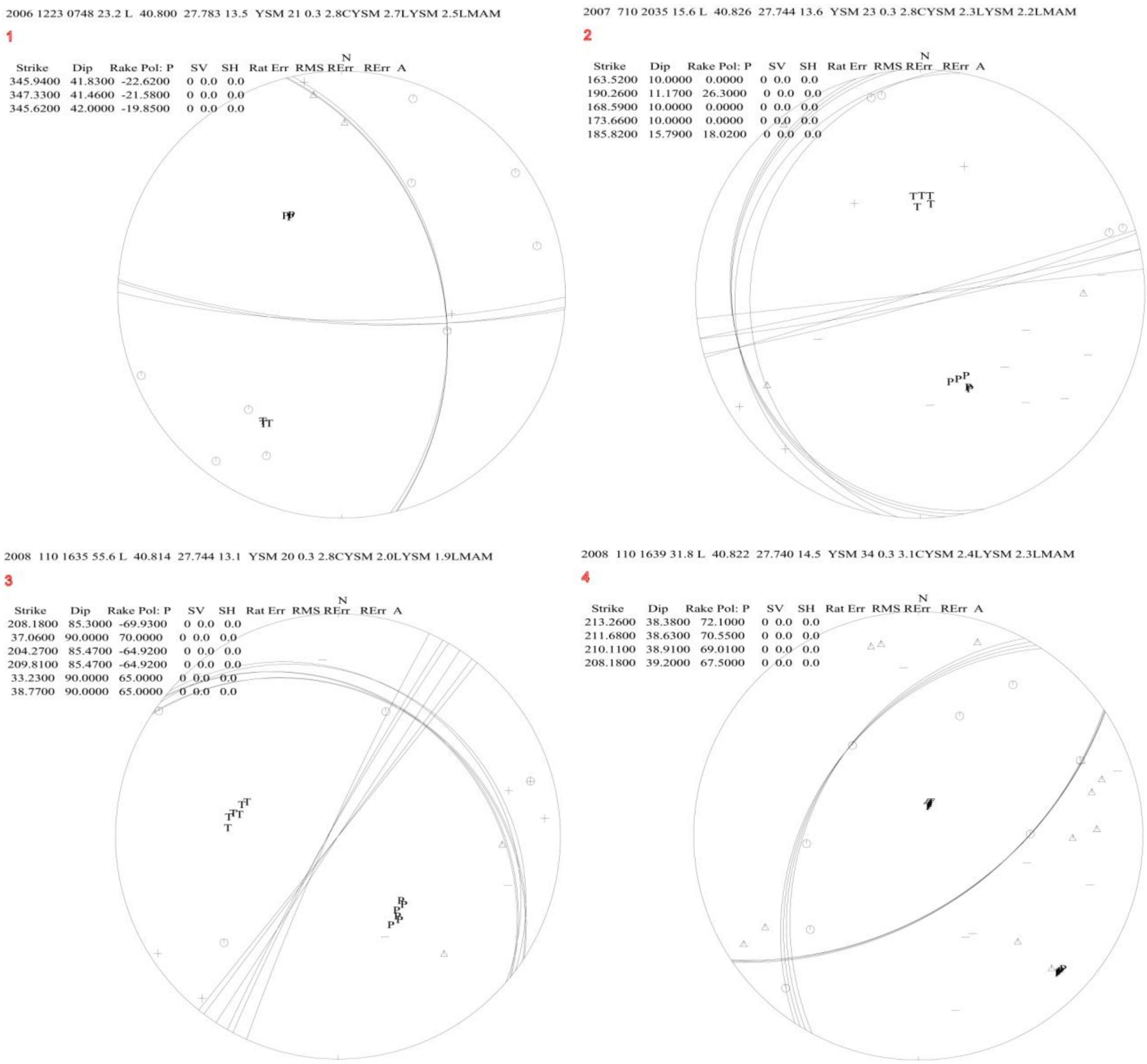

Figure D.2.1. Lower hemisphere projections of fault plane solutions obtained through the program of FOCMEC. Black circles indicate compressional P-wave first motion polarities, while black triangles show dilatational ones. Solutions are given time dependently for the Tekirdağ Basin Cluster

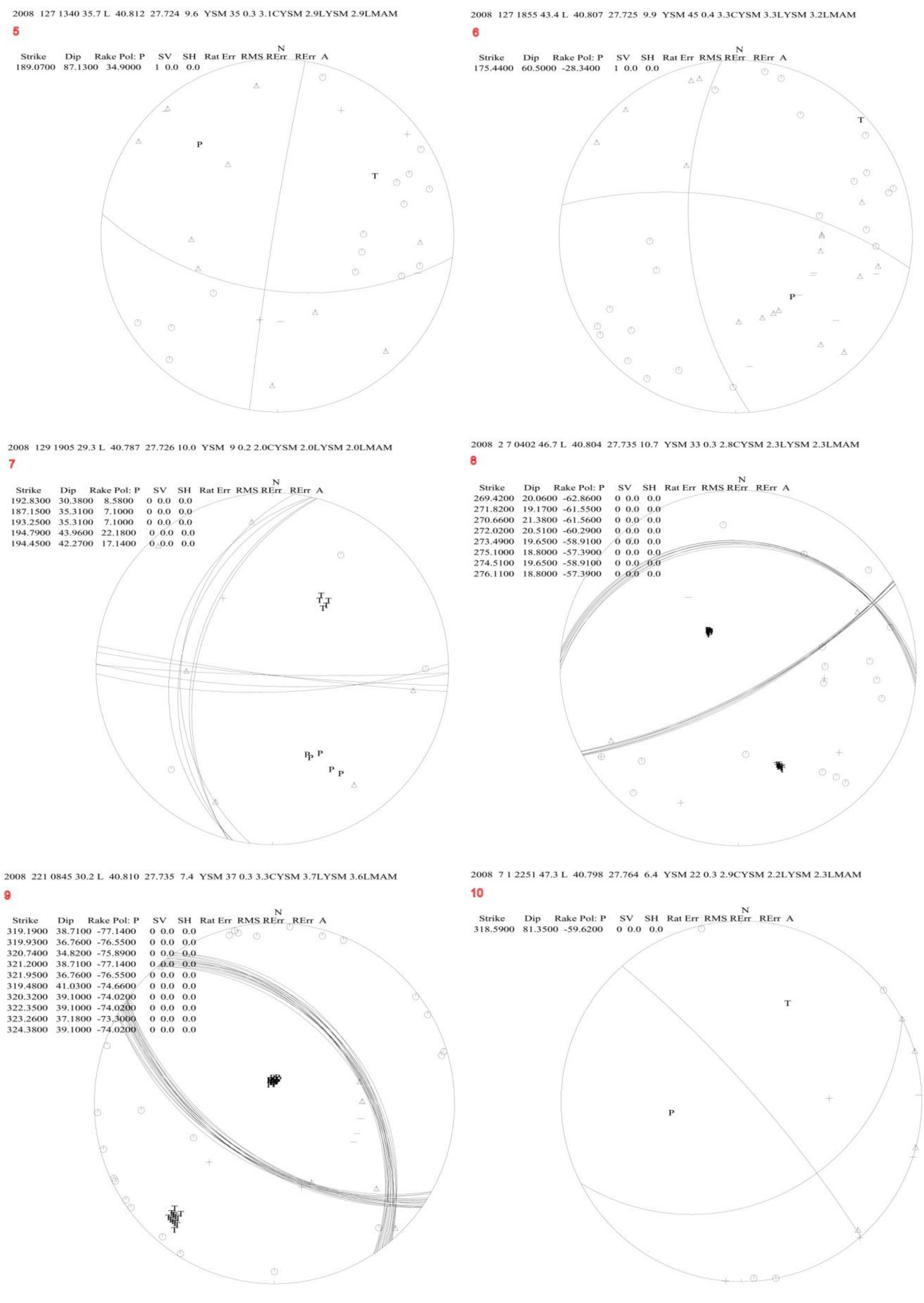

Figure D.2.2. Fault plane solutions obtained through the program of FOCMEC. Solutions are given time dependently for the Tekirdağ Basin Cluster

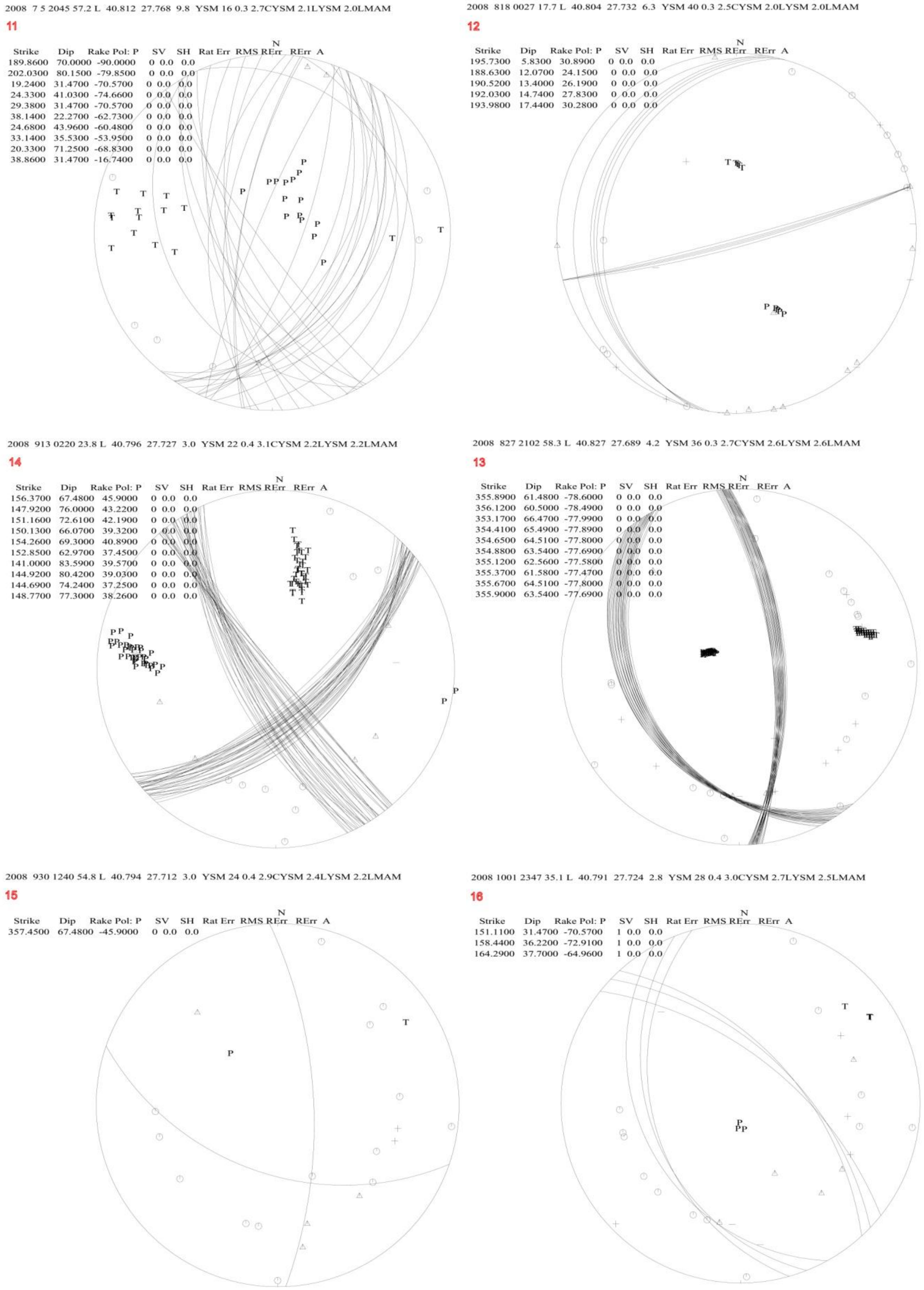

Figure D.2.3. Fault plane solutions obtained through the program of FOCMEC. Solutions are given time dependently for the Tekirdağ Basin Cluster

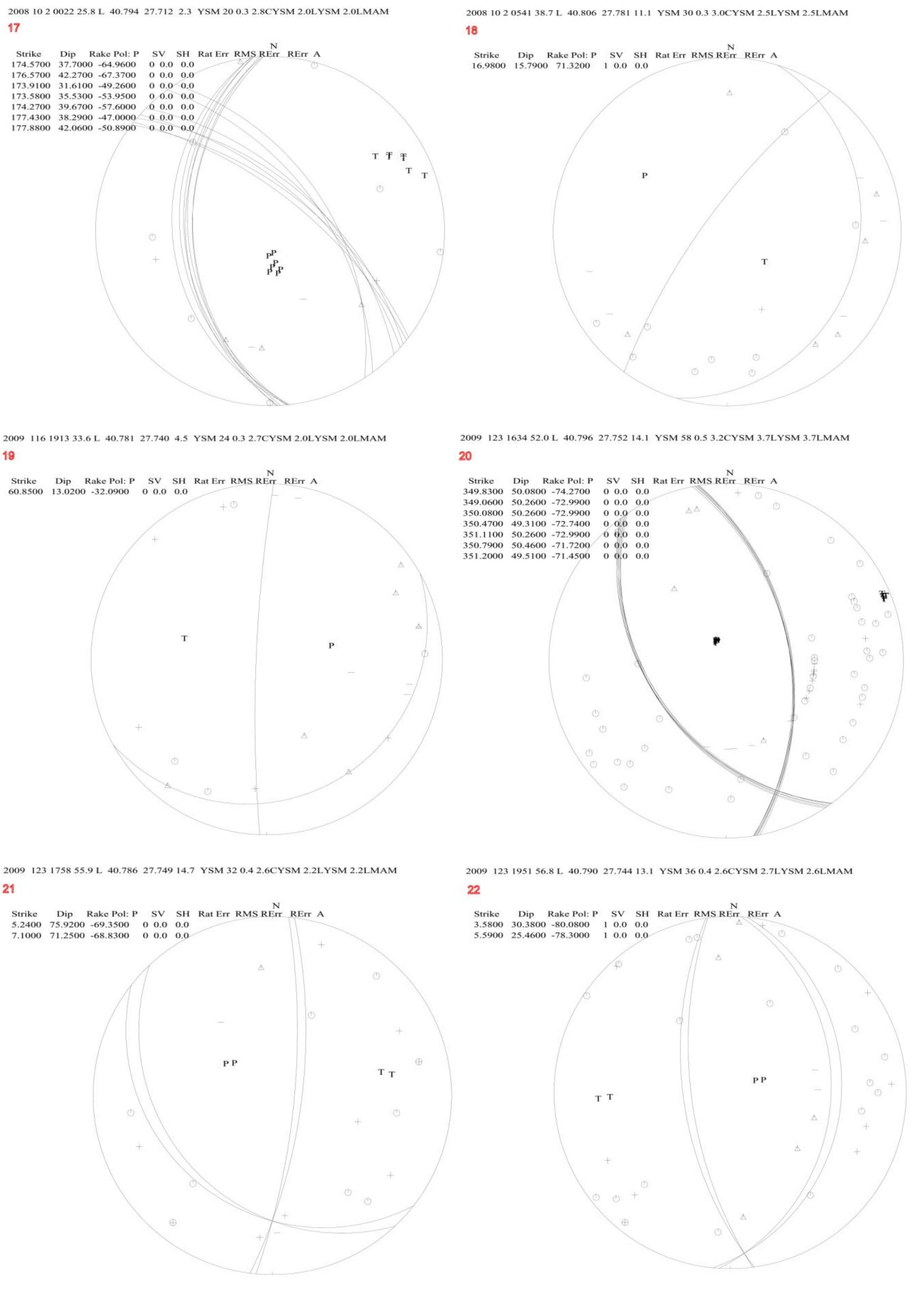

Figure D.2.4. Fault plane solutions obtained through the program of FOCMEC. Solutions are given time dependently for the Tekirdağ Basin Cluster

2009 124 1550 22.6 L 40.782 27.742 12.5 YSM 33 0.3 2.1CYSM 2.4LYSM 2.3LMAM

23

Strike	Dip	Rake	Pol: P	SV	SH	Rat	Err	RMS RErr	RErr	A
64.6500	37.0500	-86.6800	0	0.0	0.0					
65.6500	37.0500	-86.6800	0	0.0	0.0					
65.9700	37.1000	-85.0200	0	0.0	0.0					
66.9700	37.1000	-85.0200	0	0.0	0.0					
67.9700	37.1000	-85.0200	0	0.0	0.0					
67.9700	37.1800	-83.3700	0	0.0	0.0					
68.9700	37.1800	-83.3700	0	0.0	0.0					
69.9800	37.1800	-83.3700	0	0.0	0.0					
70.2800	37.2900	-81.7300	0	0.0	0.0					
71.2800	37.2900	-81.7300	0	0.0	0.0					

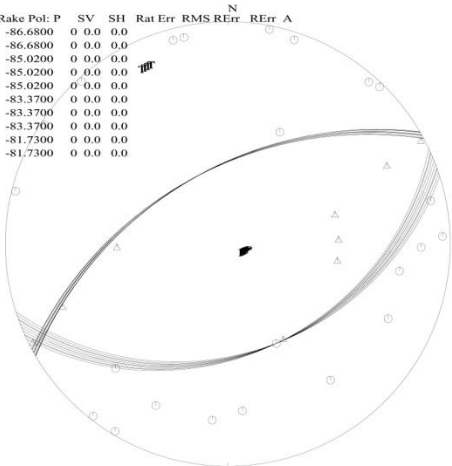

2009 124 1558 39.5 L 40.793 27.763 14.6 YSM 60 0.5 3.8CYSM 4.3LYSM 4.3LMAM

24

Strike	Dip	Rake	Pol: P	SV	SH	Rat	Err	RMS RErr	RErr	A
343.0600	54.9000	-75.2800	0	0.0	0.0					
343.1700	55.0600	-74.0700	0	0.0	0.0					
342.6900	55.2300	-72.8700	0	0.0	0.0					
342.7800	55.4100	-71.6700	0	0.0	0.0					
341.8600	56.5400	-70.7100	0	0.0	0.0					
342.2600	55.6000	-70.4800	0	0.0	0.0					
343.3000	55.6000	-70.4800	0	0.0	0.0					
341.3000	56.7300	-69.5300	0	0.0	0.0					
342.3500	56.7300	-69.5300	0	0.0	0.0					
342.7700	55.8000	-69.3000	0	0.0	0.0					

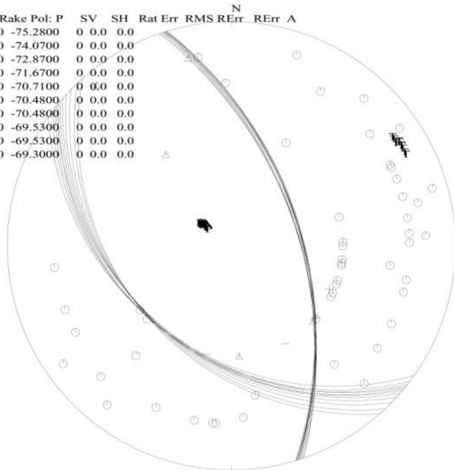

2009 124 2359 45.7 L 40.797 27.770 12.7 YSM 56 0.5 2.5CYSM 2.4LYSM 2.8LMAM

25

Strike	Dip	Rake	Pol: P	SV	SH	Rat	Err	RMS RErr	RErr	A
357.9700	46.0100	-88.6100	0	0.0	0.0					

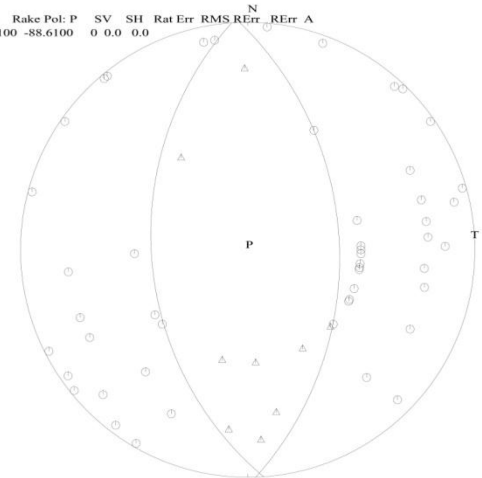

2009 125 0254 23.1 L 40.793 27.752 12.3 YSM 58 0.5 2.4CYSM 3.0LYSM 3.0LMAM

26

Strike	Dip	Rake	Pol: P	SV	SH	Rat	Err	RMS RErr	RErr	A
185.0700	47.9700	-75.1200	0	0.0	0.0					

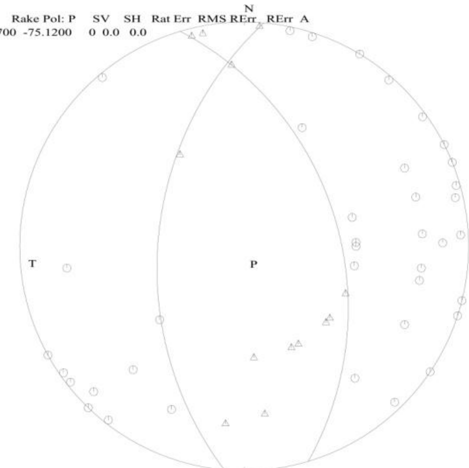

2009 125 0326 53.6 L 40.791 27.753 14.0 YSM 59 0.4 3.4CYSM 3.8LYSM 3.8LMAM

27

Strike	Dip	Rake	Pol: P	SV	SH	Rat	Err	RMS RErr	RErr	A
332.8800	60.1300	-84.2300	1	0.0	0.0					

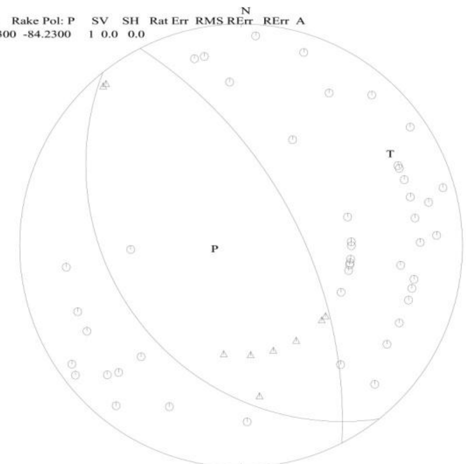

2009 125 0419 6.5 L 40.776 27.758 13.7 YSM 25 0.4 2.1CYSM 2.2LYSM 2.0LMAM

28

Strike	Dip	Rake	Pol: P	SV	SH	Rat	Err	RMS RErr	RErr	A
307.2400	63.0500	-61.7000	0	0.0	0.0					
307.8100	63.9400	-61.9400	0	0.0	0.0					
309.3600	64.1700	-60.8500	0	0.0	0.0					
309.9300	65.0400	-61.0800	0	0.0	0.0					
311.4900	65.2700	-60.0100	0	0.0	0.0					
313.6300	66.3700	-59.1700	0	0.0	0.0					
315.2100	66.6000	-58.1100	0	0.0	0.0					
315.7900	67.4600	-58.3400	0	0.0	0.0					

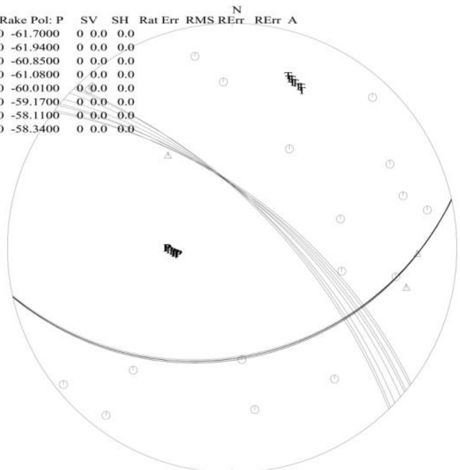

Figure D.2.5. Fault plane solutions obtained through the program of FOCMEC. Solutions are given time dependently for the Tekirdağ Basin Cluster

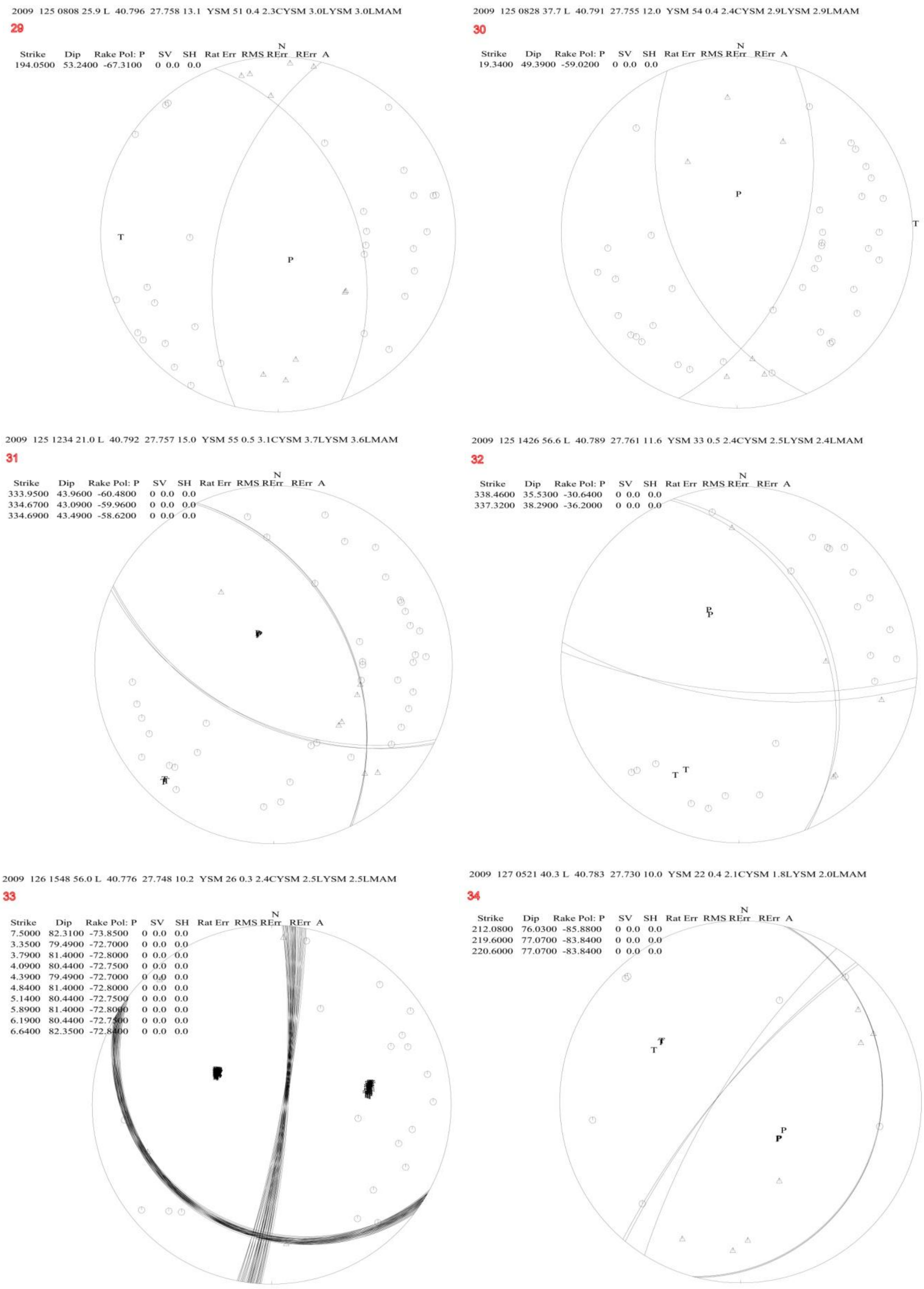

Figure D.2.6. Fault plane solutions obtained through the program of FOCMEC. Solutions are given time dependently for the Tekirdağ Basin Cluster

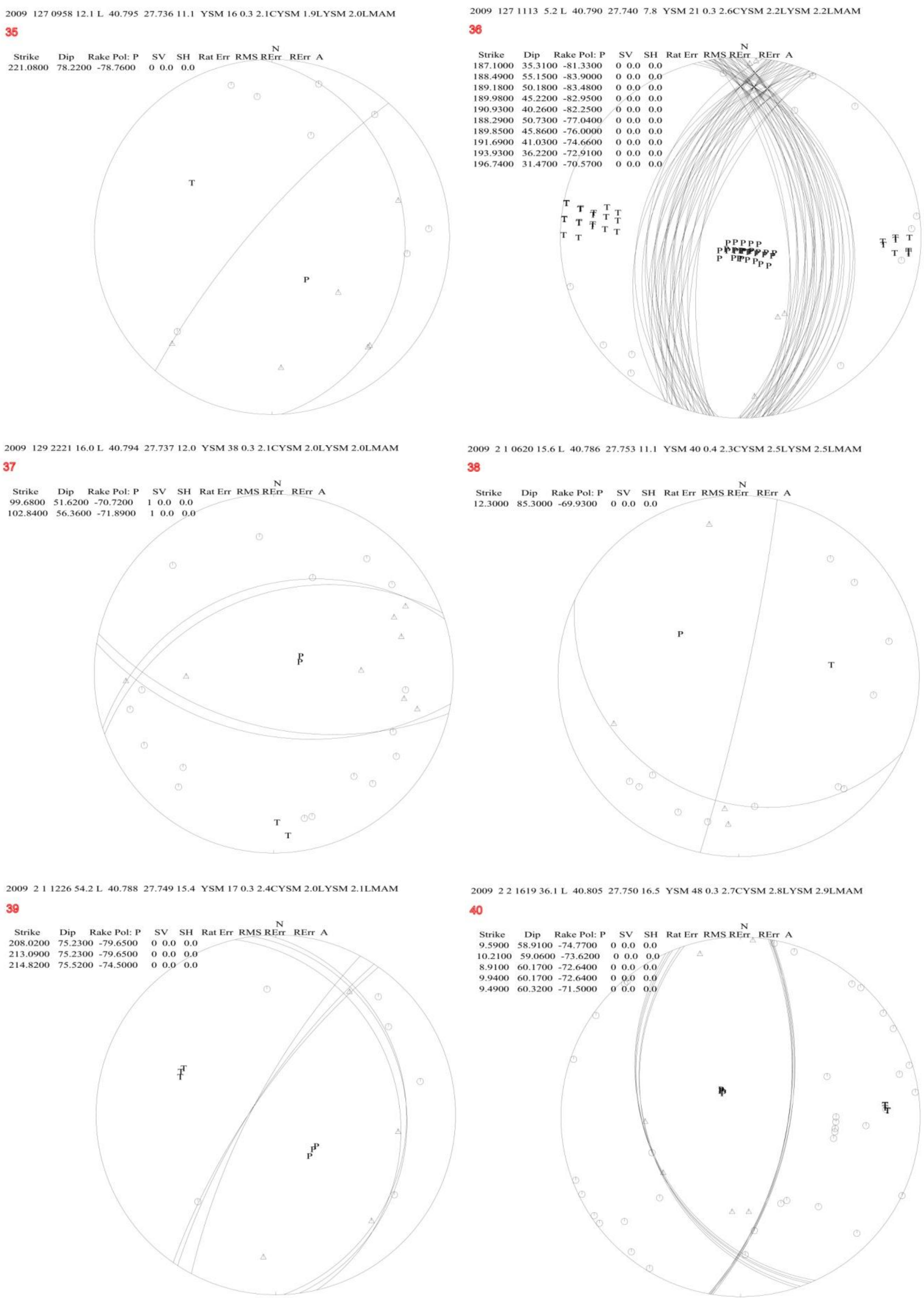

Figure D.2.7. Fault plane solutions obtained through the program of FOCMEC. Solutions are given time dependently for the Tekirdağ Basin Cluster

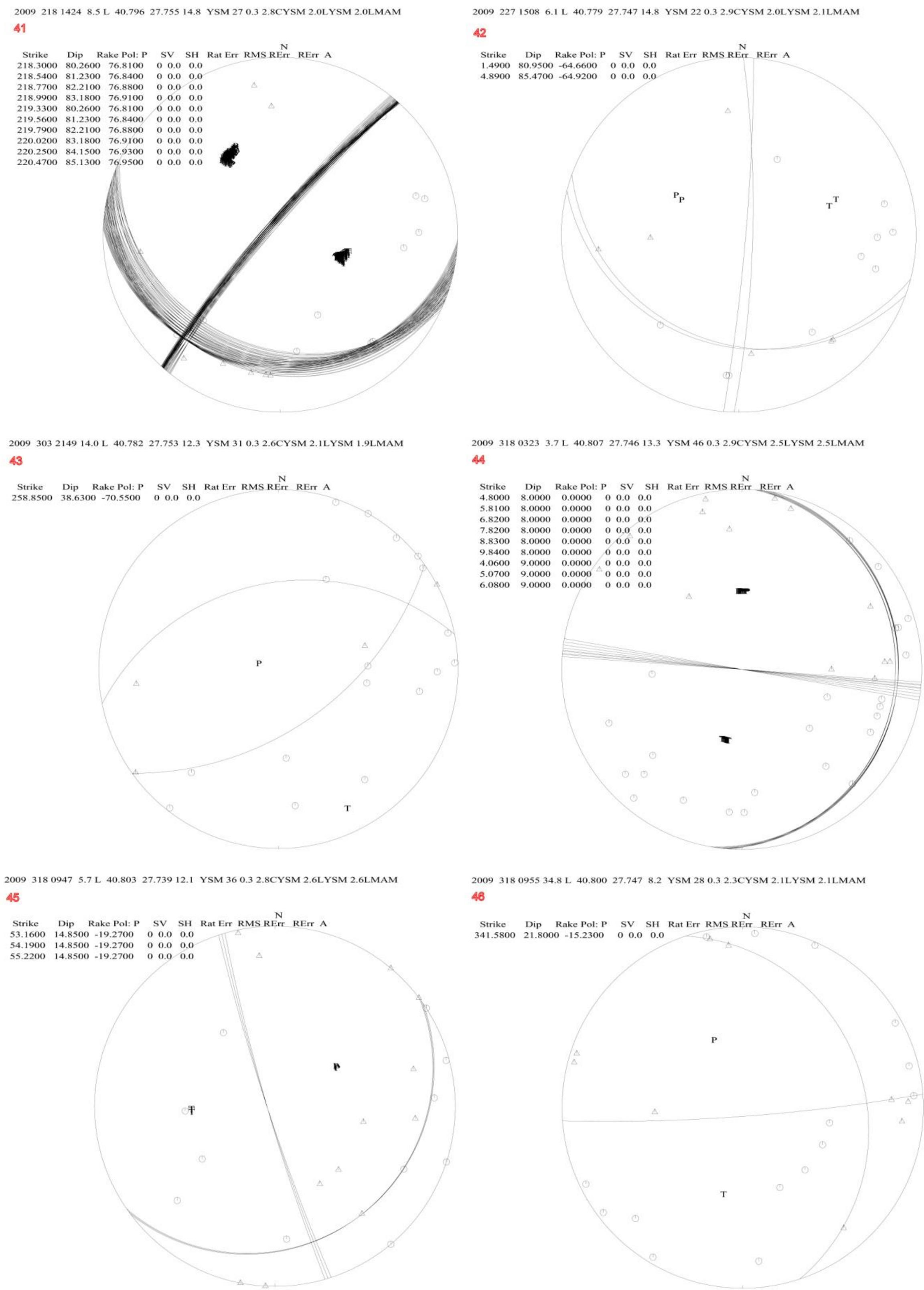

Figure D.2.8. Fault plane solutions obtained through the program of FOCMEC. Solutions are given time dependently for the Tekirdağ Basin Cluster

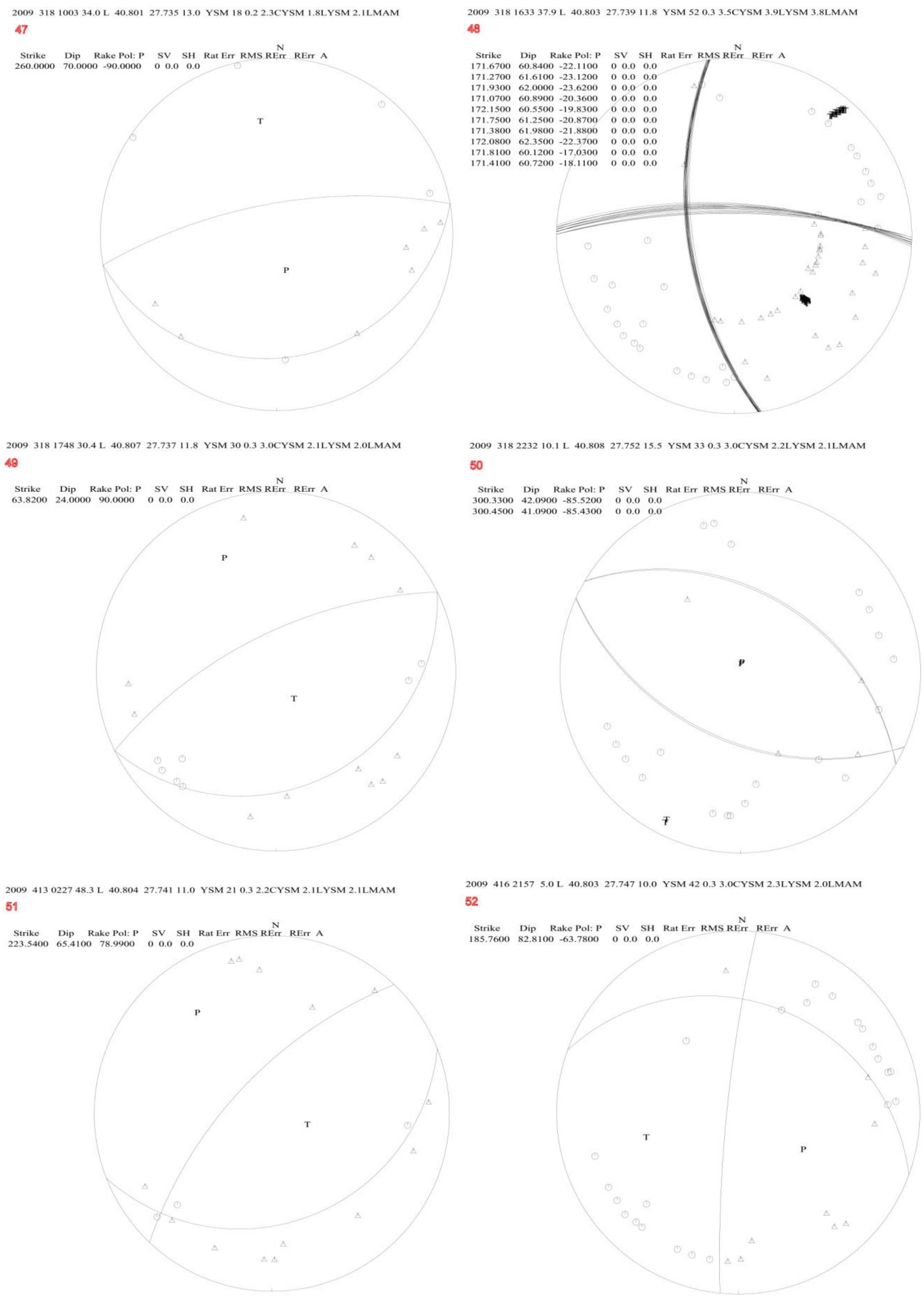

Figure D.2.9. Fault plane solutions obtained through the program of FOCMEC. Solutions are given time dependently for the Tekirdağ Basin Cluster

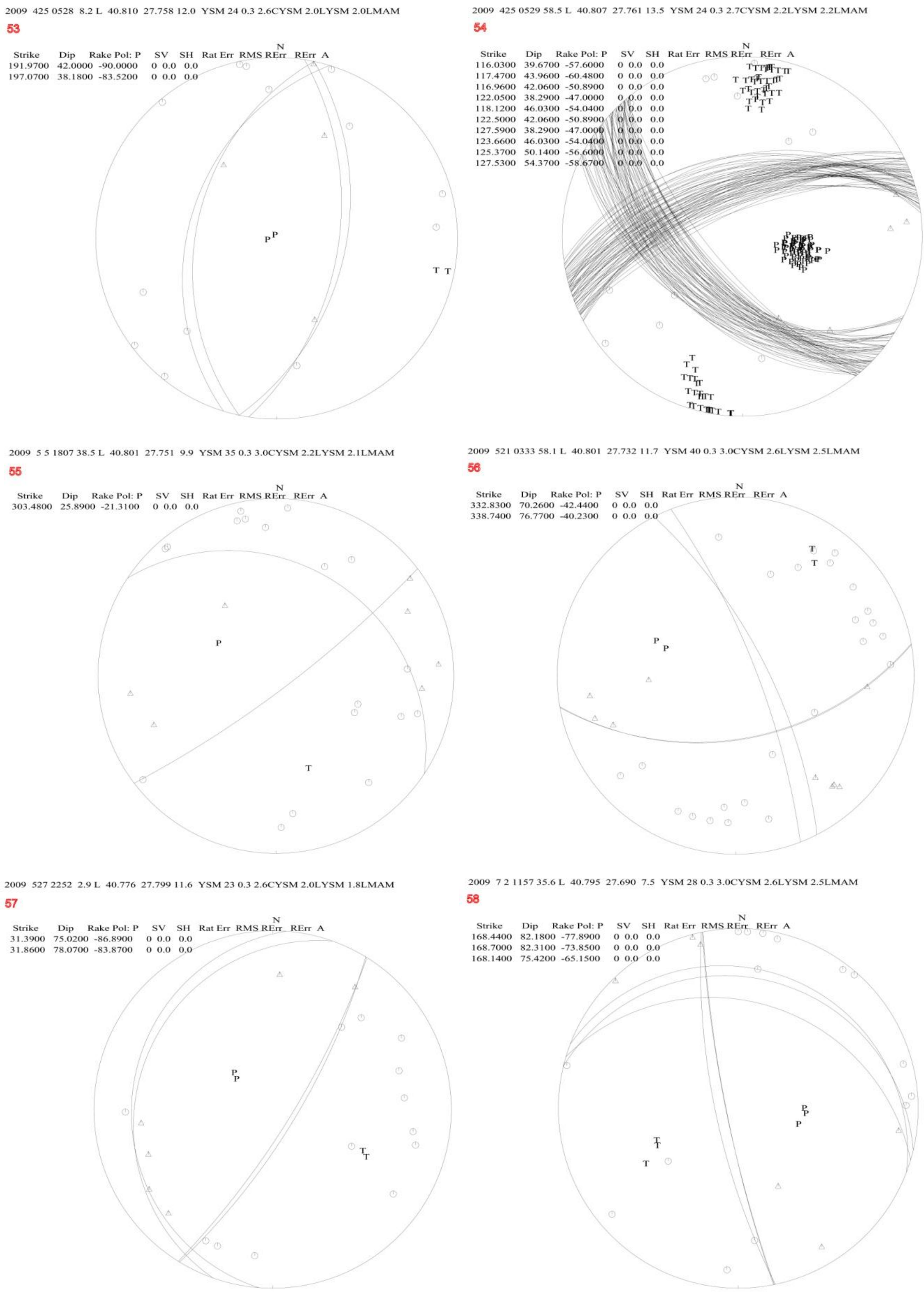

Figure D.2.10. Fault plane solutions obtained through the program of FOCMEC. Solutions are given time dependently for the Tekirdağ Basin Cluster

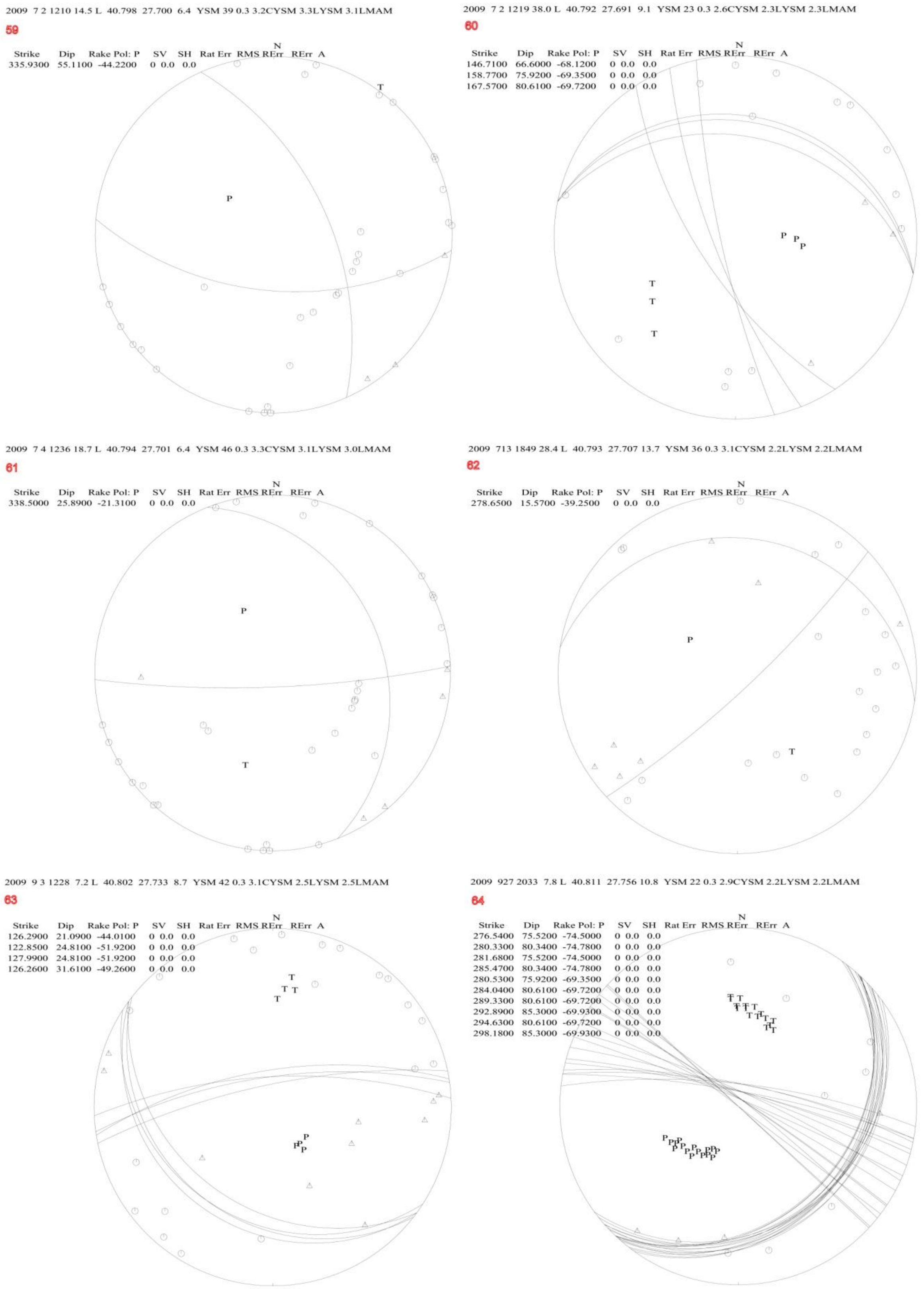

Figure D.2.11. Fault plane solutions obtained through the program of FOCMEC. Solutions are given time dependently for the Tekirdağ Basin Cluster

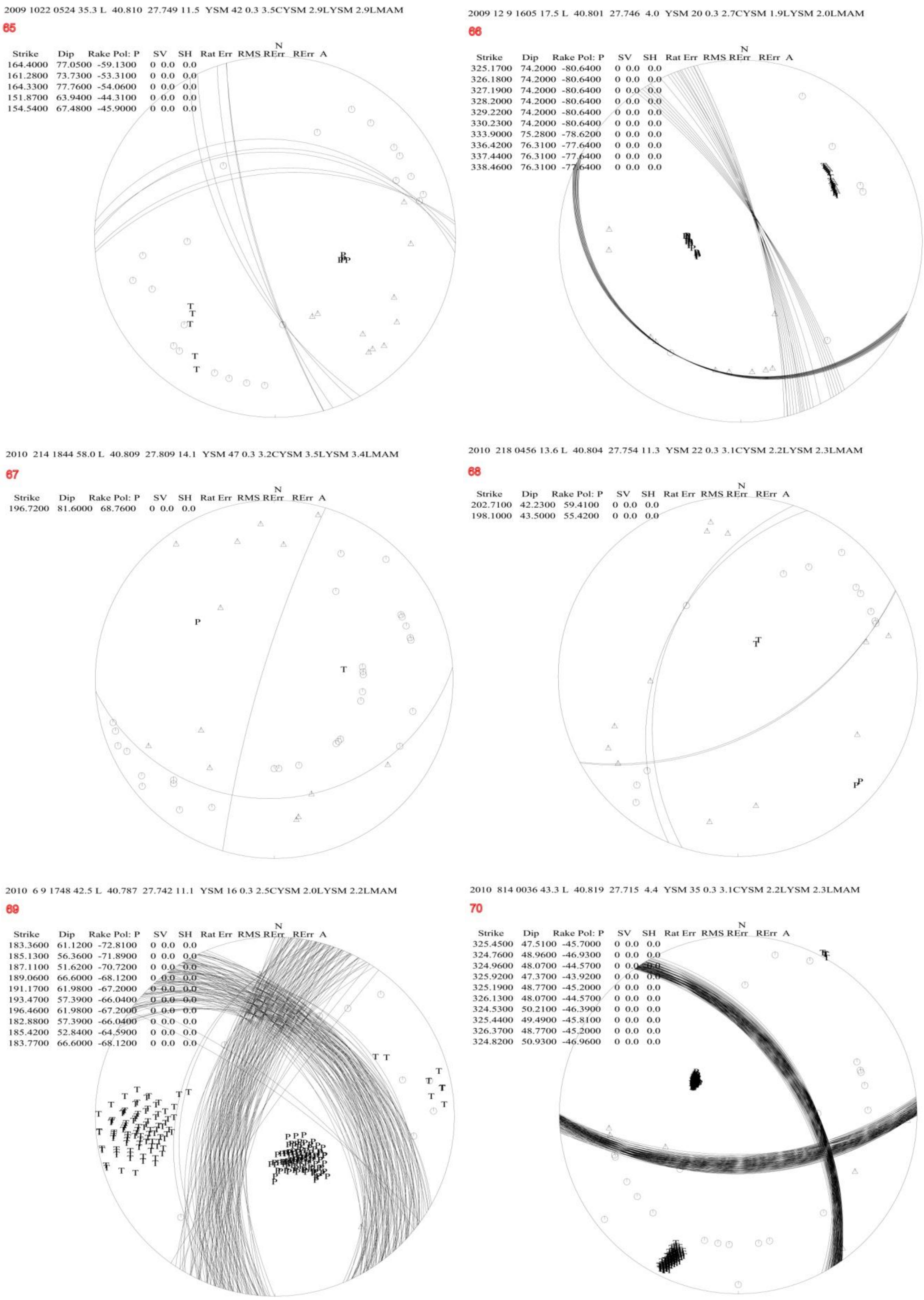

Figure D.2.12. Fault plane solutions obtained through the program of FOCMEC. Solutions are given time dependently for the Tekirdağ Basin Cluster

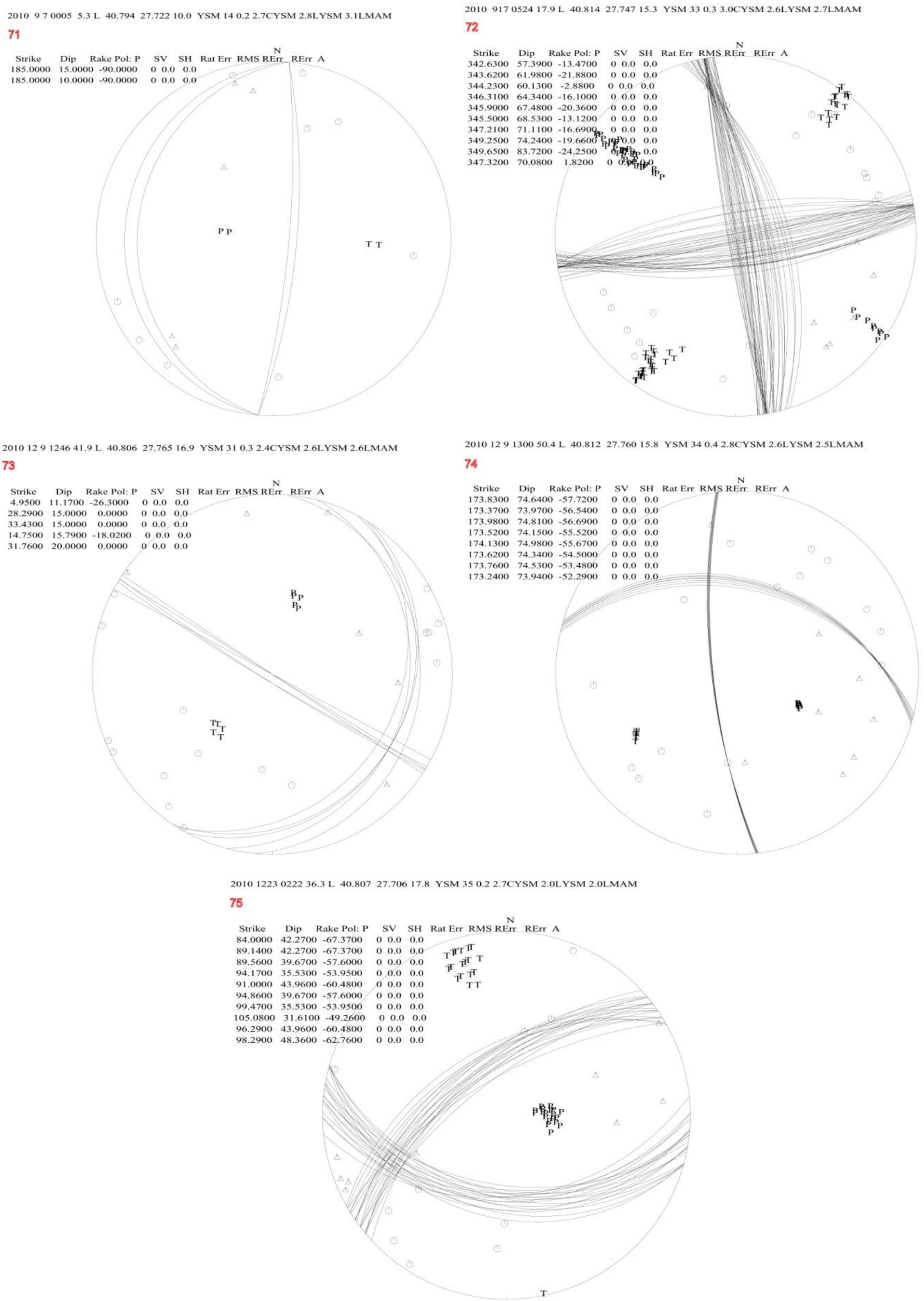

Figure D.2.13. Fault plane solutions obtained through the program of FOCMEC. Solutions are given time dependently for the Tekirdağ Basin Cluster

3. The Çınarcık Basin Cluster

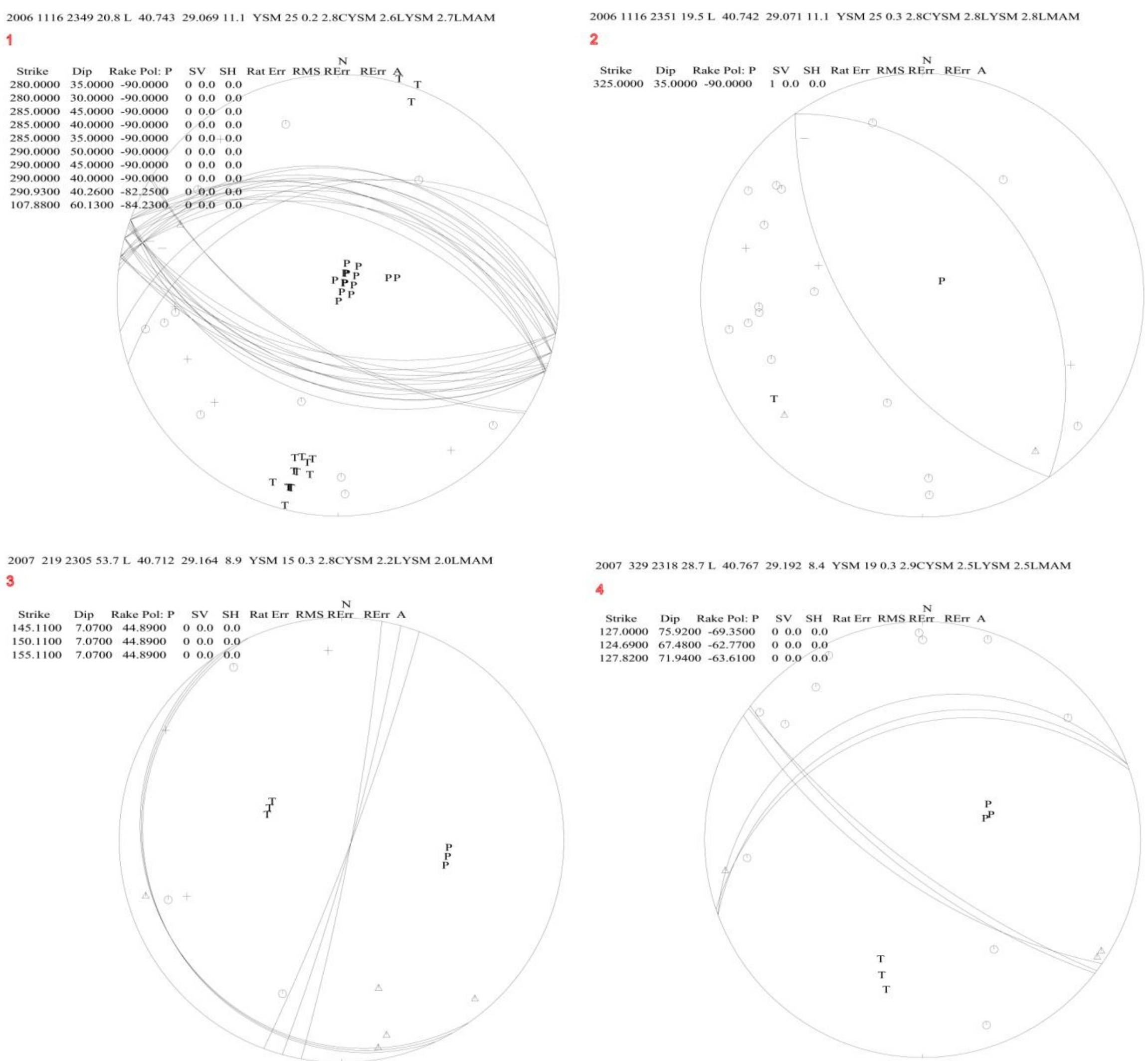

Figure D.3.1. Lower hemisphere projections of fault plane solutions obtained through the program of FOCMEC. Black circles indicate compressional P-wave first motion polarities, while black triangles show dilatational ones. Solutions are given time dependently for the Çınarcık Basin Cluster

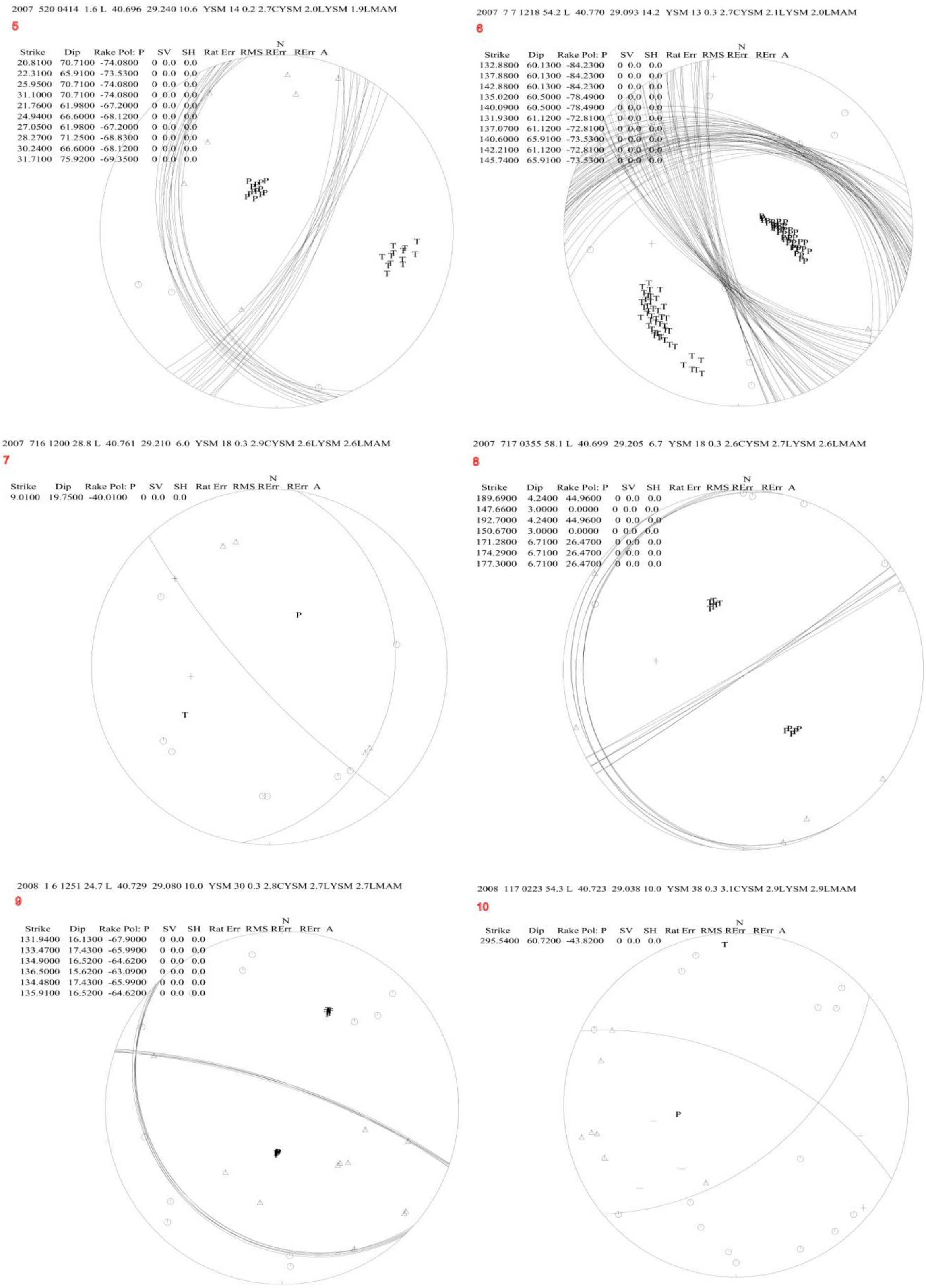

Figure D.3.2. Fault plane solutions obtained through the program of FOCMEC. Solutions are given time dependently for the Çınarcık Basin Cluster

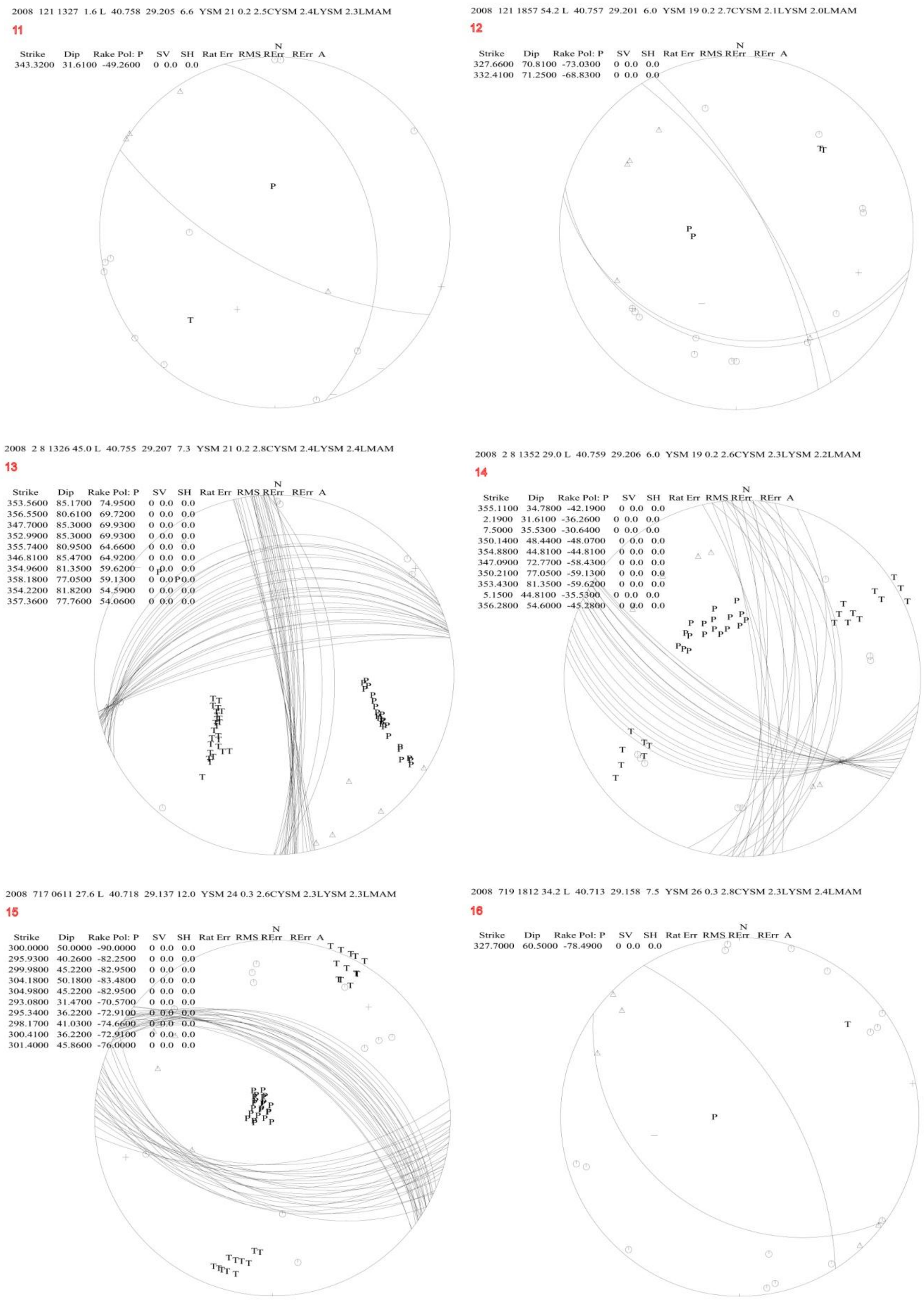

Figure D.3.3. Fault plane solutions obtained through the program of FOCMEC. Solutions are given time dependently for the Çınarcık Basin Cluster

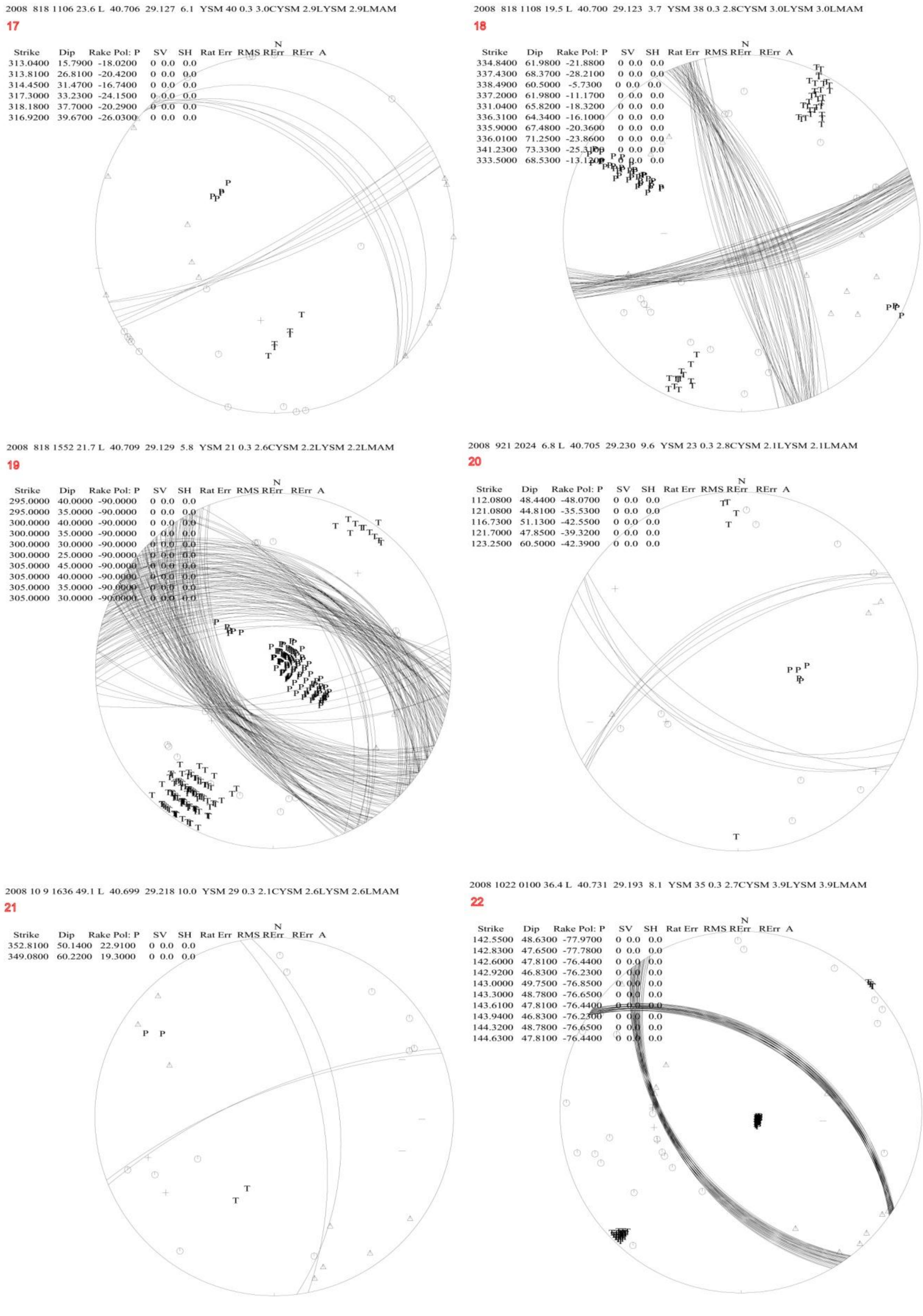

Figure D.3.4. Fault plane solutions obtained through the program of FOCMEC. Solutions are given time dependently for the Çınarcık Basin Cluster

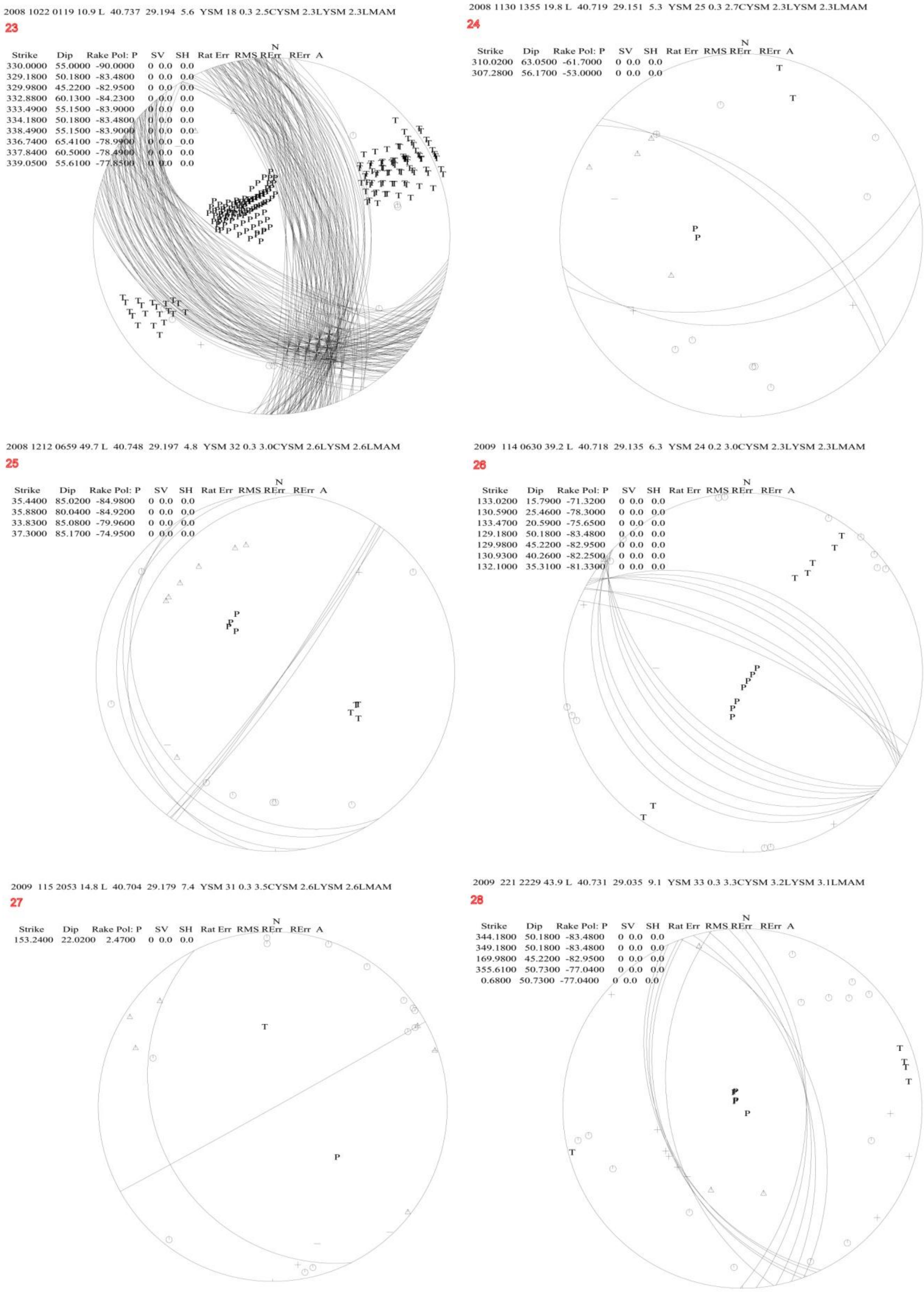

Figure D.3.5. Fault plane solutions obtained through the program of FOCMEC. Solutions are given time dependently for the Çınarcık Basin Cluster

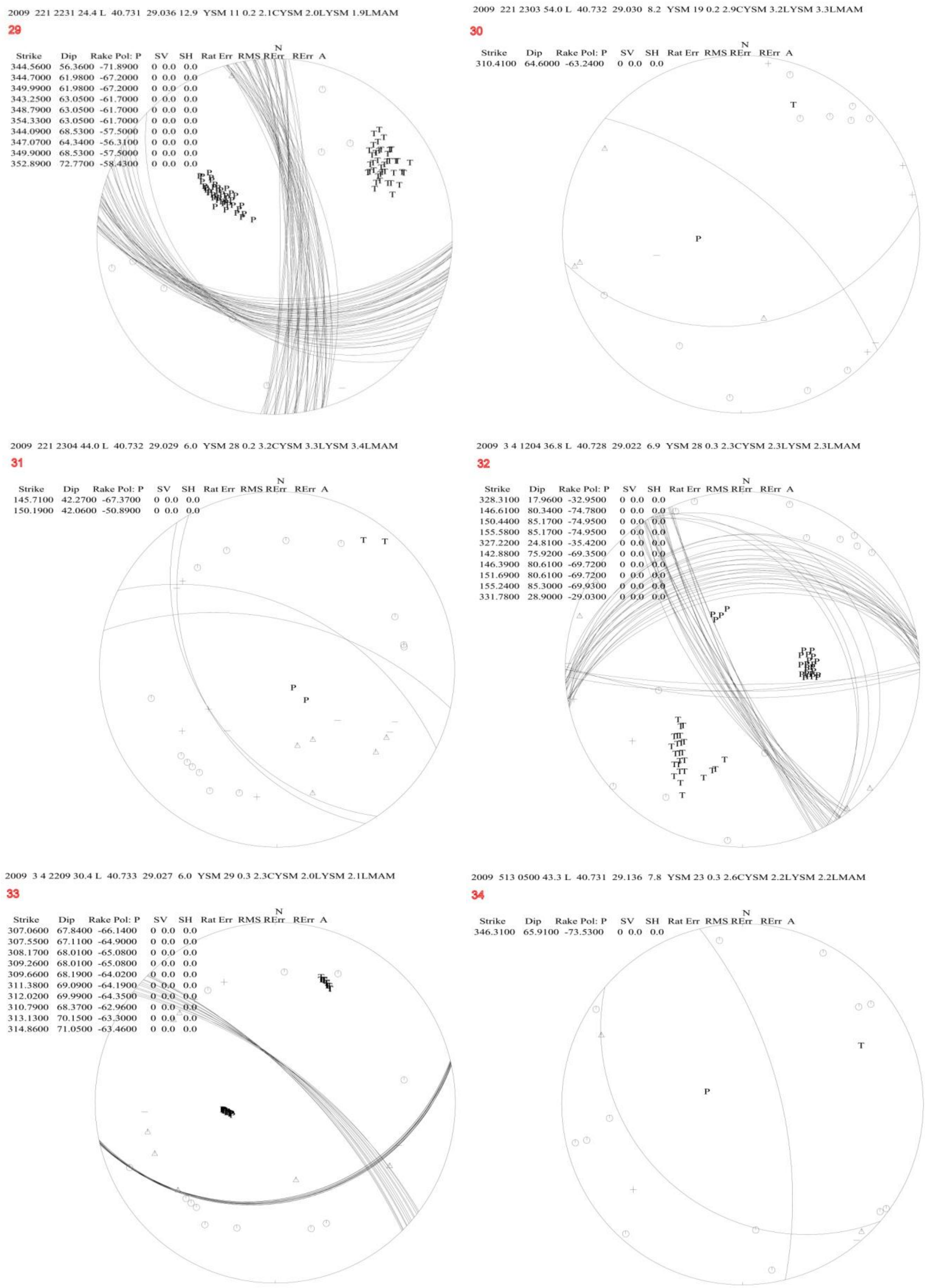

Figure D.3.6. Fault plane solutions obtained through the program of FOCMEC. Solutions are given time dependently for the Çınarcık Basin Cluster

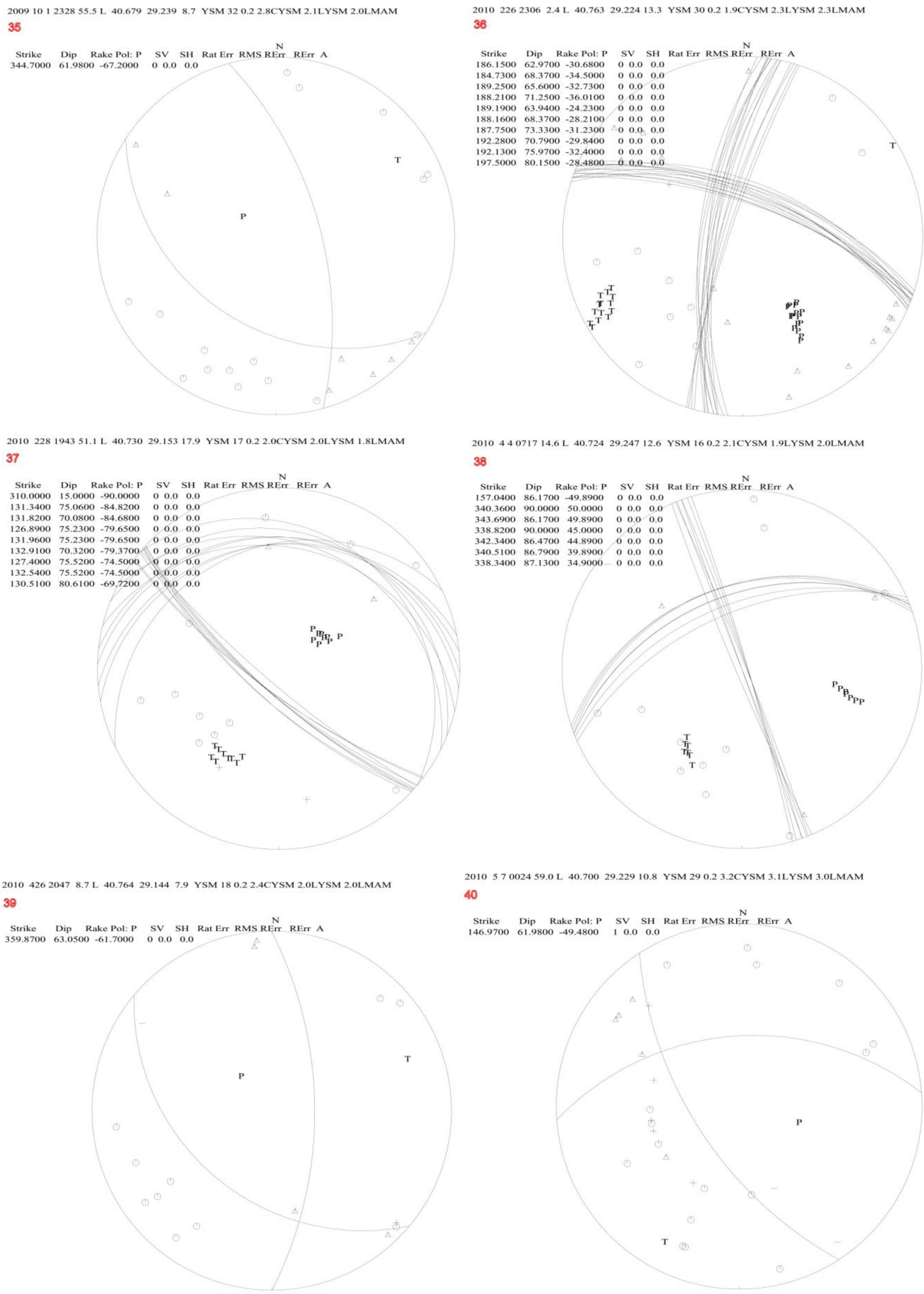

Figure D.3.7. Fault plane solutions obtained through the program of FOCMEC. Solutions are given time dependently for the Çınarcık Basin Cluster

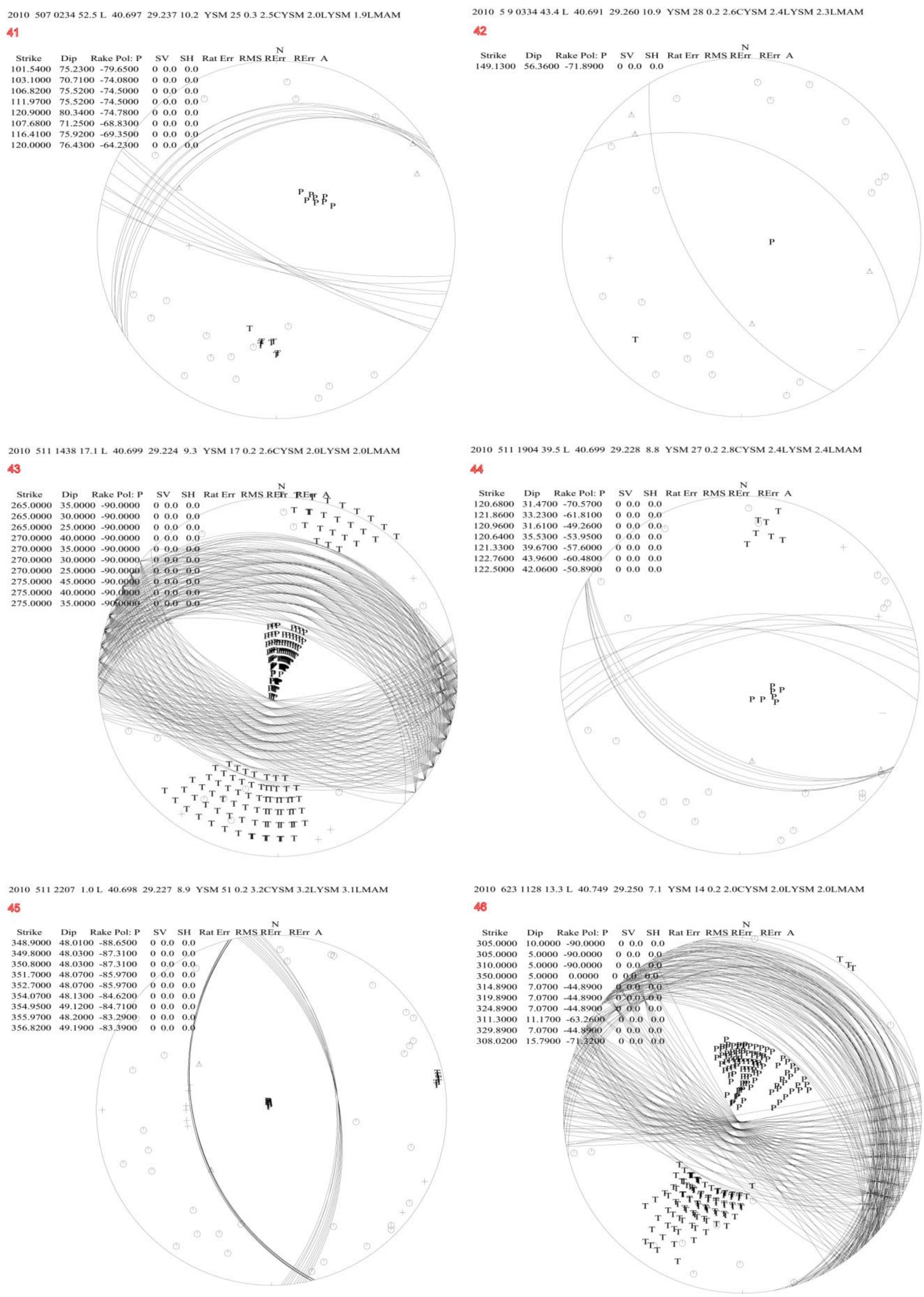

Figure D.3.8. Fault plane solutions obtained through the program of FOCMEC. Solutions are given time dependently for the Çınarcık Basin Cluster

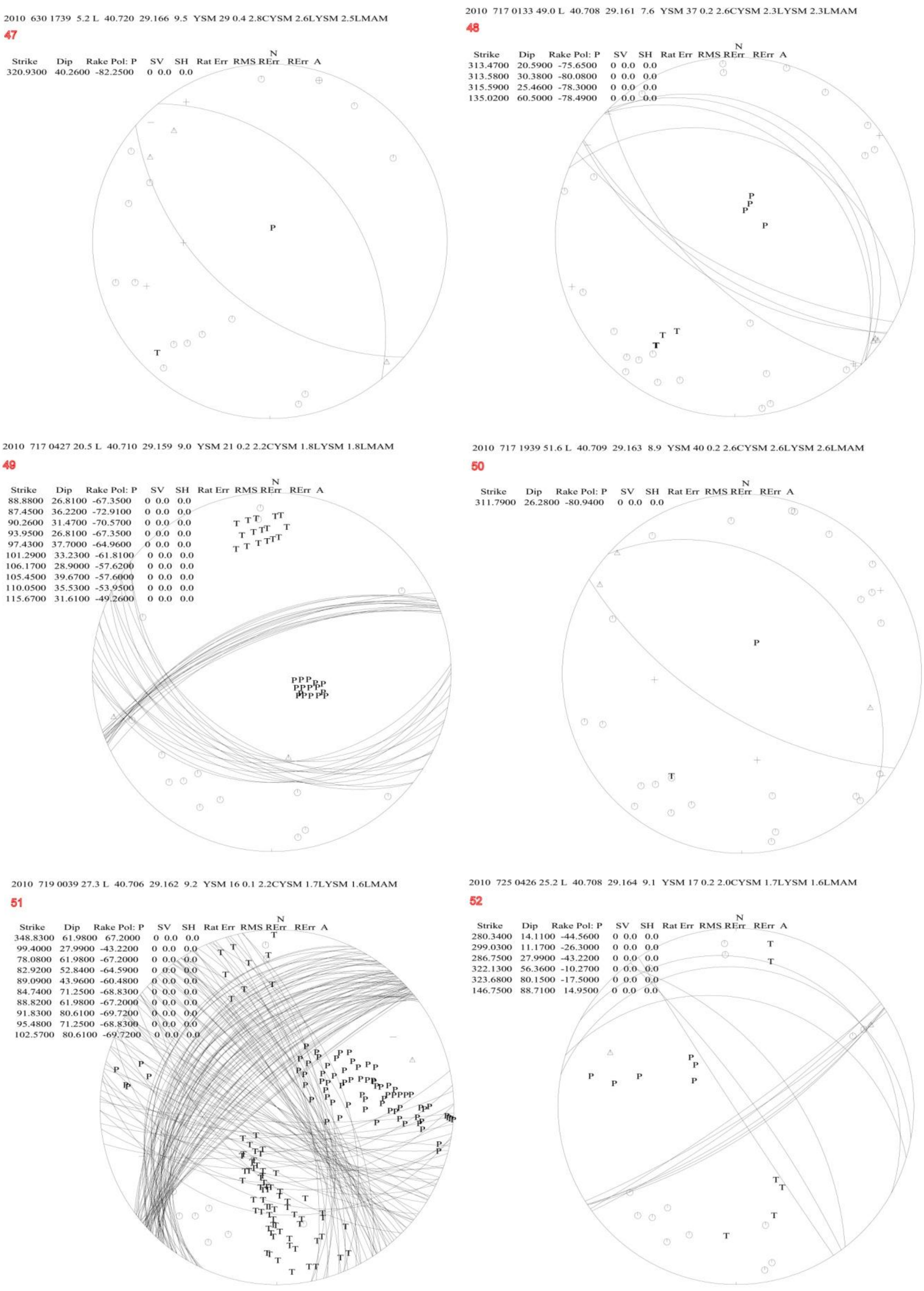

Figure D.3.9. Fault plane solutions obtained through the program of FOCMEC. Solutions are given time dependently for the Çınarcık Basin Cluster

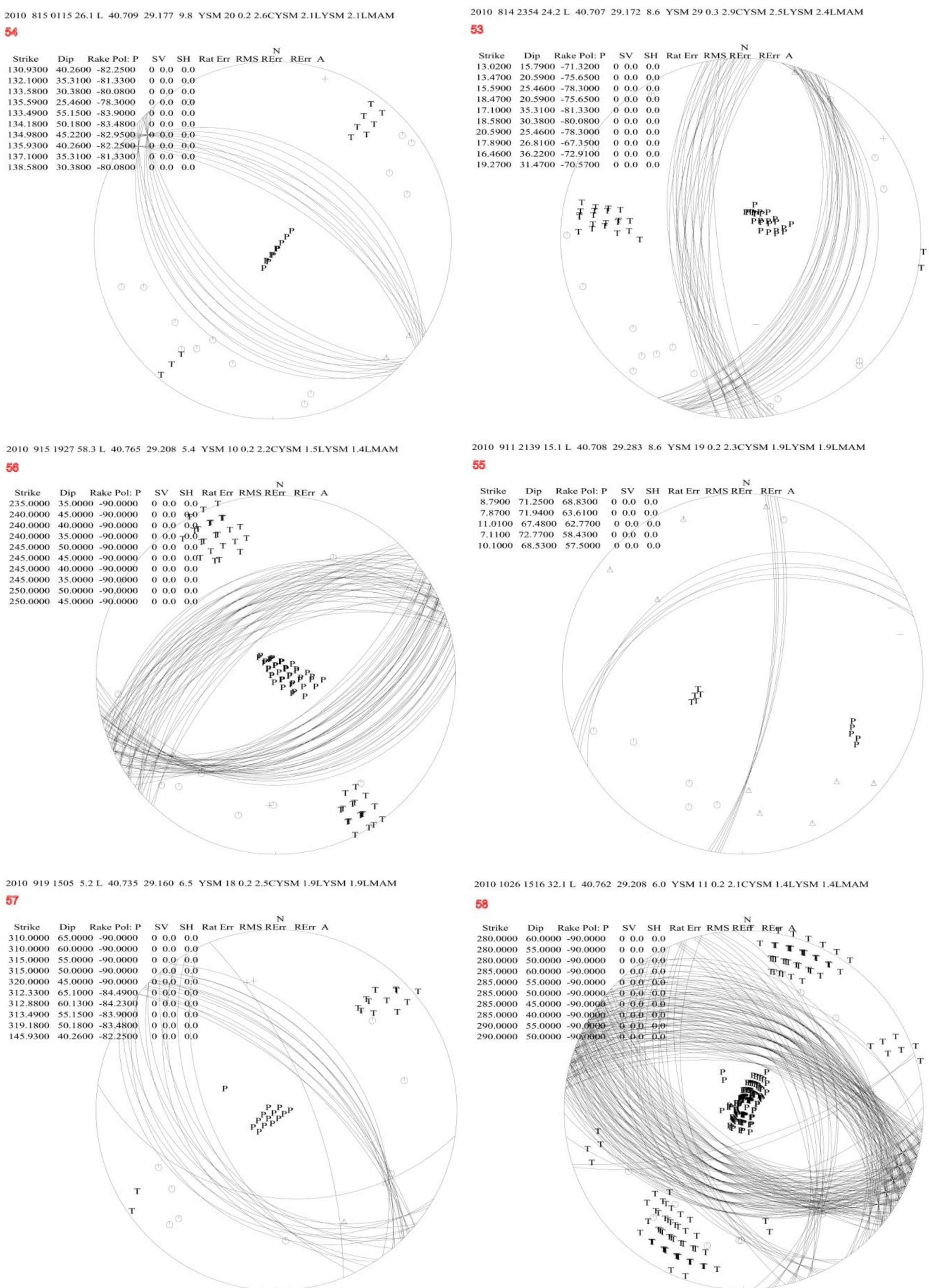

Figure D.3.10. Fault plane solutions obtained through the program of FOCMEC. Solutions are given time dependently for the Çınarcık Basin Cluster

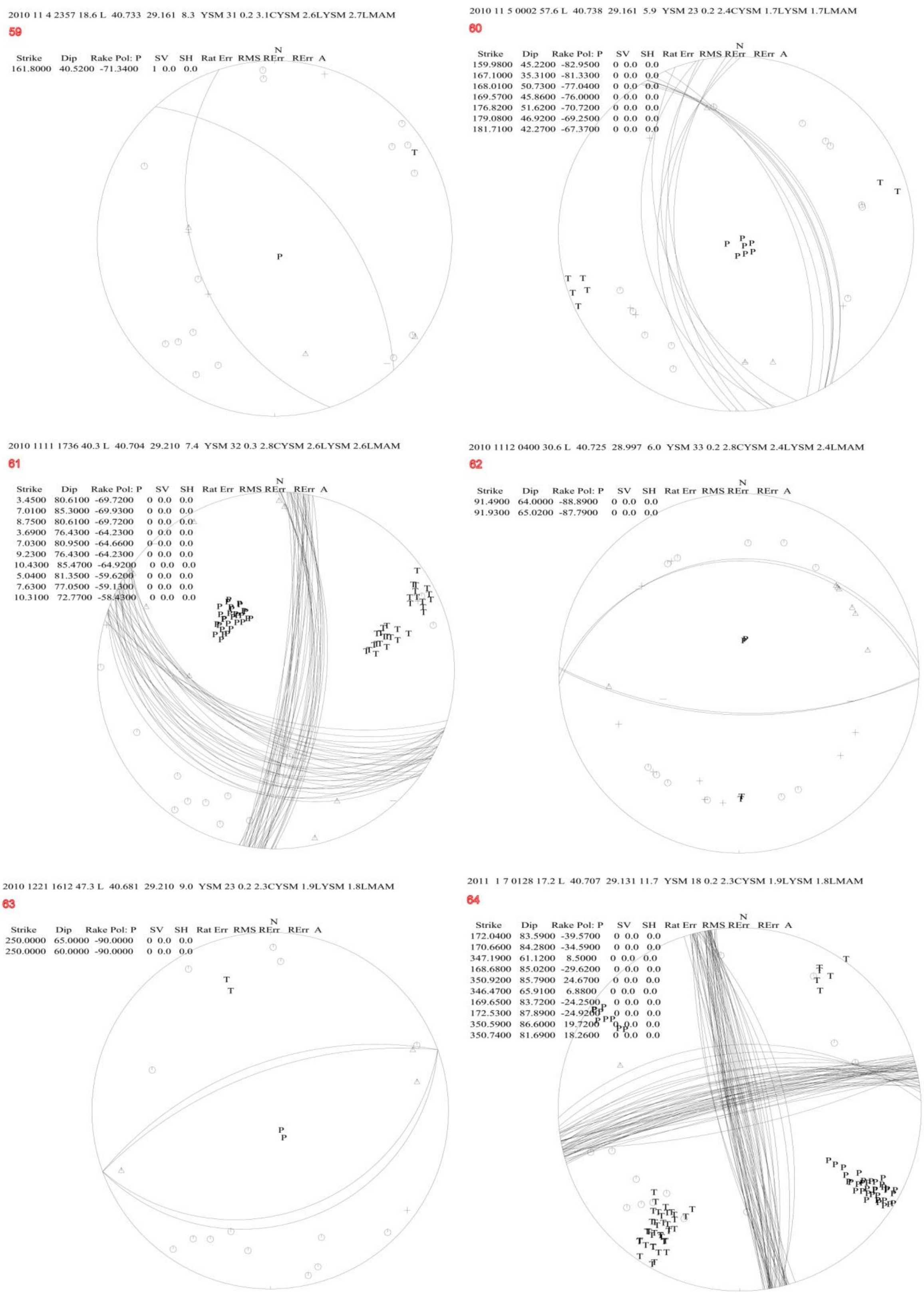

Figure D.3.11. Fault plane solutions obtained through the program of FOCMEC. Solutions are given time dependently for the Çınarcık Basin Cluster

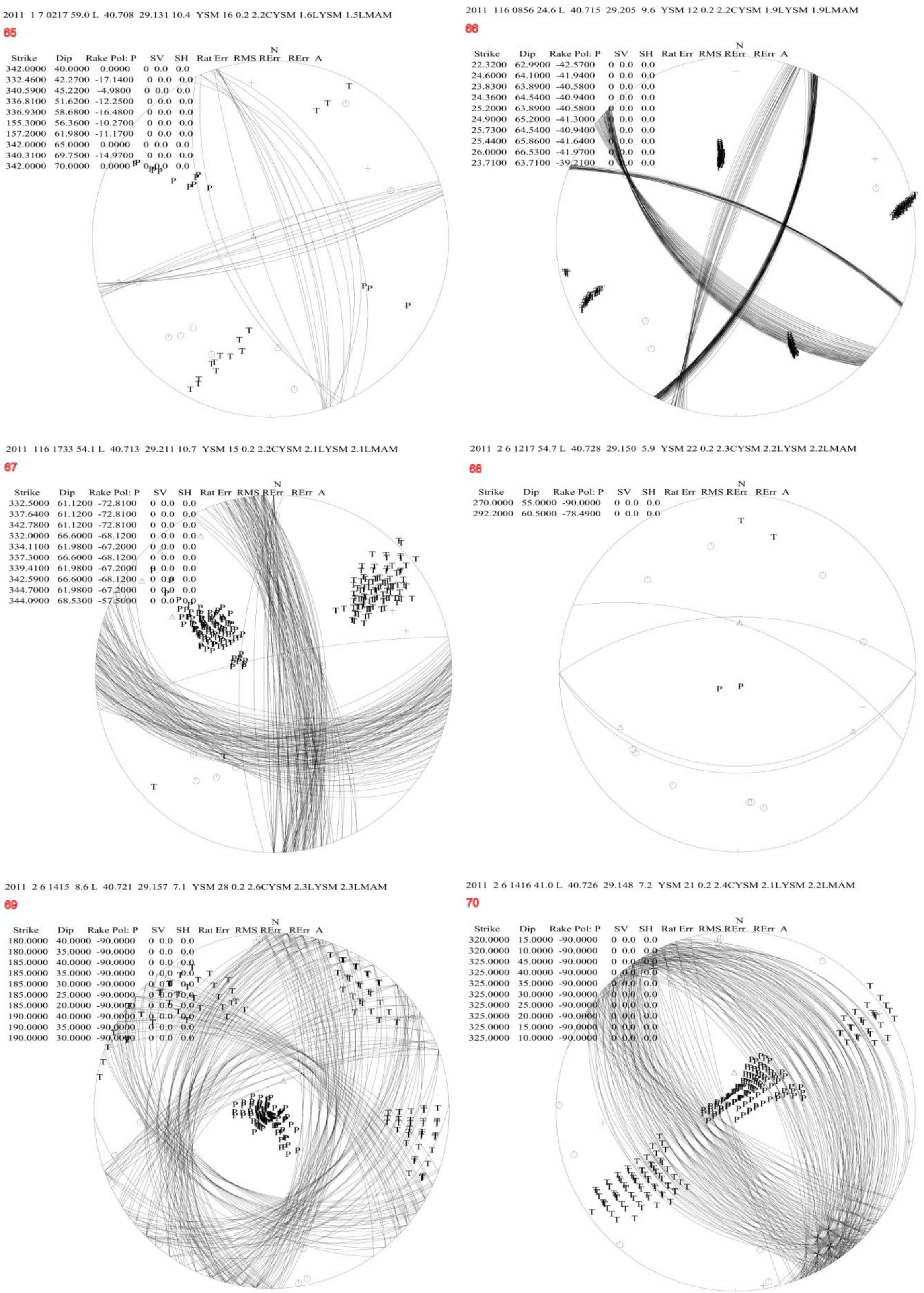

Figure D.3.12. Fault plane solutions obtained through the program of FOCMEC. Solutions are given time dependently for the Çınarcık Basin Cluster

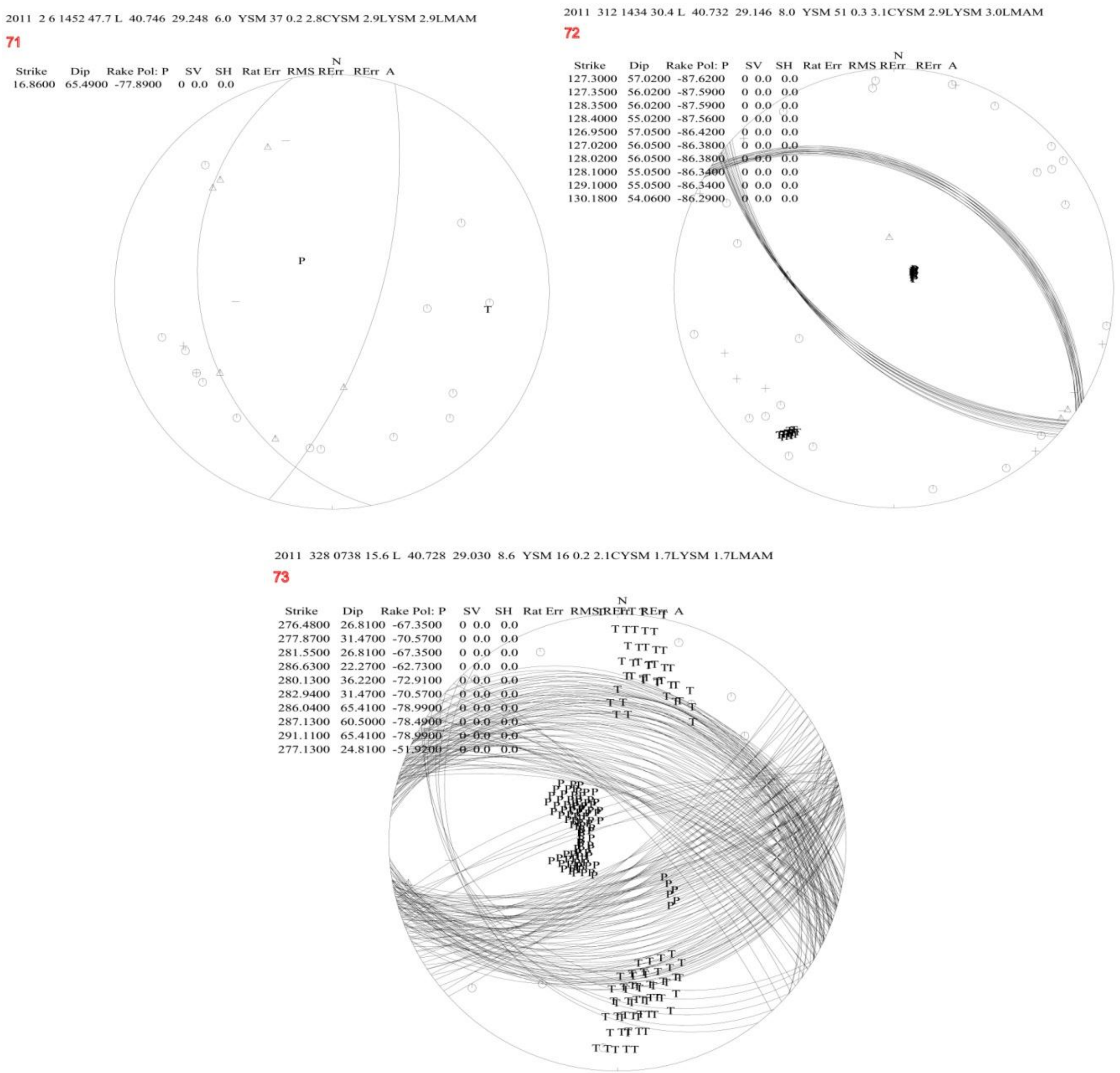

Figure D.3.13. Fault plane solutions obtained through the program of FOCMEC. Solutions are given time dependently for the Çınarcık Basin Cluster

4. The Yalova Cluster

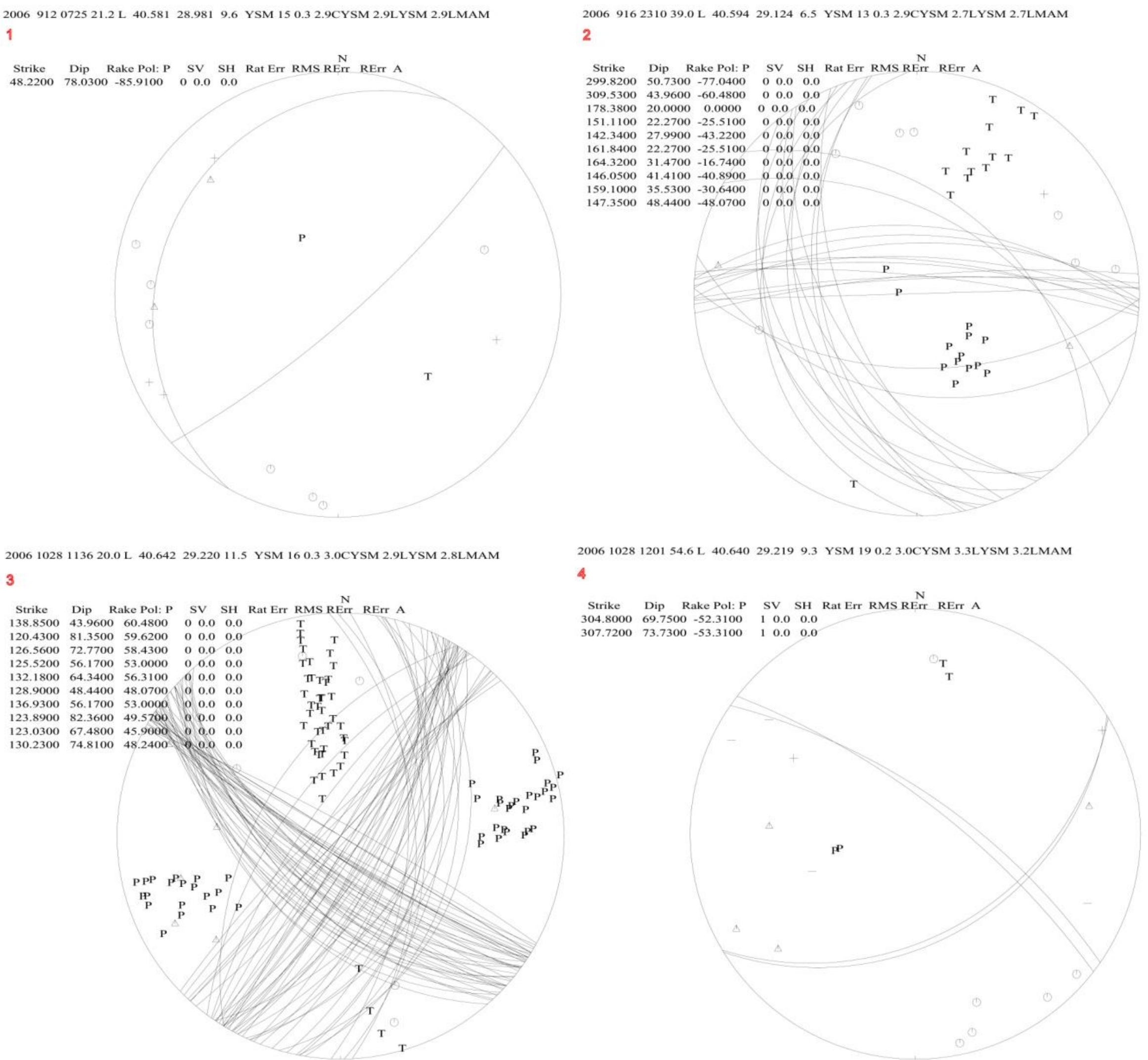

Figure D.4.1. Lower hemisphere projections of fault plane solutions obtained through the program of FOCMEC. Black circles indicate compressional P-wave first motion polarities, while black triangles show dilatational ones. Solutions are given time dependently for the Yalova Cluster

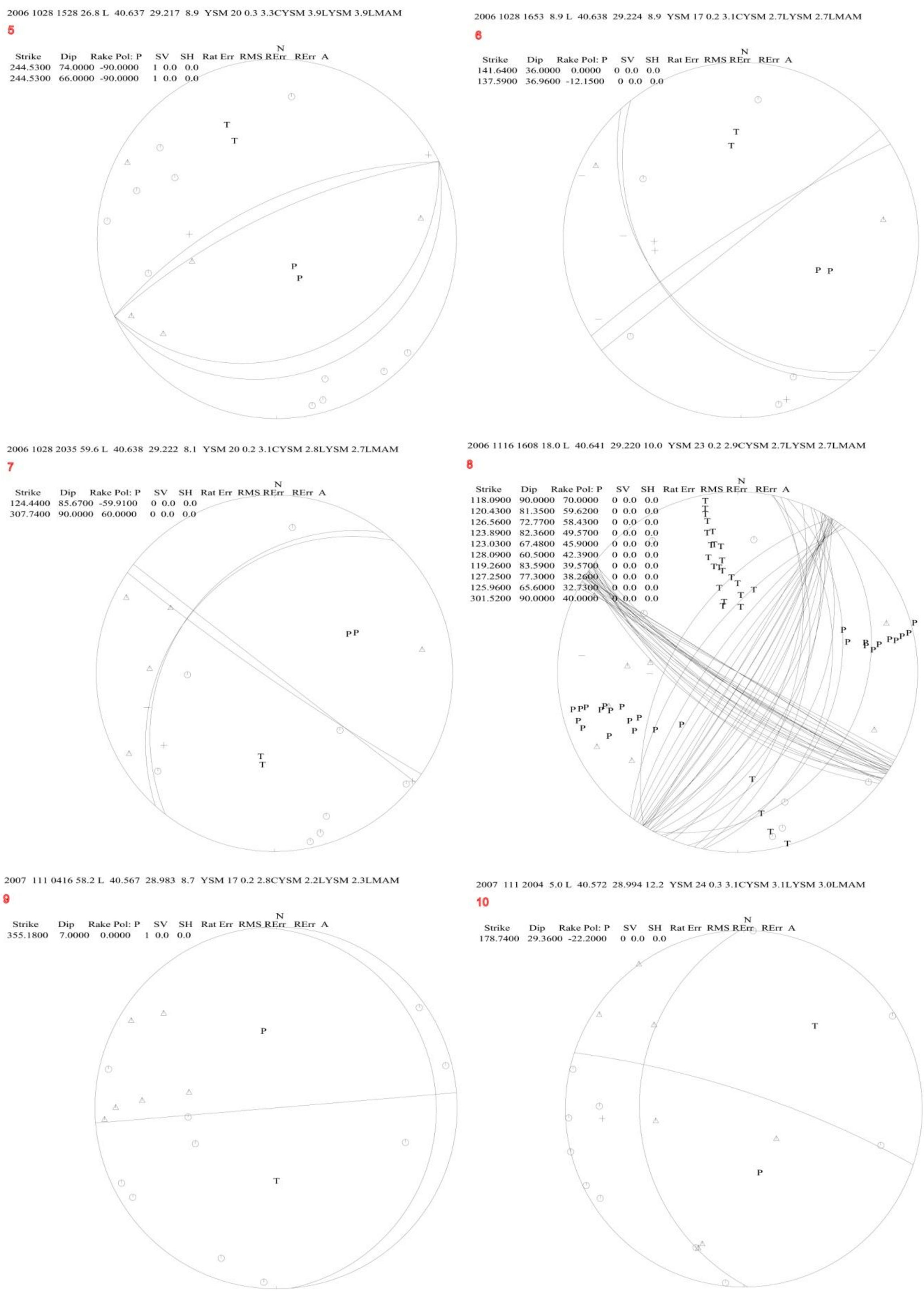

Figure D.4.2. Fault plane solutions obtained through the program of FOCMEC. Solutions are given time dependently for the Yalova Cluster

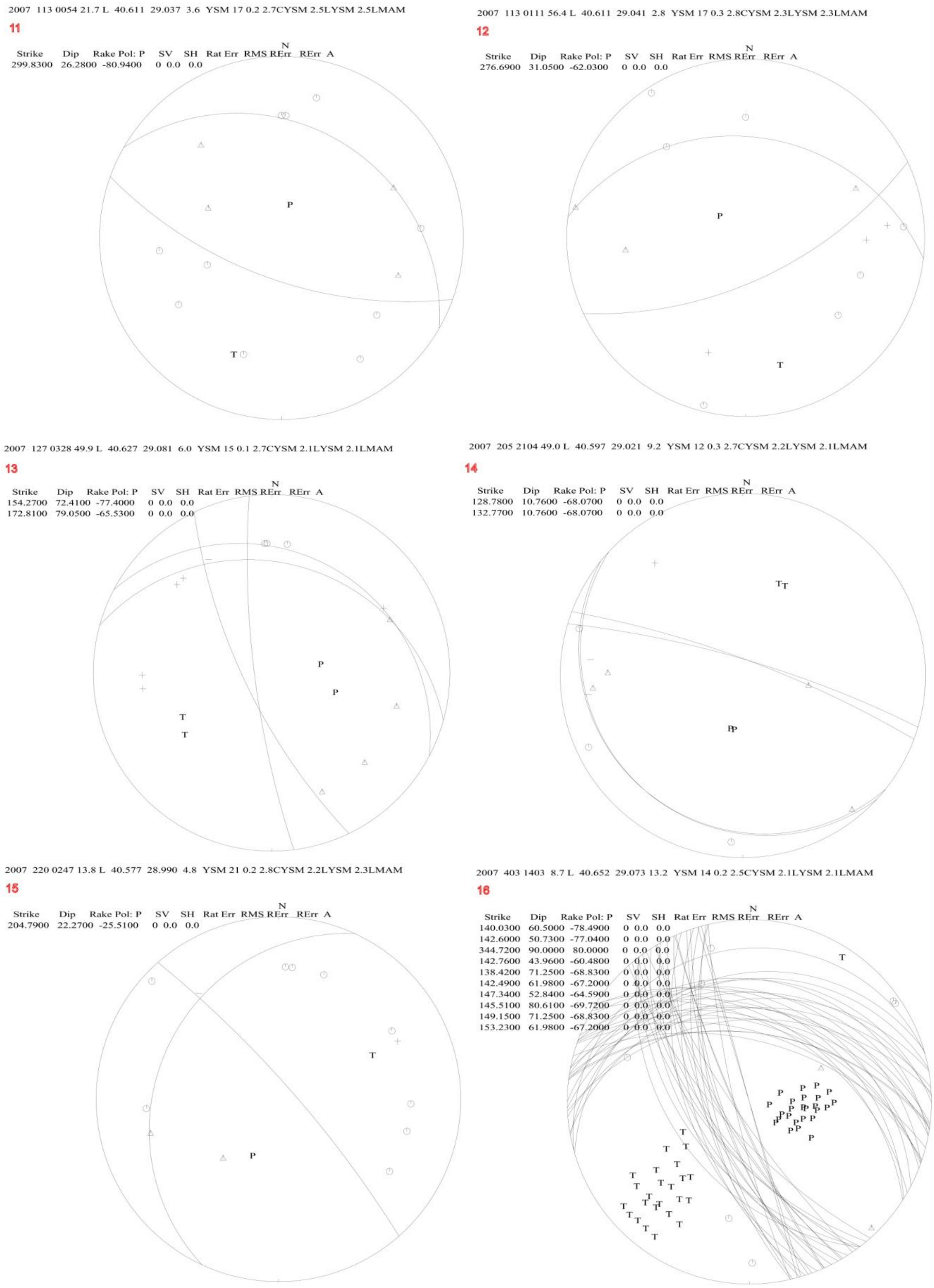

Figure D.4.3. Fault plane solutions obtained through the program of FOCMEC. Solutions are given time dependently for the Yalova Cluster

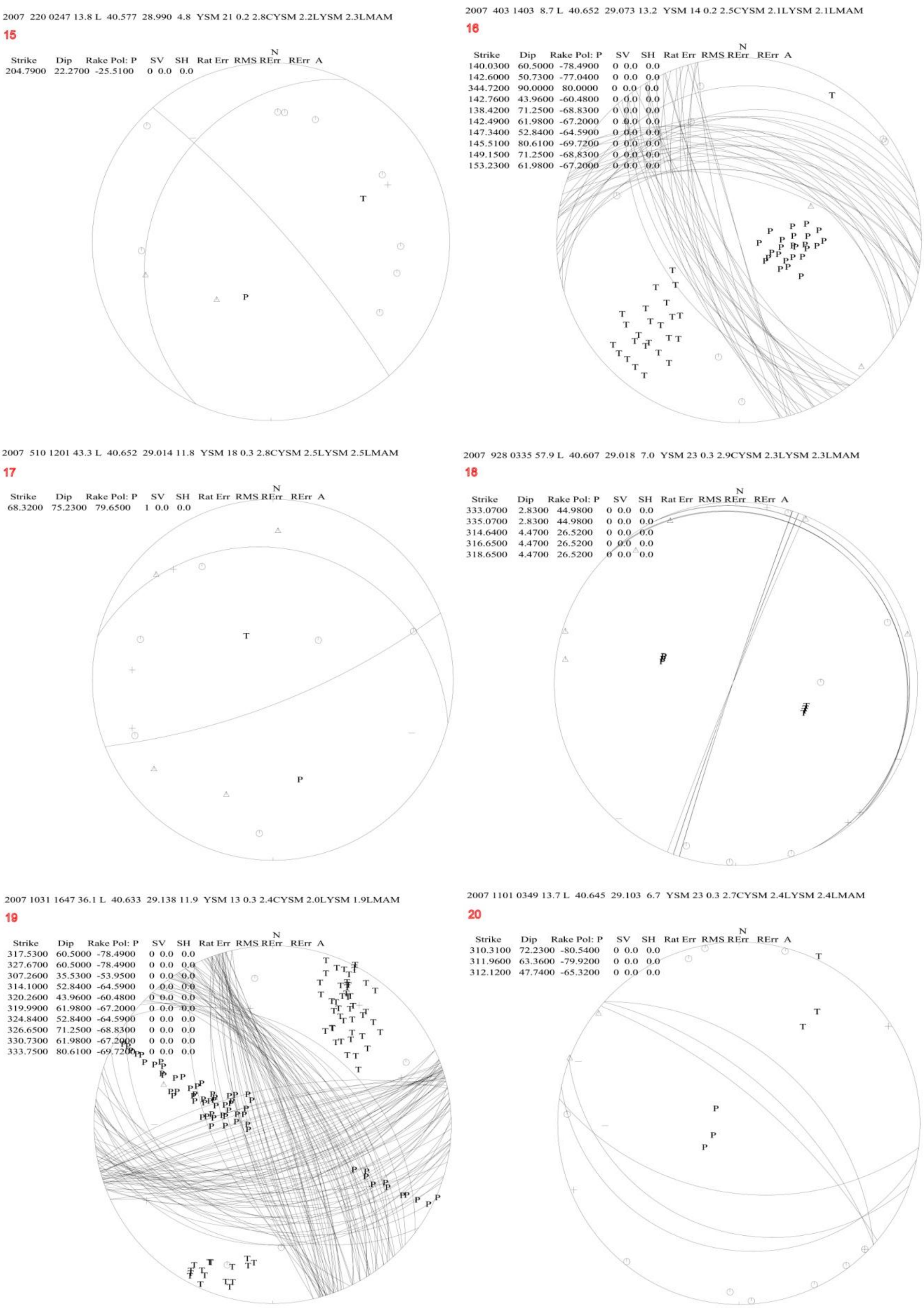

Figure D.4.4. Fault plane solutions obtained through the program of FOCMEC. Solutions are given time dependently for the Yalova Cluster

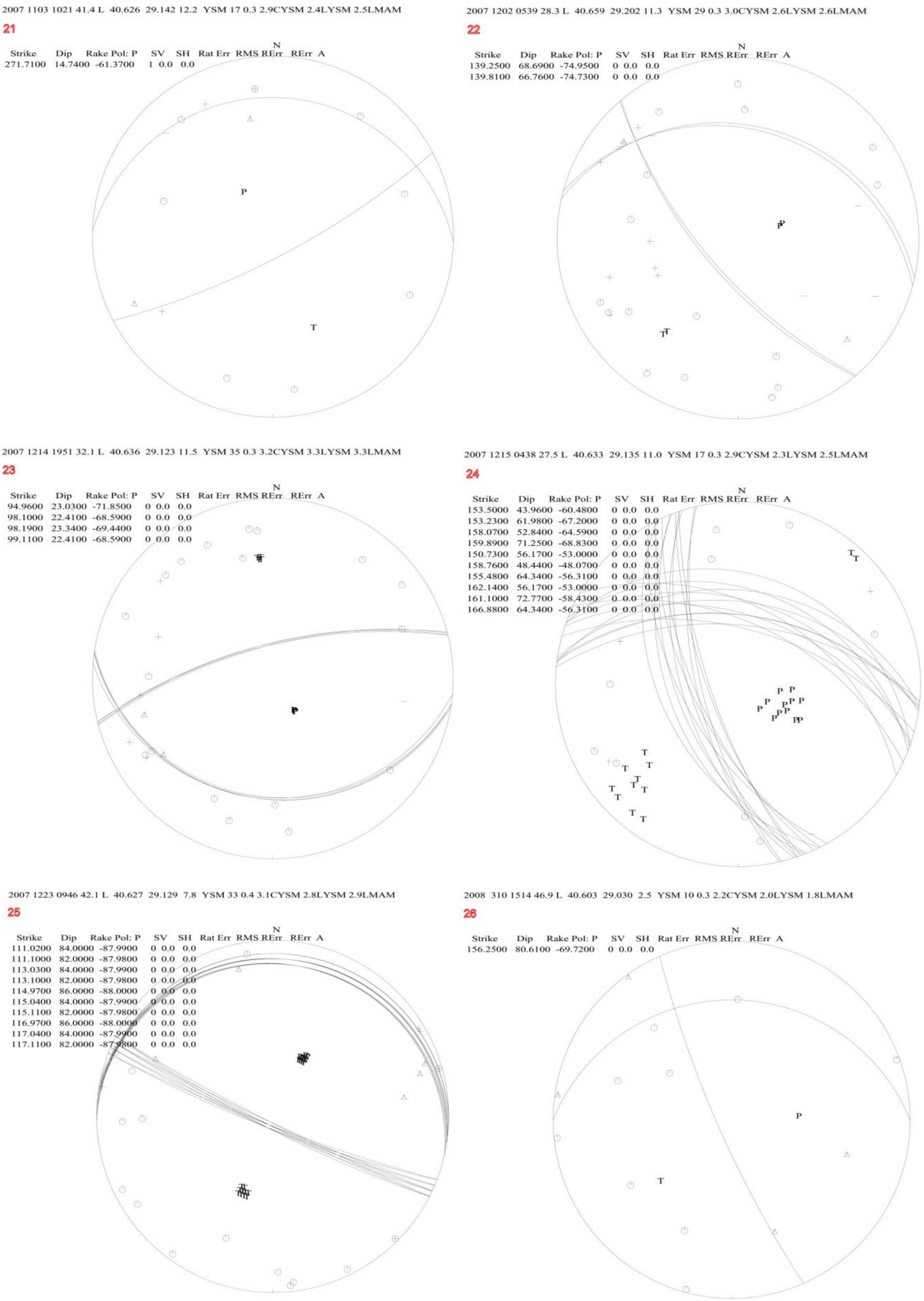

Figure D.4.5. Fault plane solutions obtained through the program of FOCMEC. Solutions are given time dependently for the Yalova Cluster

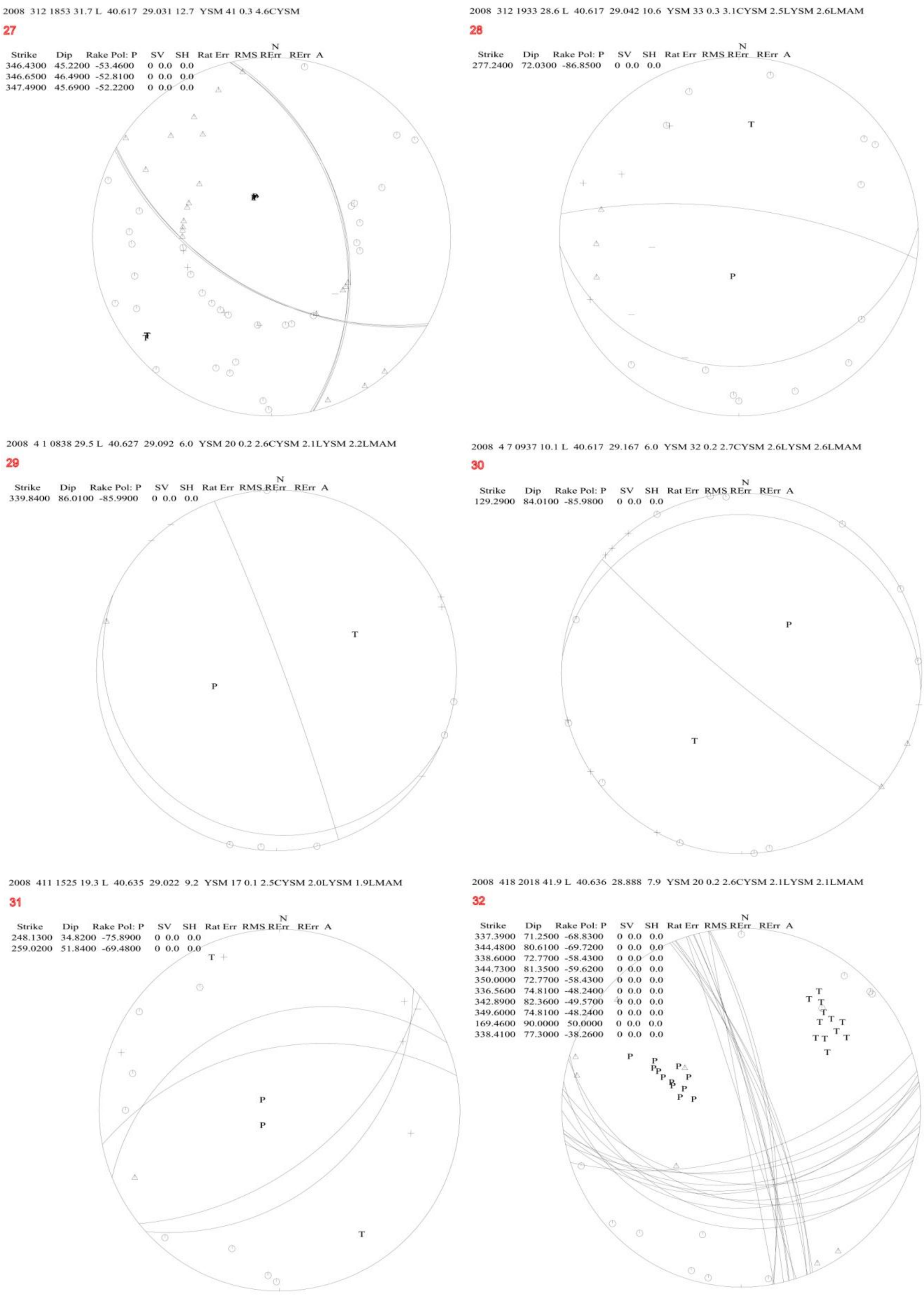

Figure D.4.6. Fault plane solutions obtained through the program of FOCMEC. Solutions are given time dependently for the Yalova Cluster

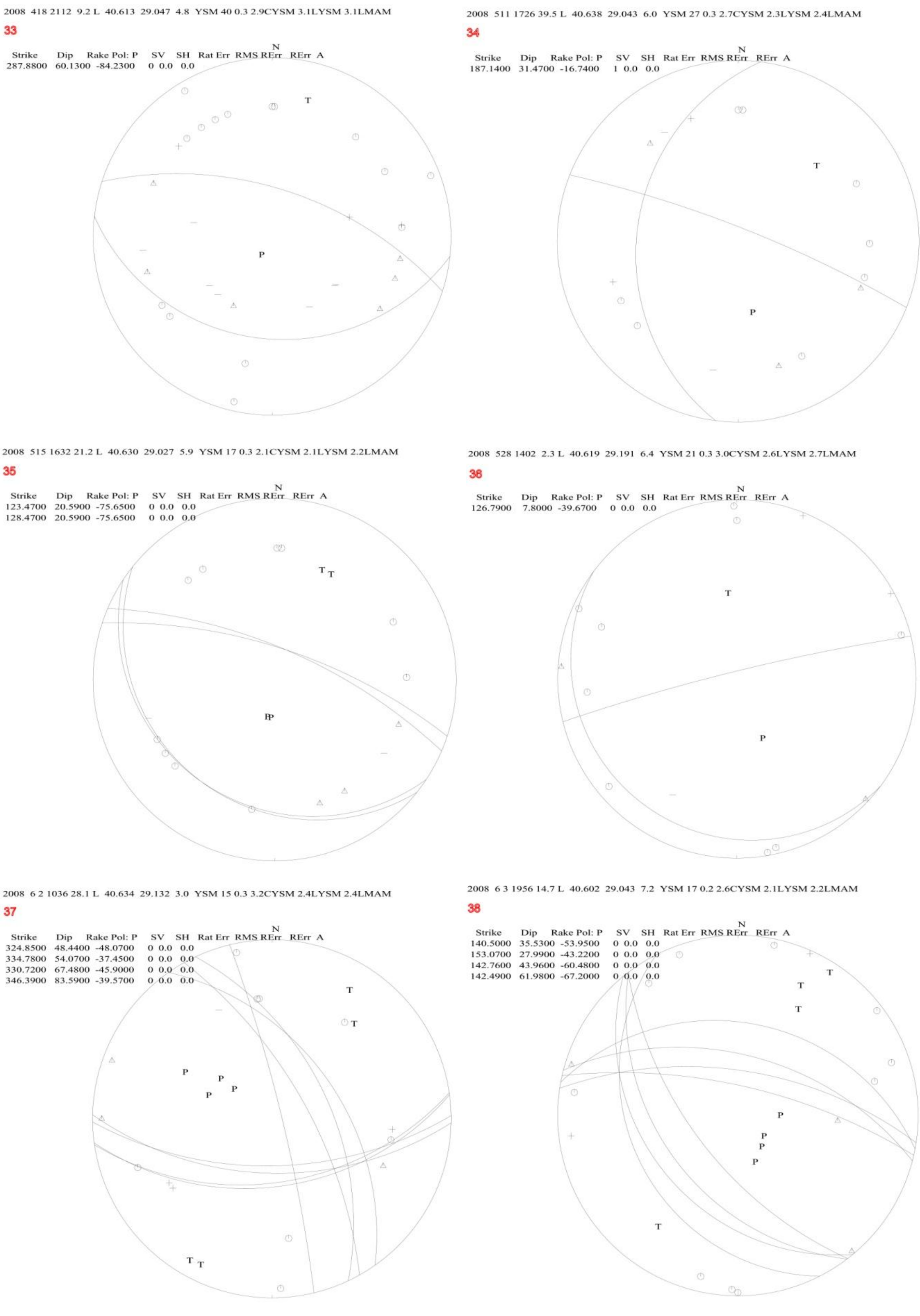

Figure D.4.7. Fault plane solutions obtained through the program of FOCMEC. Solutions are given time dependently for the Yalova Cluster

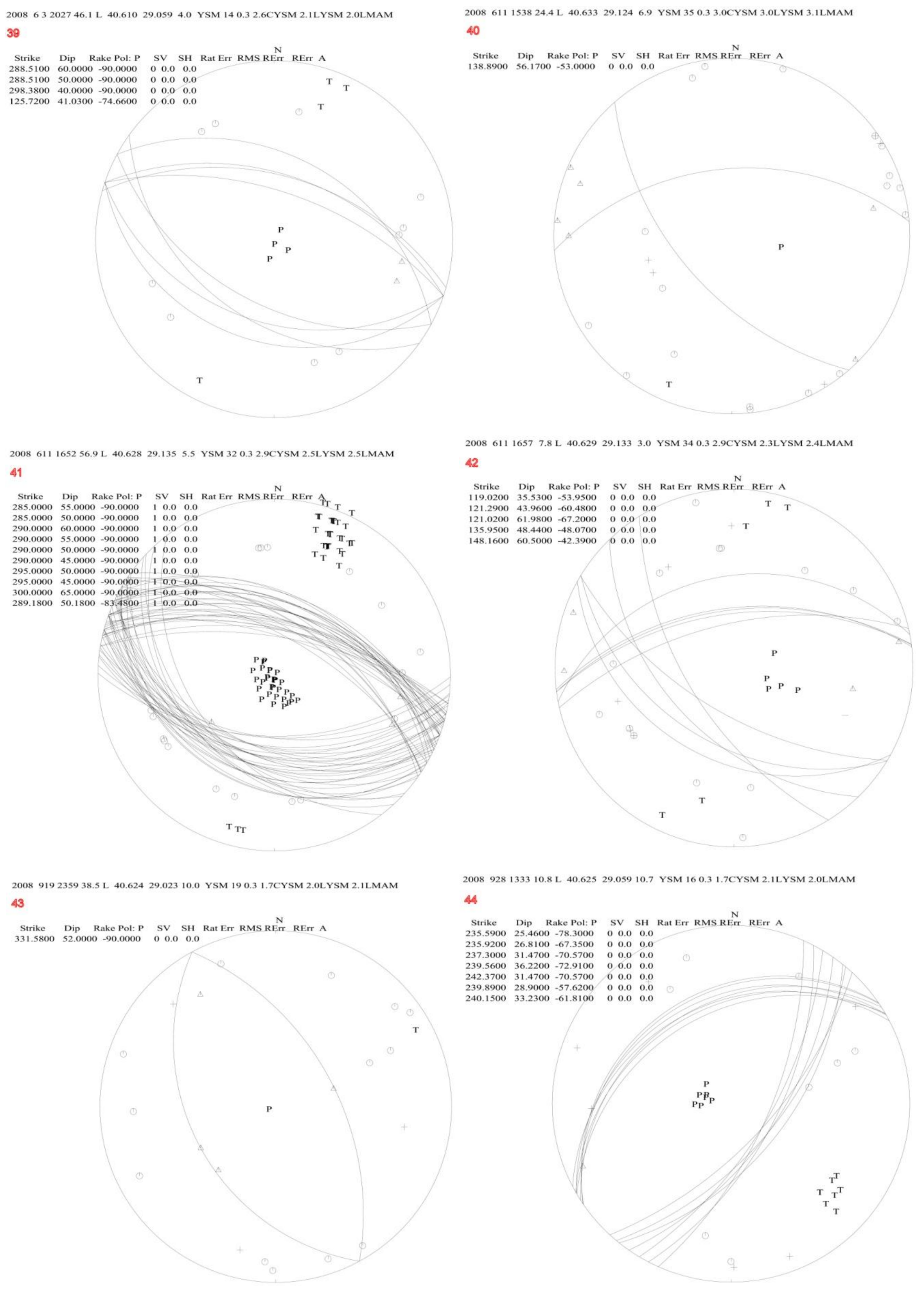

Figure D.4.8. Fault plane solutions obtained through the program of FOCMEC. Solutions are given time dependently for the Yalova Cluster

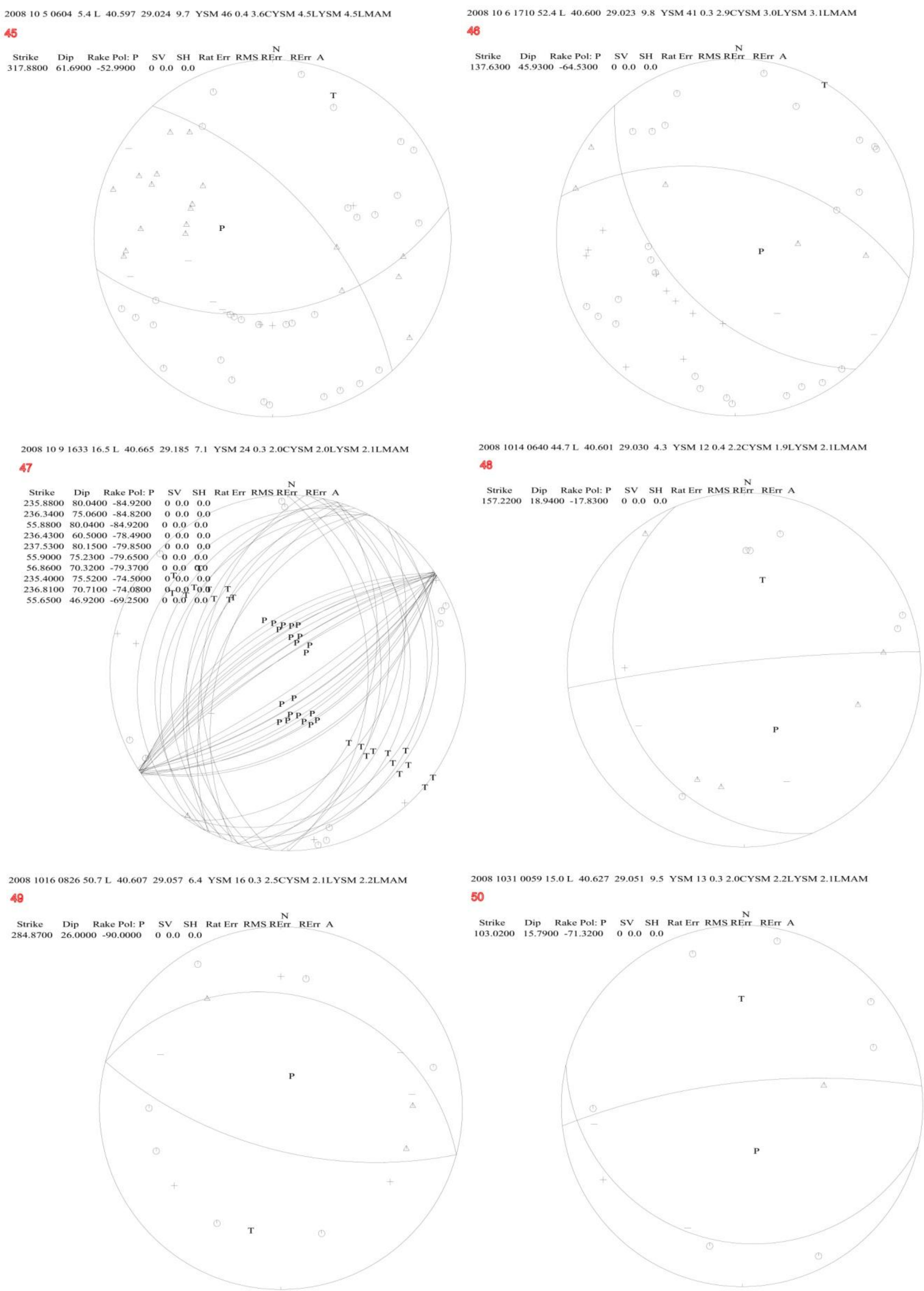

Figure D.4.9. Fault plane solutions obtained through the program of FOCMEC. Solutions are given time dependently for the Yalova Cluster

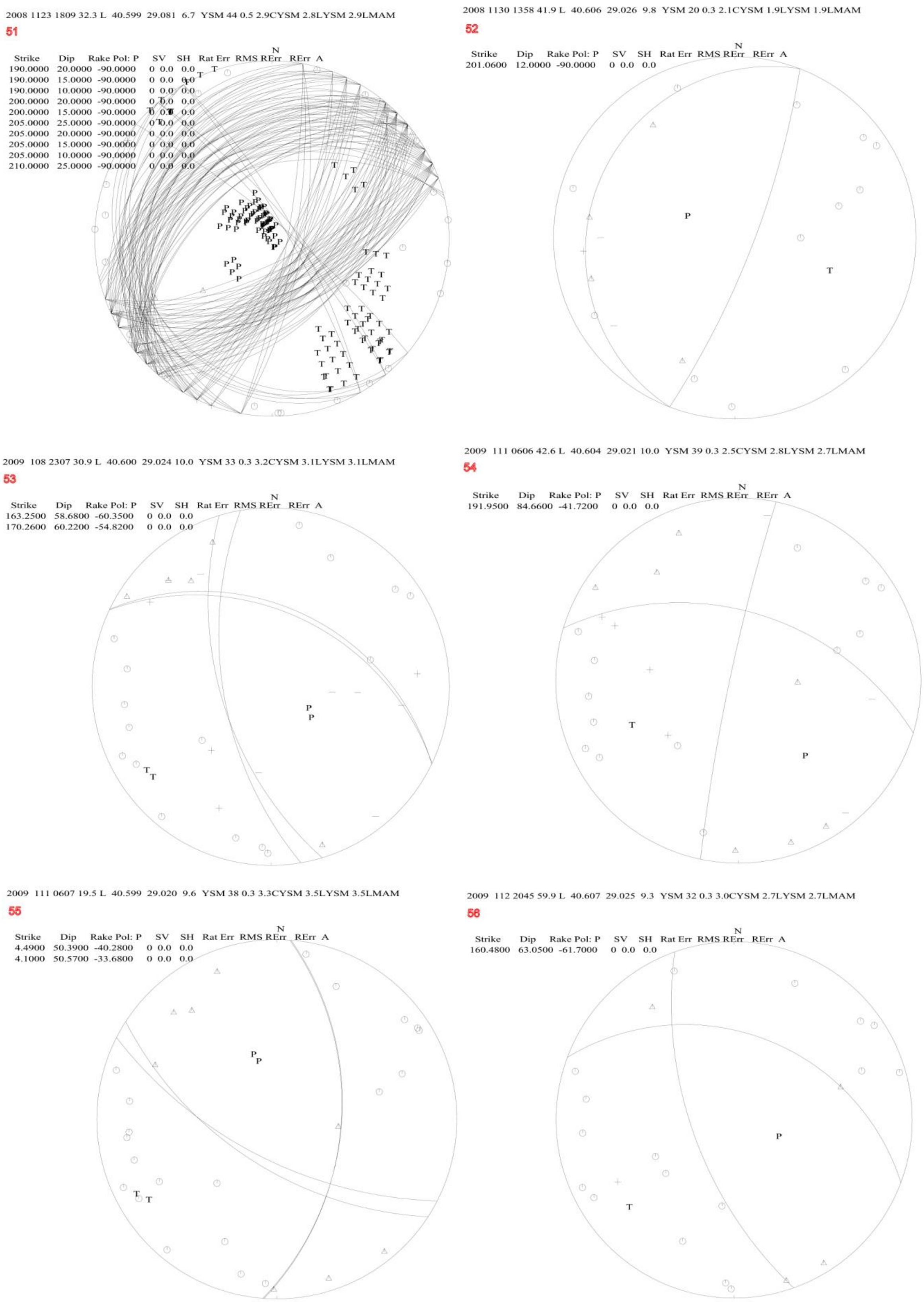

Figure D.4.10. Fault plane solutions obtained through the program of FOCMEC. Solutions are given time dependently for the Yalova Cluster

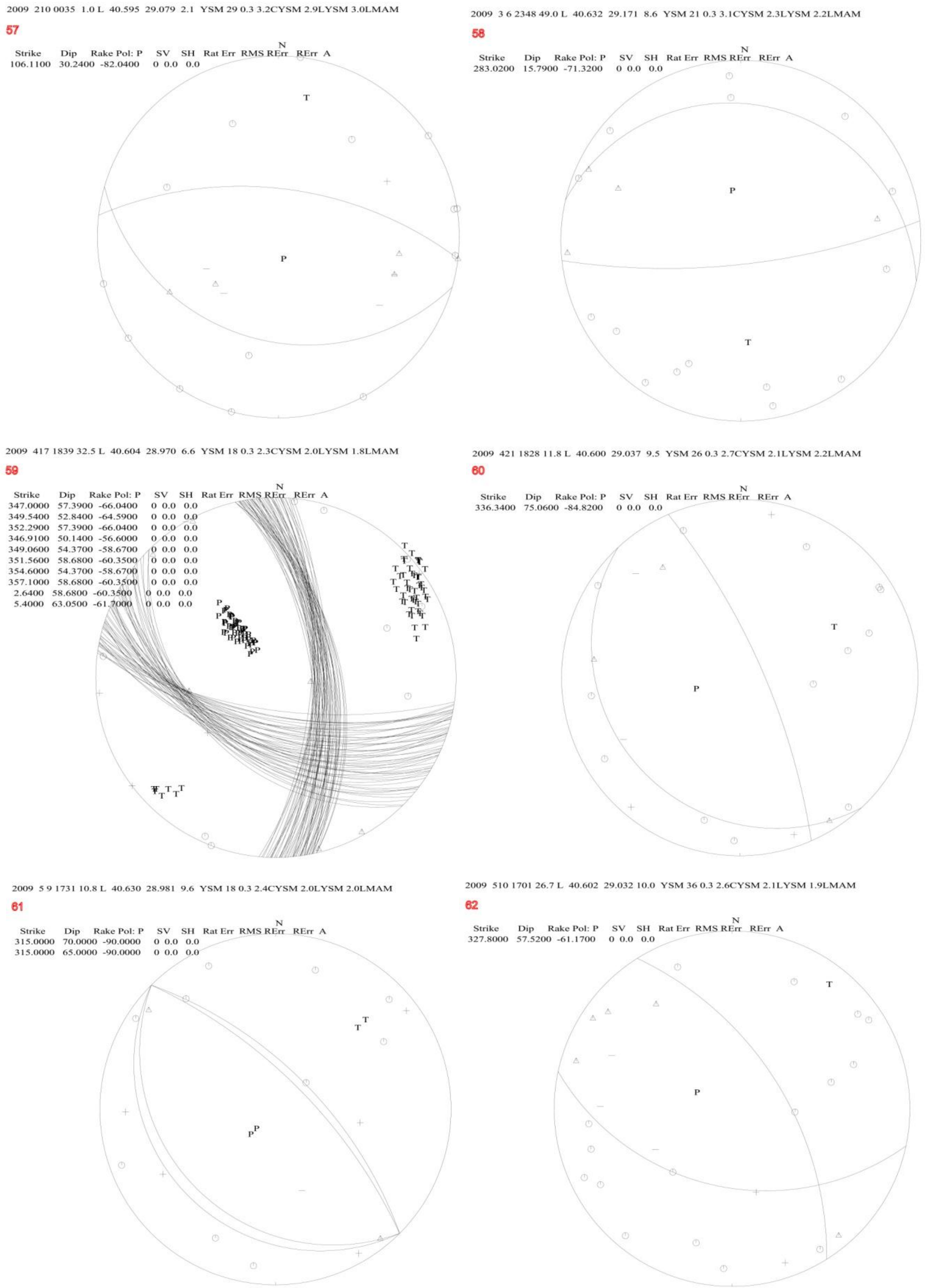

Figure D.4.11. Fault plane solutions obtained through the program of FOCMEC. Solutions are given time dependently for the Yalova Cluster

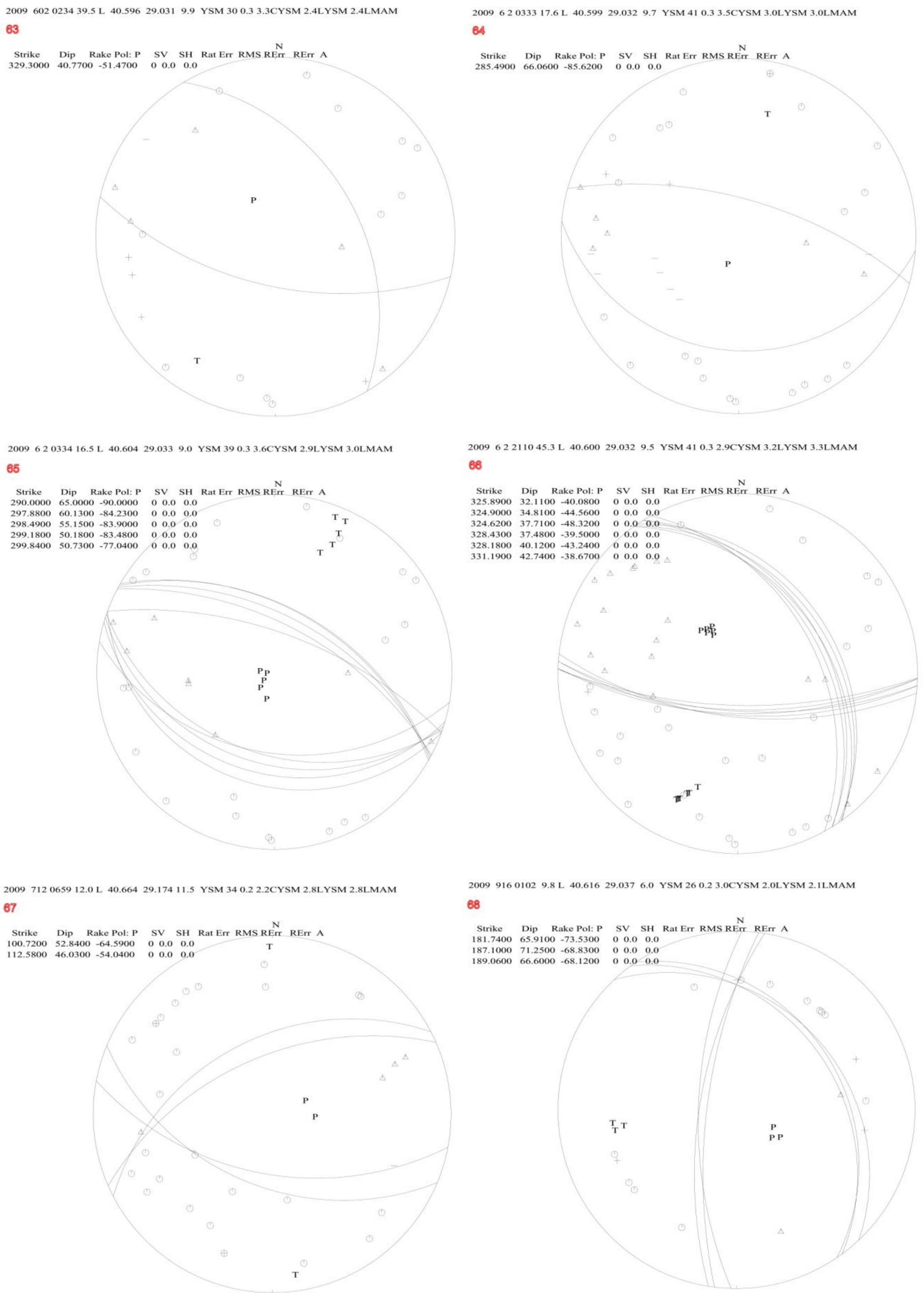

Figure D.4.12. Fault plane solutions obtained through the program of FOCMEC. Solutions are given time dependently for the Yalova Cluster

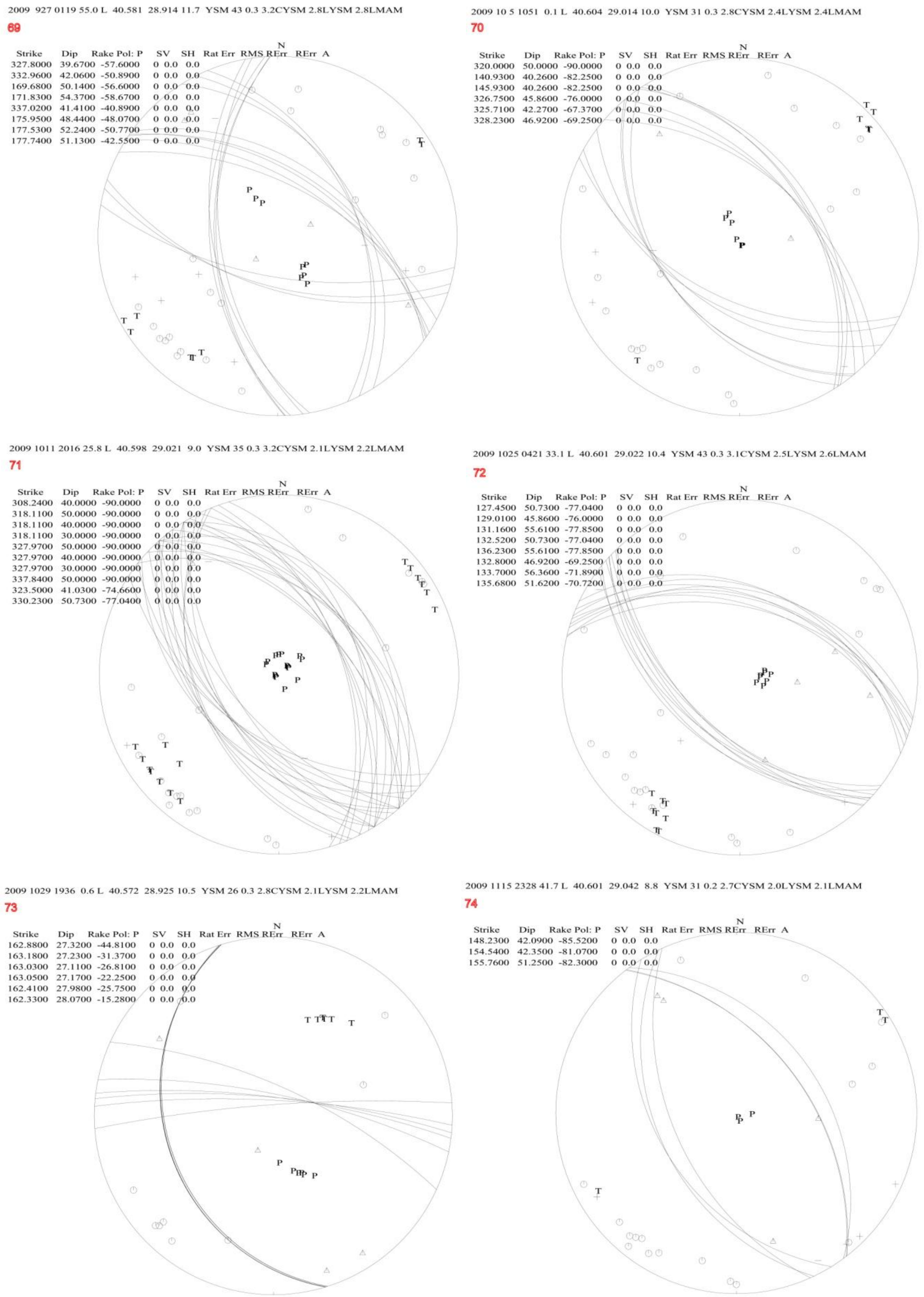

Figure D.4.13. Fault plane solutions obtained through the program of FOCMEC. Solutions are given time dependently for the Yalova Cluster

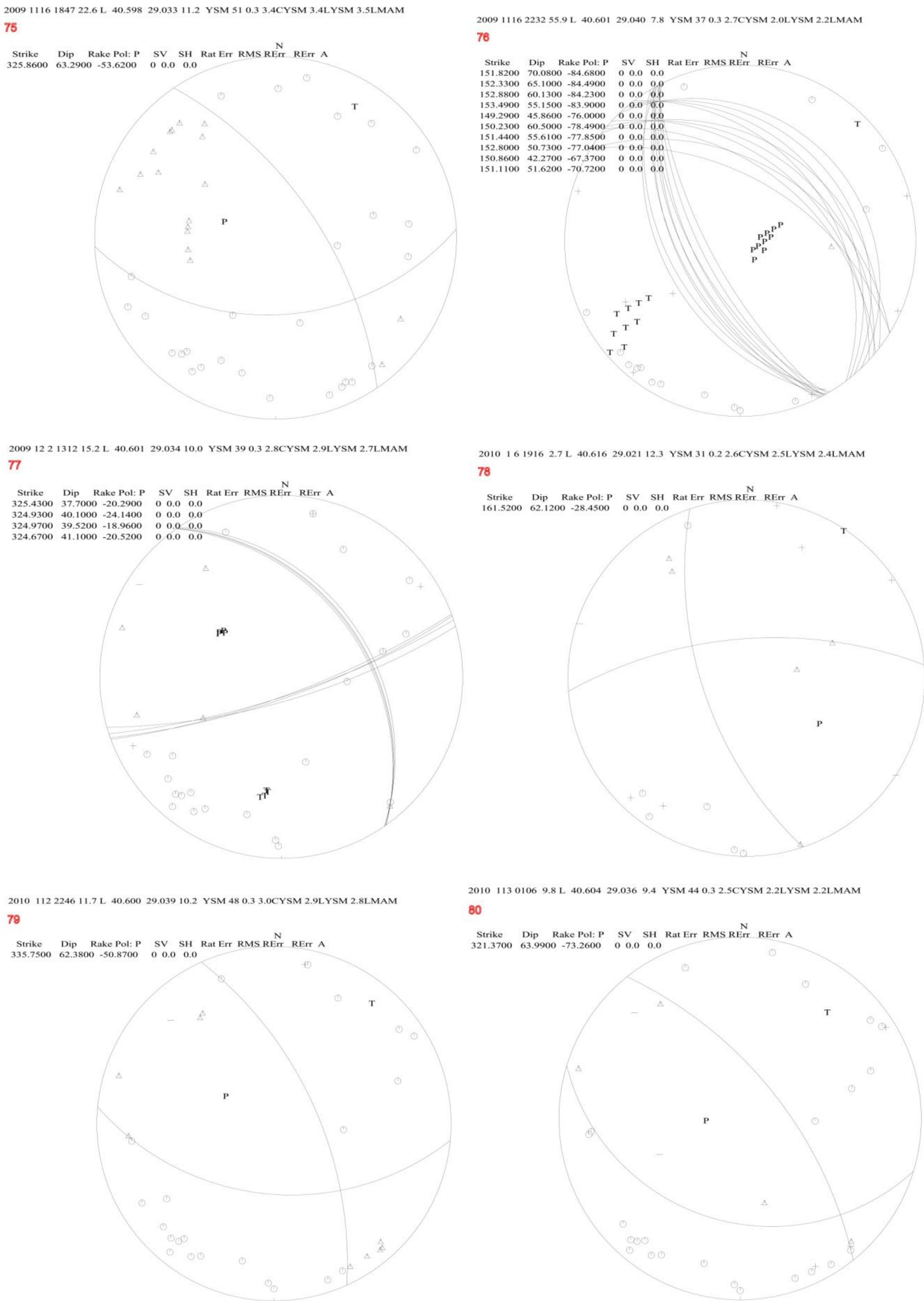

Figure D.4.14. Fault plane solutions obtained through the program of FOCMEC. Solutions are given time dependently for the Yalova Cluster

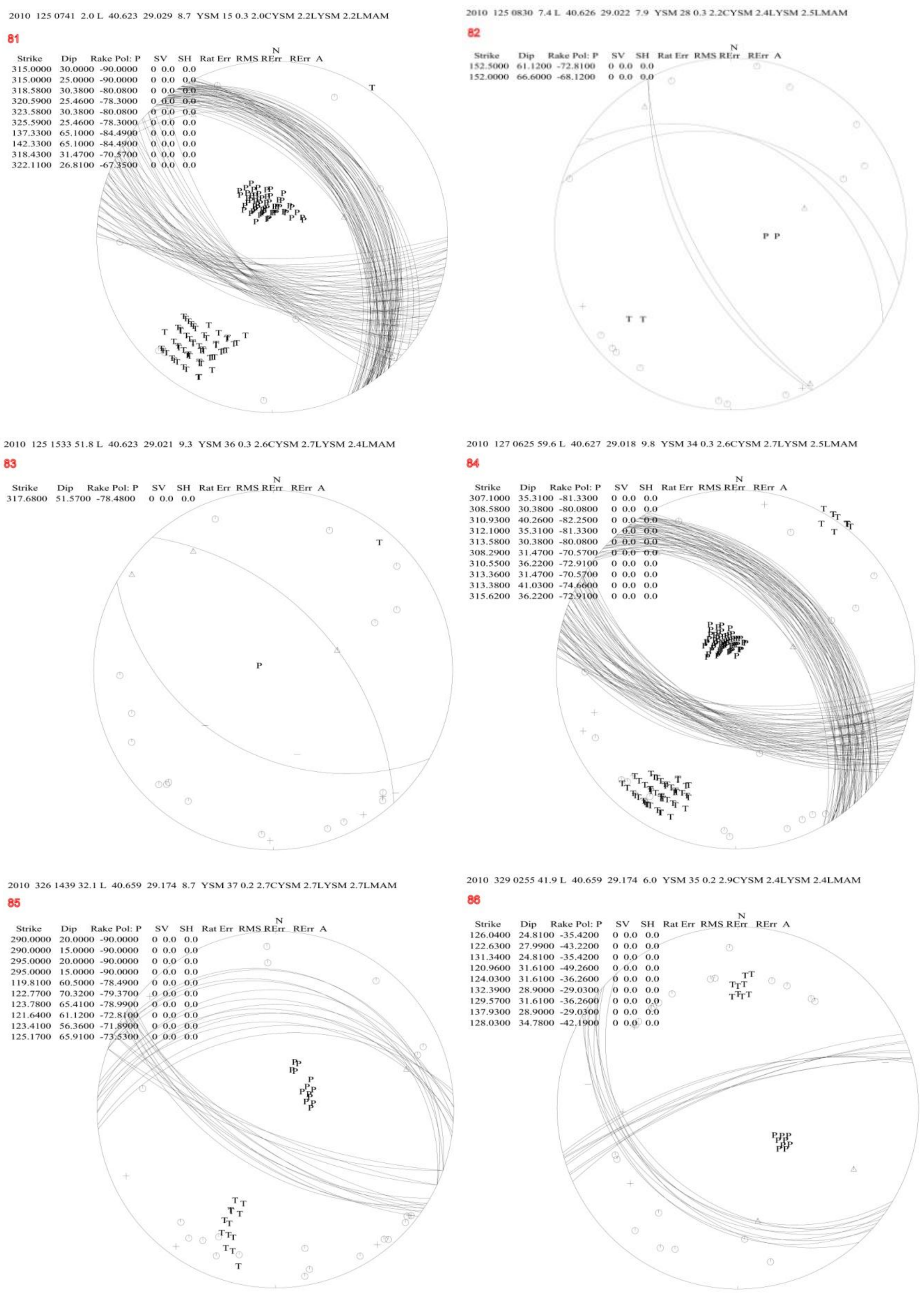

Figure D.4.15. Fault plane solutions obtained through the program of FOCMEC. Solutions are given time dependently for the Yalova Cluster

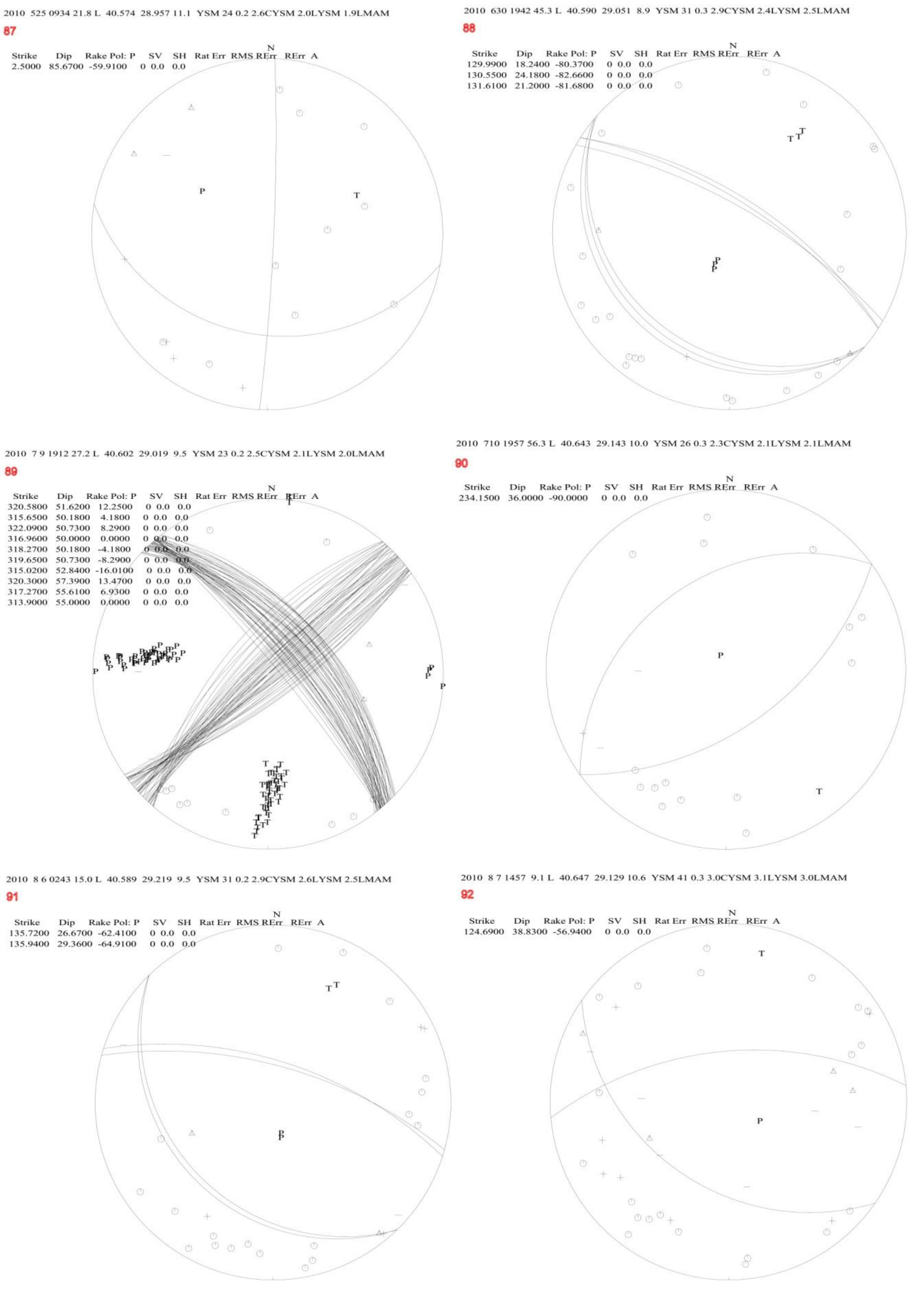

Figure D.4.16. Fault plane solutions obtained through the program of FOCMEC. Solutions are given time dependently for the Yalova Cluster

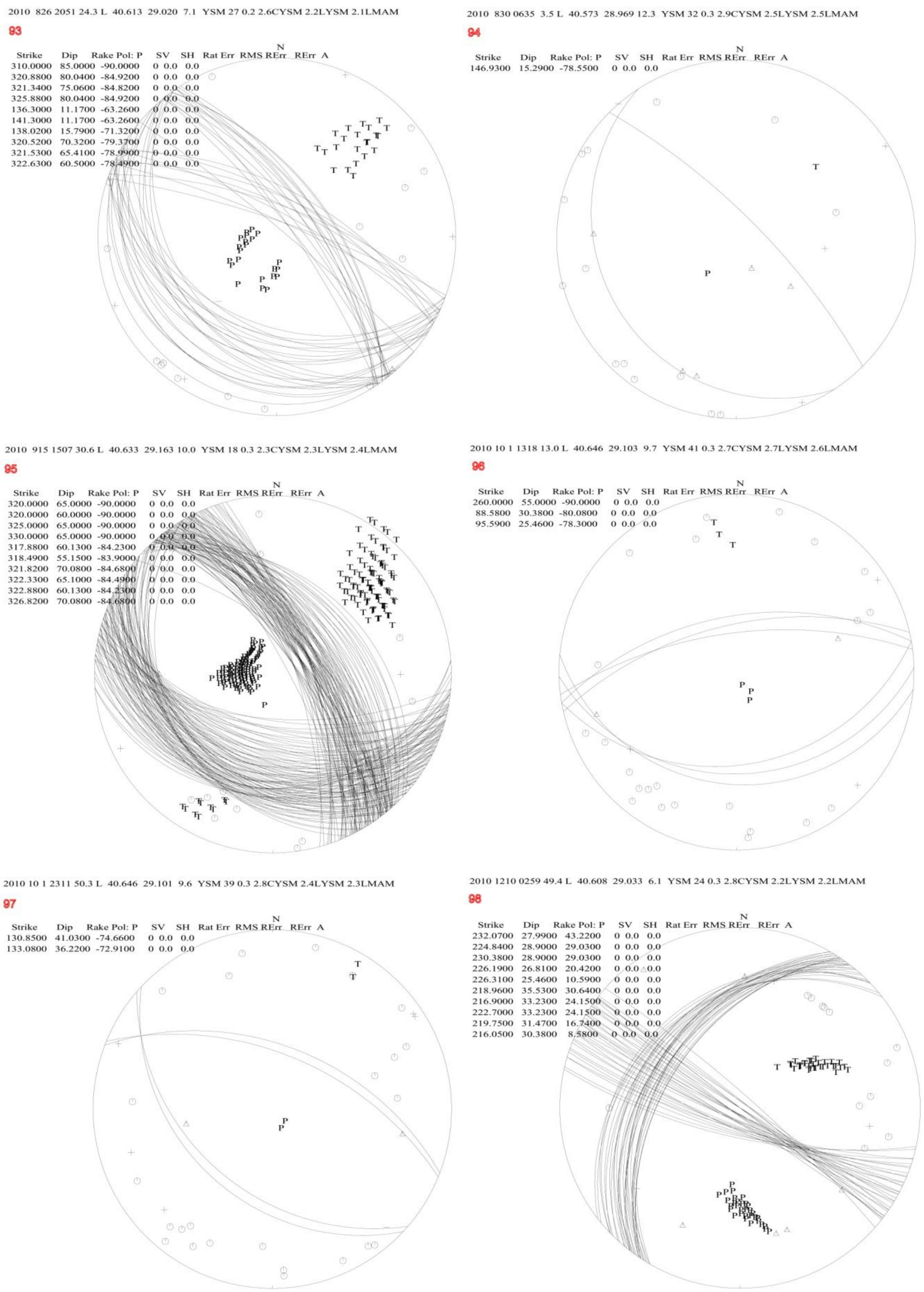

Figure D.4.17. Fault plane solutions obtained through the program of FOCMEC. Solutions are given time dependently for the Yalova Cluster

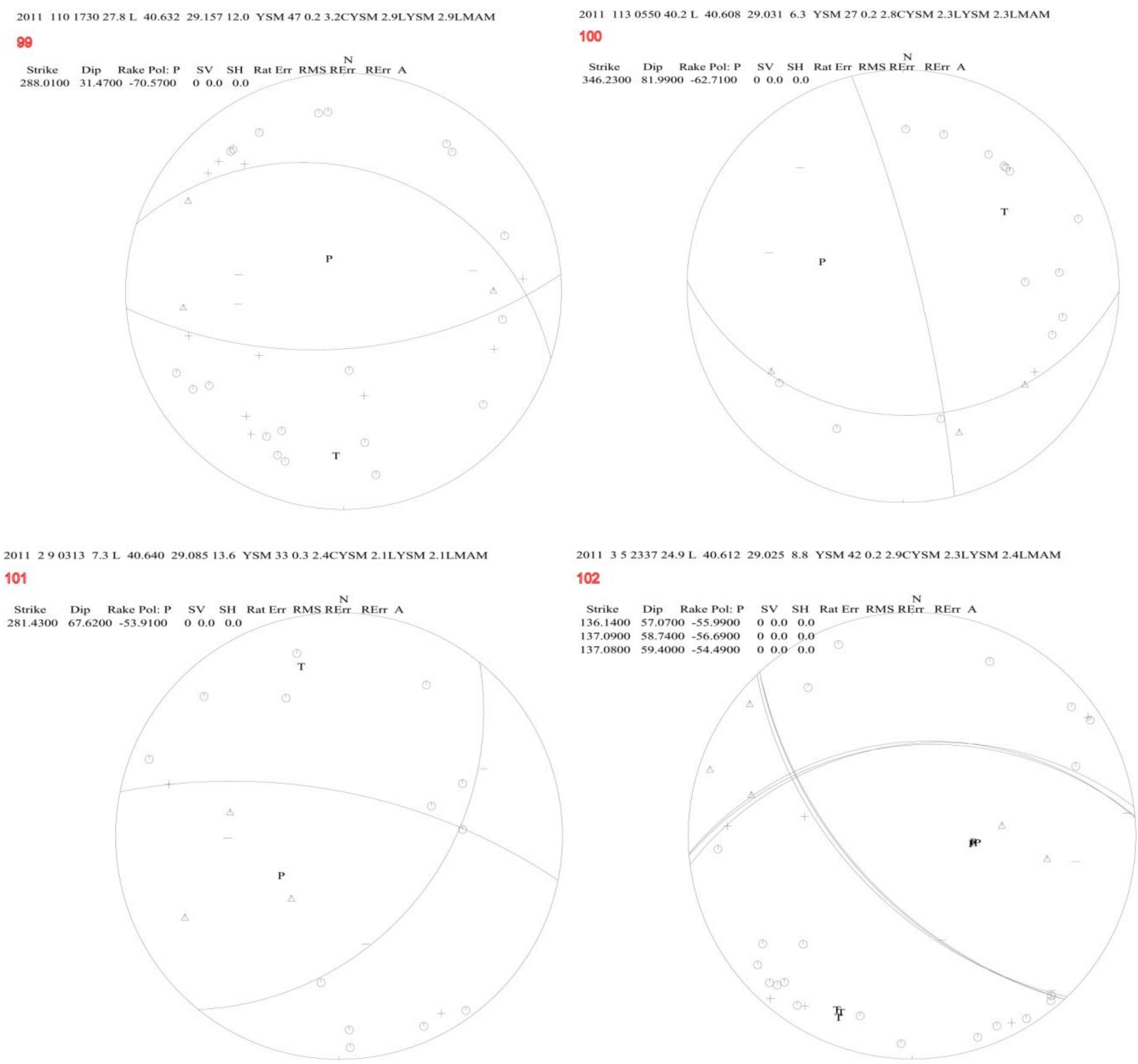

Figure D.4.18. Fault plane solutions obtained through the program of FOCMEC. Solutions are given time dependently for the Yalova Cluster

5. The Gemlik Cluster

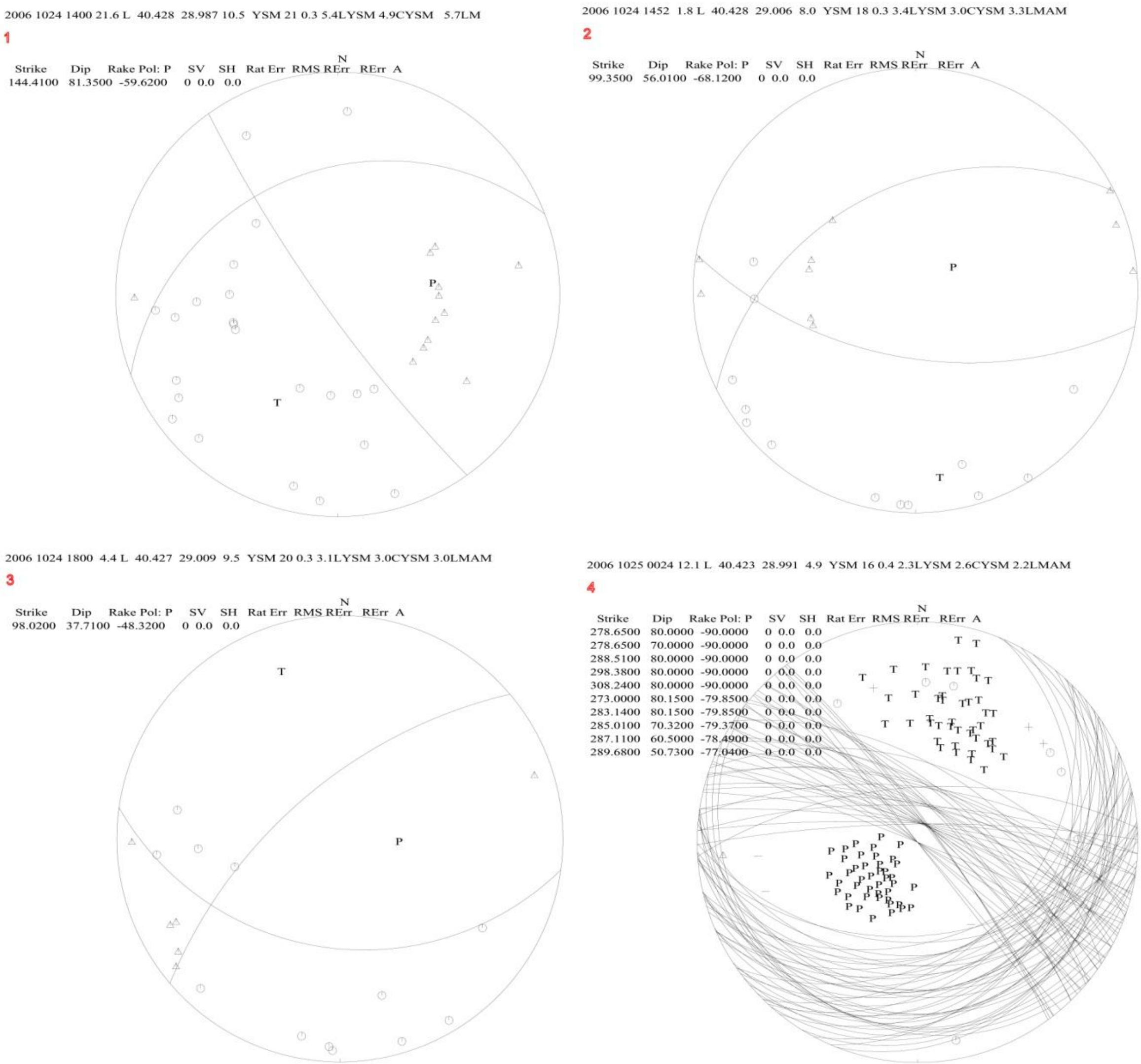

Figure D.5.1. Lower hemisphere projections of fault plane solutions obtained through the program of FOCMEC. Black circles indicate compressional P-wave first motion polarities, while black triangles show dilatational ones. Solutions are given time dependently for the Gemlik Cluster

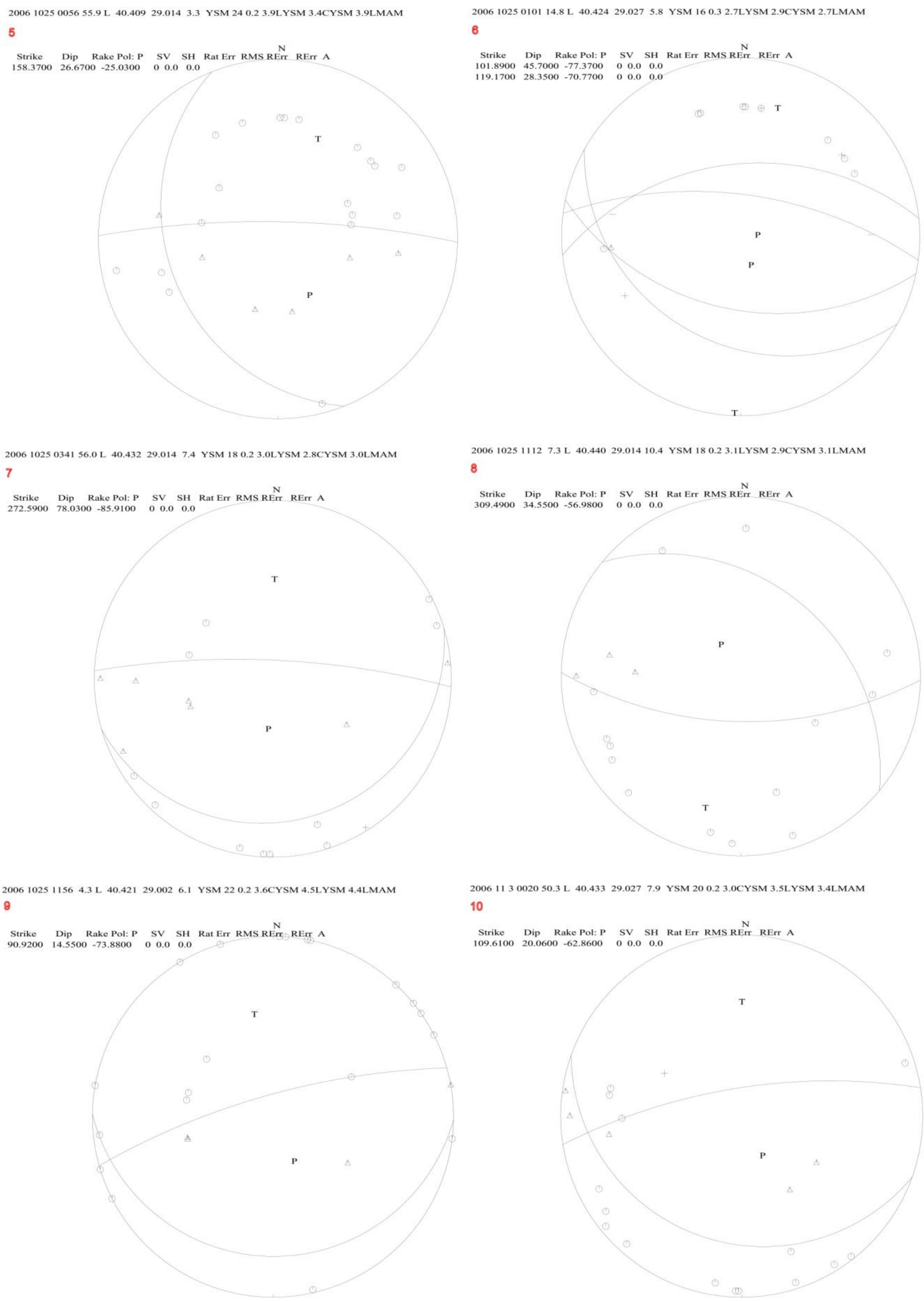

Figure D.5.2. Fault plane solutions obtained through the program of FOCMEC. Solutions are given time dependently for the Gemlik Cluster

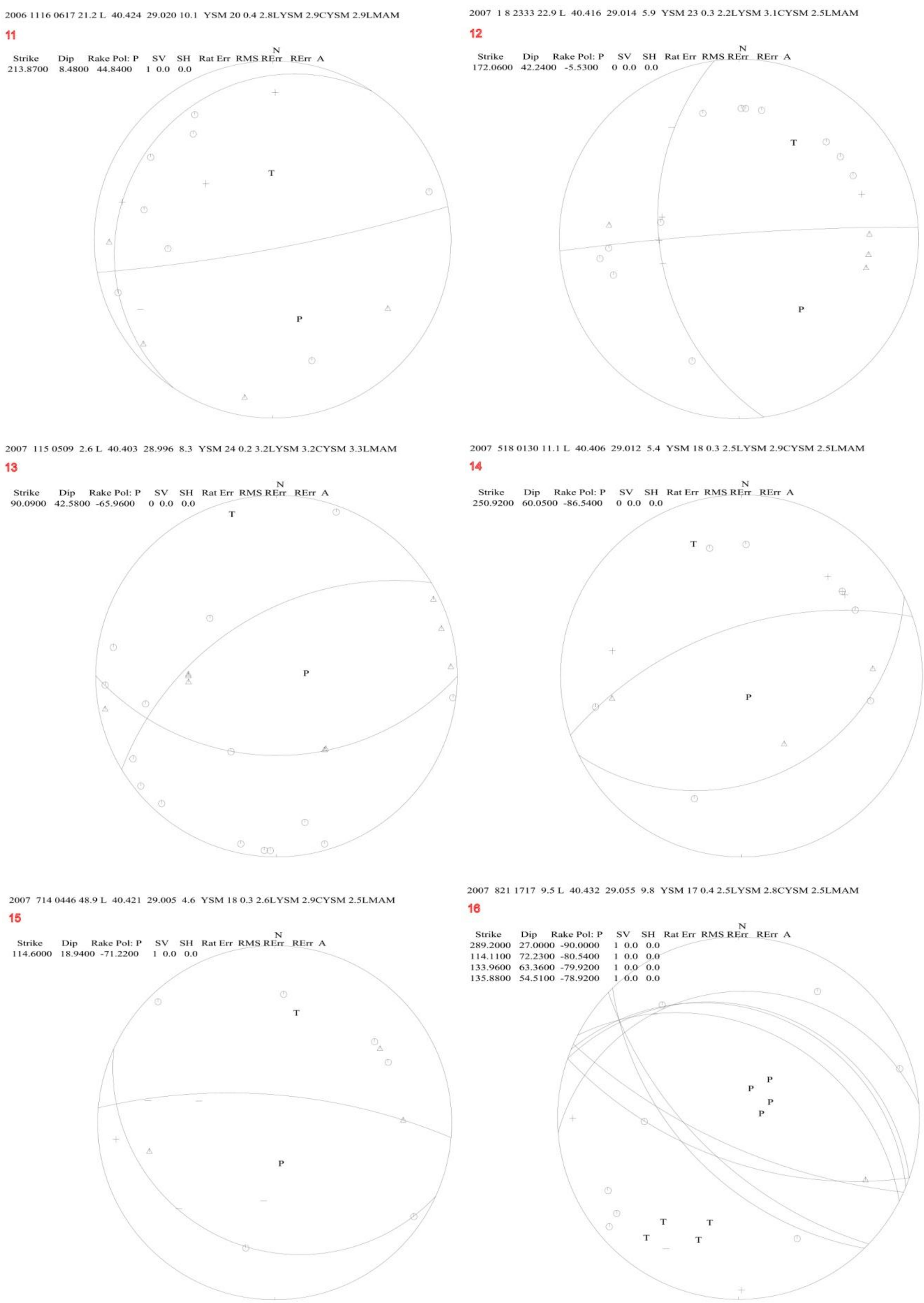

Figure D.5.3. Fault plane solutions obtained through the program of FOCMEC. Solutions are given time dependently for the Gemlik Cluster

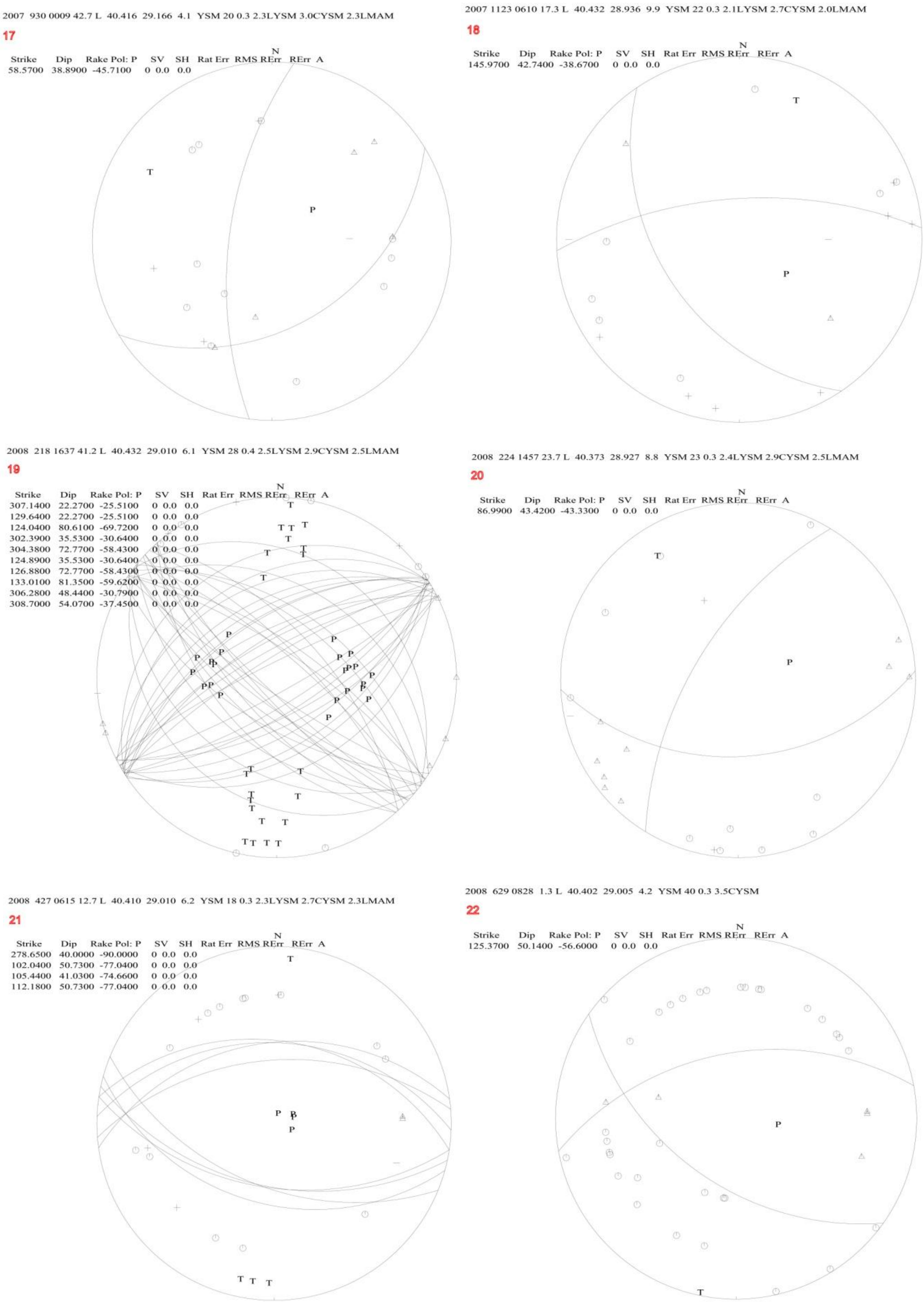

Figure D.5.4. Fault plane solutions obtained through the program of FOCMEC. Solutions are given time dependently for the Gemlik Cluster

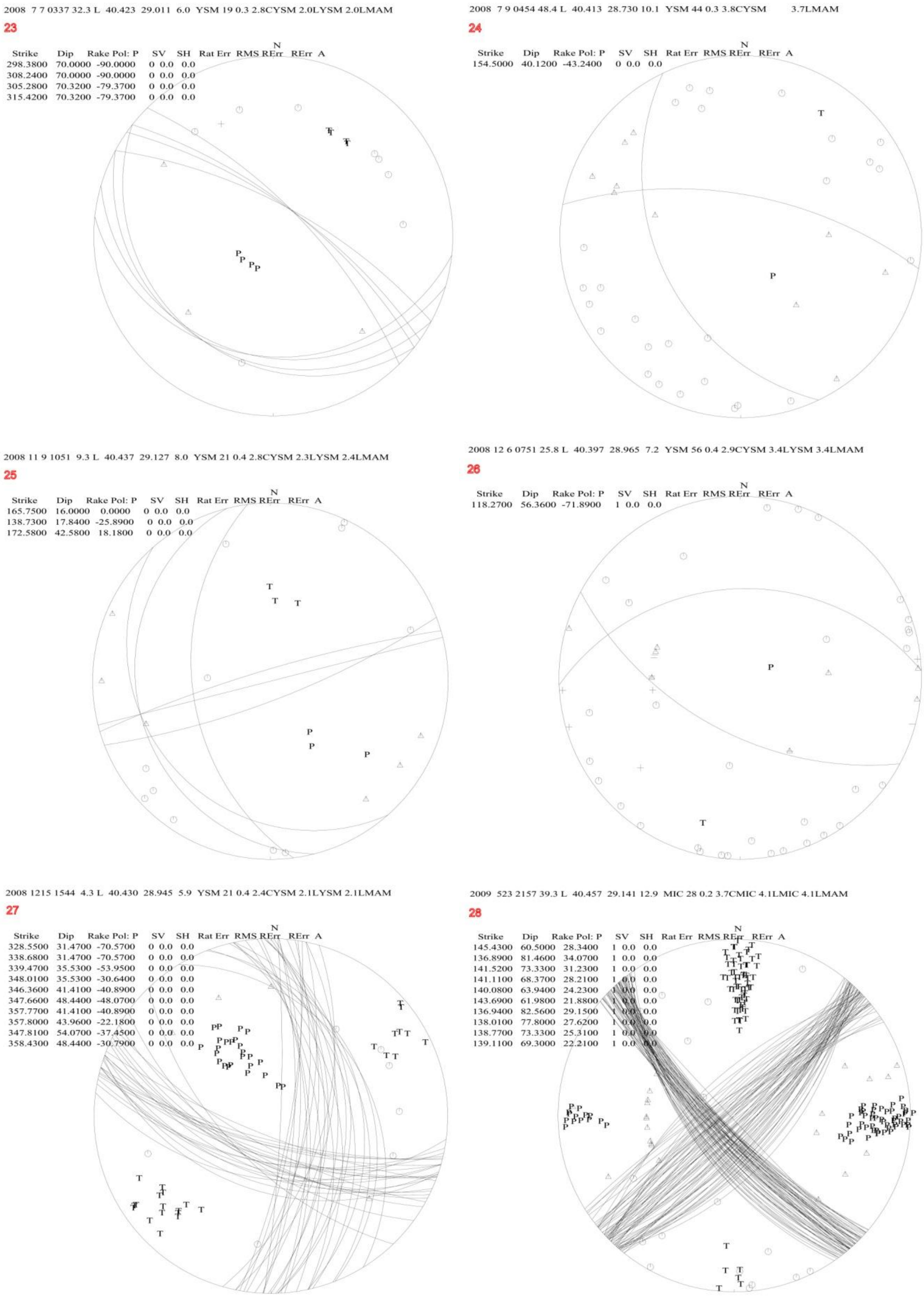

Figure D.5.5. Fault plane solutions obtained through the program of FOCMEC. Solutions are given time dependently for the Gemlik Cluster

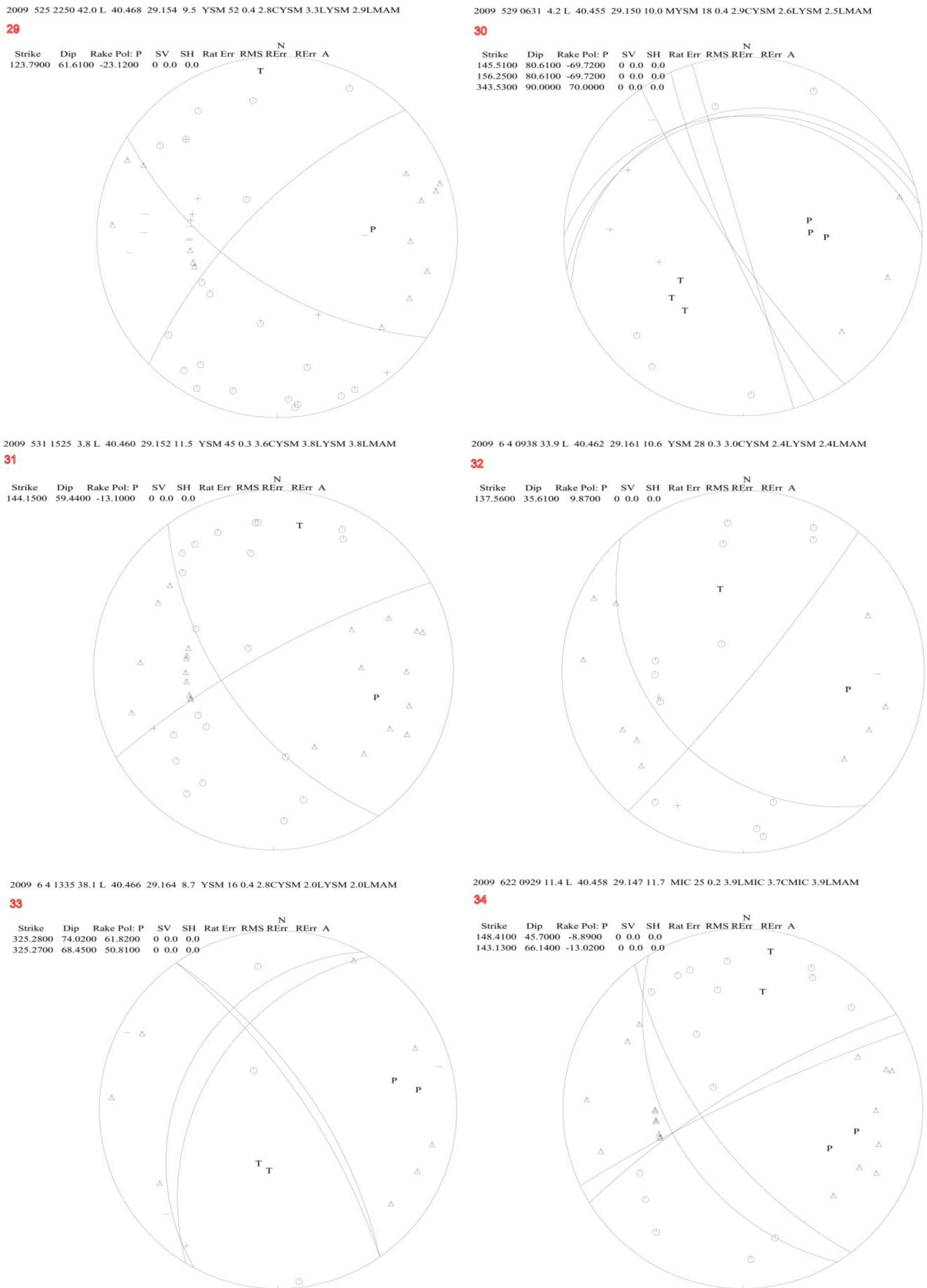

Figure D.5.6. Fault plane solutions obtained through the program of FOCMEC. Solutions are given time dependently for the Gemlik Cluster

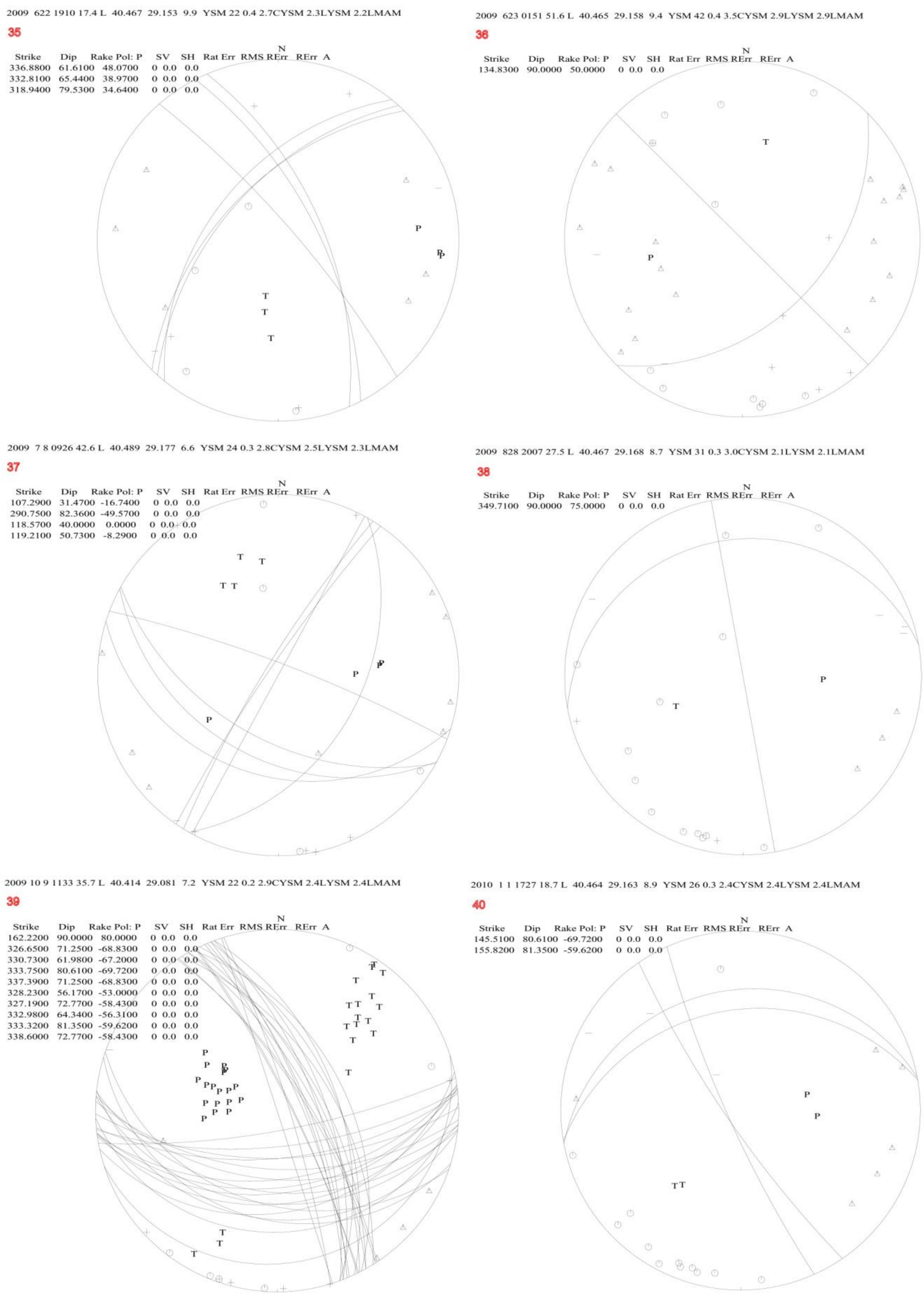

Figure D.5.7. Fault plane solutions obtained through the program of FOCMEC. Solutions are given time dependently for the Gemlik Cluster

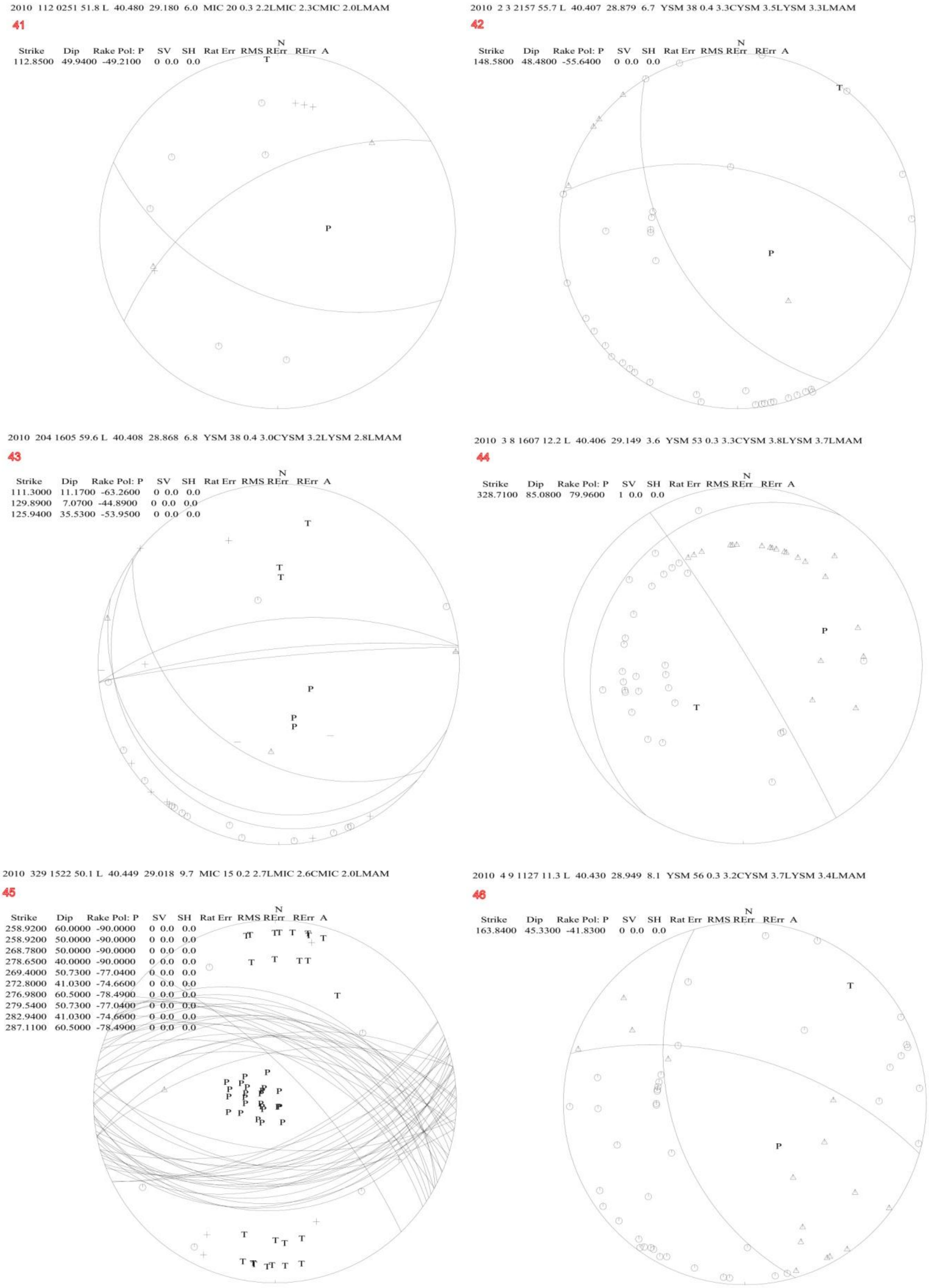

Figure D.5.8. Fault plane solutions obtained through the program of FOCMEC. Solutions are given time dependently for the Gemlik Cluster

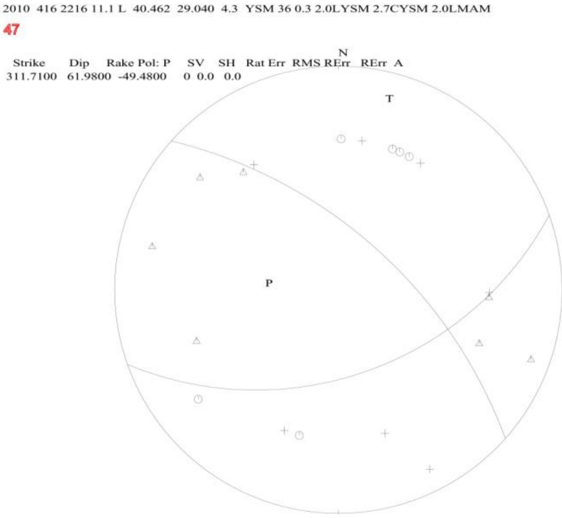

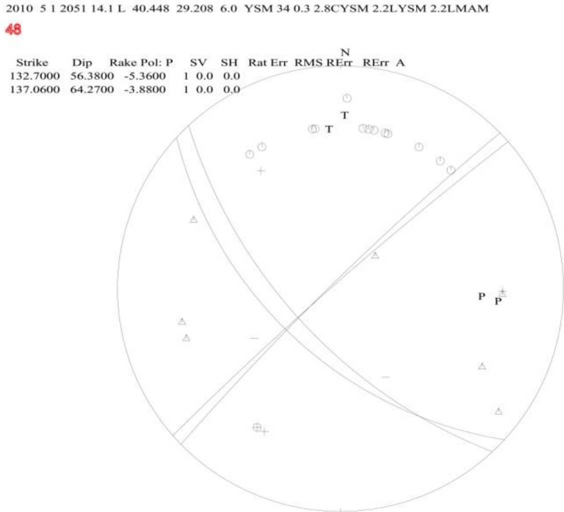

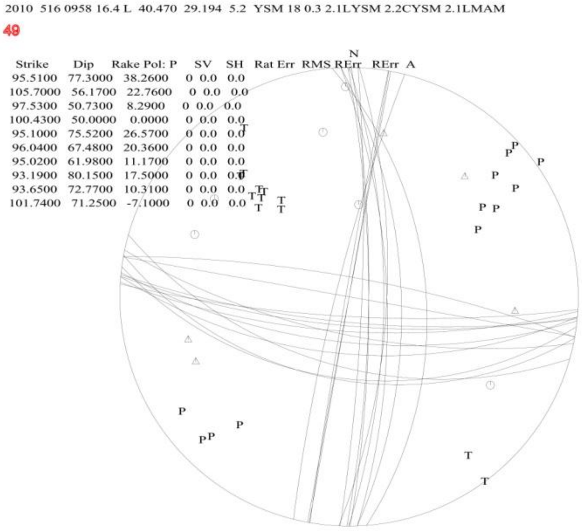

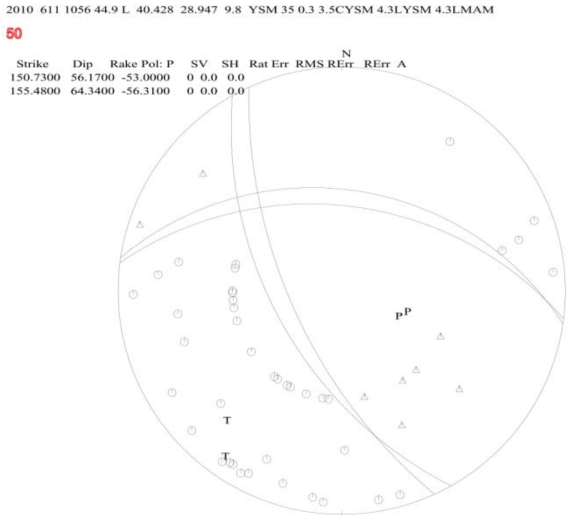

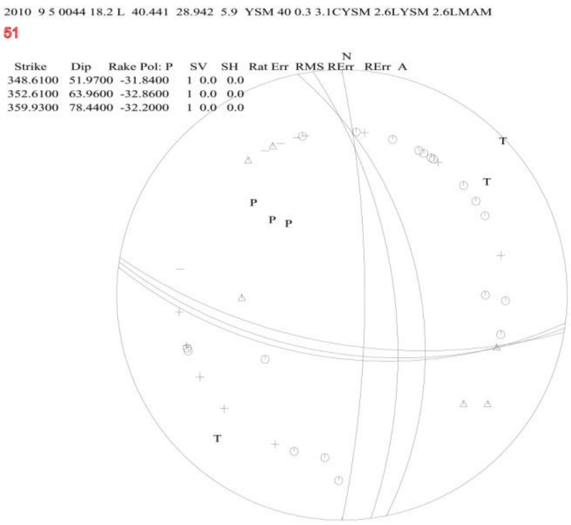

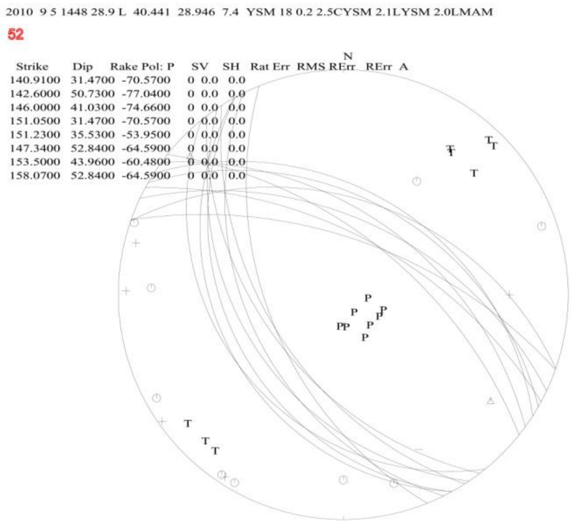

Figure D.5.9. Fault plane solutions obtained through the program of FOCMEC. Solutions are given time dependently for the Gemlik Cluster

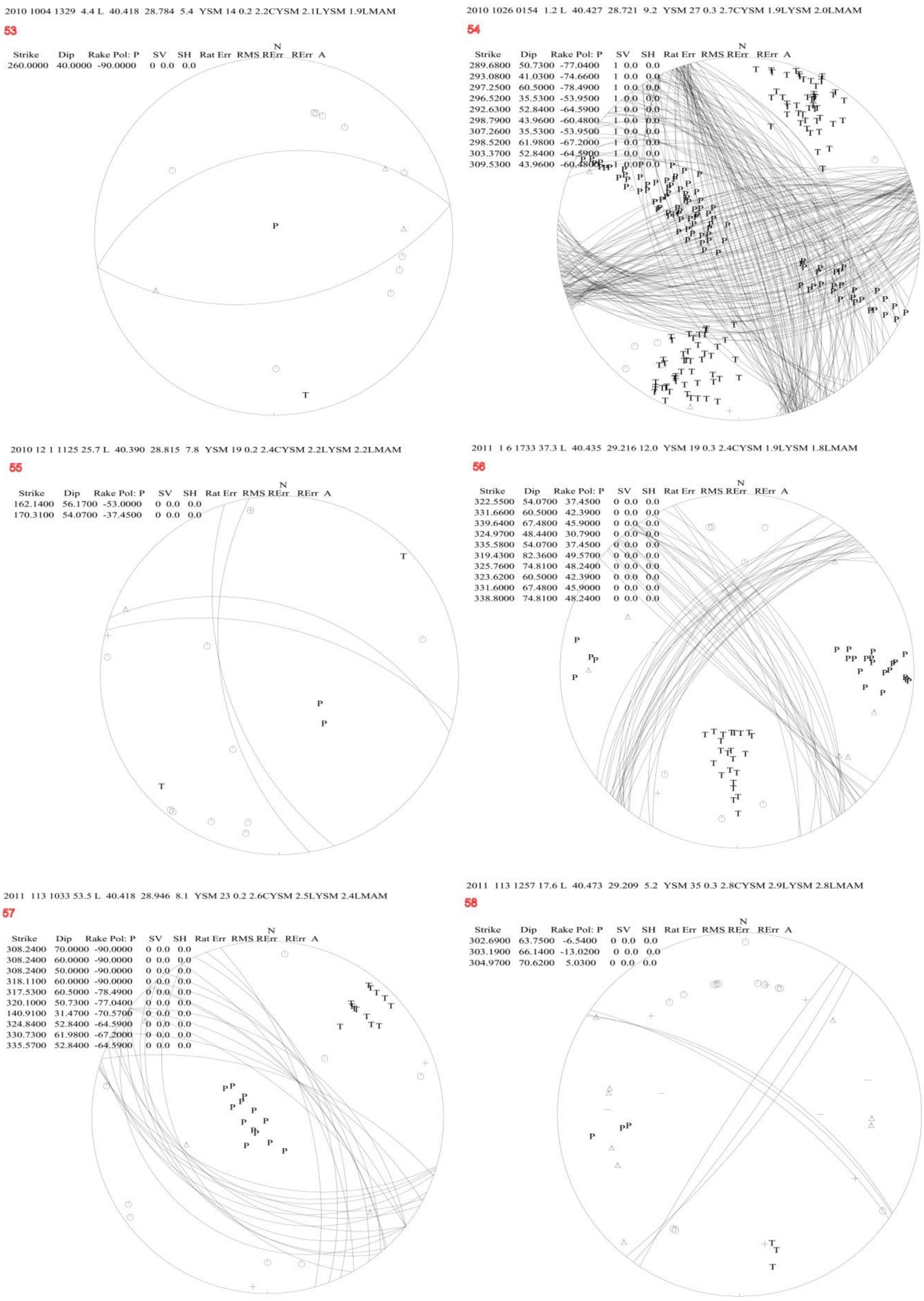

Figure D.5.10. Fault plane solutions obtained through the program of FOCMEC. Solutions are given time dependently for the Gemlik Cluster

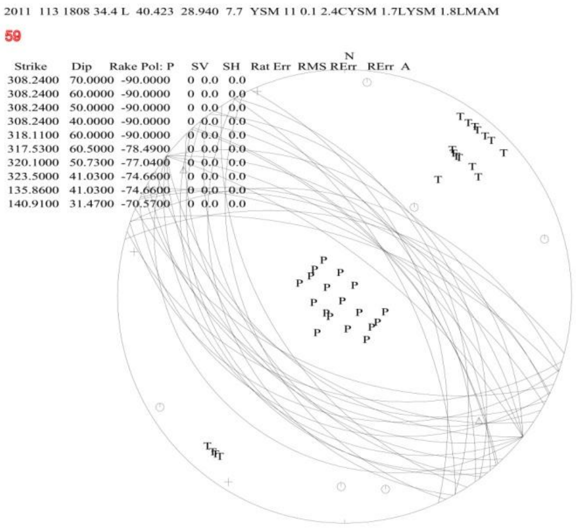

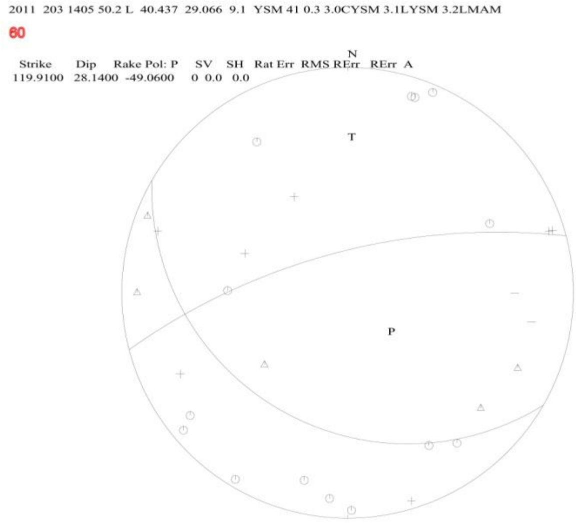

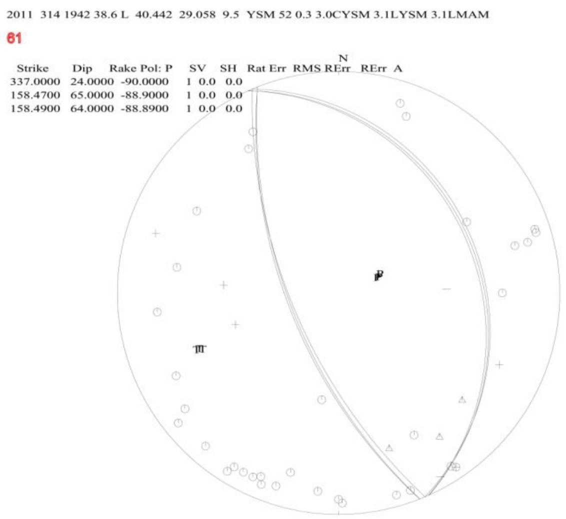

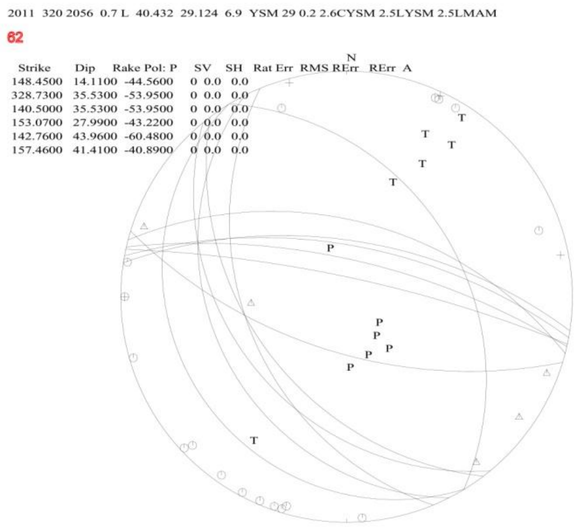

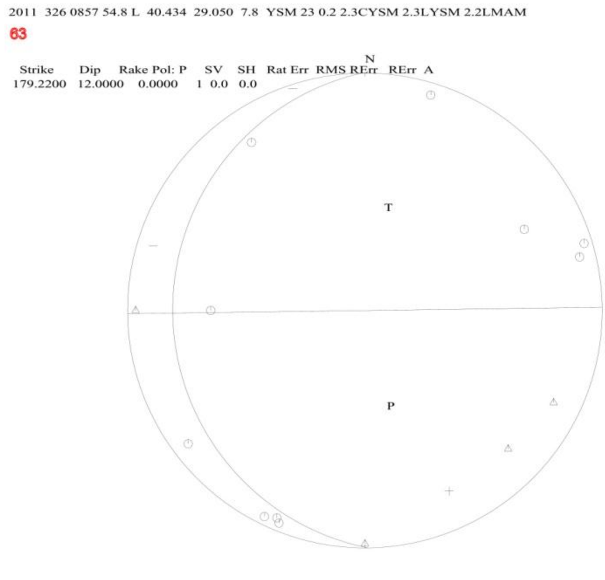

Figure D.5.11. Fault plane solutions obtained through the program of FOCMEC. Solutions are given time dependently for the Gemlik Cluster